1995

Numerical and experimental analysis for the GMAW process

Ill-soo Kim
University of Wollongong

NUMERICAL AND EXPERIMENTAL ANALYSIS FOR THE GMAW PROCESS

A thesis submitted in fulfilment of the requirements

for the award of the degree of

DOCTOR OF PHILOSOPHY

from

UNIVERSITY OF WOLLONGONG

by

ILL-SOO KIM

(B.E., Hons, M.Eng.)

Department of Mechanical Engineering

APRIL 1995

DECLARATION

This is to certify that the work presented in this thesis was carried out by the author in the Department of Mechanical Engineering of the University of Wollongong, Australia and has not been submitted for a degree to any other university or institution.

Ill-Soo Kim

ACKNOWLEDGMENTS

The author is greatly indebted to his supervisor, Assoc. Prof. Animesh Basu, for excellent guidance, supervision and constant encouragement during the period of study. The author is also grateful to Dr. Elias Siores for consultation and his continued interests in the progress of his work.

The author is very thankful to the University of Wollongong and the BHP Coated Products Division, Port Kembla, for providing the Infrared Thermography to pursue this research study. Special mention must be made of Mr. Roger for helpful discussions and comments which have been both inspirational and enjoyable. Acknowledgments also given to Mr. Des Jamieson and Mr. Ian Kirby for their valuable assistance in the use of computer hardware and software. The author wished to extend many thanks to the Department's administrative staff, Mrs. Roma Hamlet and Babara Butler for their assistance.

The author is extremely grateful to his wife Young-Sook Kim and two sons James and Andrew. Finally, the financial sacrifices and moral support of my parents are not only greatly appreciated but have also made this undertaking possible. Without them, I would not have been here today.

ABSTRACT

In recent years there has been a significant growth in the use of the automated and/or robotic welding system, carried out as a means of improving productivity and quality, reducing product costs and removing the operator from tedious and potentially hazardous environments. One of the major difficulties with the automated and/or robotic welding process is the inherent lack of mathematical models for determination of suitable welding process parameters. Developing these models is difficult because welding process parameters can affect not only weld bead geometry but also weld pool formation. Therefore, the aim of this research is to develop mathematical models to predict welding process parameters, to obtain the required weld bead geometry and to study the effects of weld process parameters on weld bead dimensions for the Gas Metal Arc Welding (GMAW) process.

In this study, the mathematical models for presenting the interrelationship between the welding process parameters and weld bead geometry were proposed. The effects of weld process parameters on weld bead profile were investigated through the empirical and theoretical mathematical models in weld pools. And finally, an infrared camera was employed to monitor the weld bead geometry. A relationship between the weld bead geometry and the surface temperature distribution was also established. An image analysis technique was employed to quantify the changes in the surface temperature distribution of the workpiece being welded. Using the infrared camera in conjunction with this image technique was shown to be one of the most sophisticated techniques to monitor perturbations occurred during welding.

Partial-penetration, single-pass, bead-on-plate welds were fabricated in 12 mm AS 1204 mild steel flats employing five different welding process parameters. The experimental results were used to develop three empirical equations: curvilinear;

polynomial; and linear equations. The results were also employed to find the best mathematical equation under eleven weld bead dimensions to assist in the procedure optimisation and the process control algorithms for the GMAW process and to correlate welding process parameters with weld bead geometry of bead-on-plates deposited. With the help of a standard statistical package program, SAS, using an IBM-compatible PC, multiple regression analysis was undertaken for investigating and modelling the GMAW process, and significance test techniques were applied for the interpretation of the experimental data.

A transient two-dimensional (2D) axisymmetric model was developed for investigating the heat and fluid flow in weld pools and determining weld bead geometry, velocity profile and temperature distribution for the GMAW process. The mathematical formulation considers four driving forces for weld pool convection: electromagnetic; buoyancy; surface tension; and plasma drag forces. The formulation also deals with the molten metal droplets. The equation was solved using a general thermofluid-mechanics computer program, PHOENICS code, which is based on the SIMPLE algorithm.

The application of infrared thermography for the adaptive control of the GMAW process was studied. Welding process parameters were purposely varied and thermal response fluctuations were recorded. Infrared images were compared and contrasted with those extracted using machine vision. It was found that reasonable correlations exist between the two systems: infrared thermography and machine vision (as far as weld pool geometry interrogation is concerned). The technique developed can help to increase productivity and weld quality by minimising the amount of post process rework and inspection efforts otherwise needed.

TABLE OF CONTENTS

LIST OF FIGURES

LIST OF TABLES

NOMENCLATURE

A_T	Weld bead total area
A_P	Weld bead penetration area
A_R	Weld bead reinforcement area
B	Magnetic flux vector
B_P	Length of weld bead penetration boundary
B_R	Length of weld bead reinforcement boundary
B_r	Radial magnetic flux
B_z	Axial magnetic flux
B_θ	Azimuthal magnetic field
C_p	Heat capacity
D	Wire diameter
DI	Weld bead dilution
E	Electric potential field
F	Rate of addition of weld material
f_L	Fraction of liquid
G	Gas flow rate
g	Gravitational acceleration
H	Weld bead height
h_c	Heat transfer coefficient
ΔH	Latent heat of fusion
I	Welding current
J	Current density vector
J_r	Radial component of current density vector
J_z	Axial component of current density vector
J_q	Current density flux at r = 0
J_{suf}	Current flux

k	Thermal conductivity
k_l	Thermal conductivity (liquid steel)
k_s	Thermal conductivity (solid steel)
L	Electrode extension
L_r	Plate radius of domain
L_z	Plate thickness of domain
Q	Heat flux
P	Weld bead penetration
P_l	Predicted weld bead penetration
P_m	Pressure
q_a	Heat density distribution of arc
R_A	Calculated results
R_T	Measured results
r	Radial coordinate
r_j	Effective radius of the current distribution
r_a	Effective radius of the velocity distribution
r_d	Drop radius
r_q	Effective radius of the heat density distribution
r_s	Source radius
S	Welding speed
u_r	Velocity component in r direction
u_z	Velocity component in z direction
t	Time
t_l	Plate thickness
T	Temperature
T_d	Drop temperature
T_{liq}	Liquid temperature (steel)
T_{sol}	Solid temperature (steel)
T_o	Initial temperature

T_r	Reference temperature for Boussinesq approximation
T_m	Melting temperature - ambient temperature
V	Welding voltage
V_r	Volumetric feed rate of electrode
W	Weld bead width
WRFF	Weld reinforcement shape factor
WRSP	Weld penetration shape factor
W_1	Predicted weld bead width
z	Axial coordinate

Greek symbol

β	Volume coefficient of thermal expansion
λ	Thermal diffusivity
ρ	Density of workpiece
η	Percentage error
μ	Dynamic viscosity
σ	Electrical conductivity
Γ	Boundary
$\frac{\partial \gamma}{\partial T}$	Surface tension temperature coefficient
σ_o	Stefan-Boltzmann constant
ε	Emissivity
ζ	Heat input efficiency
μ_m	Magnetic permeability
τ_{drag}	Shear stress
ϕ	Scalar electric potential

Subscripts

H	High grid-node location
j	Arc current
N	North grid-node location
L	Low grid-node location
P	Point grid-node location
q	Heat flux
r	Radial component
S	South grid-node location
z	Axial component

PUBLICATIONS

1. International Journals

Papers Accepted/Published

[1] I. S. Kim and A. Basu, "A study of influence of welding process variables on GMAW", Transactions of Mechanical Engineering, Australia, Vol. ME20, No. 1, P. 35 - 41.

[2] I. S. Kim and A. Basu, "An investigation of mathematical model for predicting weld bead geometry", accepted for publication in Canadian Metallurgical Quarterly, Canada.

[3] I. S. Kim, A. Basu and E. Siores, "Design of a computerized scheduling system for best rule analysis and control" accepted for publication in An International Journal of Computers and Industrial Engineering, USA.

[4] I. S. Kim and A. Basu, "The effect of welding process parameters on weld bead height in gas metal arc welding process", accepted for publication in An International Journal of Materials Processing Technology, UK.

[5] I. S. Kim and A. Basu, "Weld pool development during gas metal arc welding processes", accepted for publication in An International Journal of Materials Processing Technology, UK.

[6] I. S. Kim and A. Basu, "Mathematical models for control of weld bead penetration", accepted for publication in An International Journal of Advanced Manufacturing Technology, UK.

Papers under Review

[7] I. S. Kim and A. Basu, "The effects of input variables on weld penetration of GMAW", revised paper submitted for Journal of Intelligent Systems and Structures, USA.

[8] I. S. Kim and A. Basu, "Computational analysis of heat transfer and fluid flows in weld pool for GMAW process", revised paper submitted for the International Journal of Mathematical and Computer Modelling, USA.

[9] I. S. Kim and A. Basu, "A study of weld pool monitoring using infra-red thermography", revised paper submitted for the International Journal of Mechanical Sciences, UK.

[10] I. S. Kim and A. Basu, "Mathematical models for optimal weld bead geometry for GMAW process", revised paper submitted for the International Journal of Japan Society of Mechanical Engineers, Japan.

[11] I. S. Kim and A. Basu, "A numerical model for simulation of the GMAW process", revised paper submitted for the International Journal of Heat and Mass Transfer, UK.

2. International Conference and Others

Papers Accepted/Published

[12] I. S. Kim, A. Basu and E. Siores, "Relationships between process parameters and weld bead geometry for GMAW process", WTIA/AINDT Conference - Towards Competitive Edge, 27 September - 1 October, Wollongong, Australia, 1993, P. 170 - 176.

[13] I. S. Kim and E. Siores, "A simulation model for an automatic factory", WTIA/AINDT Conference - Towards Competitive Edge, 27 September - 1 October, Wollongong, Australia, 1993, P. 216 - 220.

[14] I. S. Kim and E. Siores, "A computer assisted scheduling system for best rule evaluation and execution", A Collection of Research Articles by Korea Overseas Students, 15, December, 1992, The Association of Korea Overseas Students, Australia, P. 13 - 23.

[15] I. S. Kim, A. Basu and E. Siores, "Design of a computerized scheduling system for best rule analysis and control", Proceedings of 16th International Conference on Computers & Industrial Engineering, 7 - 9, March, 1994, Ashikaga, Japan, P. 480 - 483.

[16] I. S. Kim, A. Basu and E. Siores, "The effect of welding parameters on weld penetration in GMAW process", Proceedings of the Pre-Assembly Symposium of 47th Annual Assembly of International Institution of Welding, 1 - 2, September, 1994, Dalian, China, P. 238 - 243.

[17] I. S. Kim, A. Basu and E. Siores, "Dynamic monitoring of weld pool formation for robotic arc welding control", Proceedings of the Pre-Assembly Symposium of 47th Annual Assembly of International Institution of Welding, 1 - 2, September, 1994, Dalian, China, P. 232 - 237.

[18] I. S. Kim, A. Basu and E. Siores, "Weld pool dynamics monitoring using infra-red thermography and machine vision sensing for GMAW process", Proceedings of the 42th National Welding Conference, 24 - 27, October, 1994, Melbourne, Australia, Vol. 2, No. 26, P. 1 - 7.

[19] I. S. Kim and A. Basu, "Mathematical models for open loop control in GMAW process", Proceedings of the 1st International Symposium on Advances in Intelligent Computer Integrated Manufacturing System, 21 - 23, November, 1994, Seoul, Korea, P. 165 - 172.

[20] I. S. Kim and A. Basu, "Robotic arc welding process using infra-red thermography", Proceedings of the 1st International Symposium on Advances in Intelligent Computer Integrated Manufacturing System, 21 - 23, November, 1994, Seoul, Korea, P. 173 - 178.

[21] I. S. Kim and A. Basu, "Mathematical models for feedback and adaptive control in GMAW", Proceedings of the 57th New Zealand Welding Conference, 15 - 17, March, 1995, Dunedin, New Zealand, P. 36 - 44.

[22] I. S. Kim and A. Basu, "A study of infra-red thermography for gas metal arc welding control", Proceedings of the Joint Applied Mechanics and Materials Summer Meeting, 28 - 30, June, 1995, Los Angels, USA, P. 478 - 478.

[23] I. S. Kim and A. Basu, "A computational model of the weld pool in GMAW process", Proceedings of the Fifth East Asia-Pacific Conference on Structural Engineering & Construction, 25 - 27, July, 1995, Gold Coast, Australia, P. 2221 - 2226.

[24] A. Basu and I. S. Kim , "Expert welding control system developed for GMAW", Proceedings of the Fifth East Asia-Pacific Conference on Structural Engineering & Construction, 25 - 27, July, 1995, Gold Coast, Australia, P. 2227 - 2232.

[25] I. S. Kim and A. Basu, "A mathematical model of heat transfer and fluid flow in the gas metal arc welding process", Proceedings of the International Conference on Advanced in Materials & Processing Technologies (AMPT'95), 7 - 11 August, 1995, Dublin, Ireland, P. 693 - 702.

[26] I. S. Kim and A. Basu, "The effect of welding process parameters on weld bead height in gas metal arc welding process", Proceedings of the International Conference on Advanced in Materials & Processing Technologies (AMPT'95), 7 - 11 August, 1995, Dublin, Ireland, P. 1147 - 1155.

[27] I. S. Kim and A. Basu, "Weld pool development during gas metal arc welding processes", accepted for presentation at the Twelfth Australasian Fluid Mechanics Conference, to be held Sydney, Australia, 10 - 15, December, 1995.

[28] I. S. Kim, "Numerical and experimental analysis for the GMAW process", (unpublished Ph.D Thesis), 1995.

[29] I. S. Kim, "A computer assisted scheduling system for best rule evaluation and execution", (unpublished Masters Thesis), 1991.

[30] I. S. Kim, "Research on material's mechanical characteristics applied by KSD 3503 steel slide", (unpublished Masters Thesis), 1982.

Papers under Review

[31] I. S. Kim and A. Basu, "Finite difference modelling of heat transfer and fluid flow for GMAW", submitted for presentation at the CSME Forum 96, to be held Hamilton, Ontario, Canada, 7 - 9, May, 1996.

[32] I. S. Kim and A. Basu, "Weld bead geometry prediction for gas metal arc welding processes", submitted for presentation at the 1996 ASME

Mechanics & Materials Conference, to be held Baltimore, USA, 12 - 14, June, 1996.

[33] I. S. Kim and A. Basu, "The effects of welding process variables on weld bead width of GMAW, submitted for presentation at the AIENG 96, to be held Southampton, UK, 11 - 13, September, 1996.

CHAPTER 1

INTRODUCTION

1.1 MOTIVATION

GMAW is generally accepted today as the preferred joining technique and commonly chosen for assembling most large metal structures such as bridges, automotive, aircraft, aerospace, shipbuilding and rolling stocks due to its joint strength, reliability, and low cost compared to other joint processes. The demand to increase productivity and quality, the shortage of skilled labour and strict health and safety requirements led to the development of the automated and/or robotic welding process to deal with many of the present problems of the welded fabrication [Hanright (1986)][61]. In the past decades, several effective and reliable welding processes have been developed into mechanised welding machines which included the power sources, wire feeders and welding control units. Robotic welders have replaced human welders in many welding applications, and reasonable seam tracking systems are commercially available, but fully adequate process control systems have not been developed due to a lack of reliable sensors and mathematical models that correlate welding process parameters to the weld bead geometry for the automated and/or robotic welding process.

To make effective use of the automated and/or robotic arc welding process, it is imperative that a mathematical model which can be programmed easily and fed to the robot, should be developed. It should give a high degree of confidence in predicting the weld bead dimensions and shape to accomplish the desired mechanical properties of the weldment. The mathematical model should also cover a wide range of material thicknesses and be applicable for all position welding.

In GMAW, the welding process parameters are known to include arc current, polarity, welding voltage, welding speed, electrode extension, electrode orientation, weld joint position, wire diameter, shielding gas composition, gas flow rate, material composition and material thickness. The parameters are interdependent and the effect of one parameter might affect another. Relationships between welding process parameters and the weld bead geometry are generally complex and the required control system will be dependent on a realistic model of the welding process. The size and shape of weld bead geometry and occurrence of various weld defects such as cratering, incomplete penetration and lack of side wall fusion are affected by all of these parameters [Chandel and Bala (1986)[22]]. This research mainly concentrated on weld bead dimensions (see figure 4.2). The development of this model and the methodology for this derivation will play an important role in the development of the automated and/or robotic welding system. Various approaches have been developed to optimise welding procedures from mathematical models based on physical principles to empirical models based on experiments. But all of them have failed to provide a practical and universal methodology for industrial applications.

An understanding of weld pool convection - which can strongly affect the various welding phenomena such as weld bead geometry, solidification model and microstructures, deformation and residual stress, and the gas porosity of the resultant weld bead - has been significant in recent years. Several mathematical models of

heat and mass transfer during GMAW processes [Tsao and Wu (1988)[184] and Kim and Na (1994)[81]] have been developed, but there exists no complete mathematical model due to a deficiency of detailed knowledge on actual welding phenomena, and physical and chemical properties over a wide range of temperatures. It is therefore necessary in the development of mathematical equations for heat transfer and fluid flow in weld pools to correlate the welding process parameters and to understand the effects of input variables on process output parameters.

A truly automated and/or robotic welding system should have three principal components: sensors which detect the condition of the welding process; a process model which provides the relationship between the welding process parameters and the welding bead geometry; and a control system which evaluates the sensor data and changes the welding process parameters using the relationship in the process model [Cook et al. 1989)[39]]. The recognition of process abnormalities during the automated and/or robotic welding process required the use of sensors. An accurate relationship between the sensed information and the welding process parameters must be presented for a control system to initiate a suitable corrective action. Many different sensing devices have been shown to provide successful monitoring of a variety of welding processes. Optical sensing techniques have displayed the ability to give detailed information on welding process parameters during the welding process.

Infrared thermography has been employed to monitor weld quality and the bond strength of resistance welded electrical components in real-time. The employed system was integrated with a microprocessor which compared the measured data against stored models of acceptable weld thermal signatures. Information related to the tensile strength of the weld was correlated with temperature profiles and heat distribution areas. Infrared thermography was also employed to assess the integrity of critical fusion welds in the aircraft and petrochemical industries [Ramsey et al.

(1963)[149], Lukens and Morris (1982)[109] and Chen and Yang (1985)[25]. Even though inspection in all applications mentioned above is performed on-line using infrared thermography, the evaluation process is confined to real-time acceptance or rejection of the finished component. This study therefore attempts to fully automate the welding process using infrared thermography as a sensing technique for real-time process monitoring and adaptive process control.

1.2 SCOPE OF THE RESEARCH WORK

A major portion of this research work is dedicated to developing the empirical and theoretical models that determine interrelationships between welding process parameters and weld bead geometry for the development of the automated and/or robotic welding process. The research concentrates on the following aspects:

1. Characterising the GMAW process and identifying the various problems that result from the GMAW process, and establishing guidelines and criteria for the most effective joint design.
2. Comparison of the experimental results to outputs obtained using sets of the published theoretical and empirical formulae relating welding process parameters to weld bead geometry. This includes remodelling the empirical equations to better predict the output of the GMAW process and finding the best mathematical model for the relationship between welding process parameters and weld bead geometry for the GMAW process.
3. Redefining the empirical equations that allow the selection of welding process parameters to be calculated from a desired weld bead size, using the theory of least squares.
4. Developing the empirical mathematical models which study the influence of welding process parameters on weld bead geometry. These models will also aid the development of an optimal welding process and assist in the

generation of process control algorithms, using multiple regression analysis with the help of a standard statistical package program, SAS, on an IBM-compatible PC.

5. Development of the transient 2D mathematical model for weld pools incorporating all important physical phenomena that control the heat transfer and convective flow condition in weld pools. This model can be employed to investigate the heat transfer and the fluid flow in the GMAW process and to generate technical information that can be employed for weld and joint design using a general thermofluid-mechanics computer program, PHOENICS code, based on the SIMPLE algorithm and developed by CHAM Limited.
6. Finding a relationship between welding process parameters and thermal image from infrared thermography, and obtaining the thermal profile characteristics. This also includes the calculation of weld bead geometry using image analysis techniques and the investigation of the interrelationship between the surface temperature distribution of the welded part and the weld bead width and weld bead height.

1.3 THESIS ORGANIZATION

The thesis is organised into 7 chapters, the outline of each chapter is given below.

Chapter 1 highlights the motivation for and details the scope of the current research work. The outline of the thesis is also included.

Chapter 2 presents a comprehensive literature review concerning all aspects of the fundamentals of the GMAW process, procedure optimisation for weld bead geometry, heat and fluid flow in weld pools, and sensing and adaptive control for the arc welding as well as a brief review of recent publications on analytical, computational and experimental techniques by different researchers.

Chapter 3 provides the investigation of the analytical and empirical formulae for understanding the relationship between welding process parameters and weld bead geometry. It also describes in detail the experimental procedure, compares theoretical with experimental results, remodels empirical equations, develops mathematical models, redefines mathematical equations and discusses the overall experimental results.

Chapter 4 covers the detailed experimental results on the effects of five welding process parameters on the eleven weld bead dimensions (see page 82) in AS 1204 mild steel flats adapting the bead-on-plate technique. It also presents empirical formulae which investigate the effects of welding process parameters on weld bead geometry.

Chapter 5 presents a transient axisymmetric mathematical model for investigating coupled conduction and convection heat transfer problems for the GMAW process. It was employed to study the effects of four driving forces (electromagnetic, buoyancy, surface tension and plasma drag forces) and the molten metal droplets on weld pools.

Chapter 6 concentrates on the application of infrared thermography in monitoring the automated and/or robotic arc welding process and its potential for weld penetration depth and seam tracking control.

Chapter 7 contains the concluding remarks and summaries of the achievements obtained during the course of this research. Suggested future work is also included at the end of this chapter.

CHAPTER 2

LITERATURE SURVEY

2.1 INTRODUCTION

Adaptive control in the automated and/or robotic welding is employed to monitor information about weld characteristics and welding process parameters and, to modify those parameters to hold weld quality within acceptable limits. Good quality of welding must have the characteristics of accurate positioning of weld pools and weld bead geometry. Typical characteristics are the weld bead geometry, composition, microstructure and appearance, while welding process parameters which govern the quality of the final weld, include arc current, welding voltage and welding speed.

In this chapter, a comprehensive review of the literature covering the fundamentals of the GMAW process, procedure optimisation for weld bead geometry, heat and fluid flow in weld pools, and sensing and adaptive control for the arc welding is given. A brief discussion on recent publications on analytical, computational and experimental techniques by different researchers is also included. Every effort has been made to cite the most recent developments.

2.2 FUNDAMENTALS OF THE GMAW PROCESS

2.2.1 Overview of the GMAW Process

GMAW, one of the oldest and fastest growing metal joining processes, has been an important component in Australia's economy because of the progress made in welding equipment, electrodes and design. Applications of the GMAW have ranged from joining thin section pipelines to assembling large metal structures such as pressure vessels, bridges, cars, trains and nuclear reactors [Heiple and Roper (1990)[67]].

The GMAW process, sometimes called Metal Inert Gas (MIG) welding, is a welding process which yields coalescence of metals by heating with a welding arc between a continuous filler metal (consumable) electrode and the workpiece. The continuous wire electrode which is drawn from a reel by an automatic wire feeder, and then fed through the contact tip inside the welding torch, is melted by the internal resistive power and heat transferred from the welding arc. Heat is concentrated by the welding arc from the end of the melting electrode to molten weld pools and by the molten metal which is being transferred to weld pools. Molten weld pools and electrode wire are protected from contaminants in the atmosphere by a shielding gas obtained from an externally supplied Ar, CO_2, or mixtures Ar with O_2, H_2, He, or CO_2 in various combinations. A controller is used to control wire feed rate, arc current and welding voltage. In some cases, it is also employed to control the gas flow rate [Brien (1990)[12]].

There are two ways that the molten metal of electrode wire may be moved to the workpiece. The first detaches from the electrode wire, accelerates through the welding arc and subsequently collides with the workpiece. The second is transferred when the electrode makes electrical contact with molten weld pools. Metal transfer is normally classified into three modes: short-circuiting; globular; and spray metal transfers, each

of these has its own scope of welding voltage, arc current, deposition rate, welding speed, applicable welding positions and manipulation techniques [Liu et al. (1989)[105]]. The mode of metal transfer also affects the welding process such as fume rate, arc stability, bead form, wetting angle and spatter.

Short-circuiting metal transfer at lower values of current (<200 A) puts together a small fast-freezing weld pool that is mostly suited for thin sections, out-of-position welding and bridging large root openings. Metal is transferred from the electrode to the workpiece only during a period when the electrode is in contact with weld pools. No metal is transposed across the arc gap.

At higher currents (200 to 250 A) globular metal transfer with a positive electrode (DCEP) occurs when droplets do not detach themselves from the electrode until their diameter is greater than that of the electrode. Globules are detached with the mechanical forces exerted by the jet stream, which in turn, is a product of the interaction of electromagnetic force on the electrode tip and the arc plasma. One component of the resultant force at the electrode tip squeezes the molten portion of the electrode and another lowers acceleration and as a result, less penetration is obtained.

Spray metal transfer with the currents (>250 A) above a critical value called the transition current and a positive electrode (DCEP) takes place when the molten electrode droplets are smaller or equal to the electrode diameter. These small droplets are easily accelerated toward the workpiece by the same mechanism of forces as in the case of globular metal transfer. Due to the inert.characteristics of the argon shield, the spray metal transfer can be employed to weld almost any metal or alloy.

It is well known that the drop formation and detachment is largely due to the balance of the four forces applied on the liquid tip. These are the forces due to surface tension, gravitation, magnetic pinch and plasma drag [Lancaster (1984)[97]].

Theoretical predictions of metal transfer achieved the limited success. The pinch instability theory provides a possible mechanism to explain metal transfer for currents above the threshold for spray transfer. It is based on the principle that the electrode has a cylindrical liquid tip before the droplet detaches. The static force balance theory assumes that retaining surface tension force is in balance with the detaching forces, which is the sum of the forces due to gravity, magnetic pinch and plasma drag, just before the detachment. This theory can predict the trend of metal transfer in the globular and spray transfer modes as tapering is allowed for, while a generally larger size is predicted comparing with experimental results. However, none of the existing theories can satisfactorily explain the metal transfer process in GMAW, and further improvement of metal transfer theory is necessary.

2.2.2 Automatic Versus Automated Welding

Welding automation reduces manpower requirements, producing consistent uniform welds, maintaining production schedules and decreasing the cost of parts welded. The major disadvantages are however the high initial cost of the welding machine involved and the need to keep automatic equipment occupied continuously [Mckee (1982)[121]].

Automatic and automated welding have many similarities, but there are major differences [Cary (1979)[19]]. Automatic welding involves carefully the dedicated fixating with tooling, work holding devices and accurate part location and orientation. It also requires detailed welding arc movement devices with predetermined sequences of welding process parameter changes and the use of limit switches or timers to form the weld joints. The automatic welding is currently employed in high volume production industries where the cost of equipment is justified by the large number of pieces to be made. The automated welding provides the same time saving and precision welding, yet it can only be applied to small-lot production and to production

of a single part. Furthermore, it has quick change capability and can adapt products without the necessity of redesigning and reworking the expensive fixtures.

The arc motion device is capable of moving in three directions; longitudinal, transverse and vertical. Extra welding positions can be obtained by mounting the workpiece on a positioner that rotates and tilts (if required). Full control is then achieved when the arc travel in all directions is accomplished within the range of the equipment and, adjustments to the welding process parameters are made during welding process. Process control is available for each part, and is employed for correctly welding the part. It only demands a positive locating point to align the robot welding torch with the part being welded and then utilising a microcomputer/controller to program it accordingly. A computer controller is employed to change welding process parameters during the welding operations if required [Cook (1981)[37]]

2.2.3 Requirement of the Automated and/or Robotic Welding System

The automated and/or robotic welding system is capable of manipulating either or both the torch and the workpiece to achieve a satisfactory weld. The mechanical structure of the robot which manipulates the torch must have the necessary working volume mobility to access all the weld points without colliding with the workpiece while maintaining the appropriate attitude of the torch relative to the seam. The manipulator must also be suitable for carrying out weave patterns and meeting various demands such as positional accuracy, repetability and travel speed [Miller (1987)[123]]. Jigs and fixtures should be controlled so that a wide range of parts can be accommodated with minimum set-up and change-over time. Nevertheless, even if the manipulator positioning system is pre-programmed for the weld sequence, and one has the completed fixtures which would ensure repetability of component placement, satisfactory and adequate welding would not be secured because the workpiece and

dimensional tolerance variations are prerequisite in the welding [Marburger (1990)[113]].

An automated and/or robotic welding system, capable of detecting and making up for such variations in the working surroundings, must consider joint tracking and welding sensing. Welding quality can be achieved by the meeting of the quality requirements such as welding bead geometry and porosity inclusions, and controlled by sensing either directly or indirectly the various welding process variables involved in the process.

Welding process parameters for the arc welding should be well established and categorised for the automated and/or robotic welding system. Electrode type and shielding methods are usually the basic considerations, and are dictated by the required weldment mechanical properties. Electrode size is related to weld joint geometry, the arc current is recommended for a particular job and the number of passes. Electrode polarity is initially established and based on whether maximum penetration or maximum deposition rate is required [Jackon (1960)[73]]. Weld pool shape and magnitudes depend on the heat input involved which in turn, relies upon welding process parameters. Arc current and welding speed dominate the weld bead penetration for single pass welds . The selection of arc current and welding speed are based on electrode size. Furthermore, welding voltage dominates the weld bead width and has an influence on the weld bead penetration since it controls the arc shape [Apps et al. (1963)[6]].

It can be clearly evident that the close control of the above mentioned interrelated welding process parameters should be applied for a form of monitoring and feedback into the process in order to achieve a full automation of welding.

2.3 PROCEDURE OPTIMISATION FOR WELD BEAD GEOMETRY

2.3.1 Overview of the Procedure Optimisation

With the advance of the automated and/or robotic welding process, procedure optimisation which selects the welding procedure and predicts weld bead geometry that will be deposited is increased. A major concern involving procedure optimisation should define a welding procedure which can be shown to be the best with respect to some standard and chosen combination of welding process parameters which give an acceptable balance between production rate and the scope of defects for a given situation [Mcglone (1982)[120]].

Typical welding procedures can be established by making a record of all the variables, defining a critical range, and specifying desired parameter values. In general, it will be classified into three categories [Cary (1979)[19]];

(1) A written description.

(2) A drawings of the weld joint design and the conditions for making each pass or bead.

(3) A record of the test results of the resulting weld.

Weld bead geometry depends on the amount and distribution of the input energy on the workpiece surface [Heiple and Roper (1990)[67]]. In the GMAW process, heat and mass inputs are coupled and offered by the welding arc to weld pools and by the molten metal which is being transferred to weld pools. The amount and distribution of the input energy are basically controlled by the distinct and cautious choice of welding process parameters to achieve the optimal weld bead geometry and the desired mechanical properties of the weldment.

2.3.2 Welding Process Parameters and Weld Bead Geometry

The factors which could be considered procedure optimisation are the equipment and labour availability, machine shop capability and workshop loading, as well as the effect of procedure change on joint preparation, inspection techniques, metallurgical quality and mechanical properties. Drayton (1972)[47] first identified twelve significant welding process parameters for Submerged Arc Welding (SAW) and classified them into four groups: preset; background; secondary; and primary variables. Preset variables decided in a early stage of the procedure development, may include material composition and thickness, weld type and weld properties. Background variables specified at the early stage of production, could contain the welding process, equipment type, consumable type and general edge preparation. Secondary variables cover the contact tip to the workpiece distance and electrode angle. Also, primary variables which usually have a major effect on the quality of the product and output rate, include welding speed, welding voltage and arc current.

For synergic pulse MIG welding process, Kumar and Parmar (1986)[96] put in two groups as follows;

(1) Primary variables - pulse current, pulse time, wire feed rate, welding speed, feed wire diameter and shielding gas composition.

(2) Secondary variables - background current level and time period, mean current, volt-ampere ratio, shielding gas flow rate, torch angle, electrode polarity, preheating condition, burn back, rise time, short circuit detect, inductance level, short-circuit current, arc length and electrode stickout.

Typically, the weld process parameters for the GMAW process that affect weld bead geometry and overall weld quality have been classified into three categories: primary adjustable; second adjustable and preselected parameters [Hobart (1964)[69]]. Second adjustable and preselected parameters are considered to be fixed, whereas primary

adjustable parameters such as welding voltage, arc current and welding speed can be altered during the GMAW process.

Primary adjustable parameters affect such output variables as welding bead geometry, deposition rate and weld soundness. The available parameters in this category will include welding voltage, arc current and welding speed. Second adjustable parameters are generally more difficult to measure, and do not directly affect weld bead geometry. Instead, these parameters generally cause a change in primary adjustable parameters based on a desired change in weld bead geometry. Variables in this category are covered wire stickout and nozzle angle. Preselected parameters are considered as factors which can only be changed in large intervals and are unfavourable as control. The parameters could also contain wire size, wire type, gas flow rate, materiel composition and material thickness.

The weld bead geometry is obtained as a result of the solidification of the liquid pool. Weld bead dimensions are generally specified with the weld bead width at the level of the plate surface, the depth below the surface to which the bead has penetrated and the height of the reinforcement dimension [Jones (1976)[76]]. These quantities can not only determine the basic mechanical properties of the weld, but also ensure the basic stress handling capabilities of the joint.

2.3.3 Research Efforts in Procedure Optimisation

Table 2.1 (a) - (d) summarises some of the important developments for procedure optimisation. Many efforts have been made to understand and to assess the effects of welding process parameters on optimal weld bead geometry.

An earlier attempt to procedure optimisation, called a tolerance box, was developed to preserve all the compiled information, to allow a rigorous determination of the effects

on the quality of any modification of the welding process parameters, and to offer a well-informed choice of the welding process parameters in terms of the constraints imposed by the production process [Jones (1976)[76] and Chandel and Bala (1986)[22]]. Nevertheless, this approach required a large number of tests and was found to be impractical for process control purposes when dealing with more than three welding process parameters.

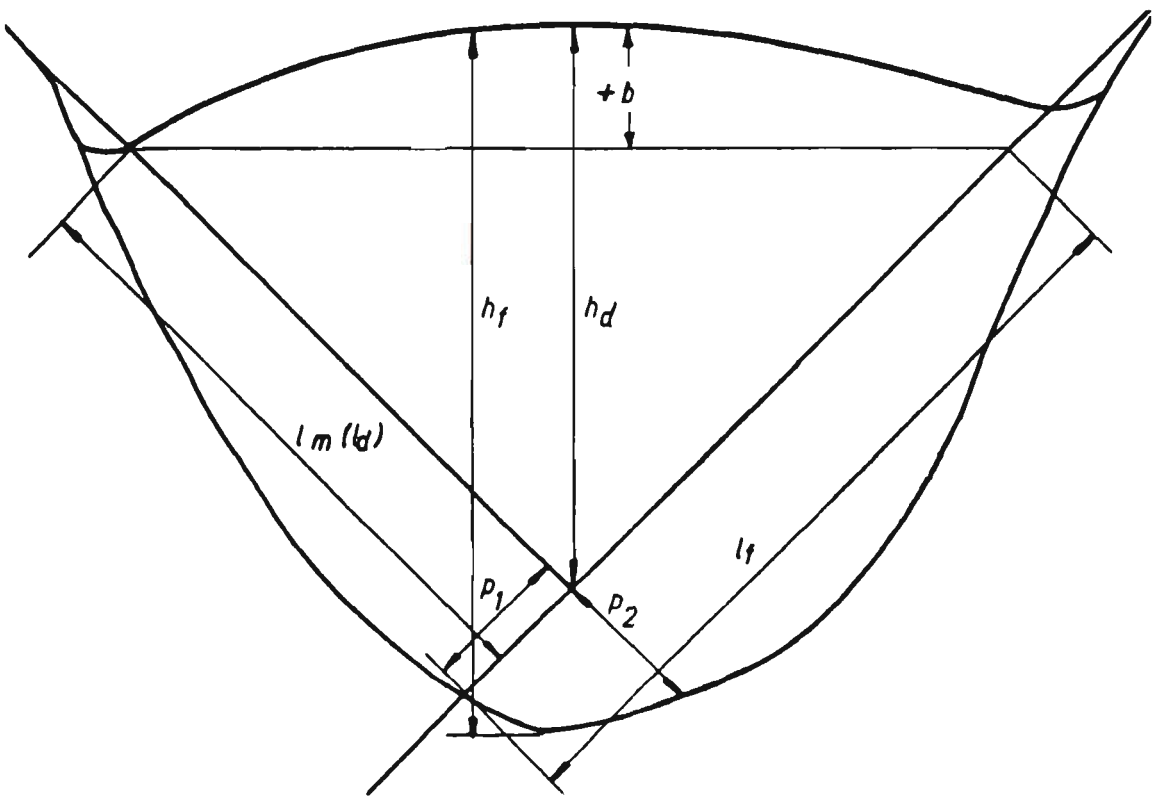

b convexity, concavity
h_d deposited metal height
h_f fused metal height
l_d deposited metal leg length
l_f fused metal leg length
l_m leg length
p penetration (p_1, p_2)]

Figure 2.1 Definition of dimensions for MIG welding with flux cored wires [Doherty (1978)[45]].

Rosenthal (1941)[156]
- an analytical mathematical equations for the arc welding

Apps et al. (1963)[6]
- the effects of six welding variables upon the shape and size of the weld bead geometry (bead width, penetration, reinforcement and the cross-sectional area)

Christensen et al. (1965)[36]
- deducing a dimensionless factor to relate temperature distribution to selected weld bead dimensions

Drayton (1972)[47]
- investigating relationships between weld bead geometry and welding process parameters for SAW
- studying the effects of arc current, current type and polarity, welding voltage and flux composition on weld bead dimensions

Jones (1976)[76]
- using tolerance box technique for SAW of close butted two pass square edge joints in 12.7 mm steel using a range of electrode and fluxes
- giving basic information regarding process capacities with existing equipment and data

Doherty and McGlone (1977)[44]
- testing the precision and accuracy of the formulae for close edge square butt SAW of mild steel plate
- mathematical relationships as a compact and flexible method of storing the necessary welding data within the computer memory

McGlone (1978)[117]
- investigating the effects of prepartion angle and depth for V close butt preparations for SAW

Table 2.1 (a) Procedure optimisation for weld bead geometry

McGlone and Chadwick (1978)[118]
- Prediction of weld bead geometry from welding process parameters
- Procedural selection of two-pass and multi-pass butt welding using an interactive predictive computer program

Thorn et al. (1982)[178]
- studying interaction of variables and their effects on weld pool dimensions for the GMAW

Doherty et al. (1978)[45]
- studying a range of procedures for flat position fillet welds made by the flux cored MIG process

Murti and Sundaresan (1983)[126]
- optimization of friction weldingparameters employed three dissimilar metal combinations

Salter and Doherty (1981)[158]
- development of an experimental and analytical technique for the selection of welding procedure

McGlone (1982)[120]
- review of procedure optimisation for SAW during the past decade

Quintino and Allum (1984)[146]
- the effects and interactions for some of the possible variables in pulsed GMAW of mild steel
- emphasizing how wire size and shield gas composition affect bead and deposition characteristics

Table 2.1 (b) Procedure optimisation for weld bead geometry

Allum and Quintino (1985)[3]
- the effects of altering mean current and welding speed on fusion characteristics of pulsed MIG welding
- a simple model for predicting fusion characteristics in pulsed current MIG welding

Kumar and Parmar (1986)[96]
- mathematical model for pulse mode on Synergic MIG welding power source

Galopin and Boridy (1986)[54]
- design of a Computer Assisted Experimentation System (CAES) to optimise welding procedure selection

Chandel and Bala (1986)[22]
- the effects of SAW parameters (current, voltage, wire diameter, electrical stickout, heat input and polarity) and groove angles on the soundness of roots bead
- observation of center-line cracking and lack of penetration

Raveendra and Parmar (1987)[150]
- mathematical models to predict weld bead geometry and shape relationships for CO_2 shielded flux cored arc welding
- welding process parameters (arc current,welding voltage, welding speed, nozzle to plate distance, gun angle)

Chandel et al. (1987)[23]
- the effect of submerged arc process variables on the penetration studied
- mathematical equation correlating penetration and welding process variables

Table 2.1 (c) Procedure optimisation for weld bead geometry

Chandel (1988)[24]
- relationships between welding process variables and weld bead geometry of bead-on-plate welds deposited by GMAW
- mathematical models to correlate the weld features with the process variables

Pandey and Parmar (1989)[138]
- the effects of wire feed arte, arc voltage, nozzle to plate distance, welding speed, touch angle and gas flow rate in MIG welding of aluminium alloy 5083

Yang et al. (1992)[190]
- the effects of welding process variables on the bead height of submerged-arc weld deposits

Liu et al. (1993)[104]
- the effects of welding process variables on pulsed Nd:YAG laser spot welds in AISI 409 stainless and AA 1100 Aluminum

Yang et al. (1993)[191]
- the effects of welding process variables on the weld deposit area of submerged arc welds

Kim et al. (1994)[79]
- comparing experimental results to outputs obtained using existing formulae
- finding the best mathematical model for automated welding process

Kim and Basu (1994)[80]
- studying the relationship between welding process parameters and welding bead geometry
- development of mathematical models

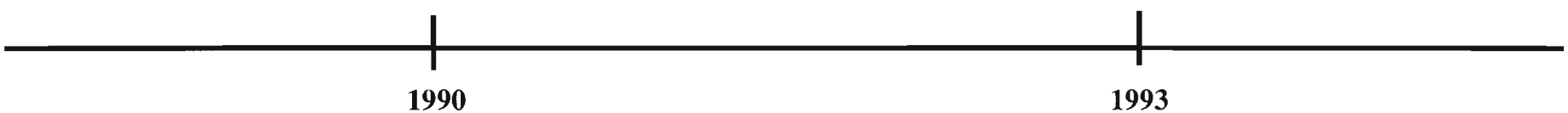

Table 2.1 (d) Procedure optimisation for weld bead geometry

Such a work published before 1978 was summarised by Shinoda and Doherty (1978)[163]. McGlone (1978)[117] and McGlone and Charwick (1978)[118] reported the mathematical analysis of the relationship between arc welding variables and weld bead geometry for SAW of square edge close butts. The SAW variables in those studies included arc current, welding voltage, welding speed, bevel angle and electrode diameters. Similar mathematical relationship between arc welding variables and fillet weld geometry shown in figure 2.1 for the GMAW using flux-cored wire has also been reported [Doherty et al. (1978)[45]].

The situation has been altered recently with the advent of increasing computer efficiency and better understanding of the usefulness of statistically designed experimentation based on factorial techniques [Galopin and Boridy (1986)[54]] which can reduce cost and provide the required information about the main and the interaction effects on the response factors. Such techniques for establishing relationships between welding process parameters and weld bead geometry have been reported for the arc welding in order to accomplish control over arc behaviour for fully mechanised and automatic welding [McGlone (1980)[119]].

Raveendra and Parmar (1987)[150] presented a mathematical model for predicting weld bead geometry and shape for CO_2 shielded flux cored arc welding as functions of welding voltage, arc current, welding speed, nozzle to plate distance and gun angle by using fractional factorial techniques and a multiple regression technique.

The experimental results have shown that a mathematical model can be an effective tool for prediction of weld bead geometry, and useful to predict the values of control variables for achieving a desired weld bead profile. Similar mathematical models relating welding process variables and weld bead geometry for the selection and control of the procedural variables have also been reported [Kumar and Parmar (1986)[96], Salter and Doherty (1981)[158], Thorn et al. (1982)[178], Murti and

Sundaresan (1983)[126], Quintino and Allum (1984)[146], Allum and Quintino (1985)[4], Chandel et al. (1987)[23] and Pandey and Parmar (1989)[138].

Chandel (1988)[24] first applied this technique to the GMAW process and investigated the relationship between process variables and weld bead geometry of bead-on-plate welds deposited by the GMAW process. These results showed that arc current has the greatest influence on weld bead geometry, and that mathematical models derived from experimental results can be used to predict weld bead geometry accurately.

Also, Yang et al. (1992)[190] carried out an experiment to determine the effects of the various process variables on the weld bead height for the SAW process. It was found that weld bead height is affected by the electrode polarity, electrode diameter, electrode extension, welding current, welding voltage and welding speed. A negative electrode polarity, a small electrode diameter, a large electrode extension, a high arc current or welding speed and a small welding voltage encourage a large weld bead height. Regression equations were represented for computing weld bead height from the welding parameters, using both linear and curvilinear multiple regression analysis techniques.

Recently, Liu et al. (1993)[104] examined experimentally the weld abilities of AA 1100 aluminium and AISI 409 stainless steel by the pulsed Nd:YAG laser welding process. The effects of Nd:YAG laser welding parameters (laser pulse time and power intensity) and material dependent variables (absorptivity and thermophysical properties) on laser spot-weld characteristics, such as weld diameter, penetration, melt rate, melting ratio, porosity and surface cratering have been studied. The experimental results showed that weld bead geometry was found to be influenced mostly by the power intensity of the laser beam and to lesser extent by the pulse duration.

Yang et al. (1993)[191] first extended their study to the weld deposit area and presented the effects of electrode polarity, extension, electrode diameter, arc current, welding voltage, travel speed, power source characteristics and flux basicity on the weld deposit area. The results of their experiment indicated that a small-diameter electrode, long electrode extension, low voltage and high welding speed produce a large deposit area, whereas the power source and flux type do not seem to have any significant effect on the weld deposit area.

2.4 HEAT AND FLUID FLOW IN WELD POOLS

Over the last few years, there has been a growing interest in quantitative representation of heat transfer and fluid flow phenomena in weld pools in order to relate the processing conditions to the quality of the weldment produced and to use this information for the optimisation and robotization of the welding process [Szekely (1989)[171]]. Normally, a theoretical model offers a powerful alternative to check out the physical concepts of the welding process, to estimate the important input parameters and to finally calculate the effects of varying any of the parameters. It is inevitable to the development of mathematical equations for heat transfer and fluid flow in weld pools to correlate the mechanical properties of the final welded structure to the welding process parameters and to understand the effects of welding process variables on weld bead geometry.

2.4.1 The Principle Driving Forces

Generally, the arc welding process is very complicated due to not only the steep changes in the physical, chemical and mechanical properties, but also phase changes in a small weld pool region. A detailed knowledge of the temperature field and thermally induced flow in weld pools is important to understand the phenomena and to develop

the improved welding techniques. Therefore, the effort of developing a theoretical model is very valuable and necessary work.

A number of studies [Heiple and Roper (1981)[65], Oreper et al. (1983)[133], Lin and Eagar (1986)[103] and Kou and Wang (1986)[85]] have represented that weld pool convection, defining the heat transfer and position of isotherms within the molten metal, can strongly affect the structure and properties of the resultant weld as well as the determination of weld pool dimensions and its associated solidification phenomena. The characteristics of weld pools affected include surface smoothness, weld pool dimensions, fume formation, macro-segregation, grain structure and gas porosity of weld bead geometry. A complete understanding of weld characteristics caused by heat transfer and fluid flow is essential to welding technology [Lancaster (1984)[97]].

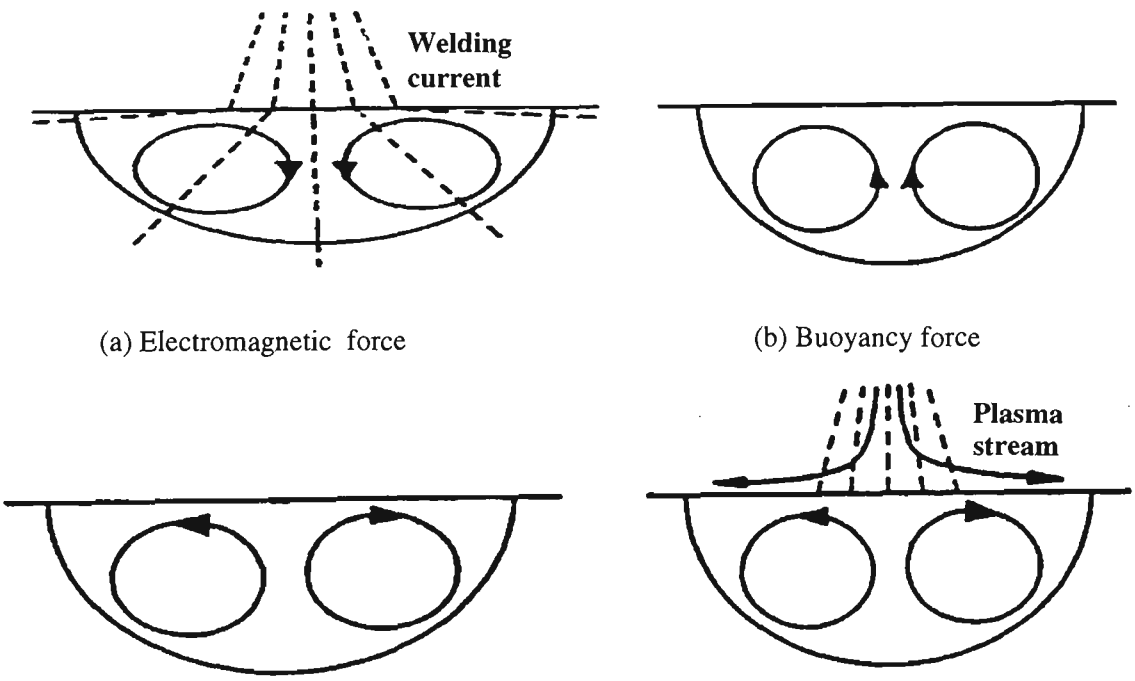

(a) Electromagnetic force (b) Buoyancy force

(c) Surface tension (d) Plasma drag force

Figure 2.2 Schematic flow profile produced by the four driving forces in weld pools.

To develop a theoretical model of heat transfer and fluid flow in weld pools, one of the most important things is to carefully examine what kind of forces are related to fluid flow in a puddle. The principal driving forces controlling weld pool convection have been identified as electromagnetic, buoyancy, surface tension and plasma drag forces [Oreper and Szekely (1984)[134]]. The former two forces are body forces which act inside weld pools, while the latter two forces are shear stresses which react on the weld pool surface. Each of these forces yields a different degree of convection and at different locations in weld pools, thus resulting in different weld bead dimensions.

Electromagnetic force is caused by the interaction between the divergent current flux from the electrode and magnetic field induced within the molten metal. Figure 2.2 (a) shows the flow pattern due to electromagnetic force ($\bar{J} \times \bar{B}$) which is the Lorentz body force.

Buoyancy force shown in figure 2.2 (b) is caused by the temperature dependence of density. The lighter liquid temperature region will ascend, but the heavier liquid at the low temperature region will submerge as weld pools are formed by the welding arc. The effect of buoyancy can be included as a distributed body force depending on temperature by means of the well known Boussinesq approximation.

The surface tension force is caused by the gradient of surface tension on weld pools due to the temperature distribution. Depending on the welding conditions and presence of impurities, the surface tension force may be inwardly or outwardly directed [Walsh and Savage (1982)[186]]. The flow pattern driven by surface tension force is schematically shown in figure 2.2 (c).

Plasma drag force is caused by the plasma jet or gas generated by decomposition of electrode coating [Kim and Na (1992)[82]]. The flow pattern driven by plasma drag

force is schematically presented in figure 2.2 (d). In summary, the principle driving forces can affect the flow field and thus weld bead geometry. It seems evident that the mathematical model, which is capable of accurate prediction of the effects of various welding parameters on welding bead dimensions, would be valuable for the development of welding procedures for automated and/or robotic applications.

2.4.2 Difficulties in Weld Pool Experiments

Generally experimental measurements of flow velocity and temperature distribution in the small, intensely heated weld pool are extremely difficult and complicated due to the presence of the welding arc over the weld surface. Also, the interactive nature of the entire welding process makes it difficult to determine the relative importance of each input parameter in affecting weld quality and productivity.

Studies of weld pools normally include surface temperature measurement [Schauer et al. (1978)[161], Geidt et al. (1984)[55], Tsai et al. (1991)[180] and Kraus (1989)[93]], surface profile shape and pressure [Lin and Eagar (1985)[101]], and arc force [Burleigh and Eagar (1983)[15] and Lin and Eagar (1986)[103]]. Apart from the studies of Kraus (1988)[92] which employed an optical spectral radiometric/laser reflectance method for high resolution of weld pool surface temperature measurements, most of the measurements entail a high degree of uncertainty because of the difficult and tedious experimental work involved in observing the welding process. Even if the experimental research involves substantial trials and errors to get a reproducible results, useful insights and trends can be obtained from such experimental studies.

However, theoretical studies based on mathematical models provide an opportunity to study the significance of heat and fluid flow as well as to understand the complex phenomena that occurred during the welding. The fundamental understanding of the interactive nature of welding process parameters can be established through methodical

and parametric analyses of the various driving forces over a range of welding conditions.

2.4.3 Research Efforts in Weld Pools

Table 2.2 (a) - (f) presents primarily the state of modelling efforts for weld pools and emphasises the advances made rather than discusses the merits and demerits of each case. A discussion of the overall direction performed by a number of researchers will also be given. Attempts at the mathematical representation of transport phenomena in the welding process date back to the 1940s. Solutions to the heat conduction equation could be found in the classical works of Rosenthal (1941)[156], Wells (1952)[188], Grosh and Trabant (1956)[60], Rykalin et al. (1960)[157] and Christensen et al. (1965)[36], and to large extent in Carslaw and Jaegar (1959)[18].

The advent of the computer age allowed the gradual introduction of numerical techniques for the welding process. The initial efforts, up to the early 1980s involved heat conduction studies, which provided a significantly improved insight into the transient temperature distributions in weldment [Myers et al. (1967)[127], Pavelic et al. (1969)[145], Hibbit and Marcal (1973)[68], Paley and Hibbert (1975)[137], Friedman (1978)[53] and Krutz and Segerlind (1978)[94]]. Lancaster (1984)[97] has a very good collection of welding pool modelling papers prior to 1980 which discuss some of the analytical solution of both linear and non-linear momentum equations from 1934. Pavelic et al. (1969)[145] showed that their mathematical model provided good predictions of the peak temperatures in the Heat Affected Zone (HAZ) within 10% of experimentally measured values. Weld pool width and length predicted by line source theory also plot parallel to the experimental results even if it did not exactly agree with experimental data.

Rosenthal (1941)[156]
- Analytical solution to point, line, and plane source
- Latent heat source neglected

Wells (1952)[188]
- implicit relationship for the maximum weld puddle width

Grosh and Trabant (1956)[60]
- temperature-dependent thermal diffusion
- Excellent agreement between experimental and analytical studies

Carslaw and Jaegar (1959)[18]
- Conduction heat transfer

Rykalin et al. (1960)[157]
- Conduction heat transfer (Analytical)

Christensen et al. (1965)[36]
- Conduction heat transfer

Myers et al. (1967)[127]
- summarise of 2D and 3D analytical theories and techniques

Pavelic et al. (1969)[145]
- a finite difference computer program for GTAW
- a radically symmetric Gaussian heat flux distribution from a welding arc

Table 2.2 (a) Heat and fluid flow in weld pools

Shercliff (1970)[162]
- semi-infinite inviscid fluid with point source
- posing singularity at axis of symmetry

Woods and Milner (1971)[189]
- A study of motion in weld pools inthe arc welding

Hibbit and Marcal (1973)[68]
- Finite element method
- a trapezoridal distributed heat source used
- including the latent heat, soild-liquid phase change, surface convection, and radiation for GMAW

Paley and Hibbert (1975)[137]
- 2D steady state model
- neglecting heat losses to the surroundings

Friedman (1975)[51]
- Gaussian heat flux model
- a thermo-mechanical FEM computer programme for GTAW

Sozou and Pickering (1976)[169]
- point source at centre of finite hemisphere
- employing free slip at free surface rather than fixed velocity

Krutz and segerlind (1978)[94]
- 2D heat flow model for predicting the strength of a weld joint via the metallurgical viewpoint

Andrews and Crane (1978)[5]
- flow in hemisphere with distributed current source
- actually point source located a few above source
- direction of flow depended on location of current source

Atthey (1980)[7]
- isothermal MHD flow in hemispherical pool
- distributed current source with inertia terms

Table 2.2 (b) Heat and fluid flow in weld pools

Oreper et al. (1983)[133]
- 2D steady convection flows with (buoyancy, MHD, Marangoni) in spot GTAW
- predefined pool shape and distributed source

Yokoya and Matsunawa (1983)[192]
- 2D combined continuity momentum/energy equations in semi-cylindrical pool with cylindrical hear source

Kou and Le (1983)[83]
- 3D finite difference technique for a moving heat source

Oreper and Szekely (1984)[134]
- 2D transient convective spot GTAW with calculated pool shape for normal and cathode spot mode current and heat fluxes

Chan et al. (1984)[20]
- 2D transient laser weld with line source and calculated pool shape (free surface assumed flat)

Goldak et al. (1984)[56]
- 2D finite element model
- a double ellipsoid power distribution proposed

Kou and Sun (1985)[84]
- 2D steady state spot GTAW with calculated pool shape
- distributed heat and current sources

Wei and Geidt (1985)[187]
- 2D steady state EBW (analytical) with keyhole

Kovitay and Lowke (1985)[87]
- 2D spot GTAW with predefined pool shape

Table 2.2 (c) Heat and fluid flow in weld pools

Oreper et al. (1986)[135]
- 2D transient weld pool development (melting and freezing) for Al, Ti, Steel

Correa and Sundell (1986)[40]
- 2D steady-state spot GTAW with predefined pool shape (uniform heat source)

Kou and Wang (1986)[86]
- 3D quasi-steady moving GTAW
- distributed heat and current sources (free surface assumed flat)

Paul and Debroy (1986)[143]
- 2D steady state LW (turbulence in increased viscosity)

Chan et al. (1986)[21]
- 3D quasi-steady LW (analytical and numerical)
- free surface assumed flat with line source
- assumed scanning speed pool characteristic velocity

Goldak et al. (1986)[57]
- review of methods, models, and software for development of mathematical model in welds

Kovitya et al. (1986)[89]
- 3D heat flow equation in a moving plate with a constant velocity

Davis et al. (1986)[41]
- 2D models of the flow of the molten metal around the keyhole in LB welding

Choi et al. (1987)[29]
- applied alloy and pure metals
- the effects of conduction, solid-liquid phase change, liquid-vapor phase change, and radiation

Oreper and Szekely (1987)[136]
- 2D transient solidification in spot GTAW

Table 2.2 (d) Heat and fluid flow in weld pools

Tekriwal and Mazumder (1988)[174]
- 3D finite element analysis
- conduction heat transfer
- Gaussian heat input with no vaporisation

Tsao and Wu (1988)[184]
- 2D GMAW spot welding
- finger penetration observed in GMAW
- metal spray in GMAW modelled via thermal energy exchange

Zacharia et al. (1988)[195]
- 3D transient spot and moving GTAW/GMAW
- deformable free surface and T-joint

Tsai and Kou (1988)[181]
- an orthogonal curvilinear coordinates in solving a free surface problems

Zacharia et al. (1989)[198]
- 3D transient model for spot/moving GTAW
- free surface deformable (prescribed heat and current sources)

Pardo and Weckman (1989)[140]
- 3D steady state thermal model
- calculation of weld width and reinforcement height

Zacharia et al. (1989)[196]
- 2D stationary GTAW/LW
- prescribed heat and current sources
- compared numerical and experimental results

Thompson and Szekely (1989)[177]
- 2D transient spot GTAW with a pre-deformed surface
- effect of Lorentz force excluded

Mclay and Carey (1989)[122]
- coupled heat transfer and viscous flow in weld pools

Table 2.2 (e) Heat and fluid flow in weld pools

Matsunawa and Yokoya (1989)[115]
- 2D stationary state model for TIG welding
- including aerodynamic drag force

Lu and Kou (1989)[108]
- power and current distribution in GMAW

Choo et al. (1990)[31]
- addressed free surface behaviour (pool collapse)
- modelled heat and current fluxes for deformed pool surface
- semi-coupling of arc and weld pool

Tsai and Kou (1990)[182]
- electromagnetic-force-induced convection studied
- 2D steady state model

Ramanan and Korpela (1990)[148]
- a study on the influence of thermocapillary and Lorentz on the flow pattern in a stationary weld pool

Ule et al. (1990)[185]
- 3D transient temperature variation during GTAW
- employing the fourth-order Runge-Kutta technique

Zacharia et al. (1991)[199]
- effects of evaporation and temperature dependent material properties on weld pools

Choo and Szekely (1991)[32]
- The role of gas shear stress on Marangoni flows in arc welding

Choo et al. (1992)[35]
- combining a mathematical model of the welding arc and the weld pool for GTAW welding

Mundra et al. (1992)[125]
- studied role of thermophysical properties in weld pool modelling

Kamala and Goldak (1993)[77]
- a method for evaluating the error of 2D and 3D temperature fields

Table 2.2 (f) Heat and fluid flow in weld pools

However, since conduction and convection heat flow in weld pools can have a marked effect in determining the quality and productivity of resultant welds, the quantitative representation of heat transfer and fluid flow phenomena in weld pools is of considerable interest. Woods and Milner (1971)[189] demonstrated that the electromagnetic force in arc welding was caused the fluid flow which boosts the mixing of weld pools. By the late 1970s, it was understood that convective flow was due to primarily electromagnetic force. In the early 1980s, researchers [Heiple and Roper (1981)[65] and Oreper and Szekely (1984)[134]] showed that surface tension has an important effect on weld pool geometry. Heiple and Roper (1981)[65] carried out a series of experimental studies on minor element effects on the depth of penetration of stainless steel during the Gas Tungsten Arc Welding (GTAW) process and insisted that the surface active elements significantly changed the temperature coefficient of surface tension from negative to positive which resulted in enlarging the depth of penetration.

As experimental research into the heat transfer and fluid flow in weld pools is limited to the measurement of the surface velocity during the actual welding process, mathematical modelling has become an essential and practical tool for the analysis of the whole process that occurs during the arc welding. This modelling was pioneered by Sozou and Pickering (1976)[169], Andrews and Crane (1978)[5] and Atthey (1980)[7].

Furthermore, Oreper, et at. (1983)[133] calculated the steady-fluid flow in weld pools of a prescribed shape caused by the combined action of surface tension, electromagnetic and buoyancy forces. The accuracy of the numerical techniques and the solutions were not discussed. Chan et al. (1984)[20] developed a 2D fluid flow model for weld pools for laser welding. They carried out a parametric study for various materials and a variety of operating conditions. Kou and Wang (1986)[85] presented the results of a quasi-steady, three-dimensional (3D) computer model for the fluid flow and heat transfer conditions in weld pools for the GTAW process.

Generally, the weld pool convection is driven by four distinct driving forces viz. buoyancy, electromagnetic, surface tension and plasma drag forces [Oreper and Szekely (1984)[134]]. However, a number of previous researchers considered only the first three forces, but the plasma drag force was not included as a driving force for mathematical models [Oreper et al. (1983)[133], Yokoya and Matsunawa (1983)[192], Kou and Le (1983)[83], Chan et al. (1986)[21], Zachria et al. (1988)[193], Thompson and Szelely (1989)[177], Mclay and Carey (1989)[122], Matsunawa and Yokoya (1989)[115], Mahin et al. (1986)[110] and Tsai and Kou (1990)[182]]. Recently, Kim and Na (1992)[82] and Choo et al. (1992)[35] developed the mathematical model of the GTAW, not the GMAW, which took account of the four driving forces of convection and calculated the effect of individual force. The computed results showed that the most important force was the electromagnetic force, and the plasma drag force which worked on the weld pool surface, increased in proportion to the increase of weld pool surface area.

It is evident from table 2.2 (a) - (f) that there have been considerable advances in modelling the heat transfer and fluid flow in weld pools. Currently, the 2D and 3D modelling of spot and moving welds are possible. The results of these modelling studies have given useful insights into the nature of convective flow in weld pools.

Even if the situation has greatly altered with the advent of increasing computer efficiency and better understanding of the physics of welding, only two papers were found as showed by Tsao and Wu (1988)[184] and Kim and Na (1994)[81]. Tsao and Wu (1988)[184] first presented a mathematical model employing the vorticity stream function and implicit finite difference method, but ignored the flow induced by the droplet surface interactions and arbitrarily fixed the parameters of volumetric heat source. Kim and Na (1994)[81] developed 3D convection model for calculating the weld bead shape, velocity field and temperature distribution by employing a

boundary-fitted coordinate system. The heat source corresponding to the metal transfer was not discussed in detail.

In GMAW processes that the welding electrode is melted and the molten metal is transferred to the work piece, the interaction of the molten metal droplets and the weld pool surface is an additional important means of generating fluid flow within weld pools. Essers and Walter (1981)[48] measured the heat transferred to the workpiece by the arc and the heat contained in the transferring metal drops with a simple water-filled calorimeter and concluded that the metal transfer has an important effect on the welding bead width and penetration. Recently, Choo et al.(1992)[30] have studied the interaction between the molten metal droplets and weld pools with a flow visualisation technique and have shown that the dominant force which controls both the direction and intensity of the pool circulation is Marangoni flow due to the surface tension differences between the molten metal droplets and weld pools. This results contradicts the previous model [Tsao and Wu (1988)[184]] which treated the droplets purely as heat and momentum sources, but not included the flow induced by the droplet surface interactions.

The motivation for modelling the welding arc stems from the objective of providing boundary conditions for weld pools through fundamental transport equations. Normally, the welding arc has been modelled independent of weld pools and vice-verse. In the case of welding arc modelling, the anode (workpiece) is assumed to be a planer, isothermal surface. On the other hand, with the weld pool, some form of Gaussian heat and current flux distributions were permitted in certain studies, these do not include the active coupling of the welding arc. Such assumptions may be valid that the arc behaviour is not affected by surface shape changes. In addition, effect such as the arc length, gas mixtures, and tip angle cannot be modelled by these heat and current Gaussian sources which are usually functions of welding voltage, arc current and size of the plasma plume. Paul and Debroy (1988)[144] also considered similar

effect in laser welding using a simple conduction model for the laser plasma plume. They strongly pointed to the importance of a dynamic coupling of the heat and current sources with the workpiece.

Szekely (1989)[171] recommended the coupling of the welding arc and weld pools. Although his paper did not actually perform the coupling studies, he reported the consistency of the welding arc model relative to the weld pool model and vice-versa. There are of course other advantages made in the numerical solution of the weld pool besides the free surface but these can generally be classified as further refinement of the mathematical model to simulate what are previously established. In fact, much of the published weld pool modelling results have similar content describing the importance of convective flows in weld pools. Recently, Choo et al. (1992)[34-35] presented the free surface temperature of GTAW pools by combing a mathematical model of the welding arc and weld pools. The computed results were quite instructive, because they provided some new, unavailable insights into weld pool behaviour.

2.5 SENSING AND ADAPTIVE CONTROL FOR ARC WELDING

2.5.1 Sensing for Arc Welding

Since sensors have widely been employed in industries and engineering, the role of sensors has become more important with increasing demand for the automated and/or robotic welding systems where problem of a poor quality weld becomes apparent if the welding process parameters are not controlled. Sensors employed in the automated and/or robotic arc welding system must detect the changes in weld characteristics and produce the output that is in some way related to the change being detected [Hohn and Holmes (1986)[70]]. To be acceptable a weld must be positioned accurately with respect

to the joints, have good appearance, sufficient penetration and have low porosity and inclusion content.

During welding, the sensor is generally exposed to extreme heat, smoke, radiation, electrical noise, spatter and inertial force from the equipment to which it is attached, and detects work shape errors, setting errors, groove shape change, tack beads, welding heat distortion and jig error [Richardson (1986)[153]]. The requirements of a welding senor are normally universal, durable, reliable, compact, non-wearing and maintenance-free. There is today no welding sensor available that satisfies all of these demands because each sensor has a limitation either in its design or application to robots. This restriction may result in the need for more than one sensor in a totally automated and/or robotic arc welding system [Malin (1986)[111]].

2.5.2 Sensor Classification

A sensor is a device that converts one type of physical quantity into another type, usually electrical quantity. Figure 2.3 illustrates the possibility of placing sensors in a welding system configuration. Point 1 can be named an input sensor. This sensor which primarily consists of electrical and flow rate monitors can be employed to monitor input conditions such as arc current, welding voltage and shielding gas flow rate.

Point 2 can be labelled a direct sensor. This sensor is probably the most important sensor in the automatic and/or robotic welding system. The sensor will provide information for control of welding operations. Weld pool size, shape and temperature distribution are examples of characteristics that direct sensor would monitor. Also this sensor monitors the final stage in the process from which information can be fed back to compensate for variations. Typical sensors are acoustic, infrared, optical sensors and on-line radiography. Point 3 can be called an output sensor. This sensor

provides confirmation and a permanent record of the process controlled during the arc welding.

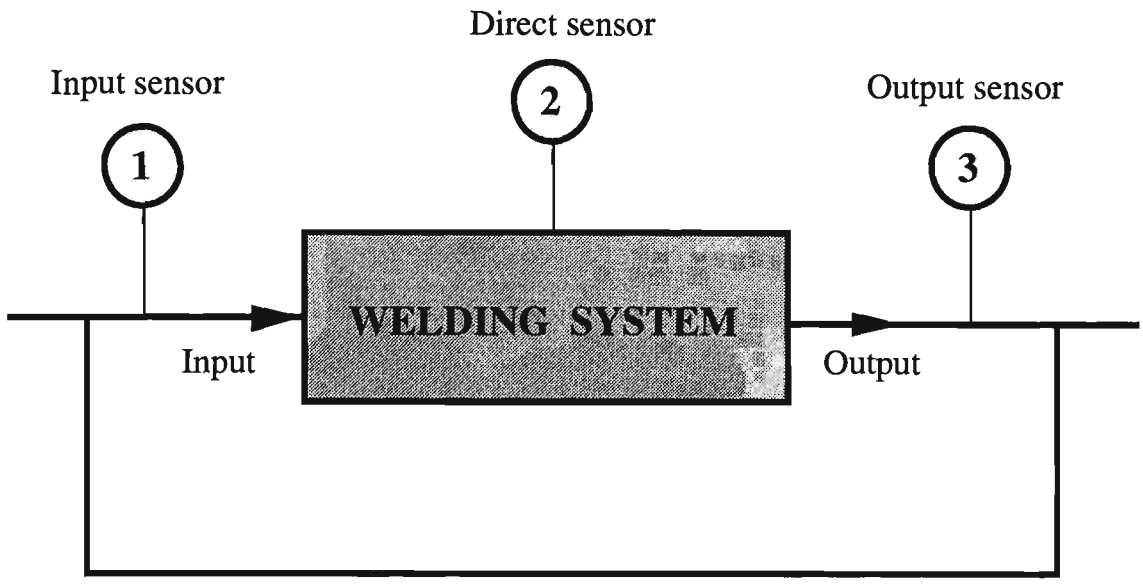

Figure 2.3 Sensors in a welding system.

There have been various techniques and sensors employed to control welding process. Sensors for adaptive control technologies can be classified with preview (optical, acoustic, ultrasonic and infrared sensing) and arc sensing, which are discussed below [Cook et al. (1989)[39]]. Table 2.3 shows applications, advantages and disadvantages of sensors used in arc welding.

2.5.2.1 Optical Sensing

Optical sensing technology has been employed and developed for a number of applications [Kraus (1988)[92], Boillet et al. (1985)[9], Hanright (1986)[61], Gonseth and Blanc (1983)[59], Agapakis et al. (1986)[2] and Deam (1989)[43]], for example, joint tracking, penetration control, arc length sensing and control, electrode extension in the GMAW, weld bead profile control and detection of surface contaminants. The main advantages of the optical sensing are non-contact operation and the ability to gain information from the spatial and spectral features of the optical output.

Table 2.3 Applications, advantages and disadvantages of sensors used in arc welding

Sensors		Applications	Advantages	Disadvantages
Preview sensing	Contact sensing	1. Joint preparation. 2. Part geometry. 3. Mechanical probes equipped with electronic sensing devices.	1. Low cost. 2. Simultaneous tracking and welding ability. 3. Universality of both welding process and weldment material type.	1. Not adaptable to suit a variety of joint geometries. 2. Probes cannot follow complex contours. 3. Contact sensors limit the welding speed.
	Non-contact sensing	1. The structured lighting/solid-state camera approach.	1. Sensing system is independent of the welding process. 2. Compensate for distortion during welding. 3. Tracking on ferrous and non-ferrous materials.	1. Sophisticated image processing is required. 2. Technology is relatively expensive, in comparison to other joint tracking alternatives.
Arc sensing		1. Automatic voltage control. 2. Vertical and lateral tracking and width control. 3. Detection of metal-transfer mode for GMAW process.	1. Relatively low cost. 2. Not affected by smoke, weld spatter, or the arc itself. 3. Ability to track and weld simultaneously. 4. Compensation corrections for heat distortion during welding.	1. Cannot track around sharp corners or turns. 2. All weld must include a weave. 3. Limited ability in the tracking of weld joints for nonferrous materials. 4. Heavy rust or mill scale will affect the joint tracking ability of the welding torch.

The optical sensing system was first investigated by Boillet et al. (1985)[9] for scanning the weld path. A fiber optic bundle was employed to transmit the infrared radiation from the surface in front of weld pools to the signal processing unit. The sensor head comprised a lens which produced an image of the fiber ends on the surface. This technique had an advantage over the infrared sensor since the lens itself was already in one unit with the torch, making it very versatile and requiring less working space. Kraus (1988)[92] employed the optical spectral radiometric/laser reflectance method to measure the pool surface temperature of SS 304, SS 316L and 8630 in the stationary GTAW.

One of the first real-time optical tracking systems was the coaxial viewing system which has been used for joint tracking and weld pool width control [Richardson et al. (1984)[152]]. In this technique, the image system is integrated into the welding torch. The point of welding is viewed coaxially with the welding electrode within the welding torch. Thus the bright core of the welding arc is blocked by the electrode /contact tip, and the entire weld area can be viewed without obstruction and distortion by the viewing angle. The system is non-intrusive and non-directional into the weld area.

2.5.2.2 Acoustic Sensing

There are various arc sounds which are characteristic of the different arc welding processes and standard procedures by which the arc sounds can be measured. A knowledge of the principles by which the welding arc produces the arc sounds, may enable researchers to control the sound levels. Various investigations have also been undertaken to correlate arc sounds to other welding characteristics. Most of these have attempted to correlate the Sound Pressure Level (SPL) to the arc characteristics such as

welding voltage, arc current and arc length [Roget et al. (1984)[155], Manz (1981)[112], Kaskinen and Mueller (1986)[78], Lewis and Dixon (1985)[100] and Jon (1985)[75]].

The acoustical emissions have been studied as a approach for real time location and characterisation of flow [Roget et al. (1984)[155]]. Also, the detection of the metal transfer mode and of the detachment of individual droplet have been employed for the automated and/or robotic welding process [Manz (1981)[112]]. The use of acoustical sensing for arc length control in the GTAW has been researched by Kaskinen and Mueller (1986)[78]. By pulsing the arc current at a rate to generate an audible tone at the welding arc, the intensity of the generated tone has been shown to be proportional to the arc length. This implies the availability of a feedback signal for arc length control. Lewis and Dixon (1985)[100] also studied a method to use acoustical emission as a method to plasma monitoring in laser beam welding. Their experiments have been aimed at studying the interrelation between the incident laser light, the plasma formation and the target material during the pulse welding with a Nd: YAG laser. A similar study was carried out by Jon (1985)[75].

2.5.2.3 Ultrasonic Sensing

Ultrasonic sensing techniques which employed both longitudinal and shear waves, have been applied to detect weld pool dimensions during the welding [Lott (1984)[106] and Hardt and Katz (1984)[62]]. Lott (1984)[106] developed a computer program to determine the source of the reflected signals and to calculate the effect of temperature gradient on the longitudinal ultrasound transmission near weld pools. The change in sound speed with temperature has two effects;

(1) Calculating the distance to the interface producing the echoes.

(2) Refracting of the sound waves in the large temperature gradient near weld pools where the sound speed changes rapidly [Carlson and Johnson (1988)[16]].

The work was then extended developing a weld inspection system that employed ultrasound to detect discontinuity in a partially completed weld [Carlson et al. (1990)[17]]. The use of ultrasonic sensing for sidewall penetration was reported by Carlson and Johnson (1988)[16] and Siores (1988)[165] who reported on the use of ultrasonics for real time monitoring and control during the SAW process. Fenn (1985)[49] has also carried out the use of ultrasonic sensing during the arc welding.

The use of ultrasonic sensing based on a shear wave technique has the potential to detect weld pool geometry in real time, and thus can be employed as a feedback signal for the control of uniform sidewall penetration. One problem which has been addressed by the researchers is that the use of piezoelectric transducers and couplant presents the potential for contamination of the weld by the coupling medium. To be useful in realistic production systems, a technique must be developed for introducing ultrasound and receiving it with non-contact sensors.

Silk (1984)[164] proposed the use of lasers for both the transmitting and receiving of ultrasound. To use lasers, a different mechanism must therefore be employed for detecting the ultrasonic energy. One of the most useful approaches to the detection of elastic waves is through the use of optical techniques specifically laser interferometry [Oreb (1990)[132]]. However, this type of highly sensitive ultrasonic reception technique in the welding environment is not viable. This approach has been reported by Carlson and Johnson (1988)[16] who incorporated laser sound generation and an Electromagnetic Acoustic Transducer (EMAT) [Maxfield et al. (1987)[116]] for ultrasound reception. Also, Fortunko and Schramm (1982)[50] studied the ability of EMAT's for ultrasonic non-destructive evaluation of butt welds.

2.5.2.4 Infrared Sensing

Infrared sensing, inherent attraction for the welding process, has had successful applications for the automated and/or robotic weld control. Infrared thermography is capable of monitoring the plate temperature distribution, which provides information for seam tracking, identification of plate geometry faults, penetration control, contamination and microstructure formation. Typical output parameters which have been investigated are cooling rate, discontinuity sensing, weld depth of penetration, contamination, seam tracking and weld pool geometry.

Ramsey et al. (1963)[149] investigated infrared thermography as a means of monitoring radiation, which is a function of both temperature and emissivity on the surface of aluminium weldment in close proximity to the welding arc. Results showed that correlation exists between the signal output and the arc welding parameters relating the control of the weld quality with heat flow patterns in the plate being welded. Infrared thermography was also employed by Lukens and Morris (1982)[109] to evaluate the weld metal cooling rates and to correlate the infrared emission intensity measurements to temperature using embedded thermocouples. Experimental results showed that the infrared radiation from the welding arc did not interfere with weld metal cooling rate and that the surface emissivity of the material would have a considerable effect on temperature.

Chin et al. (1983)[28] used the infrared thermography for sensing the arc welding process and monitored temperature distribution of the weld pool surface in order to detect variations in the welded part. Measurements were taken to determine the effect of arc current on the temperature profiles. They concluded that decreasing the arc current by 1/3 from the value required for penetration led to a decrease by 1/4 in both penetration depth and radius of the measured isotherm on the surface. Chen and Chin (1990)[26] related the surface temperature distribution to the depth of joint penetration

and weld bead width, then compared the metallographic measurement of depth of penetration and bead width with the area, magnitude and gradients of the thermal profile.

Nagarajan et al. (1989)[129] have reported on the application of infrared thermography to real time weld process monitoring. Seam tracking was obtained through using isotherm radii around the point of welding to identify the arc position relative to the joint. Weld depth of penetration control was obtained through monitoring the minor axis and ellipse isotherms which were shown to be the most sensitive variables to study the change due to variations into joint penetration depth and thickness of the plate being welded.

2.5.2.5 Arc Sensing

Arc sensing, also called through-the-arc sensing, is the most common model of the joint tracking system incorporated into commercial robotic welding systems. The technique makes use of the welding electrode as a sensor to gather information regarding welding voltage and arc current in the welding joint. In operation, the welding torch is oscillated across the joint, and current changes are sensed by the welding electrode at the joint side walls. Deviations in the current value are monitored, and feedback signals are sent to the robot controller. This feedback is essentially the method by which the welding torch is centred within the joint. To control the torch height above the joint, a preselected voltage which represents the desire welding electrode extension is programmed into the robot controller. Welding voltage measured at the welding electrode was fed back to adjust the torch height [Hanright (1986)[61]].

Commercially available joint tracking systems of this type incorporate both joint guidance and height control [Agapakis et al. (1986)[2]]. These systems assure that the welding arc will stay in the root of the joint and maintain an optimum stand off distance. The systems are however limited by the quantity and quality of information that can be obtained from the arc signal [Richardson et al. (1984)[152]].

Remwick and Richardson (1983)[151] employed arc sensing to sense the GTA pool motion and proposed the concept of using the weld pool motion as a weld bead geometry sensing technique. This concept is based on the fluid dynamics of the constrained weld pools, which depend on the properties of the molten pool material, the surface tension and the shape of weld pools [Hardt (1986)[63]]. Another application of arc sensing is the detection of the metal transfer in the GMAW. As the droplet transfer mode in the GMAW process has a great effect on weld pool metallurgy, depth of penetration and solidification, Johnson et al. (1989)[74] has attempted to correlate perturbations in the electrical arc signals with droplet transfer in order to detect the detachment of individual droplet and to distinguish the three transfer modes.

2.5.3 Adaptive Control

2.5.3.1 Open Loop Automatic Arc Welding

Manual arc welding process was automated in an attempt to gain high efficiency, high productivity and low cost. The first form of automation occurred in the United States during the 1920s. The automated welding system utilised complex jigging and mechanical devices to move the workpiece in relation to the stationary welding head in order to gain higher efficiencies and lower costs. This system was predominantly restricted to the welding of specific tasks; that is the welding machine was designed specifically for one type of manufactured item. Figure 2.4 depicts an early automatic arc welding system [Cary (1979)[19]].

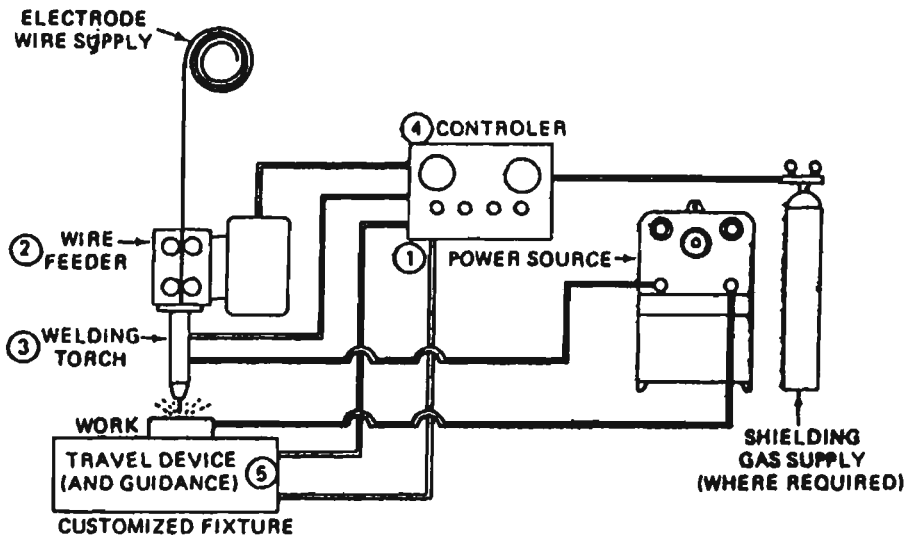

Figure 2.4 Typical early automatic arc welding system [Cary (1979)[19]].

In an effort to achieve greater flexibility, multiple axis manipulators were adapted at first by analog, and later by digital computers to perform the welding procedure. This development represented a significant improvement on the cumbersome early systems because setup times were reduced, more tasks could be performed, and routines could be stored for later use. However, as with the early systems, the later automated welding machines still relied on open loop control of the arc welding process. This is illustrated in figure 2.5.

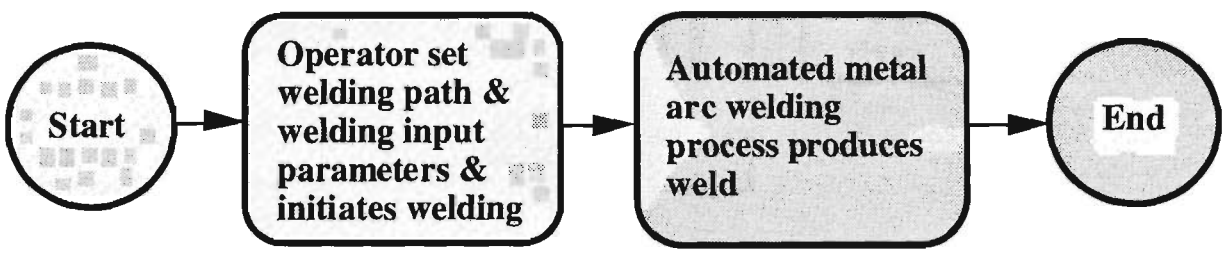

Figure 2.5 Open loop control in the automated arc welding.

It was still the operator's responsibility to select the automatic arc welder's torch path and welding process parameters such as welding voltage, gun travel speed and wire

feed rate. Algebraic models were developed in an attempt to predict the desired weld output parameters such as bead width and depth of penetration. However, these modelling systems were still dependent on the weldment being constant and did not compensate for irregularities in workpiece joint misalignment, workpiece edge distortion, or warp caused by the heat produced during the welding.

To correct problems in an open loop system, it is necessary for the operator to either stop operation immediately or wait until completion of the weld being performed. In this way, the automated welding system is much less effective in controlling the laying of a weld than manual welding. Humans make use of their senses of sound and sight to gather welding information and after processing and interpretation, take the necessary corrective measures to ensure the weld is satisfactory. Kuhne et al. (1988)[95] presented the manual arc welding control loop as depicted in figure 2.6.

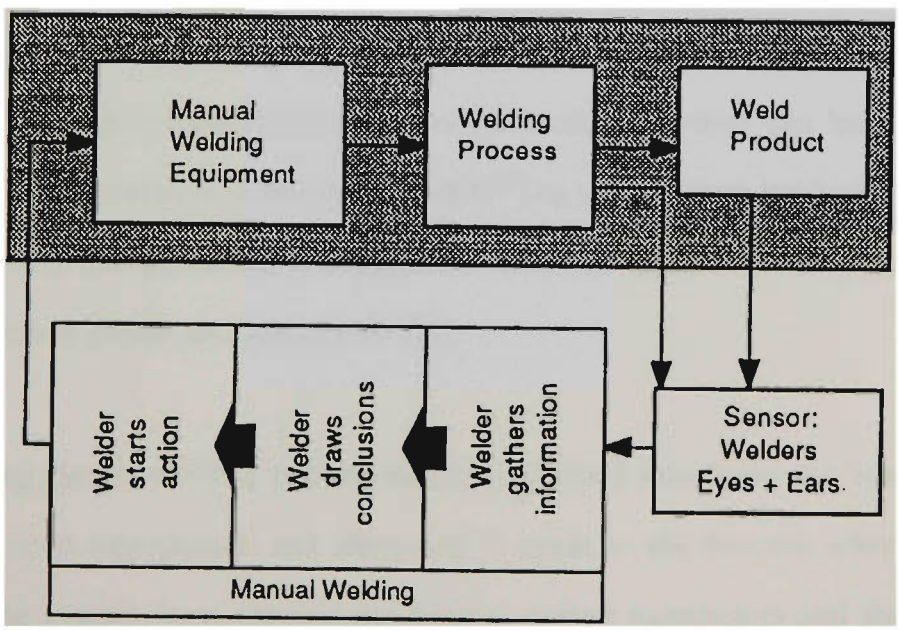

Figure 2.6 Manual arc welding control loop [Kuhne et al. (1988)[95]].

Automation without closed loop control processes the same components contained within the grey region of this figure, except that the manual welding equipment is replaced with automatic welding equipment. The operator must also utilise experience

or modelling to select the necessary input parameters to achieve the desired output parameters. As a result of these short-comings, much research and development work have concentrated on sensing and control methods to enhance the automated and/or robotic arc welding.

2.5.3.2 Closed Loop Automatic Arc Welding

With the combination of sensors and mathematical models, increased effectiveness in control of the automatic welding process was achieved. Through-the-arc sensing has been applied from width control and seam tracking [Cook (1983)[38]], to sensing of the GTAW weld pool motion [Remwick and Richardson (1983)[151]] and detection of the GMAW metal transfer models [Johnson et al. (1989)[74]]. Vision sensing has been utilised for joint tracking [Gonseth and Blanc (1983)[59]], weld bead profile sensing [Richardson (1986)[153]] and control of electrode extension [Salter and Deam (1987)[159]]. Other forms of sensing include infrared which has been used in the estimation of penetration [Chen et al. (1989)[27]] as well as seam tracking [Nagarajan et al. (1989)[128]], and ultrasonic sensing which has been applied to weld bead monitoring and inspection [Hardt and Katz (1984)[62]].

Controlling the arc welding process requires a closed loop approach whereby sensed information is interpreted, and alteration is made to the process where necessary. Firstly, the system must receive the desired output parameters and then select the necessary welding process parameters based on these output parameters, next it must initiate welding and finally monitor the welding outputs to determine the success of the weld. Subsequently, based on this process monitoring, the model must be able to take positive action for any corrections needed. This closed loop approach is represented in figure 2.7.

Many analytical approaches to process modelling have been developed from heat transfer relationships [Cook (1981)[37], Doumanidis et al. (1986)[46] and Smartt (1990)[167]], but these are regarded by Cook et al. (1989)[39] as being only reasonably accurate. Most practical models are developed statically or experimentally, and attempted to decouple the welding input parameters. However, decoupling of welding process parameters is extremely difficult since each parameter has at least some effect on the others. For instance, welding bead penetration may be able to be changed with a change in arc current level, but this may also induce unwanted changes in bead height or weld spatter.

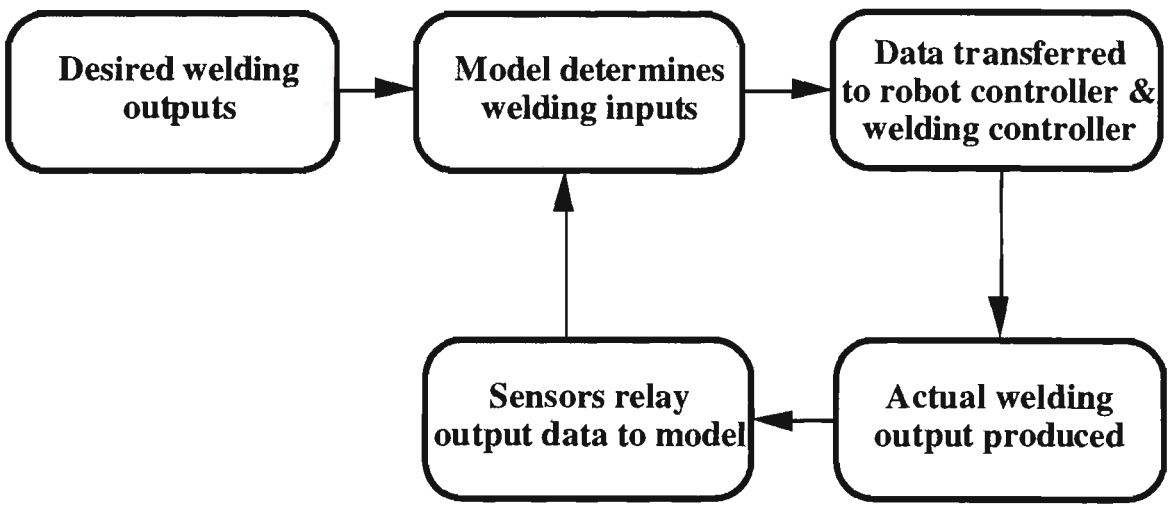

Figure 2.7 Closed loop control for the automated arc welding.

Most conventional real-time, closed loop controlled welding systems attempt to control major output parameters such as weld bead width. Hunter et al. (1988)[72] not only employed logarithmic equations to model the GMAW parameters, but also adapted capacitive distance transducers for gun positioning and ultrasonic sensing to monitor wire stickout. Sensing information on stickout length was employed on-line as an input to change voltage, wire feed rate, gun travel speed and contact tip to work distance in an attempt to maintain a constant depth of penetration. Richardson et al. (1984)[152] have been employed an optical sensor coaxially mounted with a GTAW

electrode to provide a pattern of reflected arc light for a computer algorithm to interpret joint width and location, and give successful joint tracking.

Other closed loop system has been developed by Smartt et al. (1986)[166] for real time control of reinforcement area and cooling rate. Doumanidis et al. (1986)[46] have attempted to derive simple dynamic models in their attempt to control bead width, penetration, reinforcement area, heat affected zone width and rate of cooling at the centreline of the weld. Mathematical based control systems are not suited to truly real-time adaptive control because of their inability to isolate the process input parameters, thereby resulting in excessive processing times. These systems are not capable of taking account of heuristic's and the relative effect of each input parameter. Mathematical systems are also inflexible to changes in hardware due to their rigid control laws and consequently are unable to learn from successes and errors. However, it can only consider fuzzy logic or expert systems that are capable of a learning function.

CHAPTER 3

RELATIONSHIPS BETWEEN WELDING PARAMETERS AND WELD BEAD GEOMETRY

3.1 INTRODUCTION

The GMAW process involves large number of interdependent variables which may affect product quality, productivity and cost effectiveness. The relationship between GMAW variables and weld bead geometry is complex because a number of welding process parameters are involved. Variables such as the capacity and type of equipment, material dimensions and composition may be relatively fixed, while primary adjustable variables which are characterised by welding voltage, arc current and welding speed may be altered during the welding process.

To make the automated and/or robotic arc welding, it is essential that a mathematical model that predicts weld bead geometry and accomplishes the desired mechanical properties of the weldment is developed. The model should also cover a wide range of material thicknesses and be applicable for all welding position. For the automatic welding system, the data must be available in the form of mathematical equations.

This chapter has been designed to investigate the analytical and empirical formulae for understanding the relationship between welding process parameters and weld bead

geometry. The primary purpose of this chapter is (1) to compare the experimental results to outputs obtained using sets of the published theoretical and empirical formulae relating input variables to output parameters, (2) to remodel the empirical equations in order to better predict the output of the GMAW process, (3) to develop empirical models for determining the relationship between GMAW variables and weld bead geometry, and (4) to finally redefine the mathematical equations, using the theory of least squares, that allow the selection of welding process parameters to be calculated from a desired weld bead size.

The next section represents the experimental procedure including experimental design, welding equipment and welding procedure. This is followed by the detailed description of the experimental results, comparing between measured and calculated weld bead geometry, developing empirically mathematical models, redefining mathematical equations and an overall discussion of the experimental results.

3.2 EXPERIMENTAL PROCEDURE

3.2.1 Design of Experiments

A number of problems related to the automated and/or robotic arc welding process include the modelling, sensing and control of the process. Statistically designed experiments that are based upon factorial techniques, reduce costs and give the required information about the main and interaction effects on the response factors. Among the problems, the modelling of the process is very useful for the control and analysis of the process, and determination of the appropriate welding process parameters.

Experiments were designed for developing empirically mathematical models to correlate independently controllable welding process parameters. The 3^n factorial

experiment was found to be efficient for studying the effects of two or more factors when the response is approximately linear over the range of the factor levels chosen [Montgomery (1984)[124]]. The 3^n experiment provides the smallest number of treatment combinations with which n factors can be studied in a complete factorial arrangement, and not only the main effect of a factor but also the interaction between the factors can be defined.

In this chapter the results of the experiment were however employed only for fitting the response curve. The chosen factors were wire diameter, welding voltage, welding speed and arc current, and the response was weld bead width, height and penetration. Figure 3.1 illustrates a model of welding process with input and output variables of a GMAW process.

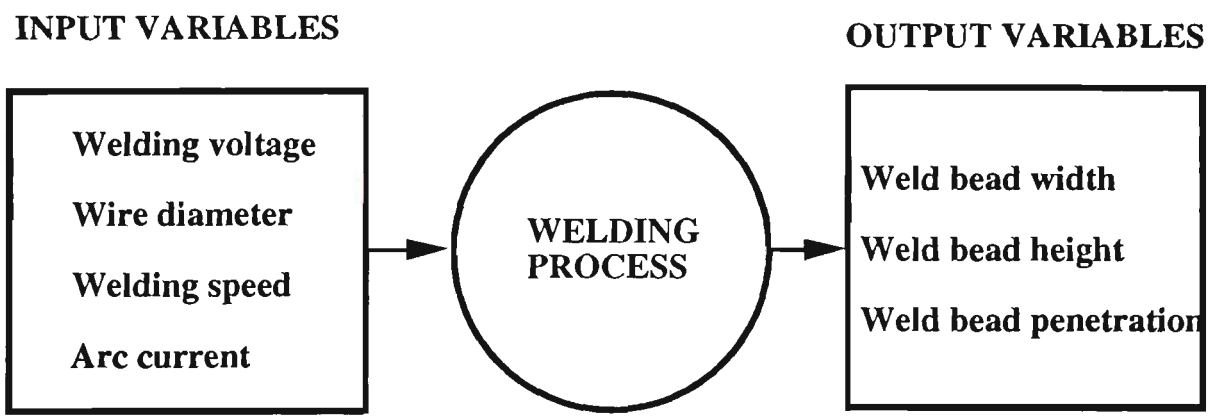

Figure 3.1 Input and output variables of the GMAW process.

In the 2×3^3 experiment to be considered the main and interaction effects, four variables, two or three levels, factorial design gave $2\times3^3 = 54$ weld runs for fitting each equation. The experimental levels and limits for four variables are given in Appendix A. For ease of recording and processing the experimental data, only one factor with two levels will be designed by the digits 0 (low) and 1 (high) respectively, while the three variables with three levels 0 (low), 1 (intermediate) and 2 (high). The design matrix and treatment combinations [Box et al. (1978)[10], Davis (1978)[42]] are

similar to those shown in Appendix A. For example, weld run No. 1 in the design matrix and the treatment combinations was made under the welding conditions coded as 0, 0, 0, 0, which means that the wire diameter, welding voltage, welding speed and arc current were 1.2mm, 20V, 250mm / min and 180A respectively (see Appendix A).

3.2.2 Welding Equipment

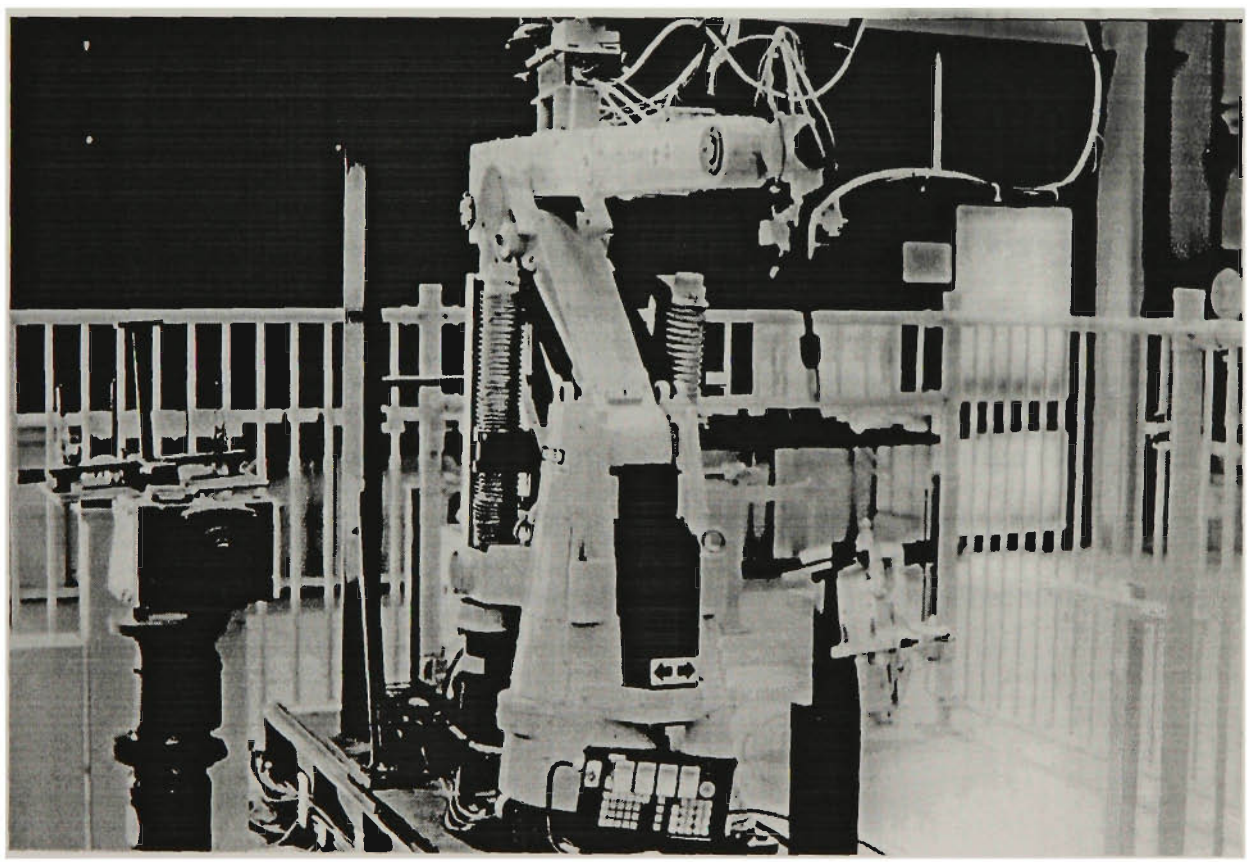

Figure 3.2 Hitachi process robot manipulator.

The welding facility at the Centre for Advanced Manufacturing and Industrial Automation (CAMIA) was chosen as the basis for the data collection and evaluation. The facility consists of a Lincoln GMAW unit which consists of a welding power source, a welder remote control unit and wire torch, and Hitachi process robot manipulator which included a robot control unit and a robot tech box. The torch positioning and motion control were achieved through monitoring the welding torch

to a Hitachi six axis robot (M6060II). This welding equipment is shown in figure 3.2.

3.2.3 Consumables and Materials

The selection of the electrode wire should be based principally upon matching the mechanical properties and physical characteristics of the base metal. Secondary consideration should be given to items such as the equipment to be used, the weld size and existing electrode inventory. 1.2 and 1.6 mm steel wire diameters were used. Typical composition of these diameters is shown in table 3.1.

To achieve equilibrium during the GMAW process, two samples were taken for observation after discarding 50 mm on each side to eliminate the end effects. Welding was carried out on experimental plates of $200 \times 75 \times 12$mm AS 1204 mild steel flats adopting a bead-on-plate technique. A chemical composition of the weld material is also shown in table 3.1. The required number of specimens were cut from 12 mm mild steel plates. The oxide scale was removed before welding using a wire brush.

3.2.4 Welding Procedure

The welding procedure to model weld bead geometry using input weld conditions was performed as following;

(1) The robot welder was taught a program path to lay out a weld. This path was illustrated in figure 3.3.

(2) A $200 \times 75 \times 12$mm mild steel as experimental test plate was located in the fixture jig.

Table 3.1 Chemical composition of the wire diameters and welding material

Item	C	Mn	Si	S	P	Cu
1.2 mm wire diameter	0.07-0.15%	1,00-1.50%	0.60-0.85%	0.035% max	0.025% max	0.50% max
1.6 mm wire diameter	0.07-0.15%	1,00-1.50%	0.60-0.85%	0.035% max	0.025% max	0.50% max
Mild steel AS 1204	0.29%		0.45%		0.050%	0.050%

(3) The required input weld conditions were manually attached to the particular weld steps in the robot path by using the robot's teach box.

Appendix A shows the design matrix and treatment combinations used during the 2×3^3 factorial welding experimental design.

(4) With welder and argon shield gas turned on, the robot was initialised and welding was executed.

(5) A new set of weld input parameters was reprogrammed for the next set of weld.

(6) Welding was once again carried out.

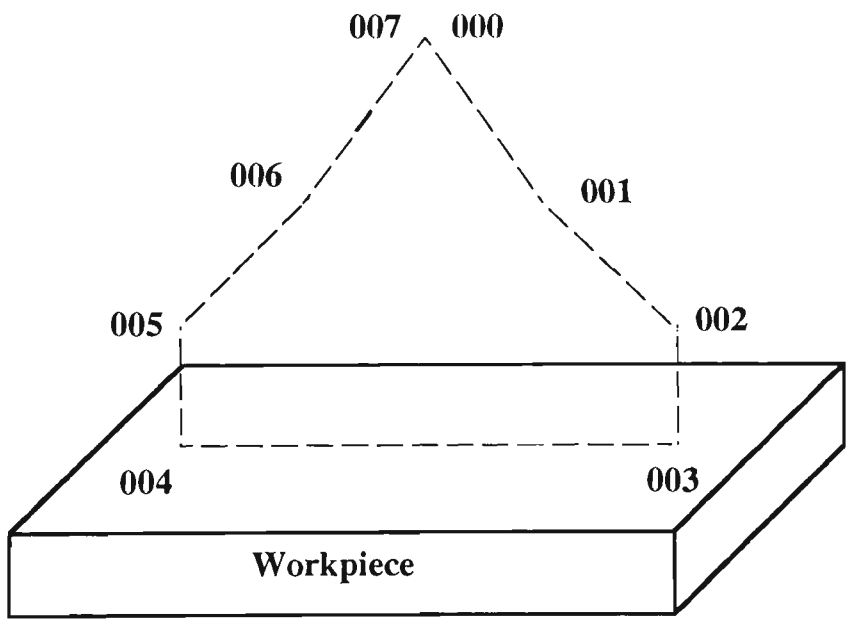

PROGRAM SETUPS

000 - Home position
001 - Full swing in home position
002 - Extend above job
003 - Slowly down to weld
004 - End of weld
005 - Move up
006 - Retract
007 - Return to home position

Figure 3.3 Robot path design for experiment.

After 54 welds, the plates were cut using a power hacksaw and the end faces were machined. Specimen end faces were polished and etched using a 2.5% nital solution to reveal grain boundaries and to display the weld bead penetration. An image analysis package, Image Analyst, manufactured in the United States by Automatix Inc., was employed to accurately measure weld bead geometry [Automatix (1990)[8]]. Appendix A shows the results of the experiment for weld bead dimensions during the GMAW process. The results of the experiment were analysed on the basis of the relationship between the input and the output parameters for the GMAW process. Figure 3.4 defines the measurement of weld bead geometry studied.

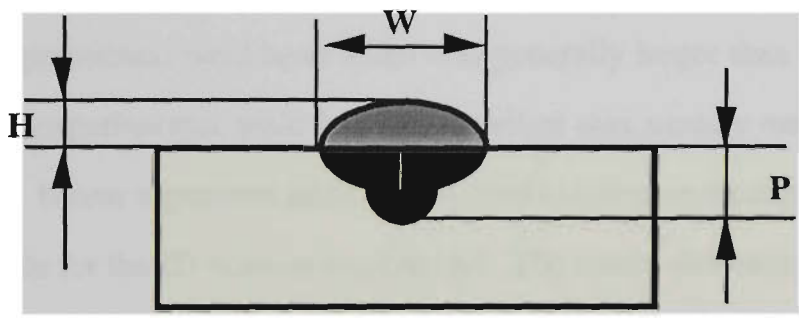

W : Bead width
H : Bead height
P : Penetration

Figure 3.4 Measurement of weld bead geometry.

3.3 RESULTS AND DISCUSSION

3.3.1 Comparing Between Theoretical and Experimental Results

Theoretical predictions of weld bead geometry can be predicted from conductive heat transfer studies. These assume that the weld completely penetrates the plate being welded and heat is conducted only in the plane of the plate. Roberts and Wells (1954)[154] have estimated the weld bead width to be given by:

$$W = \frac{1}{2}\frac{Q}{St_1}\frac{1}{\rho C_p}\frac{1}{T_m} - \frac{4}{5}\frac{\lambda}{S} \tag{3.1}$$

The weld bead penetration was assumed to be equal to a weld bead half-width, a semicircular cross section. Values of the material parameters were assumed to be $\lambda = 0.091 cm^2/sec$, $\rho C_p = 4.5 J/cm^3 C$, $T_m = 1500C$, $k = 0.41 J/cm\ C\ sec$. In GMAW, the rate of heat input to plate, is given by the product of ζ,V and I. Heat input efficiency for the GMAW process employed to weld steel plates is based on welding process parameters such as welding voltage, arc current, electrode extension and type of shielding gas. It was assumed to be 68% for the comparisons made below. The experimental weld bead width was generally larger than the theoretical one, while the experimental weld bead penetration was usually smaller than the theoretical one. Linear regression analysis was used to compare the experimental with theoretical results for the 2D mathematical model. The results obtained are as follows:

$$W_1 = 8.63374 + 0.5494W \tag{3.2}$$

$$P_1 = 0.8394 + 0.5527P \tag{3.3}$$

Table 3.2 shows the Standard Error of Estimate (SEE), coefficient of multiple correlation (R), and coefficient of determination (100 R^2) for the above described models accordingly. The values of coefficient of multiple correlation of these equations are 0.702 and 0.6035 respectively. It is noted from table 3.2 that the coefficient of multiple correlation for equation (3.2) is higher than those for equation (3.3).

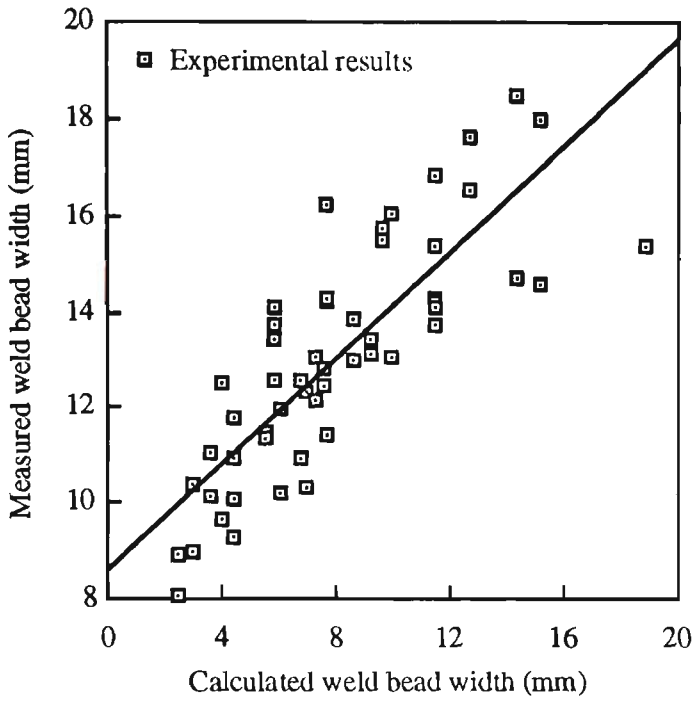

Figure 3.5 Comparison of measured and calculated weld bead width.

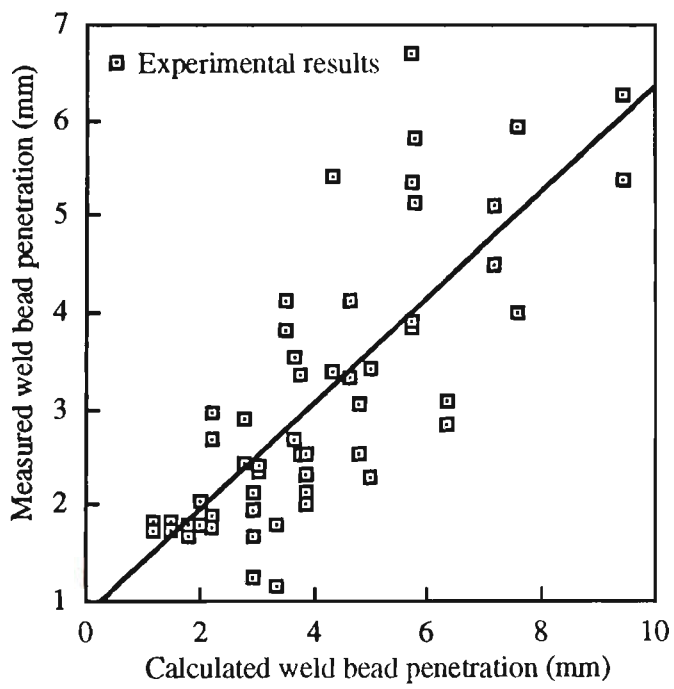

Figure 3.6 Comparison of measured and calculated weld bead penetration.

Table 3.2 Analysis of models using Roberts and Wells equation

No. of equation	Standard error of estimate	Coefficient of multiple correlation	Coefficient of determination
Weld bead width	0.50234	0.7020	0.6962
Weld bead penetration	0.34521	0.6035	0.5960

The scatter graphs of measured and calculated values of weld bead geometry are illustrated in figures 3.5 and 3.6. The line of best fit for the plotted points was drawn using linear regression computation. From figures 3.5 and 3.6, it is found that equations (3.2) and (3.3) have an inclination to overestimate the weld bead penetration, whereas the weld bead width was overall slightly larger than the values obtained during experimentation. Christensen et al. (1965)[36] have presented similar findings. Also, Friedman and Glickstein (1976)[52] have analytically shown that a larger diameter heat source tends to increase weld bead width and decrease weld bead penetration in stationary GTAW.

Christensen et al. (1965)[36] have published theoretical non-dimensional graphs showing various weld bead dimensions versus "operating parameters", n, where $n = {QS}/{4\pi\lambda k T_m}$. Their model is claimed for being suitable to all combinations of materials and welding conditions within the limitations and assumptions combined with the point source equation. The experimental results were plotted using the same non-dimensional parameters, and compared with the theoretical results obtained by Christensen et al. (1965)[36], which assumed a three dimensional (3D) conductive heat transfer configuration.

Figure 3.7 shows the non-dimensional weld bead width. Reasonable agreement between the experimental and the theoretical non-dimensional weld bead width is shown, even when the scatter about the theoretical results is considerable.

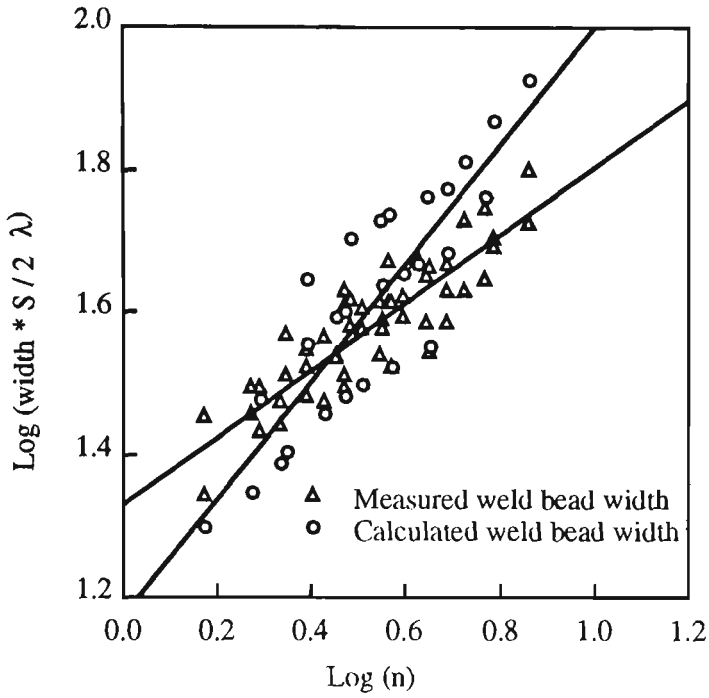

Figure 3.7 Non-dimensional weld bead measurements versus operating parameter (n) for weld bead width.

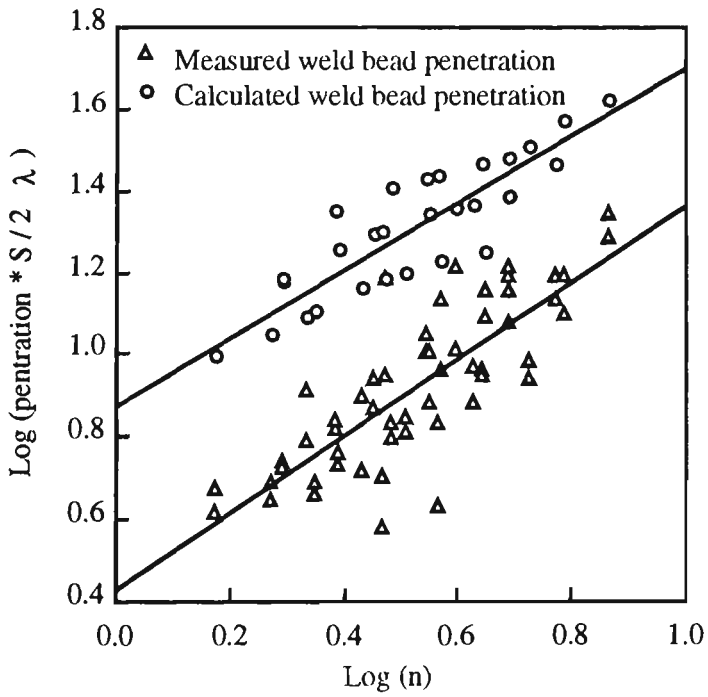

Figure 3.8 Non-dimensional weld bead measurements versus operating parameter (n) for weld bead penetration.

From figure 3.8, it appears that the theoretical equation overestimates the weld bead penetration, as has been noted by Roberts and Wells (1954)[154] and thus, presented a considerable error (60.09% variance).

In addition, it is quite evident from the above comparison that prediction of weld bead geometry with reasonable accuracy, based on various models, requires adjustments in order to achieve better agreement with experimental results. Since conductive, convective, radiative heat transfer and mass transfer in the GMAW process all take their toll, the development of an accurate analytical model can be complicated and perhaps inappropriate for either closed loop or adaptive control purposes. Instead, a regression model for weld bead geometry should be considered.

The empirical equations reported by Chandel (1988)[24] for the GMAW process were employed to predict weld bead geometry characteristics and presented as following:

$$W = \frac{(D)^{0.567}\ (L)^{0.0106}\ (I)^{0.181}\ (V)^{0.86}}{(S)^{0.614}} \times \frac{1}{(10)^{0.218}} \tag{3.4}$$

$$H = \frac{(L)^{0.38}\ (I)^{1.2}}{(D)^{1.36}\ (V)^{0.69}\ (S)^{0.45}} \times \frac{1}{(10)^{1.382}} \tag{3.5}$$

$$P = \frac{I^{2.05}\ V^{0.142}}{D^{0.86}\ L^{0.063}\ S^{0.53}} \times \frac{1}{(10)^{4.03}} \tag{3.6}$$

The welding process parameters used to produce the 54 weld runs for fitting each equation were input into the Chandel's equations to provide theoretical results for the weld bead width, height and penetration, accordingly. This allowed the accuracy of Chandel's equations to be validated using experimental findings extracted during the course of this study.

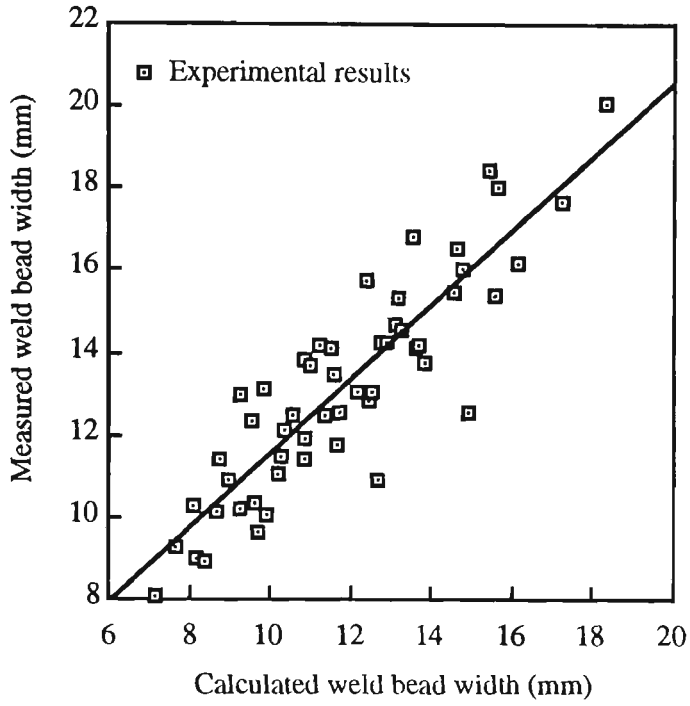

Figure 3.9 Comparison of measured and calculated weld bead width using Chandel's equations.

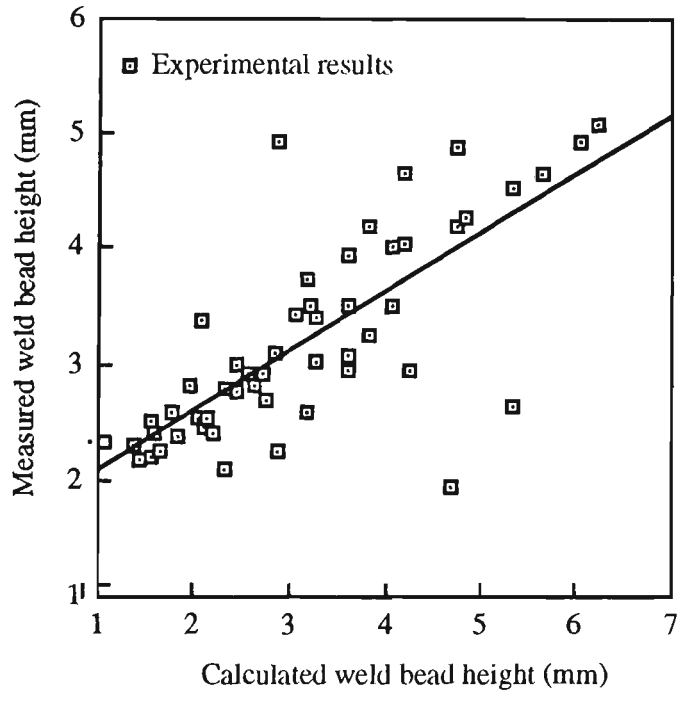

Figure 3.10 Comparison of measured and calculated weld bead height using Chandel's equations.

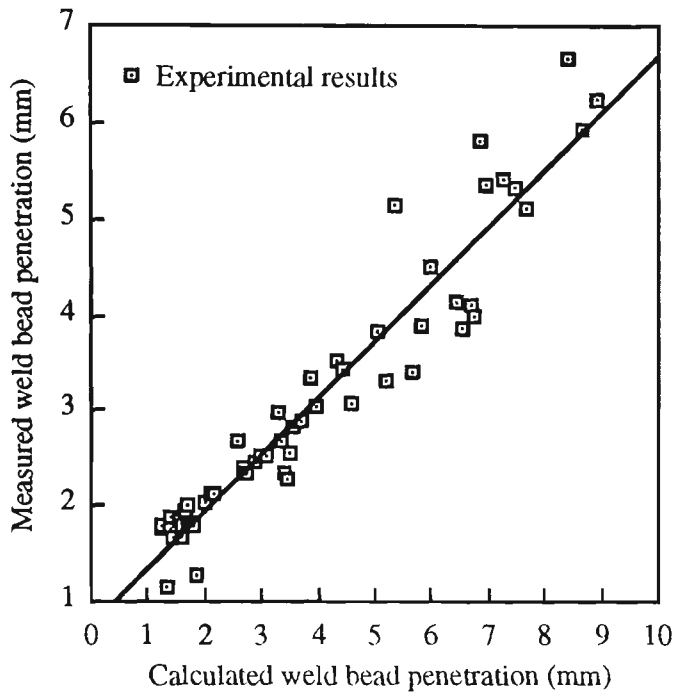

Figure 3.11 Comparison of measured and calculated weld bead penetration using Chandel's equations.

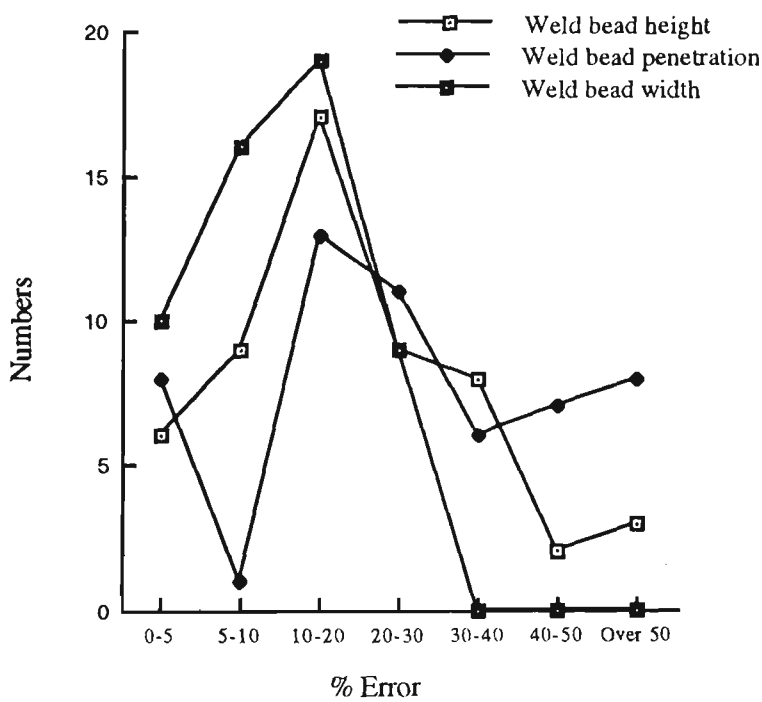

Figure 3.12 Accuracy analysis of Chandel's equations.

Results were plotted using a scatter graph for each weld bead width, height and penetration. Three graphs (figures 3.9 to 3.11) were produced for experimental versus theoretical results using Chandel's equations. The line of best fit for the plotted points was also drawn using regression computation. It is evident from these results that the model's accuracy is questionable and its universal applicability is limited.

The method chosen for assessing the accuracy of the theoretical results considered the number of theoretical results that fell within a percentage error of all the experimental results. The calculation of accuracy of the theoretical results has been used as following:

$$\eta = \frac{R_T - R_A}{R_A} \times 100 \qquad (3.7)$$

It was decided to group these into seven categories: 0-5%; 5-10%; 10-20%; 20-30%; 30-40%; 40-50% and over 50%. The results of this analysis for the welding bead dimensions (weld bead width, height and penetration) are presented in figure 3.12. This analysis indicates that Chandel's equations produced better prediction of the weld bead width, and 11 of the total weld bead dimensions were over 50 % inaccurate. The conclusions from the results of this analysis for the experimental runs show that theoretical results may not predict the experimental values with any consistent accuracy. However, when these values were plotted as data points in a scatter graph, a definite correlation appeared. This means that the mathematical equations required remodelling to suit the GMAW process with argon shield gas, the wire material type and diameter used.

3.3.2 Remodelling Mathematical Equations

The rationale to remodel the mathematical equations centres on the fact that the equations suggested by Doherty and McGlone (1977)[44] and McGlone (1978)[117] can be adjusted to suit a particular welding process. They can take the same form as the general straight line relationship. From the straight lines plotted using the original equations, the slope and the intercepts of these lines were measured and then fed into the original equations. The new equations, when plotted, produced straight lines which intersected the origin and lied at 45 degrees. Most important, the equations are capable of predicting experimental results with an improved accuracy. Using the general equation for a straight line, the modified Chandel equations were obtained as follows:

$$W = (D^{0.567} L^{0.0106} I^{0.181} V^{0.86} S^{-0.614}) \times 0.5707 + 1.8946 \qquad (3.8)$$

$$H = (D^{-1.36} L^{0.38} I^{1.2} V^{-0.69} S^{-0.45}) \times 0.02127 + 1.5926 \qquad (3.9)$$

$$P = (D^{-0.86} L^{-0.063} I^{2.05} V^{-0.142} S^{-0.53}) \times 0.00005542 + 0.75715 \qquad (3.10)$$

To evaluate the accuracy of the new equations and to observe the spread of the values, the results were again plotted using the scatter graph. These graphs of experimental versus theoretical values of weld bead geometry are presented in figures 3.13 to 3.15. As shown in figures 3.14 and 3.15, the weld bead height and penetration predictions of the modified Chandel equations produced data points located in a close proximity to the line of best fit. The results for weld bead width depicted in figure 3.13 however exhibited a degree of scatter believed to be due to the permissible amount of fluctuation in the welding speed and arc current recorded during the GMAW process.

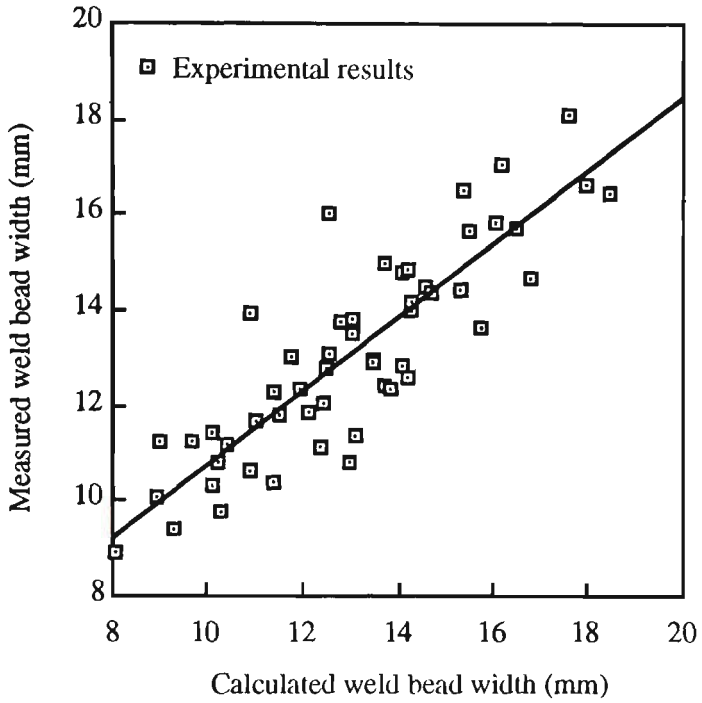

Figure 3.13 Comparison of measured and calculated weld bead width using the modified Chandel equations.

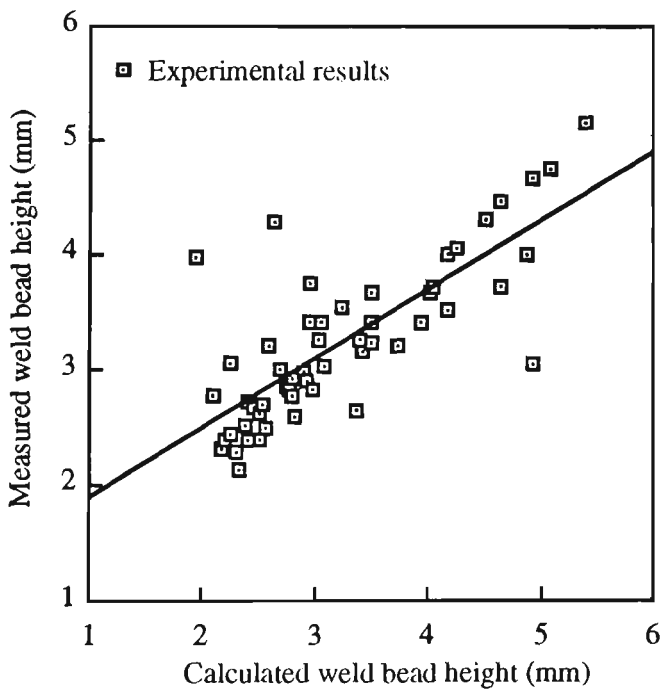

Figure 3.14 Comparison of measured and calculated weld bead height using the modified Chandel equations.

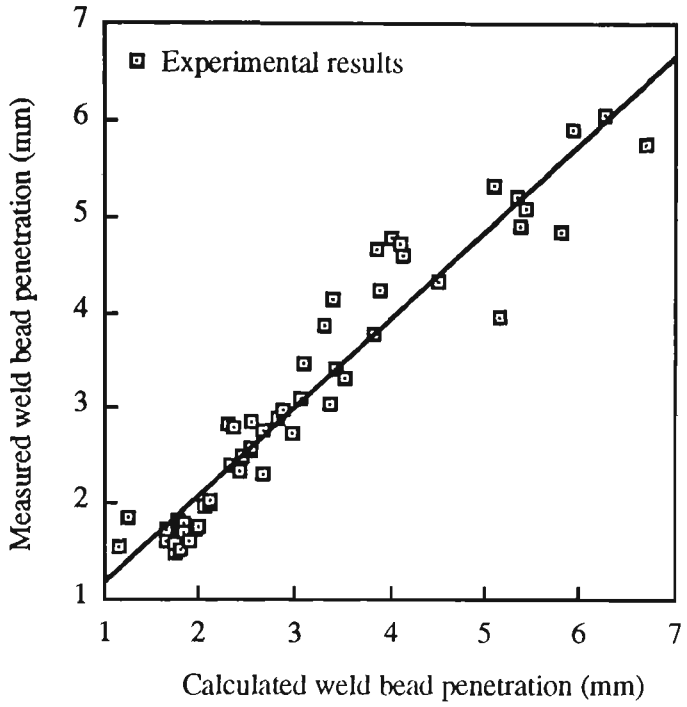

Figure 3.15 Comparison of measured and calculated weld bead penetration using the modified Chandel equations.

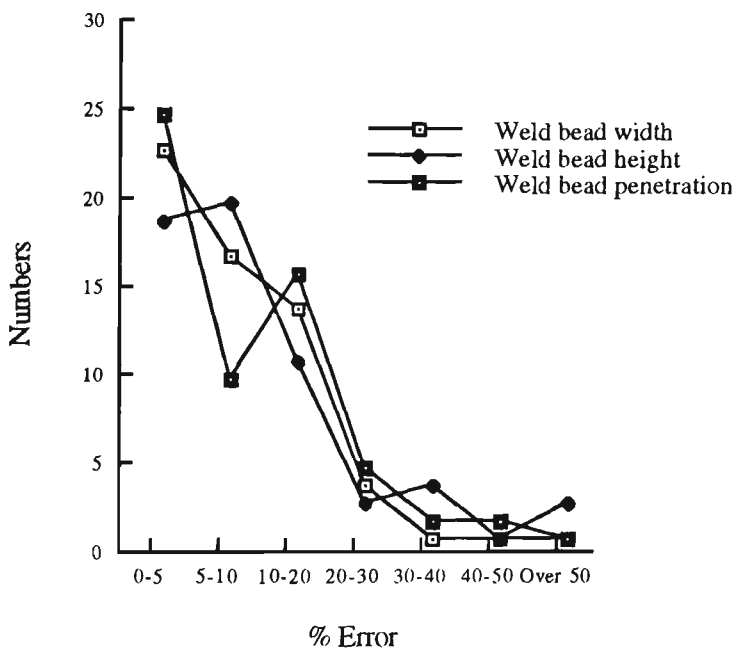

Figure 3.16 Accuracy analysis of the modified Chandel equations.

For assessing the accuracy of the theoretical results, the percentage error of each was again calculated and compared them to the experimental result. This analysis, presented in figure 3.16, exhibited a marked improvement in the percentage error when compared to the previous results produced to assess the accuracy of the original equations. It showed that the modified Chandel equations produced better predictions of weld bead width and penetration. The modified Chandel equations predicted 64 of the total weld bead dimensions to be within 0-5 % of the experimental results.

3.3.3 Development of Mathematical Models

In order to quantitatively evaluate the effects of welding process variables on weld bead geometry, the following adjusted mathematical relationship between welding process parameters and weld bead geometry has been developed. In general, the response function can be represented as follows:

$$Y = f(D, V, I, S) \tag{3.11}$$

Assuming a linear relationship for the narrow range and considering all the main effects together with the two factor interactions, the above equation suggested by McGlone and Chadwick (1978)[118] can be expressed as follows:

$$Y = a_1 (D)^{a_2} (V)^{a_3} (I)^{a_4} (S)^{a_5} \tag{3.12}$$

where a_1, a_2, a_3, a_4 and a_5 are constants.

The values of a_1, a_2, a_3, a_4 and a_5 were computed by the method of regression [Montgomery (1984)[124], Box et al. (1978)[10] and Davis (1978)[42]]. These analyses were carried out with the help of a standard statistical package, SAS, using IBM-

compatible PC [SAS (1988)[160]]. The following equations correlating welding process parameters to weld bead geometry were obtained from the experimental data:

$$W = (D^{0.4294} V^{0.7083} I^{0.3518} S^{-0.4590} 10^{-0.0905}) \quad (3.13)$$

$$H = (D^{-0.1255} V^{-0.7183} I^{0.6387} S^{-0.2395} 10^{0.3339}) \quad (3.14)$$

$$P = (D^{-0.5668} V^{0.0130} I^{1.4005} S^{-0.3641} 10^{-2.3098}) \quad (3.15)$$

The adequacy of the models and the significance of coefficients were tested by applying the analysis of variance technique respectively. Table 3.3 shows the standard error of estimate (SEE), coefficient of multiple correlation (R) and coefficient of determination (100 R^2) for the above mentioned equations, respectively.

Table 3.3 Analysis of variance tests for mathematical equations

No. of equation	Standard error of estimate	Coefficient of multiple correlation	Coefficient of determination
Weld bead width	0.85437	0.9398	0.9259
Weld bead height	0.73431	0.9037	0.8960
Weld bead penetration	0.67543	0.9056	0.8979

The mathematical models were employed to calculate the theoretical results of regression analysis, to compare the experimental results measured with the set of existing empirical findings reported by Chandel and the set of modified empirical equations. To ensure the accuracy of the new equations and to survey the spread of the values, results were again plotted using the scatter graph. These graphs of experimental versus theoretical values of weld bead dimension are presented in figures 3.17 to 3.19 for weld bead width, height and penetration, respectively.

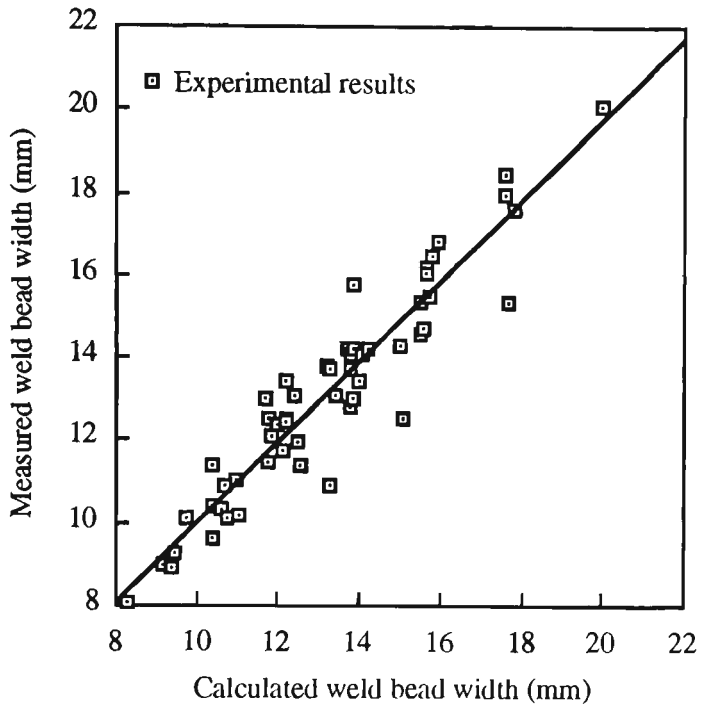

Figure 3.17 Comparison of measured and calculated weld bead width using mathematical equations.

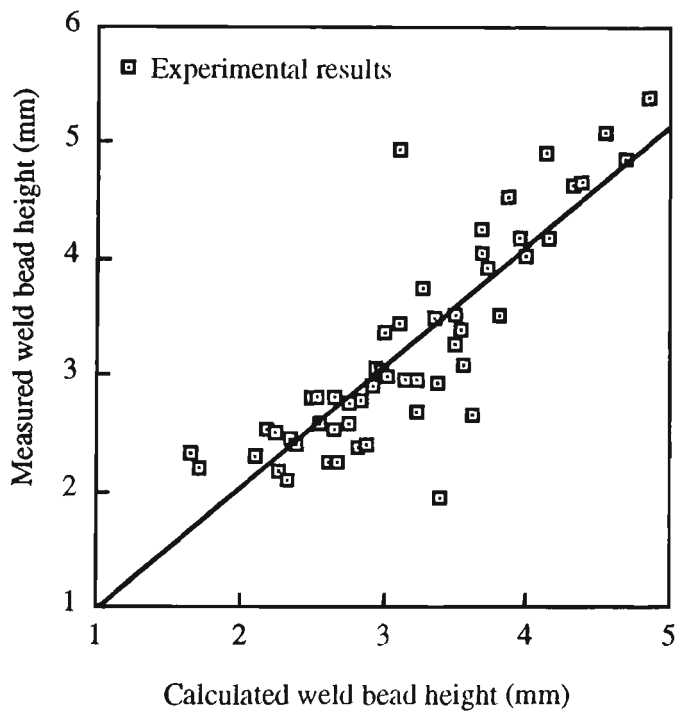

Figure 3.18 Comparison of measured and calculated weld bead height using mathematical equations.

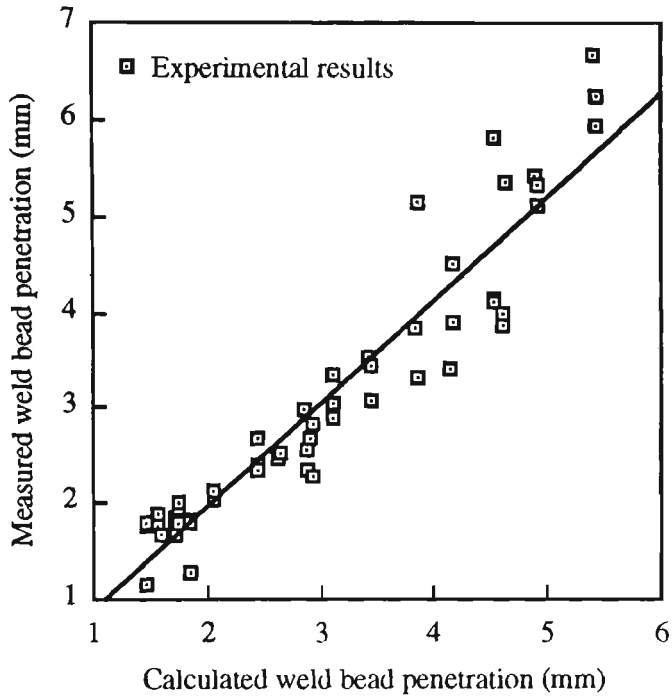

Figure 3.19 Comparison of measured and calculated weld bead penetration using mathematical equations.

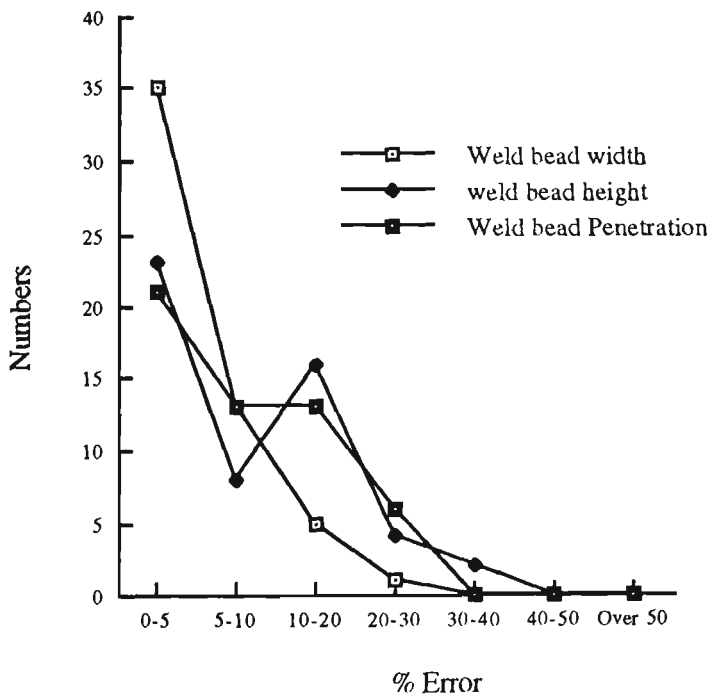

Figure 3.20 Accuracy analysis of mathematical equations.

For assessing the accuracy of the theoretical results, the percentage error of each was again calculated, compared them to the experimental result and presented in figure 3.20. This analysis indicated that the mathematical models provided better predictions of the weld bead dimensions. When welding bead dimensions were totalled in columns, results showed that the models developed produced 79 weld bead dimensions that were within 0-5 % accurate. The remaining totals lay predominantly in the 5-10 % and 10-20 % groups. During the analysis of the results, it was observed that the empirical mathematical models for the GMAW process yielded more accurate weld bead dimensions.

3.3.4 Redefining Mathematical Model into a Useable Format

The empirical equations previously defined yielded the values for weld bead width, height and penetration for respective values of wire diameter, arc current, welding voltage and travel speed. The process operation requires these in a different form. Once weld bead geometry have been specified, the formula are required to calculate the welding process parameters to achieve weld bead geometry.

Figures 3.17 to 3.19 indicate that the empirical formulae predicted experimental result better than the set of the published equations suggested by Chandel, the set of modified Chandel equations or the set of theoretical formula. For this reason, the newly established mathematical models were chosen to carry on the ensuing work in redefining the equations.

Using the theory of least squares [Lawson and Hanson (1974)[98]], the setting of the wire diameter, welding voltage, arc current and welding speed can be calculated by the following equation in terms of weld bead width, height and penetration:

$$\theta = (\Phi^T \Phi)^{-1} \Phi^T y \qquad (3.16)$$

where $y = [y_1 \quad y_2 \quad \cdots \quad y_n]$ $\theta = [\theta_1 \quad \theta_2 \quad \cdots \quad \theta_n]$ $\Phi = \begin{bmatrix} \varphi(x_1) \\ . \\ . \\ . \\ \varphi(x_n) \end{bmatrix}$

To reduce the complexity of the mathematics, the equations (3.13) to (3.15) will be rewritten as following:

$$W^{\nabla} = (D^{0.4294} V^{0.7083} I^{0.3518} S^{-0.4590}) \tag{3.17}$$

$$H^{\nabla} = (D^{-0.1255} V^{-0.7183} I^{0.6387} S^{-0.2395}) \tag{3.18}$$

$$P^{\nabla} = (D^{-0.5668} V^{0.0130} I^{1.4005} S^{-0.3641}) \tag{3.19}$$

where

$$W^{\nabla} = \frac{W}{0.81189}, \quad H^{\nabla} = \frac{H}{2.15725}, \quad P^{\nabla} = \frac{P}{0.0049}$$

Taking the natural logarithms (In) from both sides of the above equations yields the following:

$$\ln W^{\nabla} = (0.4294 \ln D) + (0.7083 \ln V) + (0.3518 \ln I) + (-0.4590 \ln S) \tag{3.20}$$

$$\ln H^{\nabla} = (-0.1255 \ln D) + (-0.7183 \ln V) + (0.6387 \ln I) + (0.2395 \ln S) \tag{3.21}$$

$$\ln P^{\nabla} = (-0.5668 \ln D) + (0.0130 \ln V) + (1.4005 \ln I) + (-0.3641 \ln S) \tag{3.22}$$

The above equations can be defined by the following vectors and rewritten in matrix form:

$$y = \theta \ \Phi \tag{3.23}$$

where

$$y = \begin{bmatrix} W^{\nabla} \\ H^{\nabla} \\ P^{\nabla} \end{bmatrix}, \quad \theta = \begin{bmatrix} \ln D \\ \ln V \\ \ln I \\ \ln S \end{bmatrix}, \quad \Phi = \begin{bmatrix} 0.4294 & 0.7083 & 0.3518 & -0.4590 \\ -0.1255 & -0.7183 & 0.6387 & 0.2395 \\ -0.5668 & 0.0130 & 1.4005 & -0.3641 \end{bmatrix}$$

Using the equation (3.16), the determinant of system is:

$$\begin{bmatrix} \ln D \\ \ln V \\ \ln I \\ \ln S \end{bmatrix} = \begin{bmatrix} 0.8633 & 2.0610 & -1.0337 \\ 19.5313 & -1.6094 & 30.0391 \\ 3.8125 & 3.5566 & 10.4570 \\ 13.1875 & -2.8203 & 18.8281 \end{bmatrix} \begin{bmatrix} W^{\nabla} \\ H^{\nabla} \\ P^{\nabla} \end{bmatrix} \tag{3.24}$$

Therefore, the equations of wire diameter, welding voltage, arc current and travel speed should be represented as following:

$$\ln D = 0.8633 \ln W^{\nabla} + 2.0610 \ln H^{\nabla} - 1.0337 \ln P^{\nabla} \tag{3.25}$$

$$\ln V = 19.5313 \ln W^{\nabla} - 1.6094 \ln H^{\nabla} + 30.0391 \ln P^{\nabla} \tag{3.26}$$

$$\ln I = 3.8125 \ln W^{\nabla} + 3.5566 \ln H^{\nabla} + 10.4570 \ln P^{\nabla} \tag{3.27}$$

$$\ln S = 13.1875 \ln W^{\nabla} - 2.8203 \ln H^{\nabla} + 18.8281 \ln P^{\nabla} \tag{2.28}$$

This produced four simplified equations of W^{∇}, H^{∇} and P^{∇}, each being expressed as a function of weld bead width, height and penetration. The principle of least squares was applied to the above set of equations and produced four new equations which described $\ln D, \ln V, \ln I$ and $\ln S$ in terms of W^{∇}, H^{∇} and P^{∇}. From the

above equations, it can be seen that this model is considered to be useful for the process automation such as weld seaming tracking in the GMAW processes. The main advantage of the experimental model is its simple form which allows the easy calculation of the weld bead dimension for various welding conditions.

To utilise these equations and to determine the value of weld bead width, height and penetration, the values of wire diameter, welding voltage, arc current and welding speed are first determined. The values of the gas flow rate and wire stickout, not yet included in the model, can be chosen according to material type and thickness. It must be demonstrated that the mathematical models developed can be applied to other joint types, processes, and materials. These variables are the subject of future research work with the view of incorporating them into a more comprehensive model.

3.4 SUMMARY OF RESULTS

The effects of welding process parameters on weld bead geometry when bead-on-plate welds are deposited using the GMAW process have been studied and the following conclusions reached:

1. The universality of results obtained after using empirical equations taken from existing models developed by Chandel proved to be limited in predicting experimental bead shapes for the GMAW process. After the equations were adjusted and the process was remodelled, the accuracy of weld bead dimension substantially improved.
2. Comparison between weld bead geometry experimental findings and those proposed by the conductive heat transfer model showed that the theoretical analysis generally overestimates penetration and suitably predict the weld bead width, even if considerable scatter is found in the overall results.

3. Results from redefining the mathematical models should be put into perspective with the standard GMAW power source that was employed to conduct the experimental work.
4. Mathematical models developed from the observed data in the course of this work can be used to control the welding process parameters in order to achieve desired weld bead geometry outcomes and indeed weld quality.

CHAPTER 4

MATHEMATICAL MODELS FOR PREDICTING WELD BEAD GEOMETRY

4.1 INTRODUCTION

Since the GMAW process is well suited for mass production and the automated and\or robotic welding application, all commercial metals; carbon steel, stainless steel, aluminium, copper and titanium could be welded by selecting the suitable welding process parameters and shielding gas. One of the most important tasks in the GMAW process is to understand how welding process parameters affect welding bead geometry and to subsequently develop the mathematical models for predicting the desired weld bead dimensions. By carefully choosing and closely controlling welding process parameters, high quality welds may be made in all environments for the GMAW process.

This chapter presents the results obtained in detailed experimental study regarding the effects of five welding process parameters on the eleven weld bead dimensions in AS 1204 mild steel flats adopting the bead-on-plate technique. The objectives are to fully characterise welding process parameters in which accurate and reproducible outputs could be generated, and to develop the mathematical models which study the influence of welding process parameters on weld bead geometry and help the development of optimal welding process and the generation of process control algorithms. The

models developed will be useful for identifying the various problems that result from the GMAW process and establishing guidelines and criteria for effective joint design.

4.2 EXPERIMENTAL WORK

4.2.1 Selection of Welding Process Parameters

A trial and error method within a narrow range of variables is often used to seek optimisation of the welding process. However, this approach can be time consuming and expensive as well as self defeating [Apps et al (1963[6])]. Another method, termed the 'tolerance box' technique is an effective, systematic approach to determine process parameters, tolerances and production rates, but it is to expensive and time consuming, and can not deal with more than three process parameters [Jones (1976)[76]].

Generally, a major difficulty in the procedure optimisation is many welding process parameters involved. The usual single variable experiment which has been varied one variable at a time but kept the others constant, is burdensome and unsuitable in complex system such as the GMAW process. However the statistical design of experiment based on the factorial technique, involves simultaneous variations of all the variables, greatly reduces the number of trials and enables mathematically reliable predictions to be made of the optimum conditions [Harris and Smith (1983)[64]]. This approach has been successfully employed in other field such as chemical engineering and agriculture. Therefore, it was decided to use the well established statistical tool of three level fractional factorial technique for designing the experiments which reduced the experimental runs to the minimum possible.

The welding process parameters which could affect weld bead geometry and overall weld quality during the GMAW process (described in chapter 2) could be classified into three categories and described as following [Hobart (1964)[69]]:

(1) Arc current.

(2) Polarity.

(3) Welding voltage.

(4) Welding speed.

(5) Electrode extension.

(6) Electrode orientation.

(7) Weld joint position.

(8) Wire diameter.

(9) Shielding gas composition.

(10) Gas flow rate.

For achieving satisfactory weld bead geometry and studying the effects of those parameters which definitely affect the metal transfer mode and the amount of heat input to the workpiece, it is essential to control the above welding process parameters. Welding process parameters included in this study were however wire diameter, gas flow rate, welding speed, arc current and welding voltage. All other parameters, except these variables under considerations, were kept constant. Figure 4.1 illustrates a model of the GMAW process with input and output variables. Appendix B shows experimental conditions and their limits to investigate the relationship between input and output variables which based on experimental runs and criterion being good weld bead appearance and configurations. The other welding process parameters were fixed as following:

(1) Polarity: negative.

(2) Electrode extension: 15 mm.

(3) Electrode orientation: 90 degrees.

(4) Material thickness: 12 mm.

(5) Shielding gas : 80% A_r + 20% CO_2.

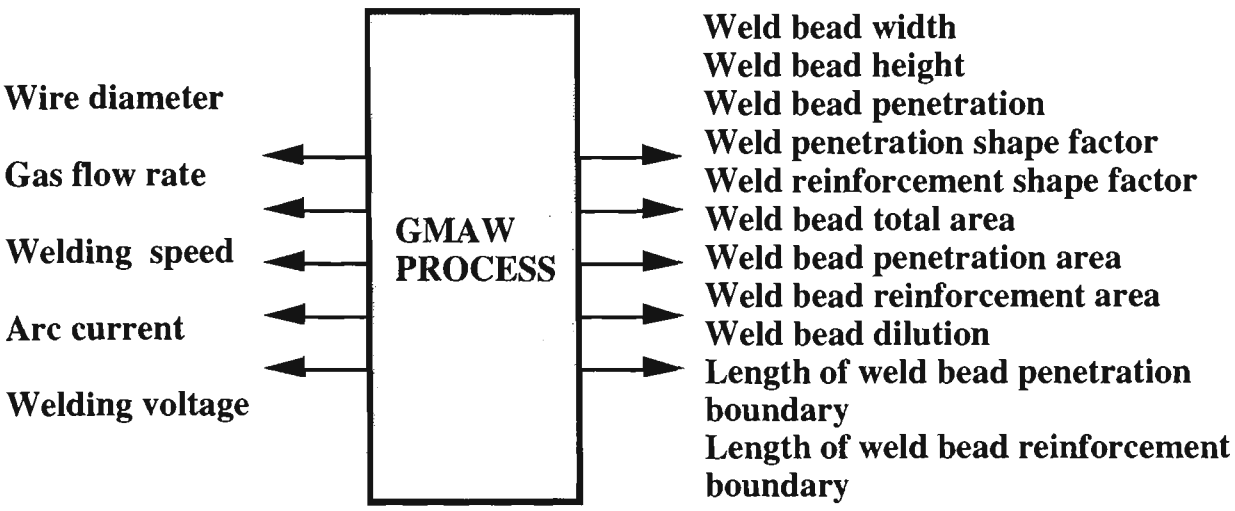

Figure 4.1 A model of GMAW process with input and output parameters.

4.2.2 Definition of Weld Bead Geometry

To investigate the effects of the welding process parameters on the resultant GMAW, a number of output variables called weld bead geometry were measured from the specimens of the workpiece. A definition of weld bead geometry, as the basic of a control system for the automatic and/or robotic GMAW process, describes its shape and derives other dimensions which should be meaningful in determining the acceptability of the weld. These parameters also determine the basic mechanical properties of the weld and the basic stress handling capabilities of the joints. Figure 4.2 gives a schematic representation in which weld bead dimensions will be defined as follow:

(1) Weld bead width.

(2) Weld bead height.

(3) Weld bead penetration.

(4) Weld penetration shape factor, the ratio of weld bead penetration to weld bead width.

(5) Weld reinforcement shape factor, the ratio of weld bead height to weld bead width.

(6) Weld bead total area.

(7) Weld bead penetration area.

(8) Weld bead reinforcement area.

(9) Weld bead dilution, the ratio of weld bead penetration area to weld bead total area at a given cross section.

(10) Length of weld bead penetration boundary.

(11) Length of weld bead reinforcement boundary.

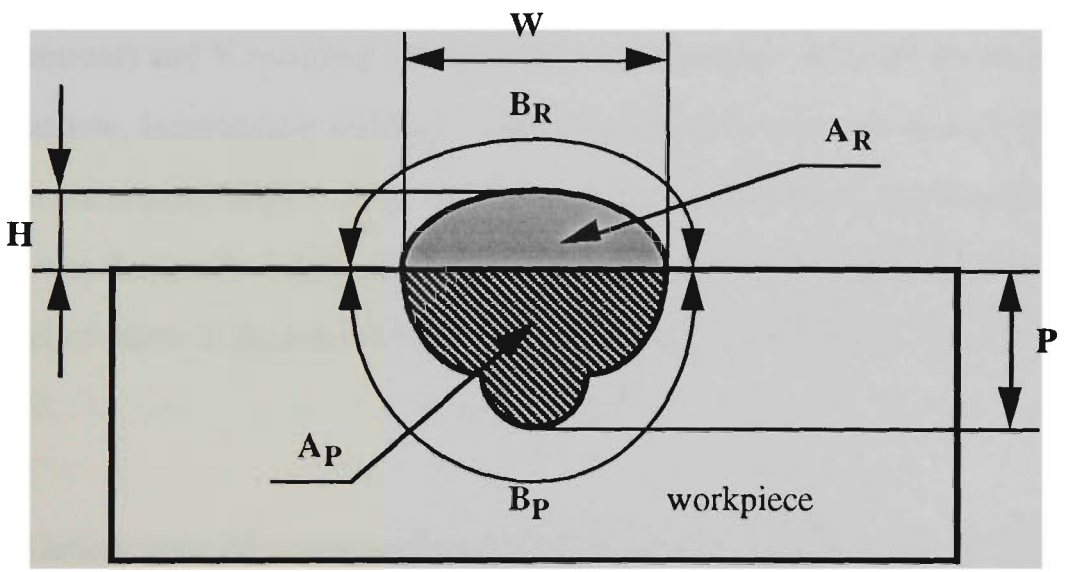

B	Weld bead width
H	Weld bead height
P	Weld bead penetration
A_P	Weld bead penetration area
A_R	Weld bead reinforcement area
B_P	Length of weld bead penetration boundary
B_R	Length of weld bead reinforcement boundary

Figure 4.2 Schematic representation of weld bead dimensions.

4.2.3 Development of Design Matrix

This experiment plan, a 3^5 fractional factorial experiment which could be expected to provide sufficient data for determining the relationship and interaction between the welding process parameters and weld bead dimensions, was designed on three levels around the limitations described above (see Appendix B). The levels were selected, partly in anticipation of known consequences of change and partly in respect of quality control. Conventionally welding process parameters in the fractional factorial designs are known as factors and weld bead geometry as effects. In all planes, the 5 factors were denoted by capital letter D (wire diameter), G (gas flow rate), S (welding speed), I (arc current) and V (welding voltage) and investigated at the three levels of each factor as low, intermediate and high. They were designated by the digits 0 (low), 1 (intermediate) and 2 (High). Each treatment combination in the 3^5 fractional factorial design was designated by X_1, X_2, X_3, X_4, X_5, where X_1 is the level of factor D, X_2 the level of factor G, X_3 the level of factor S, X_4 the level of factor I, X_5 the level of factor V.

Capital letters were also employed to present the various main effects and interactions associated with the respective factors. Main effects had 2 degrees of freedom and were designed by capital letters alone. Two factor interactions had 4 degrees of freedom and could be split into two parts, each having 2 degrees of freedom. With respect to factors D and G, the parts of two factor interactions were denoted by DG and DG^2. For finding the effects of 5 independent factors, a three level full factorial design should require 243 trials. However, a half replicate of tests of 81 trials for fitting each equation called a fractional factorial design was employed to evaluate the main and interaction effects of five factors at three levels rather than a full experiment of 243 tests. Appendix B shows the combinations of factor levels, for each of which the eleven effects were measured.

In this chapter, experimental results for studying linear and first order interactive effects between five welding process parameters and eleven weld bead dimensions, were only employed for fitting the response curve. The chosen factors were wire diameter, gas flow rate, welding speed, arc current and welding voltage. The response was weld bead width, weld bead height, weld bead penetration, weld penetration shape factor, weld reinforcement shape factor, weld bead total area, weld bead penetration area, weld bead reinforcement area, weld bead dilution, length of weld bead penetration boundary and length of weld bead reinforcement boundary.

4.2.4 Experimental Procedure

81 welded samples from AS 1204 mild steel flats adopting the bead-on-plate technique were employed in the experiment because the workpiece offered a convenient reference plane for measurement of weld bead geometry, and the influences arising from joint preparation were removed. The chemical composition of weld material and the three different wire diameters (0.9, 1.2 and 1.6 mm) were the same employed in chapter 3. Experimental test plates were located in the fixture jig by the robot controller and the required input weld conditions were fed into the particular weld steps. With welder and shield gas turned on, the robot was initialised and welding was executed. This continued until the fractional factorial experimental design runs were completed.

The measurements of weld bead geometry as shown in figure 4.2 were made using a metallurgical microscope interfaced with an image analysis system. Images are represented by a 256 level Gray scale, and the program can be employed to identify areas of the same shade and to calculate the distance between them or their individual area. The fractional factorial matrix was assumed to link the mean values of the eleven measured results with changes in the five welding process parameters for determining local features of the response surface.

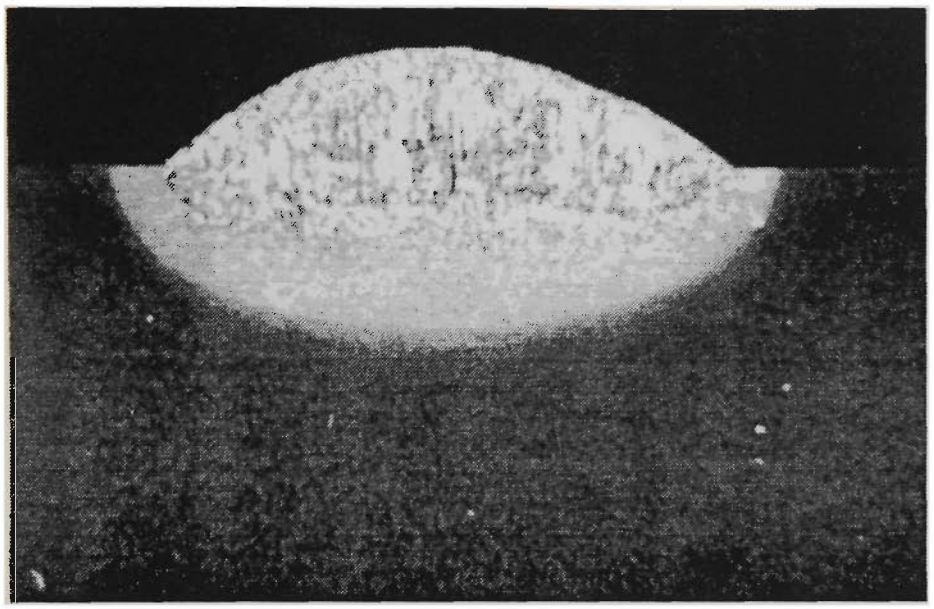

(a)

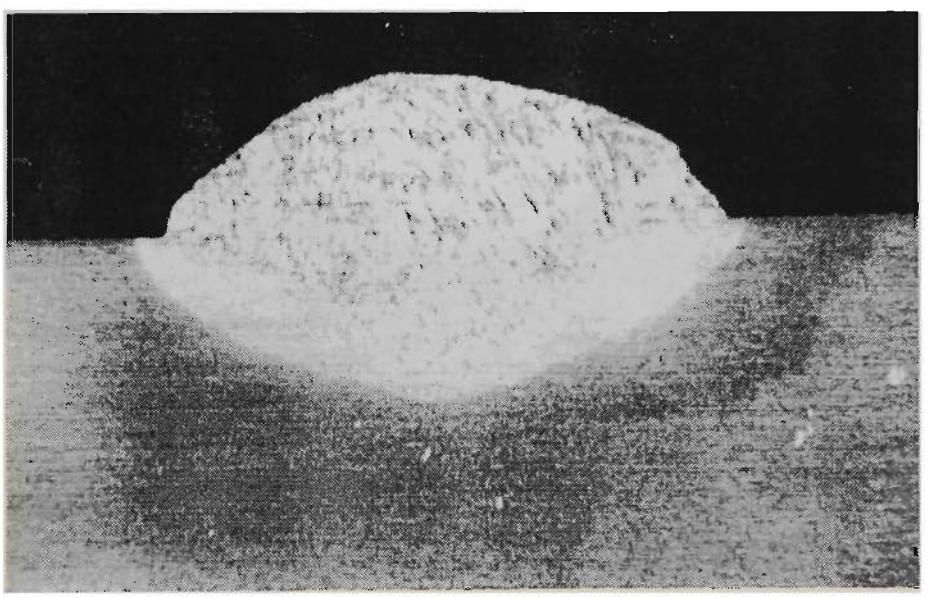

(b)

Figure 4.3 Metallurgical sections of welds according to the various combination of welding process parameters.
(a) D=1.2 mm, G=6 ℓ, S=250 mm/min, I=180 Amp, V=30 Volt
(b) D=1.2 mm, G=6 ℓ, S=330 mm/min, I=360 Amp, V=30 Volt

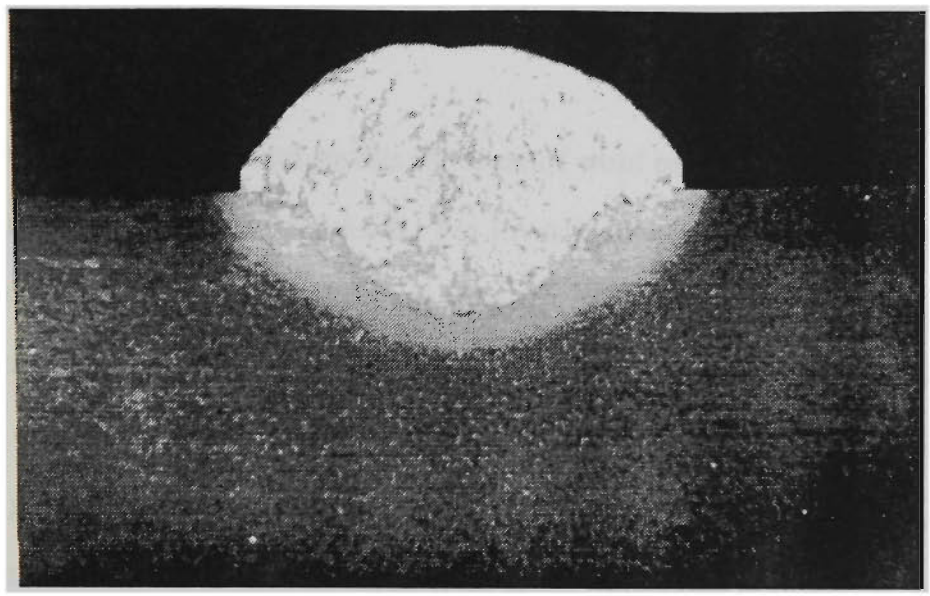

(c)

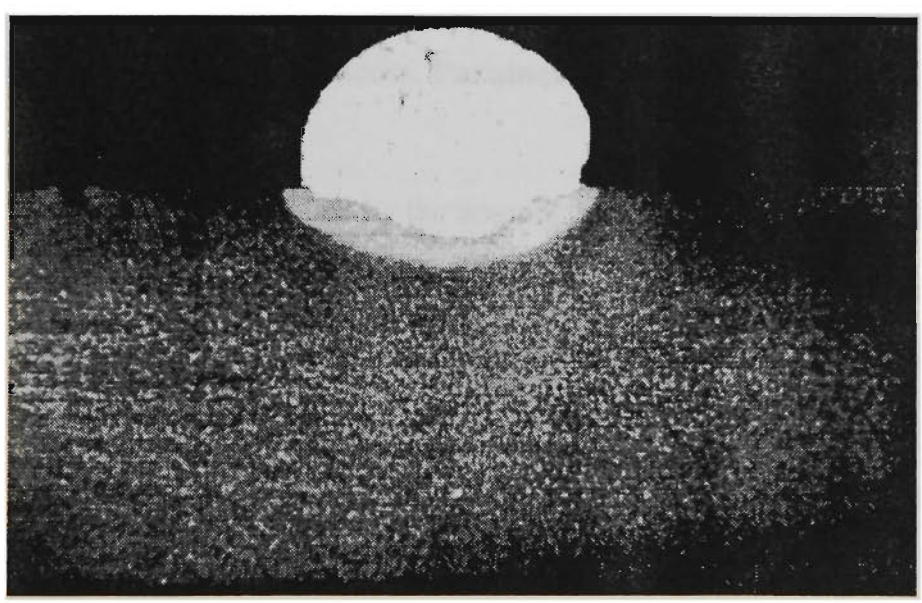

(d)

Figure 4.3 Metallurgical sections of welds according to the various combination of welding process parameters.
(c) D=1.6 mm, G=6 ℓ, S=410 mm/min, I=360 Amp, V=20 Volt
(d) D=0.9 mm, G=6 ℓ, S=330 mm/min, I=250 Amp, V=20 Volt.

4.3 EXPERIMENTAL RESULTS AND DISCUSSION

The summary of experimental results in terms of weld process parameters and weld bead geometry is given in Appendix B. For investigating weld quality and measuring weld bead geometry, the metallurgical sections of four welds made using various welding process parameters are also presented in figure 4.3. Figures 4.4 to 4.14 show the effect of each welding process parameter on the weld bead width, weld bead height, weld bead penetration, weld penetration shape factor, weld reinforcement shape factor, weld bead total area, weld bead penetration area, weld bead reinforcement area, weld bead dilution, length of weld bead penetration boundary and length of weld bead reinforcement boundary.

4.3.1 Effects of Welding Process Parameters on Weld Bead Width

The weld bead width is determined by the amount of the wire melting and the manner in which this molten metal is spread over the workpiece surface. The factors that affect the melting rate are arc current, wire diameter and electrode extension [Chandel (1988)[24] and Raveendra and Parmar (1987)[150]]. The mode of spreading over the workpiece surface is governed by welding voltage, wire diameter and welding speed [Chandel (1988)[24] and Raveendra and Parmar (1987)[150]]. Figures 4.4 (a) - (d) show the effects of five welding process parameters on weld bead width. The coupled effects of gas flow rate and wire diameter on the average weld bead width are represented in figure 4.4 (a). The average weld bead widths were calculated by taking the average of all measured values with the same gas flow rate for a particular wire diameter, but without considering the effects of welding speed, arc current and welding voltage. It is evident that a higher weld bead width is obtained with a larger wire diameter, while the effect of gas flow rate on weld bead width seems to have little significance. Figure 4.4 (b) shows the average weld bead width against welding speed for wire diameters of 0.9, 1.2 and 1.6 mm.

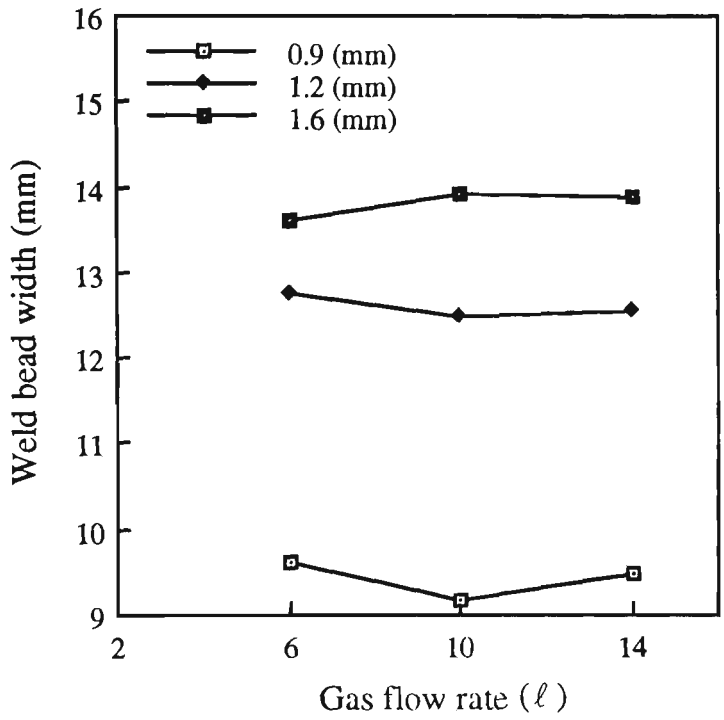

Figure 4.4 (a) The effect of gas flow rate on average weld bead width.

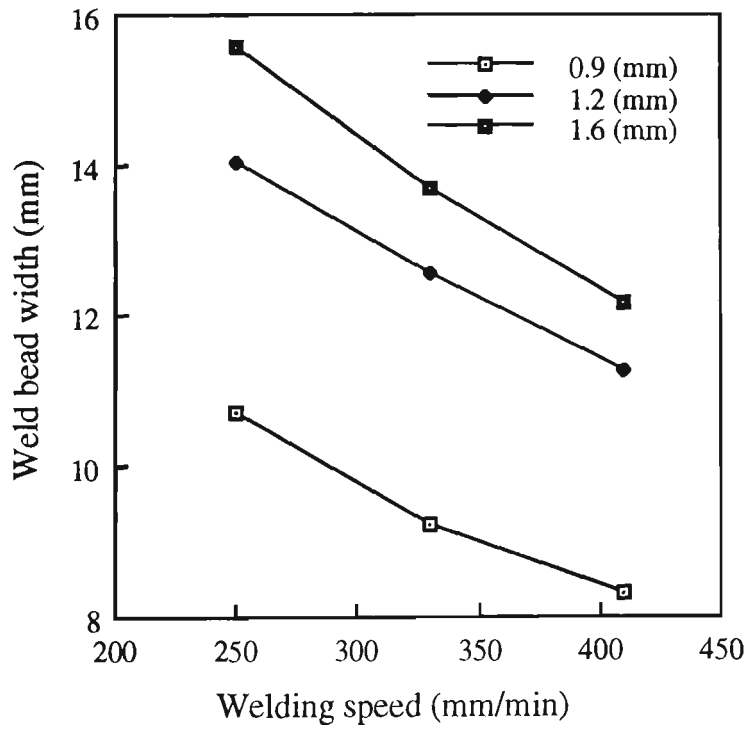

Figure 4.4 (b) The effect of welding speed on average weld bead width.

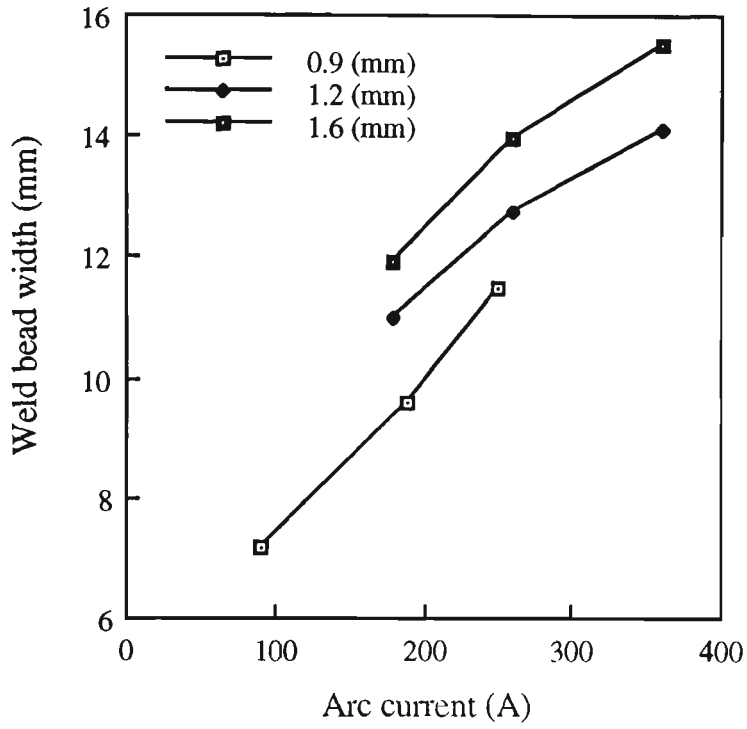

Figure 4.4 (c) The effect of arc current on average weld bead width.

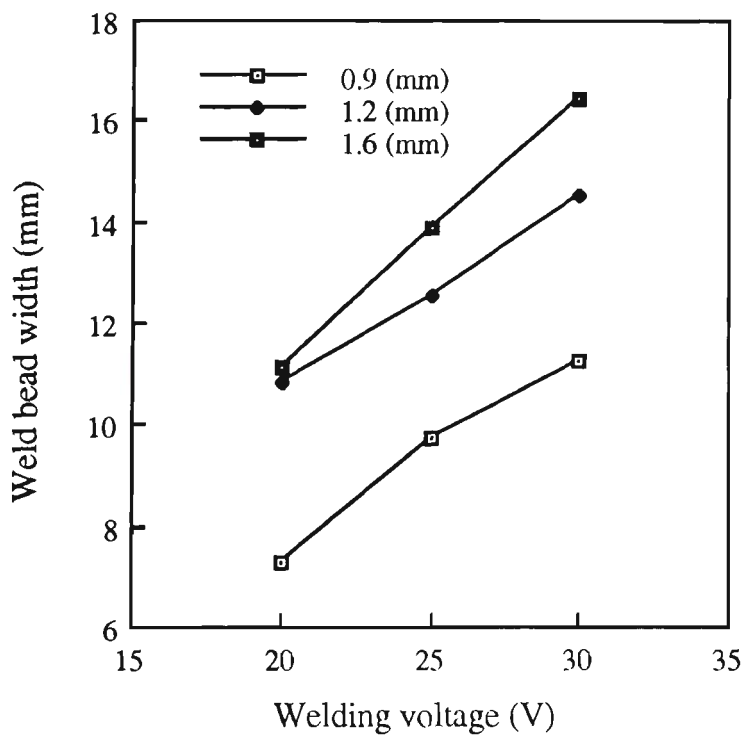

Figure 4.4 (d) The effect of welding voltage on average weld bead width.

Weld bead widths were produced by taking the average of all values for welds deposited with the same welding speed for a given wire diameter, but ignoring the effects of gas flow rate, arc current and welding voltage. It is noted that there is a decrease in weld bead width as welding speed increases.

Figure 4.4 (c) presents the effect of arc current on weld bead width for three different wire diameters, respectively. The average weld bead widths were found by taking the average of all measured values with the same arc current for a particular wire diameter, without taking account of the effects of gas flow rate, welding speed and welding voltage. It can be seen from figure 4.4 (c) that the weld bead width increases as arc current increases. The effect of welding voltage on weld bead width is shown in figure 4.4 (d). The average weld bead widths were produced by taking the average of all measured values with the same welding voltage for a specific wire diameter, yet ignoring the effects of gas flow rate, welding speed and arc current. It is apparent from figure 4.4 (d) that the weld bead width increases when there is an increase in welding voltage.

4.3.2 Effects of Welding Process Parameters on Weld Bead Height

The effects of five welding process parameters on weld bead height are shown in figures 4.5 (a) - (d). The coupled effects of gas flow rate and wire diameter on the average weld bead height are represented in figure 4.5 (a), which indicate that there is a decrease in weld bead height with an increase in the gas flow rate and wire diameter. Weld bead heights were computed by taking the average of all measured values for welds deposited with the same gas flow rate for a particular wire diameter, but without considering the effects of welding speed, arc current and welding voltage. Figure 4.5 (b) displays the effect of welding speed on weld bead height for a specific wire diameter. Weld bead heights were produced by taking the average of all values for welds with the same welding speed, but ignoring the effects of gas flow rate, arc

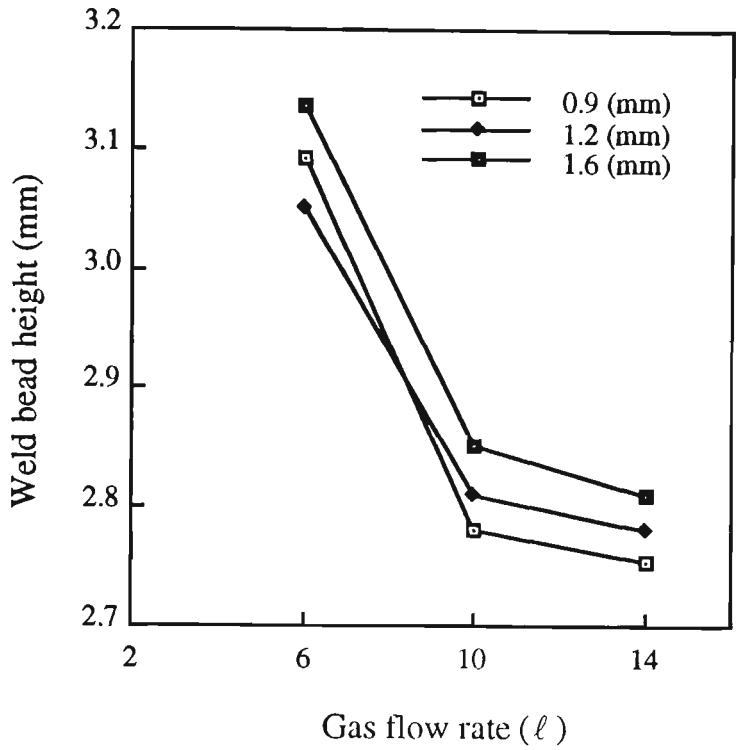

Figure 4.5 (a) The effect of gas flow rate on average weld bead height.

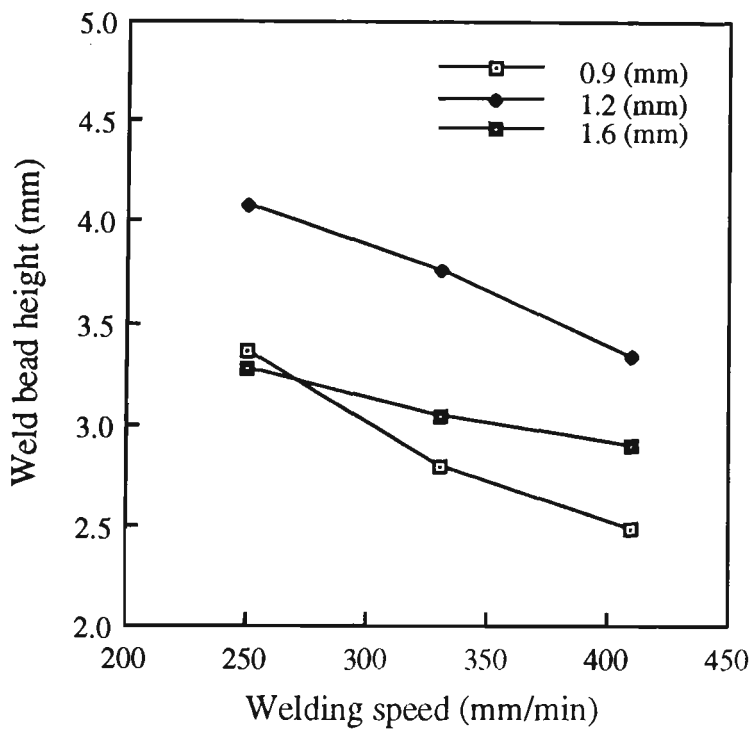

Figure 4.5 (b) The effect of welding speed on average weld bead height.

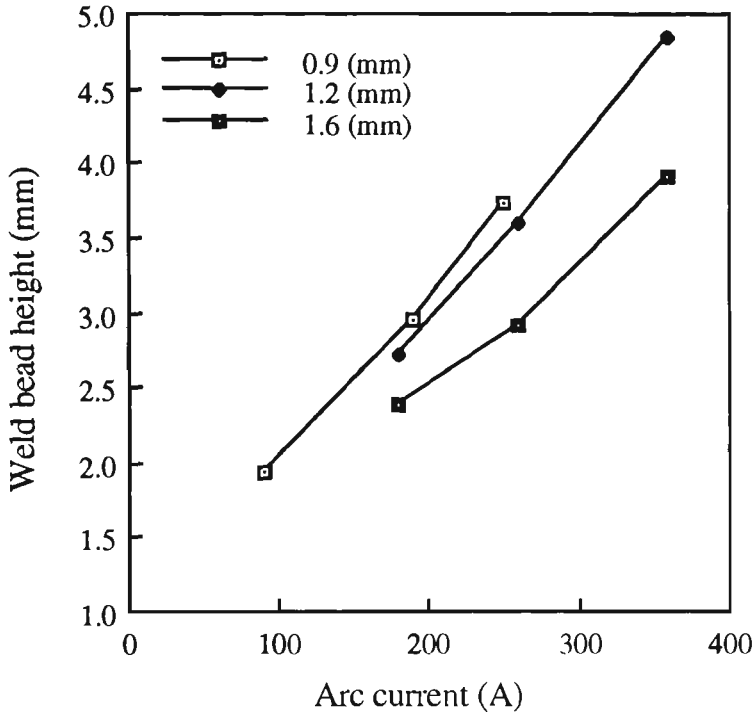

Figure 4.5 (c) The effect of arc current on average weld bead height.

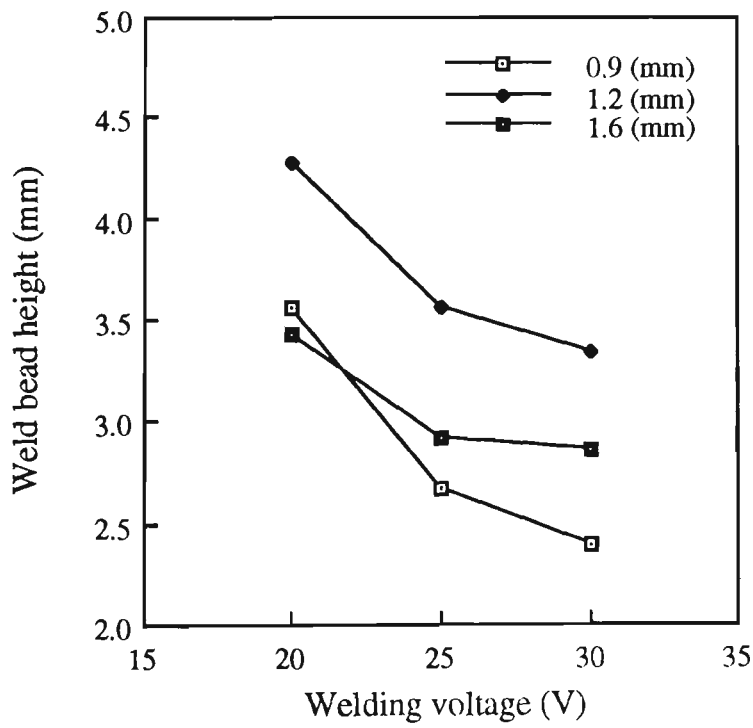

Figure 4.5 (d) The effect of welding voltage on average weld bead height.

current and welding voltage. As shown in figure 4.5 (b), it is evident that for a particular wire diameter, there is a decrease in weld bead height as welding speed increases.

Figure 4.5 (c) reveals the average weld bead height against arc current for a given wire diameter. It is evident from figure 4.5 (c) that the weld bead height increases when arc current increases. The average weld bead heights were found by taking the average of all measured values with the same arc current for a given wire diameter, but without taking account of the effects of gas flow rate, welding speed and welding voltage. Figure 4.5 (d) shows the effect of welding voltage on weld bead height for a particular wire diameter. Weld bead heights were counted by taking the average of all measured values with the same welding voltage for a specific wire diameter, yet ignoring the effects of gas flow rate, welding speed and arc current. Evidence from figure 4.5 (d) shows that the weld bead height decreases when there is an increase in welding voltage.

4.3.3 Effects of Welding Process Parameters on Weld Bead Penetration

The weld bead penetration is the result of the workpiece melting. As a result, welding process parameters influence the weld bead penetration. The effects of five welding process parameters on weld bead penetration are given in Figures 4.6 (a) - (d). Figure 4.6 (a) shows the effects of gas flow rate and wire diameter on the average weld bead penetration. The average weld bead penetrations were adjusted by taking the average of all measured values with the same gas flow rate for a particular wire diameter, but without considering the effects of welding speed, arc current and welding voltage. It can be seen here that a higher weld bead penetration is obtained with a larger wire diameter, while the effect of gas flow rate on weld bead penetration seems to have little significance.

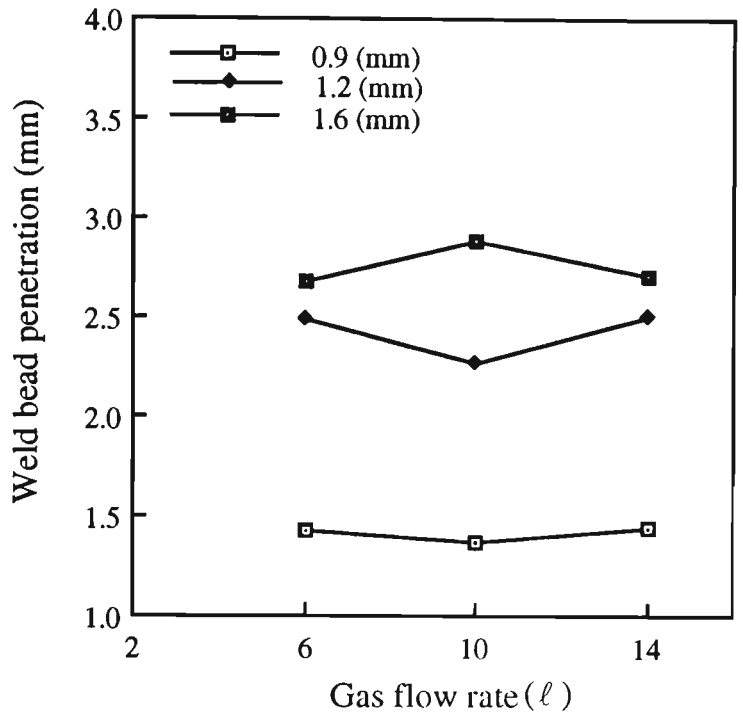

Figure 4.6 (a) The effect of gas flow rate on average weld bead penetration.

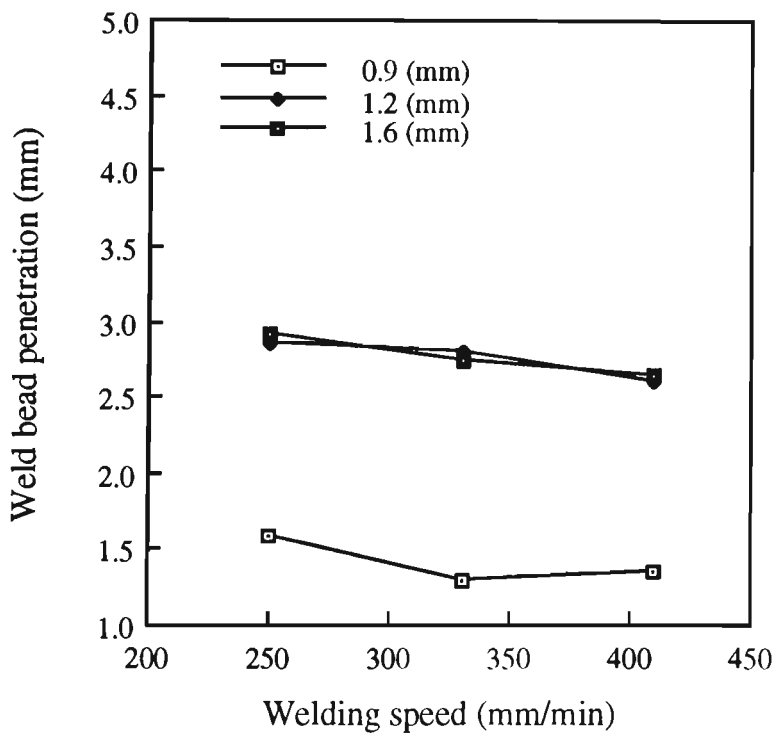

Figure 4.6 (b) The effect of welding speed on average weld bead penetration.

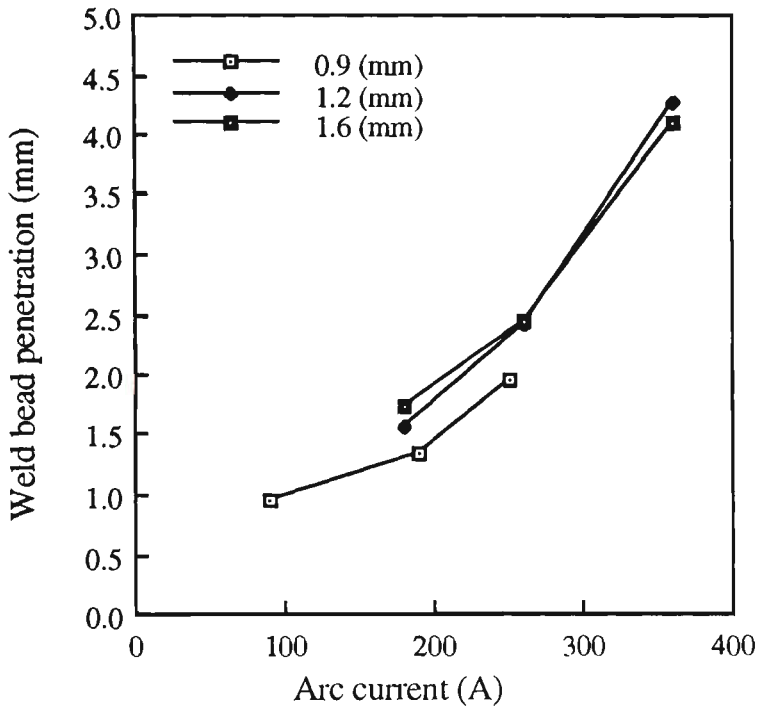

Figure 4.6 (c) The effect of arc current on average weld bead penetration.

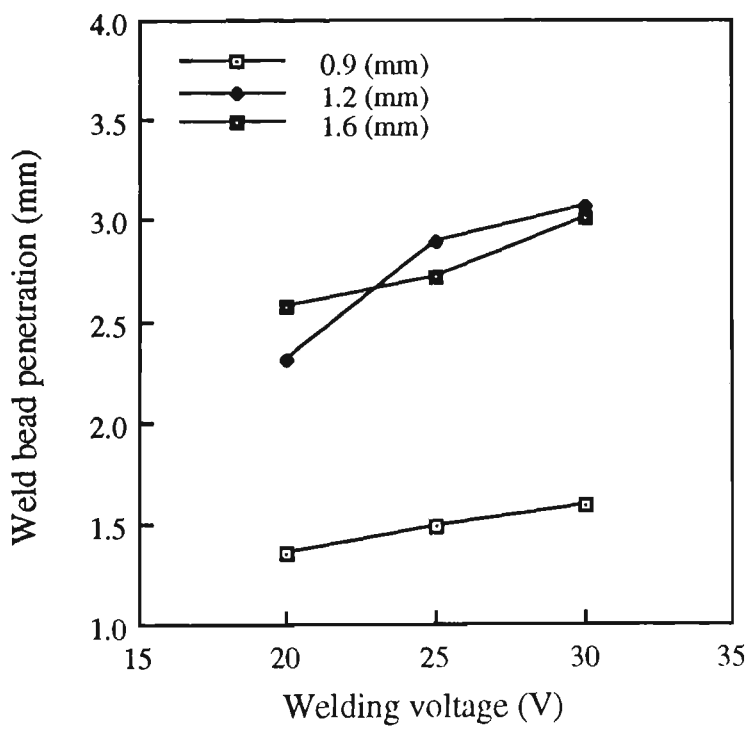

Figure 4.6 (d) The effect of welding voltage on average weld bead penetration.

The effect of welding speed on average weld bead penetration shown in figure 4.6 indicates that there is a decrease in weld bead penetration as welding speed increases. The average weld bead penetrations were produced by taking the average of all values for welds deposited with the same welding speed for a specific wire diameter, but ignoring the effects of gas flow rate, arc current and welding voltage.

When arc current increases, the weld bead penetration increases as can be seen in figure 4.6 (c). The average weld bead penetrations were found by taking the average of all measured values with the same arc current for a given wire diameter, without taking account of the effects of gas flow rate, welding speed and welding voltage. Figure 4.6 (d) displays the effect of welding voltage on weld bead penetration for a given wire diameter. Weld bead penetrations were produced by taking the average of all measured values for welds deposited with the same welding voltage for a specific wire diameter, yet ignoring the effects of gas flow rate, welding speed and arc current. It seems from figure 4.6 (d) that there is an increase in weld bead penetration as welding voltage increases.

4.3.4 Effects of Welding Process Parameters on Weld Penetration Shape Factor

Figures 4.7 (a) - (d) exhibit the effects of five welding process parameters on weld penetration shape factor. The effect of gas flow rate on the average weld penetration shape factor for a particular wire diameter is represented in figure 4.7 (a), which represents that there is a decrease in weld penetration shape factor with larger wire diameter, and the effect of gas flow rate on weld penetration shape factor seems to have little significance. Weld penetration shape factors were computed by taking the average of all measured values with the same gas flow rate for a particular wire diameter, but without considering the effects of welding speed, arc current and welding voltage.

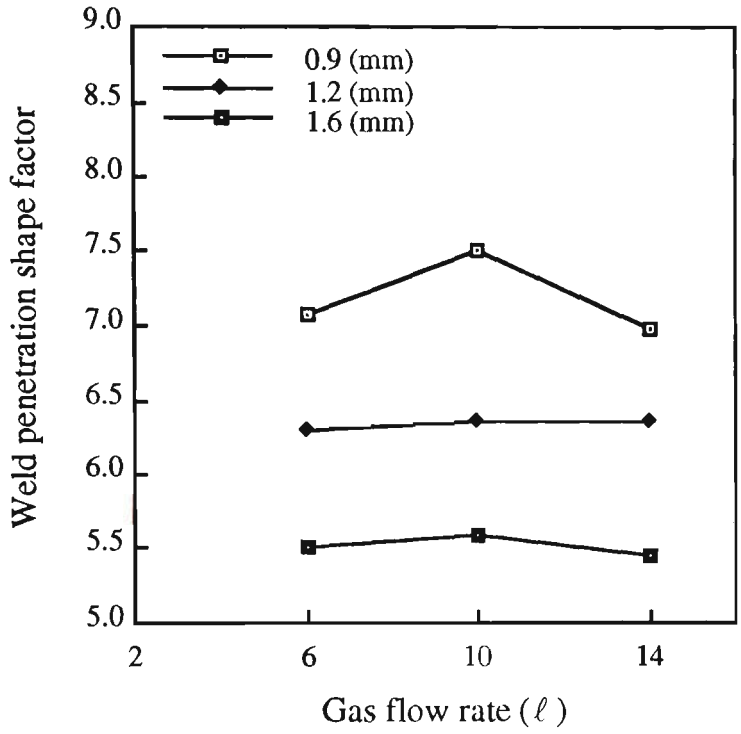

Figure 4.7 (a) The effect of gas flow rate on average weld penetration shape factor.

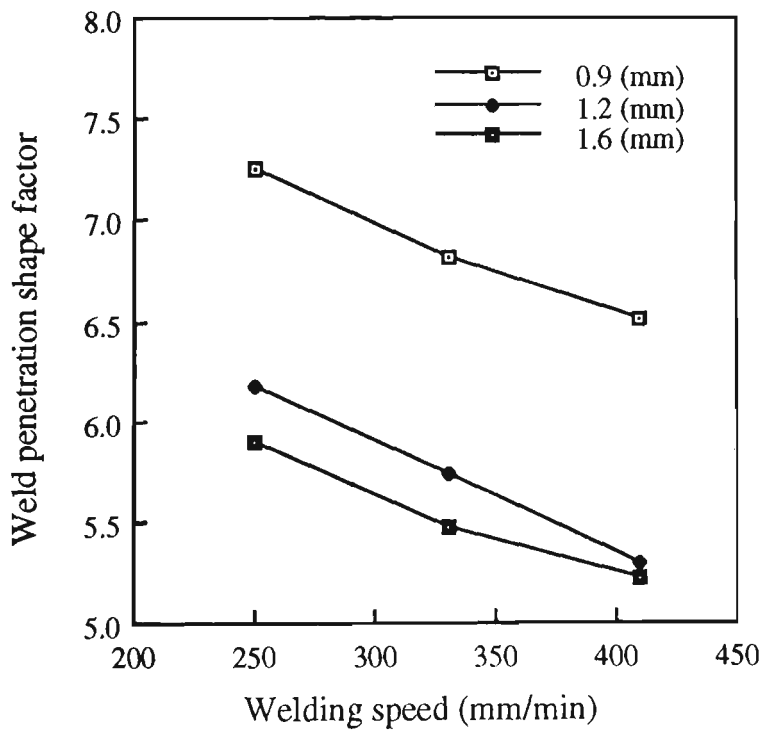

Figure 4.7 (b) The effect of welding speed on average weld penetration shape factor.

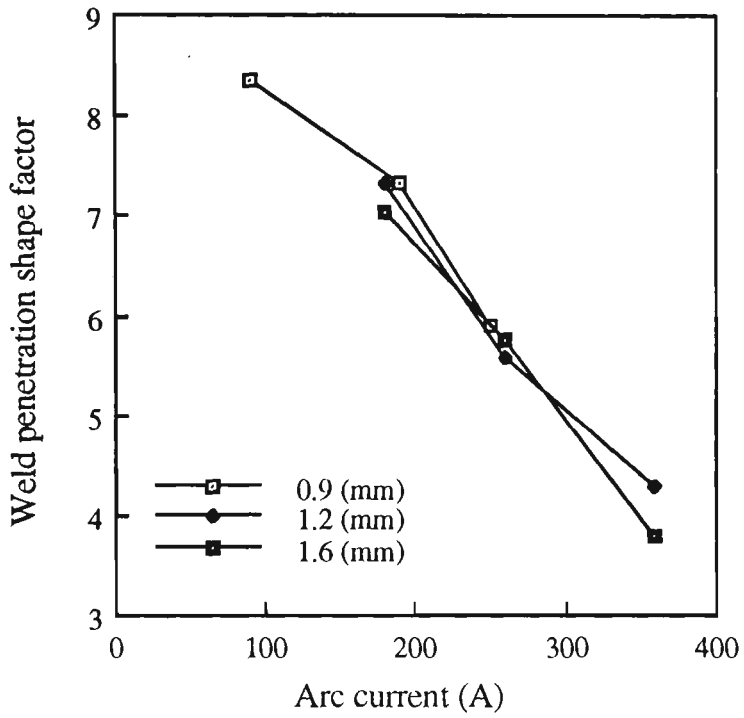

Figure 4.7 (c) The effect of arc current on average weld penetration shape factor.

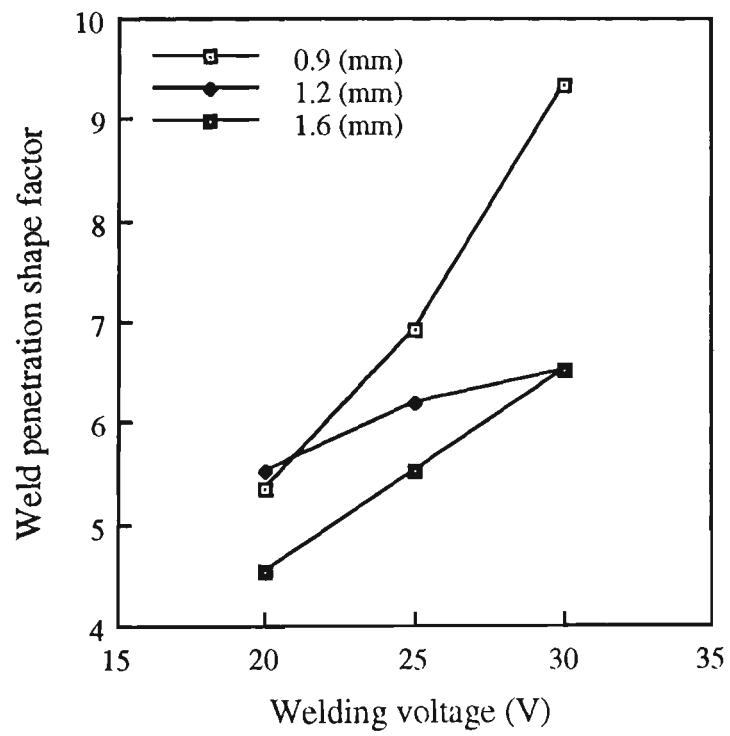

Figure 4.7 (d) The effect of welding voltage on average weld penetration shape factor.

When higher welding speeds are used, a lower weld penetration shape factor is achieved as can be seen in figure 4.7 (b). Weld penetration shape factors were calculated by taking the average of all values for welds deposited with the same welding speed for a particular wire diameter, but ignoring the effects of gas flow rate, arc current and welding voltage.

Figure 4.7 (c) presents the effect of the arc current on weld penetration shape factor for three different wire diameters. As shown in figure 4.7 (c), weld penetration shape factor decreases when arc current increases. Weld penetration shape factors were adjusted by taking the average of all measured values for welds deposited with the same arc current for a particular wire diameter, but without taking account of the effects of gas flow rate, welding speed and welding voltage. The effect of welding voltage on weld penetration shape factor shown in figure 4.7 (d) illustrates that the weld penetration shape factor increases with an increase in welding voltage. Weld penetration shape factors were calculated by taking the average of all measured values with the same welding voltage for a given wire diameter, yet ignoring the effects of gas flow rate, welding speed and arc current.

4.3.5 Effects of Welding Process Parameters on Weld Reinforcement Shape Factor

The relationship between five welding process parameters and weld reinforcement shape factor is shown in figures 4.8 (a) - (d). The coupled effects of gas flow rate and wire diameter on average weld reinforcement shape factor represented in figure 4.8 (a) indicate that a higher weld reinforcement shape factor is obtained with a larger wire diameter, while the effect of gas flow rate on weld reinforcement shape factor does not seem to have any significant effect. Weld reinforcement shape factors were calculated by taking the average of all measured values with the same gas flow rate for a particular wire diameter, but without considering the effects of welding speed, arc

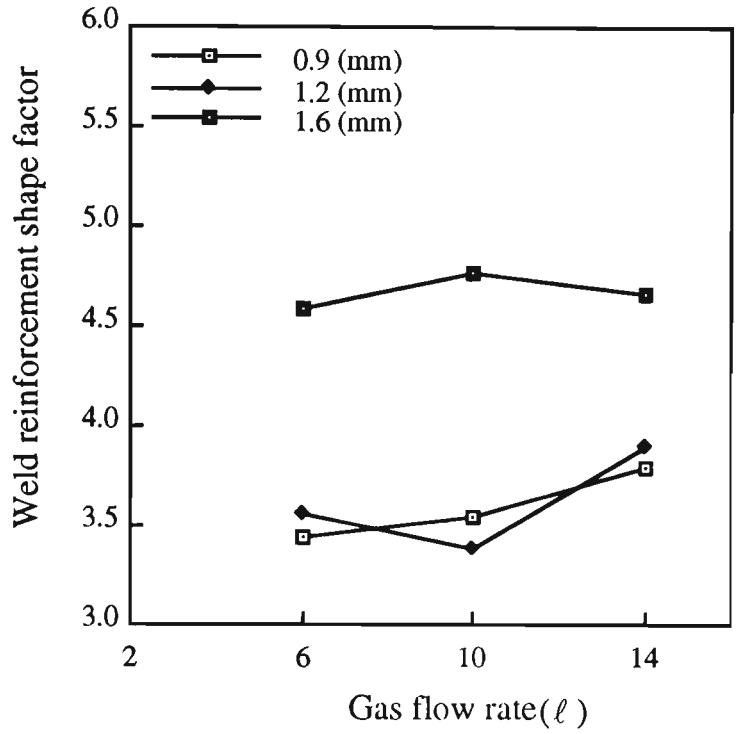

Figure 4.8 (a) The effect of gas flow rate on average weld reinforcement shape factor.

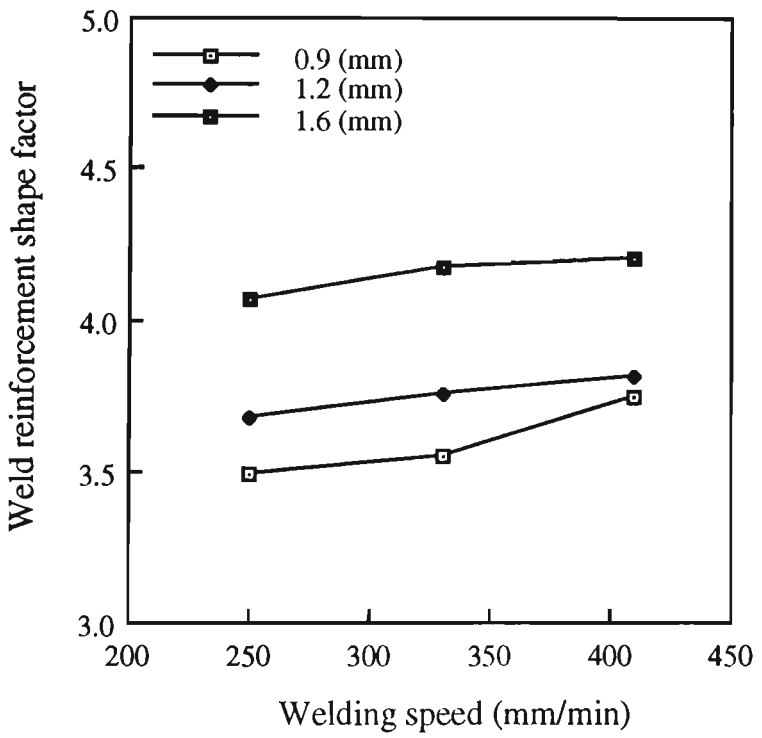

Figure 4.8 (b) The effect of welding speed on average weld reinforcement shape factor.

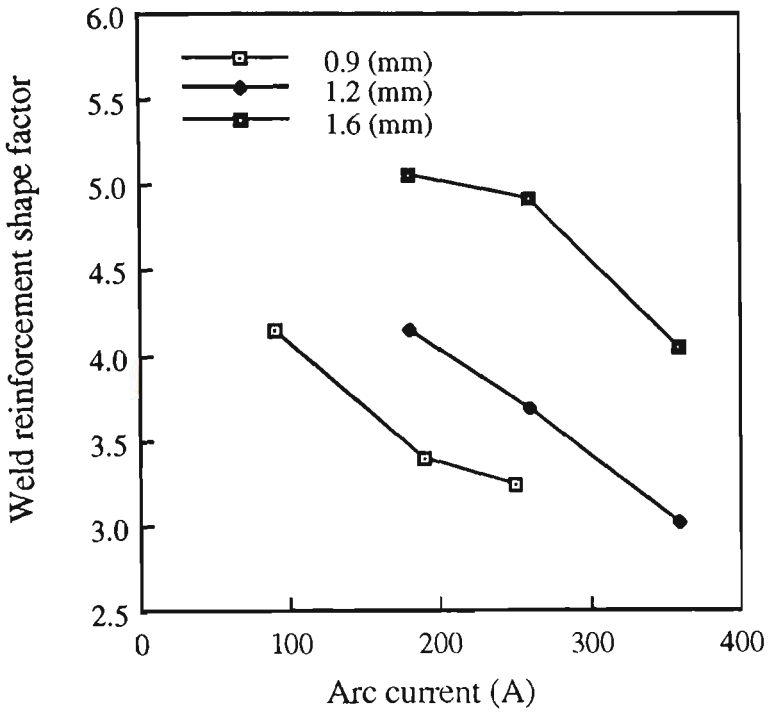

Figure 4.8 (c) The effect of arc current on average weld reinforcement shape factor.

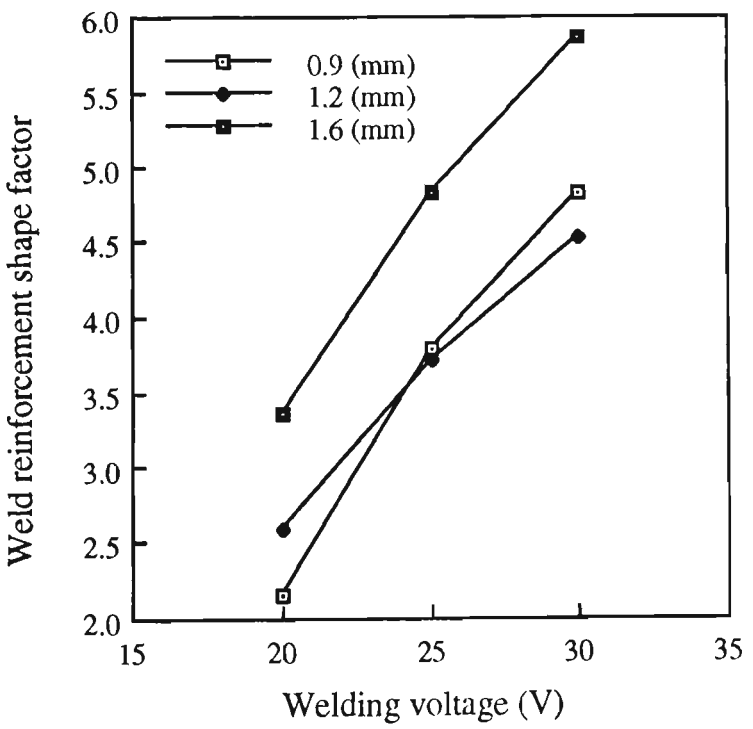

Figure 4.8 (d) The effect of welding voltage on average weld reinforcement shape factor.

current and welding voltage. Figure 4.8 (b) shows the effect of welding speed on weld reinforcement shape factor for a specific wire diameter. The average weld reinforcement shape factors were produced by taking the average of all values for welds deposited with the same welding speed for a given wire diameter, but ignoring the effects of gas flow rate, arc current and welding voltage. It is evident from figure 4.8 (b) that there is no significant effect on weld reinforcement shape factor when welding speed increases.

Figure 4.8 (c) illustrates that the weld reinforcement shape factor decreases as arc current increases. Weld reinforcement shape factors were found by taking the average of all measured values with the same arc current for a particular wire diameter, without taking account of the effects of gas flow rate, welding speed and welding voltage. The effect of welding voltage on weld reinforcement shape factor shown in figure 4.8 (d) indicates that there is an increase in weld reinforcement shape factor when welding voltage increases. The average weld reinforcement shape factors were produced by taking the average of all measured values with the same welding voltage for a specific wire diameter, yet ignoring the effects of gas flow rate, welding speed and arc current.

4.3.6 Effects of Welding Process Parameters on Weld Bead Total Area

The weld bead total area is comprised of the workpiece and wire melting area so that any welding process parameter will eventually influence the weld bead total area. It is well known that higher wire melting rates are obtained when higher current and smaller wire diameter are employed [Chandel (1988)[24] and Raveendra and Parmar (1987)[150]]. Figures 4.9 (a) - (d) display the effects of five welding process parameters on weld bead total area. The coupled effects of gas flow rate and wire diameter on average weld bead total area are represented in figure 4.9 (a), which indicate that a higher weld bead total area is obtained with a larger wire diameter, while the effect of gas flow rate on weld bead total area does not seem to

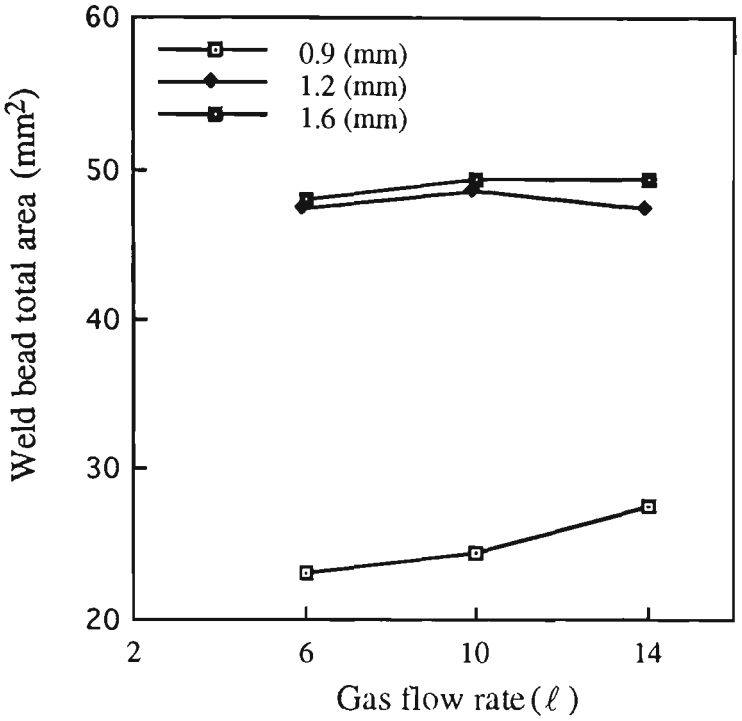

Figure 4.9 (a) The effect of gas flow rate on average weld bead total area.

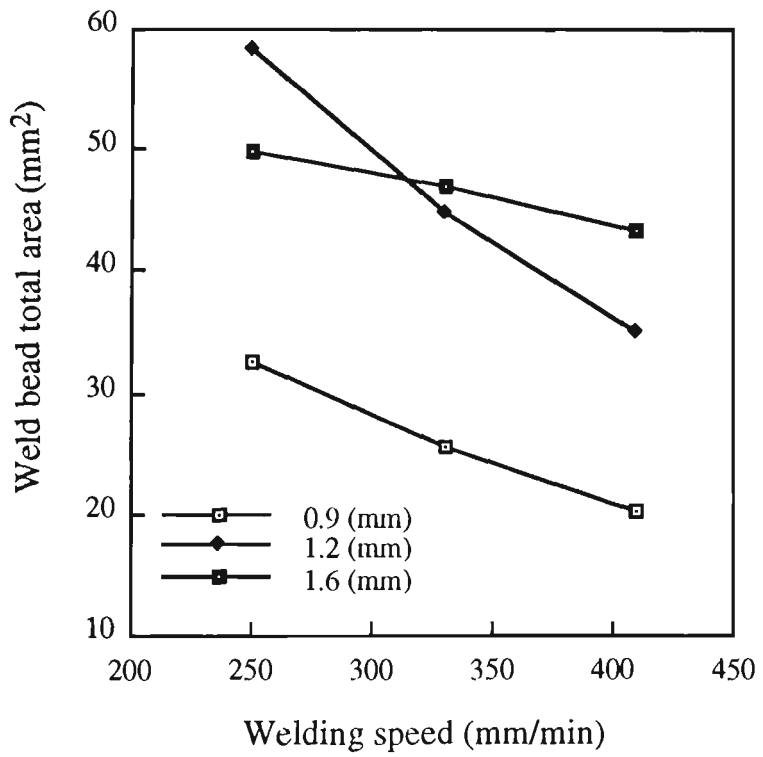

Figure 4.9 (b) The effect of welding speed on average weld bead total area.

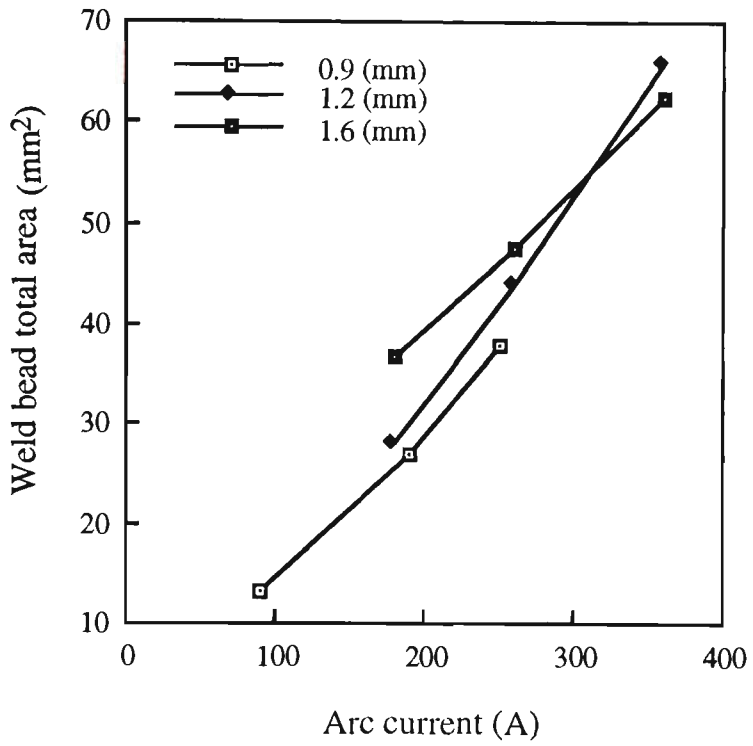

Figure 4.9 (c) The effect of arc current on average weld bead total area.

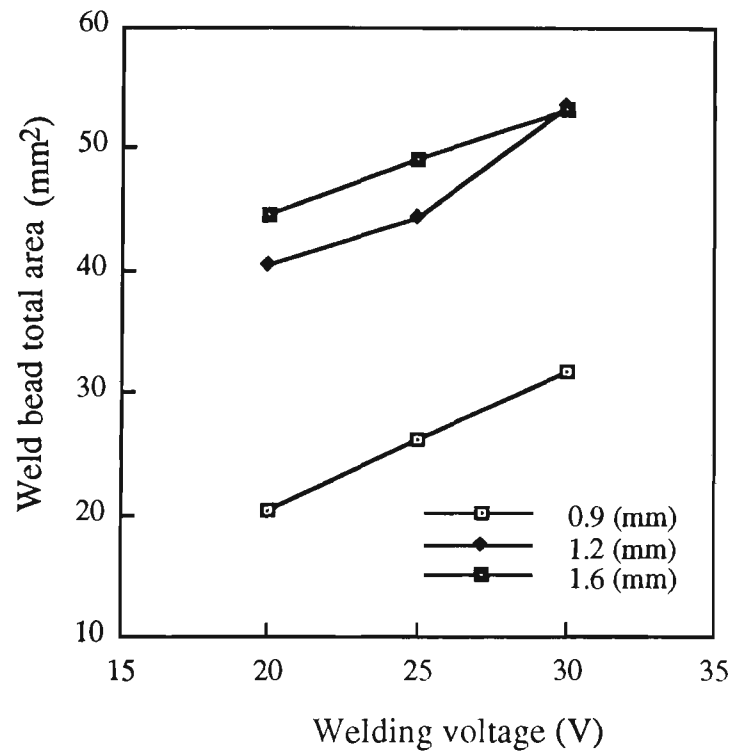

Figure 4.9 (d) The effect of welding voltage on average weld bead total area.

have any significant effect. The average weld bead total areas were calculated by taking the average of all measured values with the same gas flow rate for a particular wire diameter, but without considering the effects of welding speed, arc current and welding voltage. Figure 4.9 (b) shows the effect of welding speed on the average weld bead total area for a specific wire diameter. Weld bead total areas were produced by taking the average of all values for welds deposited with the same welding speed for a specific wire diameter, but ignoring the effects of gas flow rate, arc current and welding voltage. It is evident from figure 4.9 (b) that there is a decrease in weld bead total area as welding speed increases.

When a higher arc current is used, a higher weld bead total area is produced as can be seen in figure 4.9 (c). Weld bead total areas were found by taking the average of all measured values with the same arc current for a particular wire diameter, but without taking account of the effects of gas flow rate, welding speed and welding voltage. The effect of welding voltage on weld bead total area is shown in figure 4.9 (d), which indicates that there is an increase in weld bead total area as welding voltage increases. The average weld bead total areas were produced by taking the average of all measured values for welds deposited with the same welding voltage for a specific wire diameter, yet ignoring the effects of gas flow rate, welding speed and arc current.

4.3.7 Effects of Welding Process Parameters on Weld Bead Penetration Area

The effects of the five welding process parameters on weld bead penetration area are exhibited in figures 4.10 (a) - (d). The effects of gas flow rate and wire diameter on average weld bead penetration area are represented in figure 4.10 (a) which indicate that there is an increase in weld bead reinforcement area as wire diameter is increased, but the effect of gas flow rate on weld bead penetration area seems to have little significance.

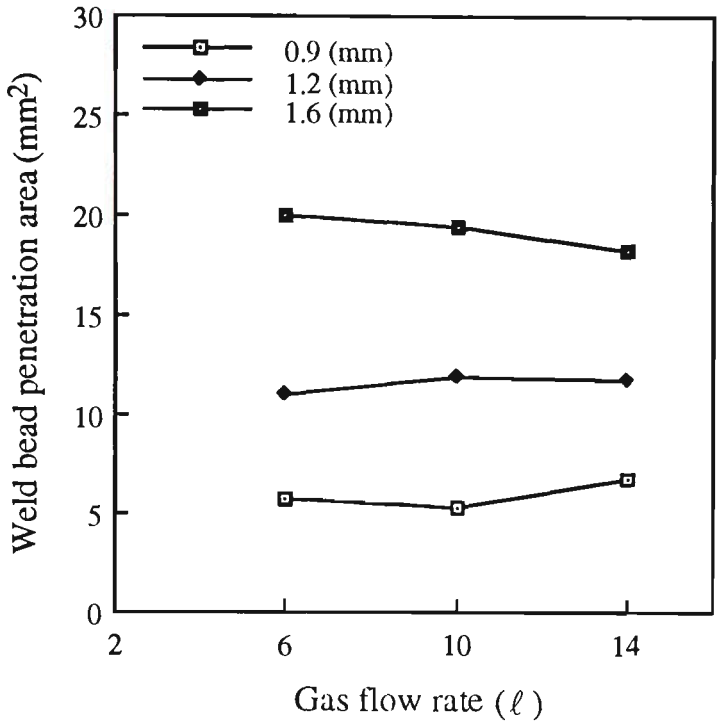

Figure 4.10 (a) The effect of gas flow rate on average weld bead penetration area.

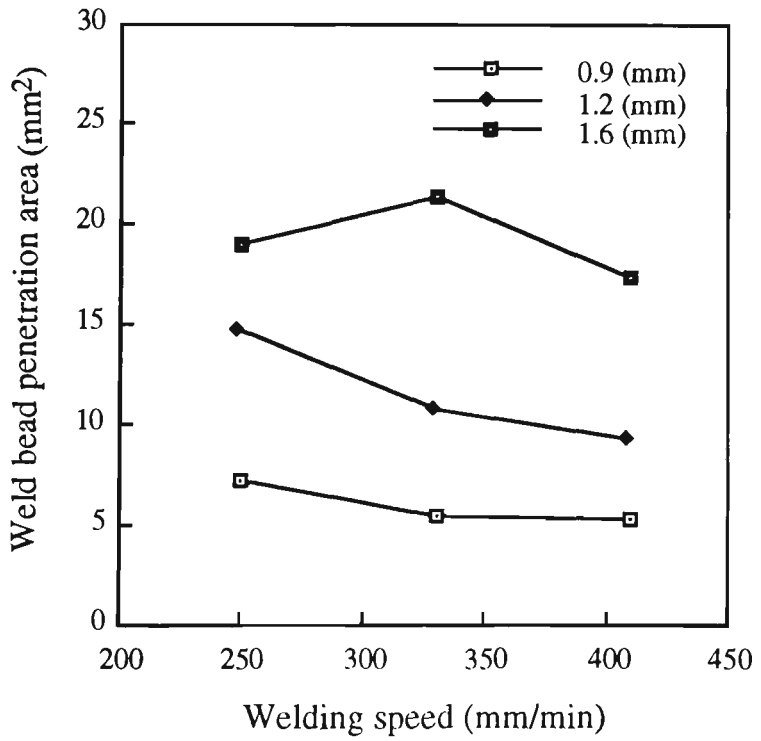

Figure 4.10 (b) The effect of welding speed on average weld bead penetration area.

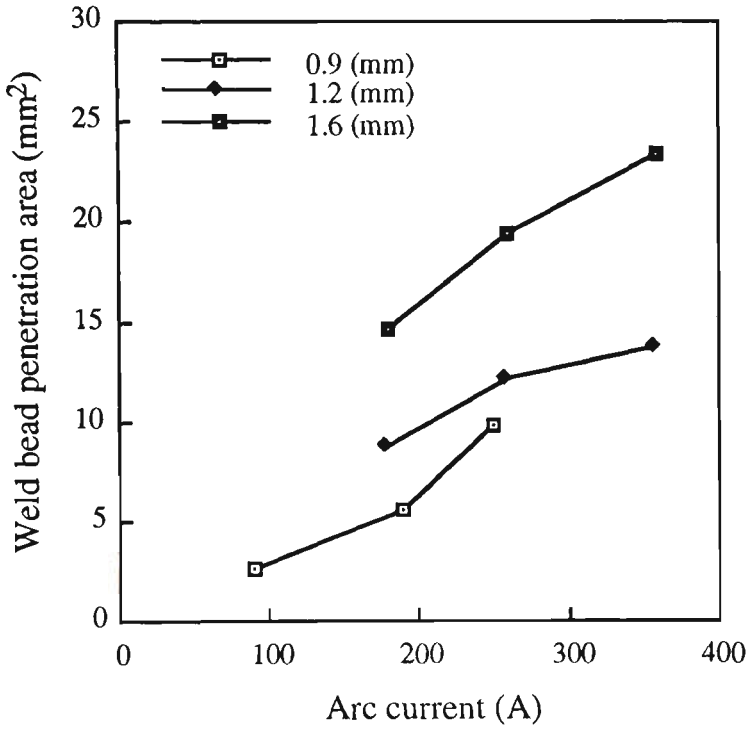

Figure 4.10 (c) The effect of arc current on average weld bead penetration area.

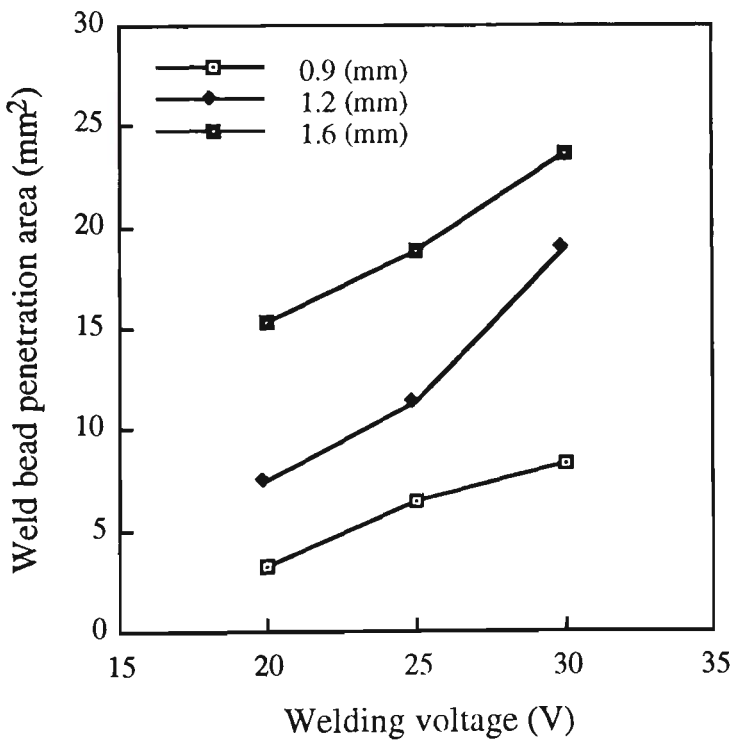

Figure 4.10 (d) The effect of welding voltage on average weld bead penetration area.

Weld bead penetration areas were calculated by taking the average of all measured values with the same gas flow rate for a particular wire diameter, but without considering the effects of welding speed, arc current and welding voltage. Figure 4.10 (b) shows the effect of welding speed on the average weld bead penetration area for a specific wire diameter. The average weld bead penetration areas were produced by taking the average of all values for welds deposited with the same welding speed for a given wire diameter, but ignoring the effects of gas flow rate, arc current and welding voltage. As shown in figure 4.10 (b), the effect of welding speed on weld bead penetration area does not seem significant.

The effect of arc current on weld bead penetration area shown in figure 4.10 (c), illustrates that the weld bead penetration area increases when arc current increases. The average weld bead penetration areas were found by taking the average of all measured values with the same arc current, without taking account of the effects of gas flow rate, welding speed and welding voltage. When a higher welding voltage is used, a higher weld bead penetration area is obtained as can be seen in figure 4.10 (d). Weld bead reinforcement areas were produced by taking the average of all measured values with the same welding voltage for a specific wire diameter, yet ignoring the effects of gas flow rate, welding speed and arc current.

4.3.8 Effects of Welding Process Parameters on Weld Bead Reinforcement Area

The effects of five welding process parameters on weld bead reinforcement area are shown in figures 4.11 (a) - (d). The coupled effects of gas flow rate and wire diameter on the average weld bead reinforcement area represented in figure 4.11 (a) indicate that a higher weld bead reinforcement area is obtained with a larger wire diameter, while the effect of gas flow rate on weld bead reinforcement area seems to have little significance.

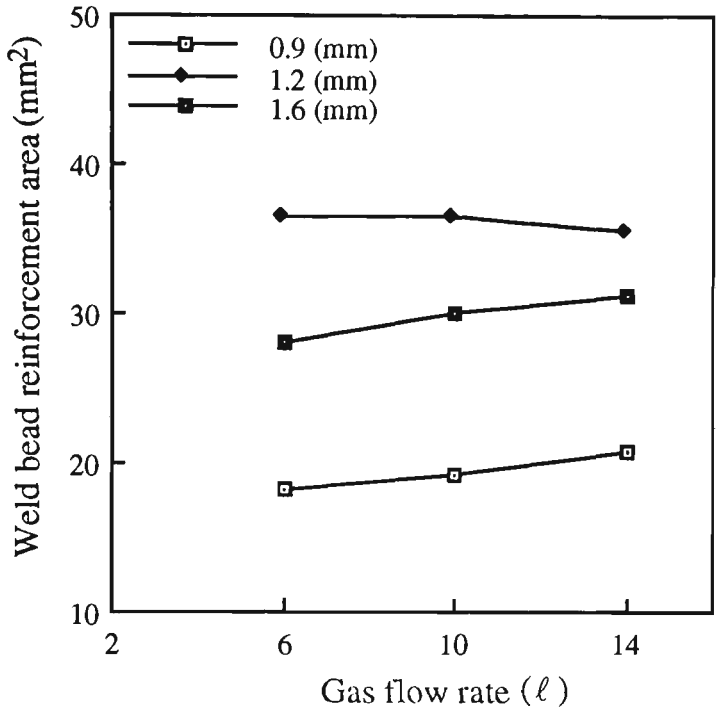

Figure 4.11 (a) The effect of gas flow rate on average weld bead reinforcement area.

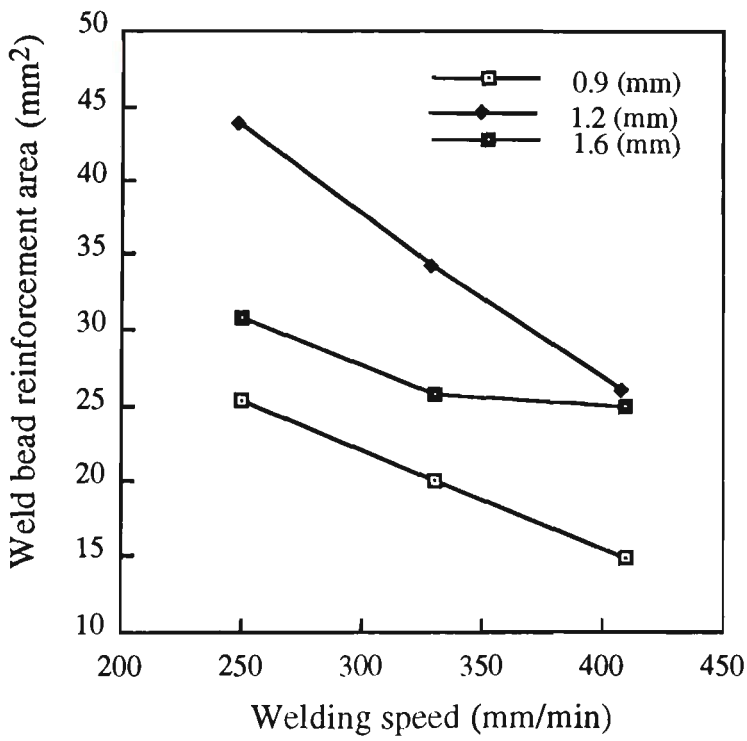

Figure 4.11 (b) The effect of welding speed on average weld bead reinforcement area.

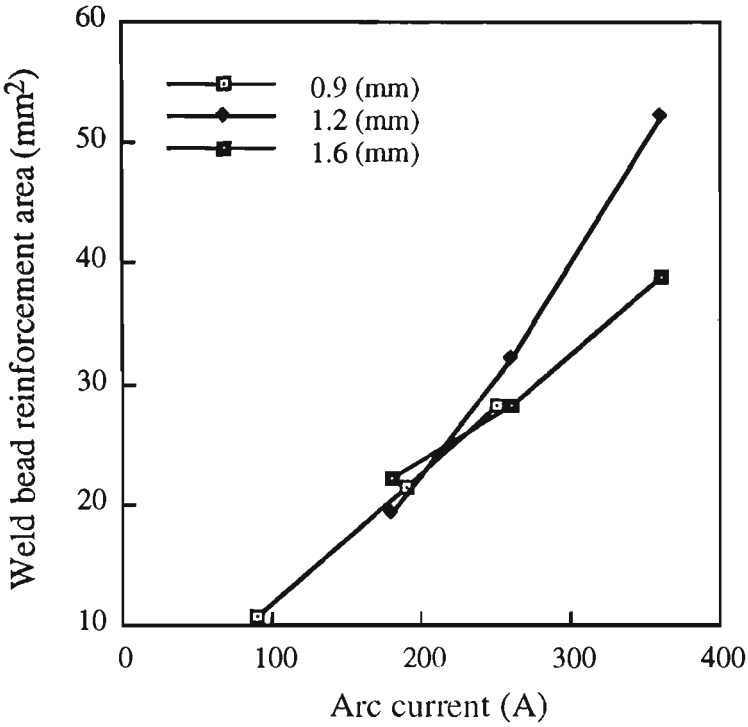

Figure 4.11 (c) The effect of arc current on average weld bead reinforcement area.

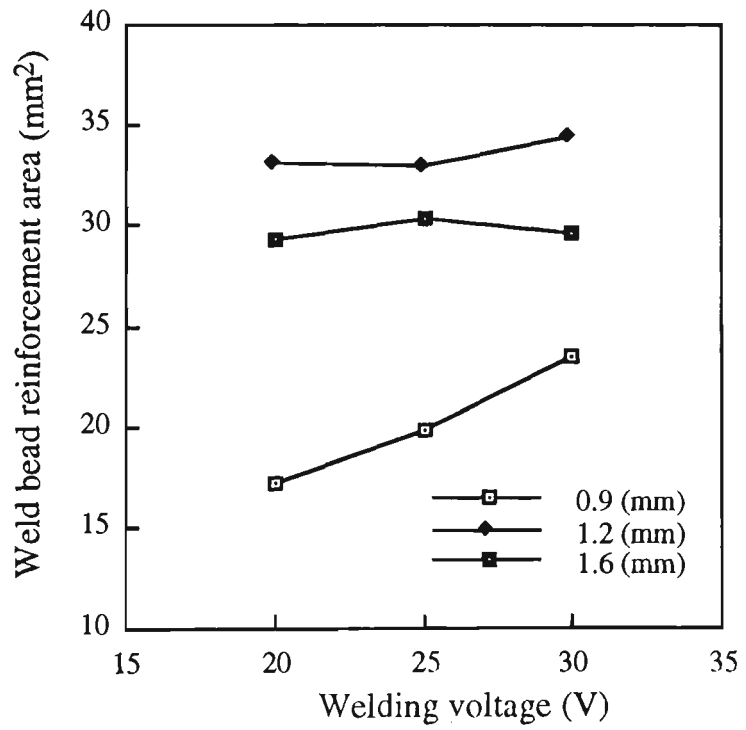

Figure 4.11 (d) The effect of welding voltage on average weld bead reinforcement area.

Weld bead reinforcement areas were calculated by taking the average of all measured values with the same gas flow rate for a particular wire diameter, but without considering the effects of welding speed, arc current and welding voltage. Figure 4.11 (b) exhibits the effect of welding speed on average weld bead reinforcement area for a specific wire diameter. The average weld bead reinforcement areas were produced by taking the average of all values for welds deposited with the same welding speed for a given wire diameter, but ignoring the effects of gas flow rate, arc current and welding voltage. It is noted that there is a decrease in weld bead reinforcement area as welding speed increases.

The relationship between arc current and weld bead reinforcement area is mixed as shown in figure 4.11 (c). This may be due to scattering effects (experimental error). The average weld bead reinforcement areas were found by taking the average of all measured values with the same arc current for a particular wire diameter, but without taking account of the effects of gas flow rate, welding speed and welding voltage. The effect of welding voltage on weld bead reinforcement area is revealed in figure 4.11 (d). Weld bead reinforcement areas were produced by taking the average of all measured values with the same welding voltage for a given wire diameter, yet ignoring the effects of gas flow rate, welding speed and arc current. It is shown in figure 4.11 (d) that the effect of welding voltage on weld bead reinforcement area has not had any significant effect.

4.3.9 Effects of Welding Process Parameters on Weld Bead Dilution

The effects of five welding process parameters on weld bead dilution are shown in figures 4.12 (a) - (d). The coupled effects of gas flow rate and wire diameter on weld bead dilution shown in figure 4.12 (a) represent that the weld bead dilution increases with an increase in wire diameter, but the effect of gas flow rate on weld bead dilution does not seem to have any significance.

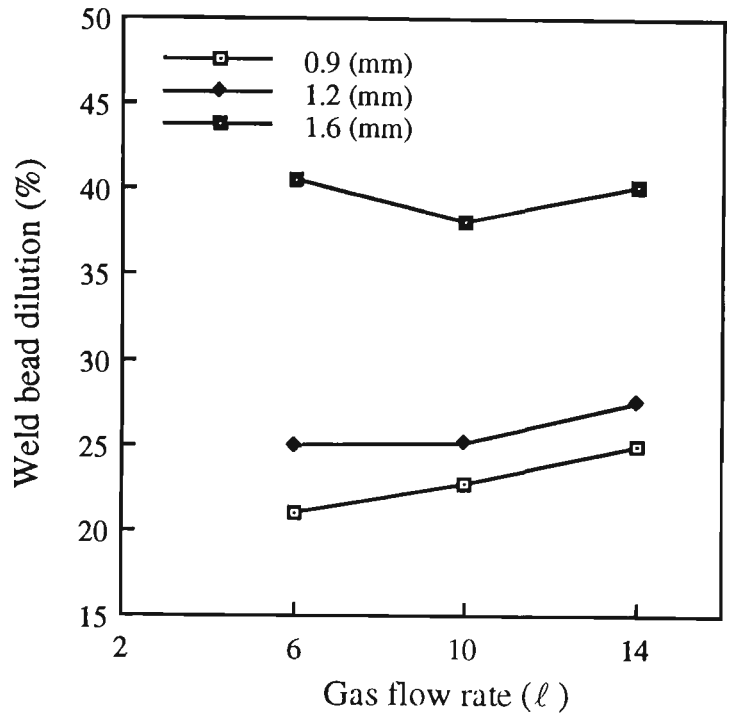

Figure 4.12 (a) The effect of gas flow rate on average weld bead dilution.

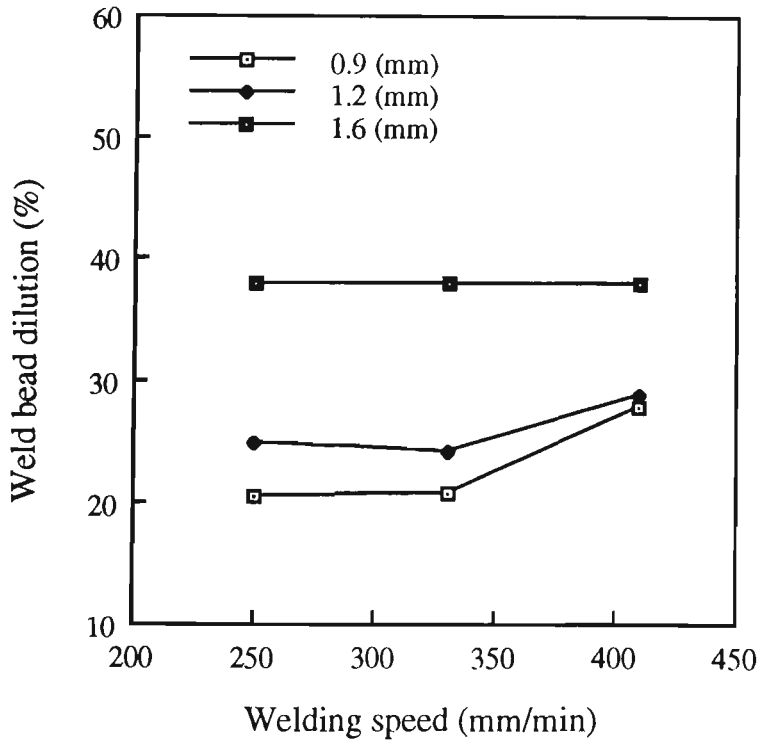

Figure 4.12 (b) The effect of welding speed on average weld bead dilution.

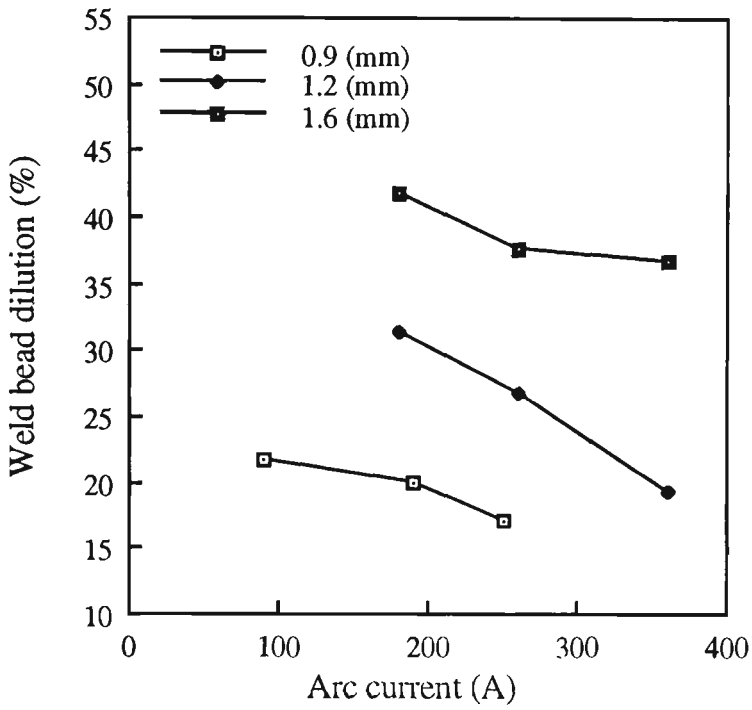

Figure 4.12 (c) The effect of arc current on average weld bead dilution.

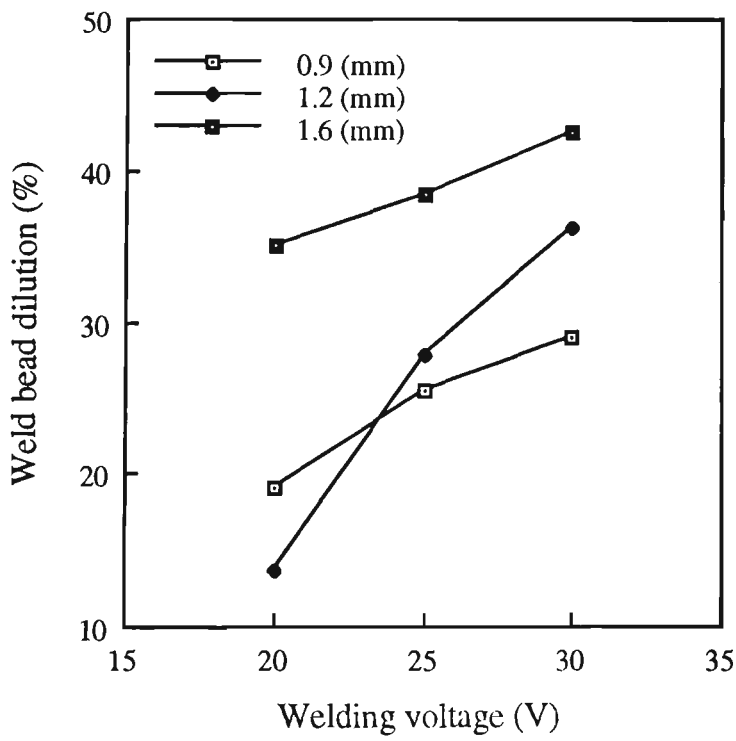

Figure 4.12 (d) The effect of welding voltage on average weld bead dilution.

The average weld bead dilutions were calculated by taking the average of all measured values with the same gas flow rate for a particular wire diameter, but without considering the effects of welding speed, arc current and welding voltage. When a higher welding speed is employed, a higher weld bead dilution is produced as shown in figure 4.12 (b). The average weld bead dilutions were produced by taking the average of all values for welds deposited with the same welding speed for a given wire diameter, but ignoring the effects of gas flow rate, arc current and welding voltage.

Figure 4.12 (c) presents the weld bead dilution against arc current for wire diameters of 0.9, 1.2 and 1.6 mm. Weld bead dilutions were found by taking the average of all measured values with the same arc current for a given wire diameter, but without taking account of the effects of gas flow rate, welding speed and welding voltage. It can be concluded from figure 4.12 (c) that the weld bead dilution decreases when arc current increases. The effect of welding voltage on weld bead dilution is shown in figure 4.12 (d), which reveals that the weld bead dilution increases with an increase in welding voltage. Weld bead dilutions were produced by taking the average of all measured values for welds deposited with the same welding voltage for a specific wire diameter, yet ignoring the effects of gas flow rate, welding speed and arc current.

4.3.10 Effects of Welding Process Parameters on Length of Weld Bead Penetration Boundary

The length of the weld bead penetration boundary is the linear length of the solidified line. This length would depend on the amount of the workpiece melting. Figures 4.13 (a) - (d) show the effects of five welding process parameters on length of weld bead penetration boundary. The effects of gas flow rate and wire diameter on length of weld bead penetration boundary are represented in figure 4.13 (a). Length of weld bead penetration boundaries were calculated by taking the average of all measured values for welds deposited with the same gas flow rate for a given wire diameter, but

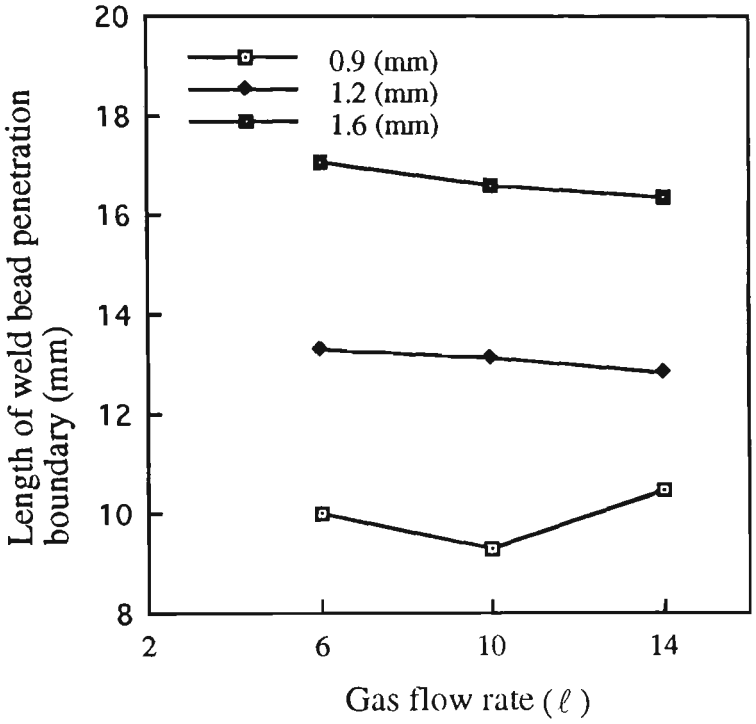

Figure 4.13 (a) The effect of gas flow rate on average length of weld bead penetration boundary.

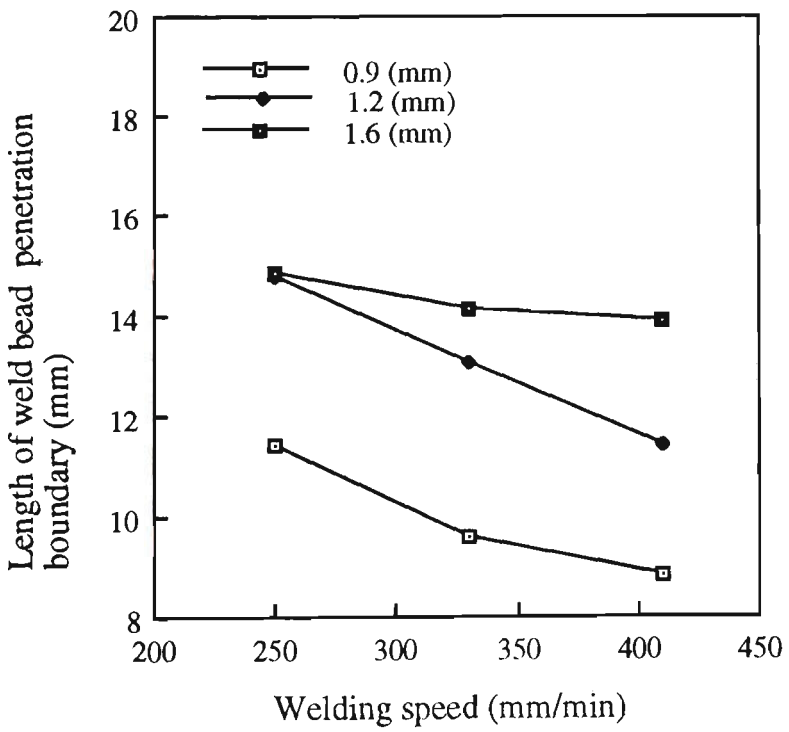

Figure 4.13 (b) The effect of welding speed on average length of weld bead penetration boundary.

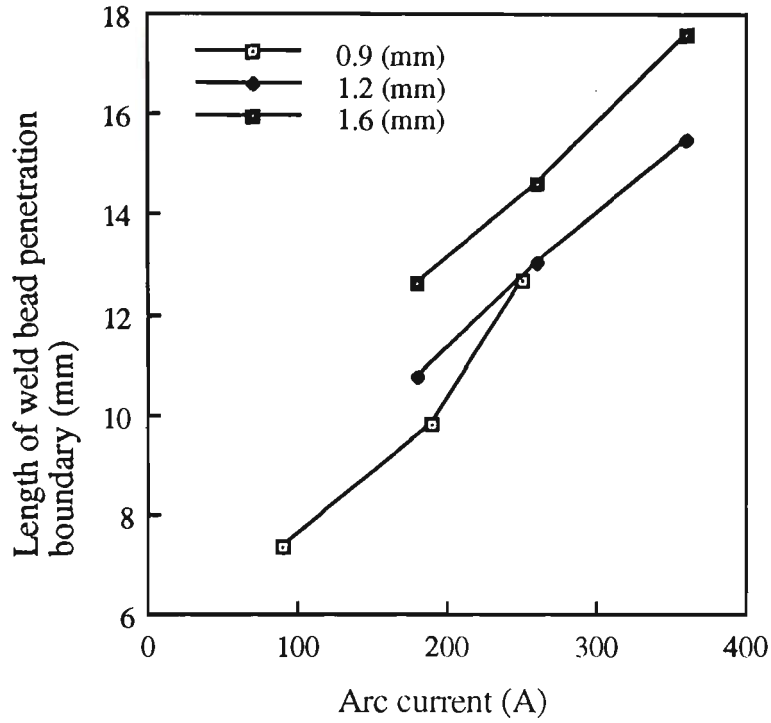

Figure 4.13 (c) The effect of arc current on average length of weld bead penetration boundary.

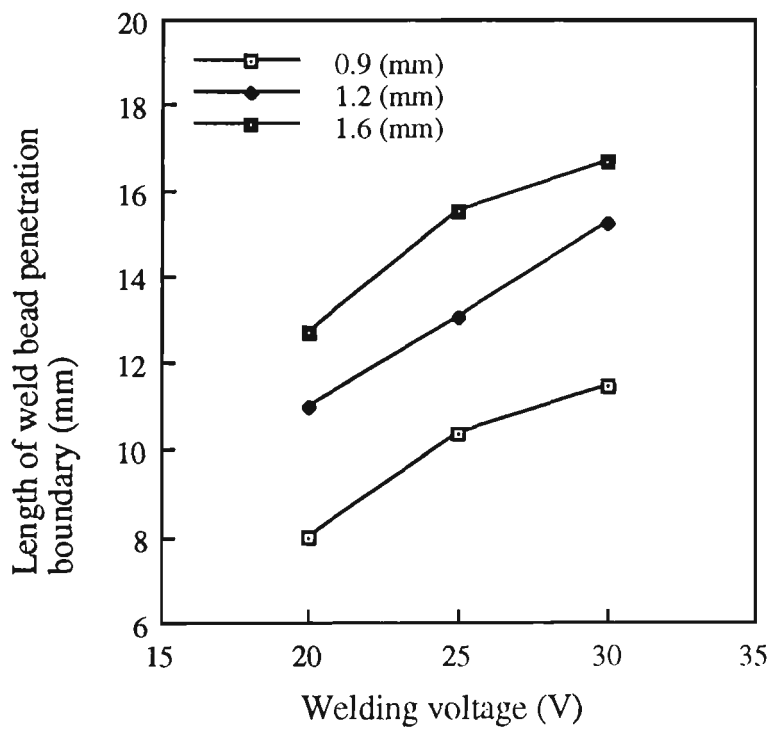

Figure 4.13 (d) The effect of welding voltage on average length of weld bead penetration boundary.

without considering the effects of welding speed, arc current and welding voltage. As shown in figure 4.13 (a), there is an increase in length of weld bead penetration boundary as wire diameter increases, while the effect of gas flow rate on length of weld bead penetration boundary seems to have little significance. Figure 4.13 (b) shows the effect of welding speed on length of weld bead penetration boundary for a specific wire diameter. The average length of weld bead penetration boundaries were produced by taking the average of all values with the same welding speed for a given wire diameter, but ignoring the effects of gas flow rate, arc current and welding voltage. It is evident from figure 4.13 (b) that there is a decrease in length of weld bead penetration boundary when welding speed increases.

The effect of arc current on length of weld bead penetration boundary shown in figure 4.13 (c) indicates that length of weld bead penetration boundary increases when arc current increases. Length of weld bead penetration boundaries were found by taking the average of all measured values with the same arc current for a particular wire diameter, without taking account of the effects of gas flow rate, welding speed and welding voltage. Figure 4.13 (d) shows the effect of welding voltage on length of weld bead penetration boundary for a particular wire diameter. The average length of weld bead penetration boundaries were produced by taking the average of all measured values with the same welding voltage for a specific wire diameter, but ignoring the effects of gas flow rate, welding speed and arc current. It seems from figure 4.13 (d) that length of weld bead penetration boundary increases with an increase in welding voltage.

4.3.11 Effects of Welding Process Parameters on Length of Weld Bead Reinforcement Boundary

The effects of five welding process parameters on length of weld bead reinforcement boundary are shown in figures 4.14 (a) - (d). The coupled effects of gas flow rate and

wire diameter on length of weld bead reinforcement boundary are represented in figure 4.14 (a). The average length of weld bead reinforcement boundaries were calculated by taking the average of all measured values with the same gas flow rate for a particular wire diameter, but without considering the effects of welding speed, arc current and welding voltage. It is noted that a higher length of weld bead reinforcement boundary is obtained with a longer wire diameter, but the effect of gas flow rate on length of weld bead reinforcement boundary seems to have little significance as shown in figure 4.14 (a). Figure 4.14 (b) represents the effect of welding speed on length of weld bead reinforcement boundary for a specific wire diameter.

The average length of weld bead reinforcement boundaries were produced by taking the average of all values for welds deposited with the same welding speed, but ignoring the effects of gas flow rate, arc current and welding voltage. As shown in figure 4.14 (b), there is a decrease in length of weld bead reinforcement boundary as welding speed increases.

Figure 4.14 (c) indicates the average length of weld bead reinforcement boundary against arc current for three different wire diameters. Length of weld bead reinforcement boundaries were found by taking the average of all measured values with the same arc current for a particular wire diameter, but without taking account of the effects of gas flow rate, welding speed and welding voltage. It is clear from figure 4.14 (c) that length of weld bead reinforcement boundary increases with an increase in arc current. The effect of welding voltage on length of weld bead reinforcement boundary is displayed in figure 4.14 (d), which indicates that there is an increase in length of weld bead reinforcement boundary when welding voltage increases. Length of weld bead reinforcement boundaries were produced by taking the average of all measured values for welds deposited with the same welding voltage for a given wire diameter, yet ignoring the effects of gas flow rate, welding speed and arc current.

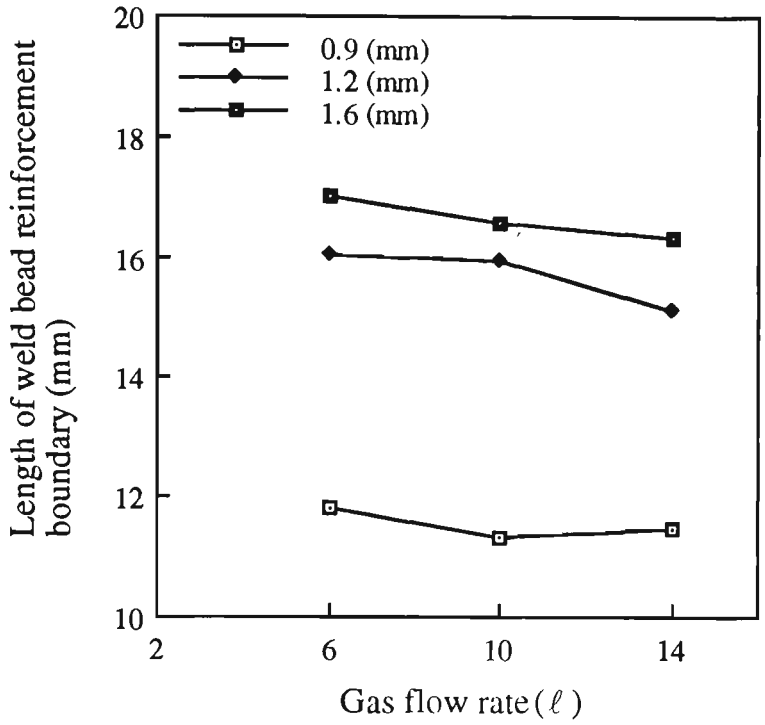

Figure 4.14 (a) The effect of gas flow rate on average length of weld bead reinforcement boundary.

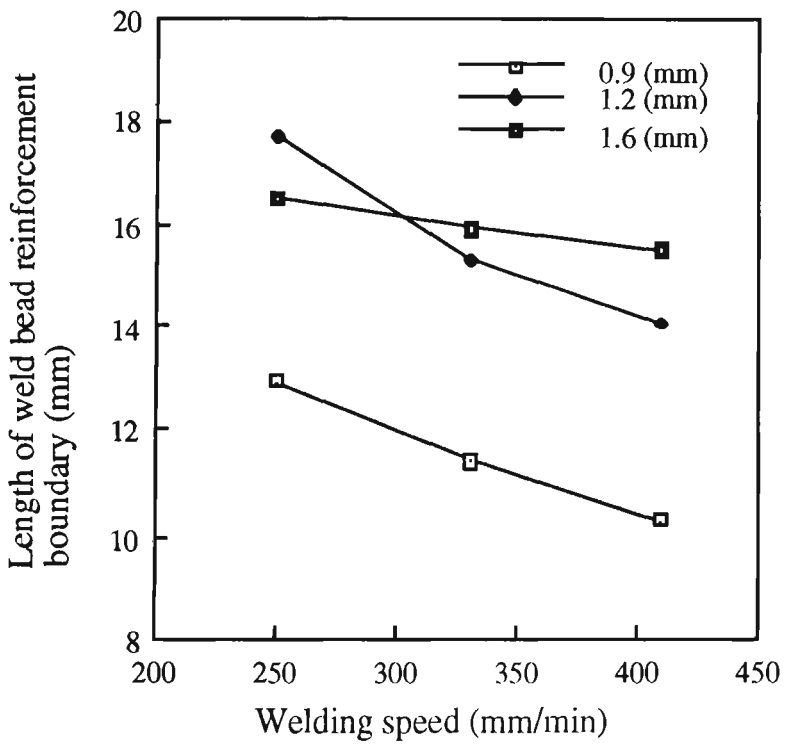

Figure 4.14 (b) The effect of welding speed on average length of weld bead reinforcement boundary.

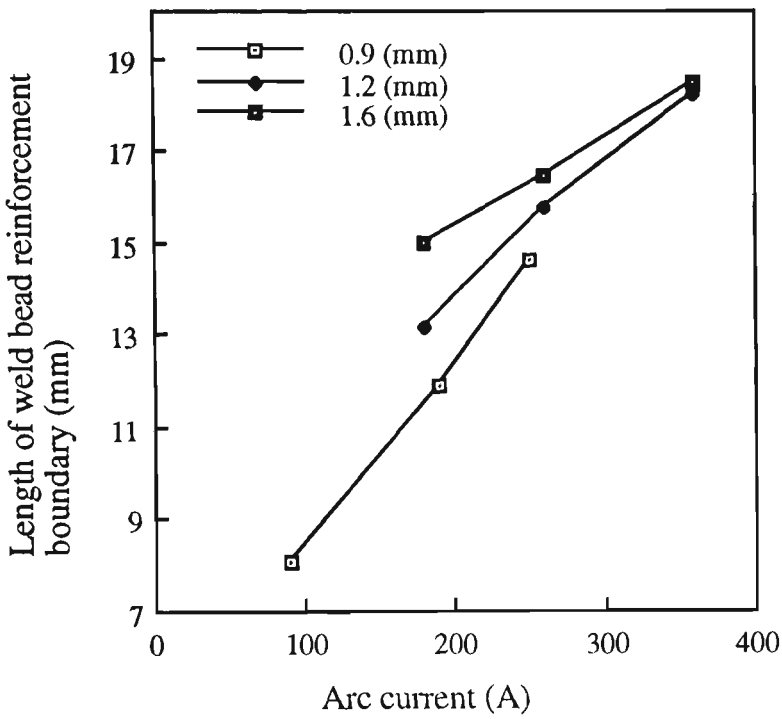

Figure 4.14 (c) The effect of arc current on average length of weld bead reinforcement boundary.

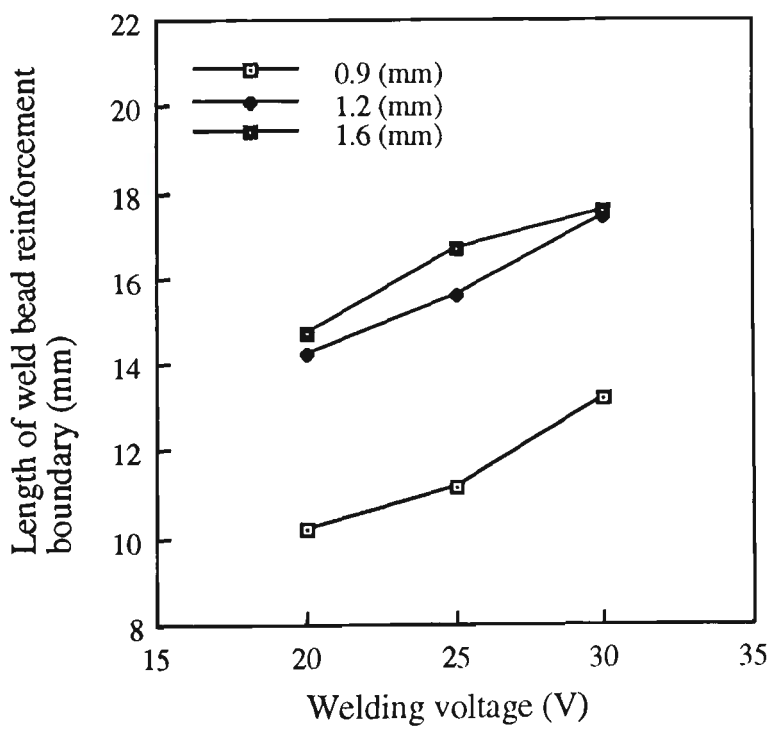

Figure 4.14 (d) The effect of welding voltage on average length of weld bead reinforcement boundary.

4.4 DEVELOPMENT OF MATHEMATICAL MODELS

4.4.1 Selection of a Mathematical Model

The experimental results have shown that weld bead geometry is influenced by wire diameter, gas flow rate, welding speed, arc current and welding voltage. It was therefore thought that a formalised approach to procedure optimisation could successfully establish combinations of welding process parameters which would produce welds of a given quality standard. With five welding process parameters, the response parameter (Y) could be any of weld bead dimensions under considerations and express as follows:

$$Y = f(D,G,S,I,V) \tag{4.1}$$

The empirical mathematical model can be categorically divided into three parts:

(1) Curvilinear equation [McGlone (1978)[117], McGlone and Chadwick (1978)[118], Doherty et al. (1978)[45], Galopin and Boridy (1986)[54] and Chandel (1988)[24].

(2) Polynomial equation [Raveendra and Parmar (1987)[150] and Pandey and Parmar (1989)[138].

(3) Linear equation [Yang et al. (1992)[190].

The primary aim of this chapter is to develop all mathematical equations and to find the best mathematical model under eleven weld bead dimensions in order to investigate the effects of welding process parameters on the weld bead geometry and the relationship between input and output parameters.

McGlone and Chadwick (1978)[118] introduced a curvilinear formula which assumed a linear relationship for the close range and considered all the main effects together with the two factor interactions, and represented as following:

$$Y = b_1 (D)^{b_2} (G)^{b_3} (S)^{b_4} (I)^{b_5} (V)^{b_6} \quad (4.2)$$

where b_1, b_2, b_3, b_4, b_5 and b_6 are constant.

The procedure of this technique was carried out first by an analysis of the variance (ANOVA) which quantified the effects of welding process parameters on each weld bead dimension in order to verify the significance of each welding process parameter and to detect whether there were any interaction effects among the welding process parameters themselves. Second the multiple correlation coefficient and the Fisher's F-ratio (F) were employed to gauge goodness of fit and to indicate the significance at the 1% level on Fisher's F-ratio for including the physical considerations about the logical shape of the equations. As a result, a function based on the analysis of variance was developed for describing the experimental results.

Raveendra and Parmar (1987)[150] also proposed a portion of the power series-algebraic polynomial which includes the main effects of welding process parameters and first order interactions as follows:

$$Y = c_1 + c_2 D + c_3 G + c_4 S + c_5 I + c_6 V + c_7 DG + c_8 DS + c_9 DI + c_{10} DV + c_{11} GS + c_{12} GI + c_{13} GV + c_{14} SI + c_{15} SV + c_{16} IV \quad (4.3)$$

where $c_1, c_2, c_3, c_4, c_5, c_6, c_7, c_8, c_9, c_{10}, c_{11}, c_{12}, c_{13}, c_{14}, c_{15}$ and c_{16} are constant.

Finally, the linear equation [Yang et al. (1992)[190]] could be expressed as following:

$$Y = d_1 + d_2 D + d_3 G + d_4 S + d_5 I + d_6 V \quad (4.4)$$

where d_1, d_2, d_3, d_4, d_5 and d_6 are constant.

4.4.2 Mathematical Models Developed

Best fit equations for investigating the interrelation between the five welding process parameters and eleven weld bead dimensions were computed by using the standard statistical techniques such as multiple regression analysis. These analyses were employed a standard statistical package program, SAS (1988)[160].

4.4.2.1 Weld Bead Width

The following curvilinear, polynomial and linear equations for predicting weld bead width and correlating weld process parameters with weld bead width were obtained from the experimental results:

For curvilinear equation:

$$W_{cur} = \frac{D^{0.3647} I^{0.4151} V^{0.9273}}{S^{0.4873} 10^{0.0097}} \tag{4.5}$$

For polynomial equation:

$$W_{pol} = 5.0102 - 0.2283D - 0.0035G - 0.0179S + 0.0098I + 0.1405V + 0.1497DV + 0.0005IV \tag{4.6}$$

For linear equation:

$$W_{lin} = -2.3053 + 3.5131D - 0.0035G - 0.0179S + 0.0213I + 0.4331V \tag{4.7}$$

Table 4.1 Analysis of variance tests for mathematical models for weld bead width

No. of equation	Standard error of estimate	Coefficient of multiple correlation	Coefficient of determination
Equation 4.5	0.712	0.9810	96.24
Equation 4.6	0.791	0.9734	94.76
Equation 4.7	0.832	0.9697	94.04

The variance technique was employed to analyse and check the adequacies of the developed mathematical models. The standard error of estimate SEE, coefficient of multiple correlation R and coefficient of determination 100 R^2 for equations (4.5) to (4.7) are given in table 4.1. It is noted that the value of coefficient of multiple correlation for equation (4.5) is higher than those for equations (4.6) and (4.7), but all the models are adequate.

4.4.2.2 Weld Bead Height

The three equations to predict weld bead height and to correlate weld process parameters with weld bead height were computed from the experimental results:

For curvilinear equation:

$$H_{cur} = \frac{I^{0.7475} 10^{0.8607}}{D^{0.4092} G^{0.0844} S^{0.4327} V^{0.6649}} \qquad (4.8)$$

For polynomial equation:

$$H_{pol} = 7.8333 - 0.5866D - 0.1093G - 0.0118S + 0.0175I - 0.1893V$$
$$+0.0653DG - 0.0054DI + 0.0003SV \qquad (4.9)$$

For linear equation:

$$H_{lin} = 5.9411 - 1.1584D - 0.0288G - 0.0042S + 0.0109I - 0.0882V \quad (4.10)$$

Table 4.2 Analysis of variance tests for mathematical models for weld bead height

No. of equation	Standard error of estimate	Coefficient of multiple correlation	Coefficient of determination
Equation 4.8	0.387	0.9348	87.40
Equation 4.9	0.380	0.9363	87.66
Equation 4.10	0.406	0.9239	85.36

To check the adequacies of the mathematical models, the standard error of estimate, coefficient of multiple correlation and coefficient of determination for the equations (4.8) to (4.10) given table 4.2 indicate that the value of coefficient of multiple correlation of equation (4.9) is higher than those of equations (4.8) and (4.10), but all equations are equally useful for prediction of weld bead height due to small differences.

4.4.2.3 Weld Bead Penetration

The three formulae for predicting weld bead penetration as well as correlating weld process parameters with weld bead penetration were calculated from the experimental results:

For curvilinear equation:

$$P_{cur} = \frac{D^{0.3945}\ G^{0.1187}\ I^{0.9557}\ V^{0.1529}}{10^{2.2959}} \quad (4.11)$$

For polynomial equation:

$$P_{pol} = 6.1869 - 1.0168D + 0.0605G - 0.0016S - 0.0235I - 0.2202V$$

$$-0.0136DG + 0.0066DI + 0.0011IV \qquad (4.12)$$

For linear equation:

$$P_{lin} = -1.9503 + 0.3428D + 0.0438G - 0.0016S + 0.0121I + 0.0417V \qquad (3.13)$$

The statistical data to analyse the adequancies of equations (4.11) to (4.13) are respectively tabulated in table 4.3. It can be seen from table 4.3 that the value of coefficient of multiple correlation for equation (4.12) is better than those of equations (4.11) and (4.13), but those equations are similarly employed to predict the weld bead penetration.

Table 4.3 Analysis of variance tests for mathematical models for weld bead penetration

No. of equation	Standard error of estimate	Coefficient of multiple correlation	Coefficient of determination
Equation 4.11	0.738	0.8411	70.75
Equation 4.12	0.651	0.8824	77.87
Equation 4.13	0.762	0.8273	68.44

4.4.2.4 Weld Penetration Shape Factor

For predicting weld penetration shape factor and correlating weld process parameters with weld penetration shape factor, the following curvilinear, polynomial and linear equations were obtained from the experimental results:

For curvilinear equation:

$$WRSP_{cur} = \frac{D^{0.0178} \quad V^{0.4989} \quad 10^{2.1229}}{S^{0.2746} \quad I^{0.5932}} \qquad (4.14)$$

For polynomial equation:

$$WRSP_{pol} = -8.3062 - 5.8524D - 0.0788G - 0.0048S + 0.0798I + 0.8377V + 0.2269DV - 0.0039IV \quad (4.15)$$

For linear equation:

$$WRSP_{lin} = 7.5922 - 0.1804D - 0.0788G - 0.0048S - 0.0169I + 0.2018V \quad (4.16)$$

Table 4.4 Analysis of variance tests for mathematical models for weld penetration shape factor

No. of equation	Standard error of estimate	Coefficient of multiple correlation	Coefficient of determination
Equation 4.14	1.830	0.6905	47.68
Equation 4.15	1.372	0.8485	72.01
Equation 4.16	1.855	0.6884	47.39

Table 4.4 shows the standard error of estimate, coefficient of multiple correlation and coefficient of determination for the equations (4.14) to (4.16). As shown in table 4.4, the value of coefficient of multiple correlation of equation (4.15) is 0.8485, while the values of coefficient of multiple correlation of equations (4.14) and (4.16) are not high, which show an indication of the inconsistency of weld penetration shape factor equation and of the uncertain nature of weld penetration shape factor prediction.

4.4.2.5 Weld Reinforcement Shape Factor

To predict weld reinforcement shape factor and to correlate weld process parameters with weld reinforcement shape factor, the following three equations were obtained from the experimental results:

For curvilinear equation:

$$WRFF_{cur} = \frac{D^{0.7738} \quad G^{0.0752} \quad V^{1.5924}}{I^{0.3324} \quad 10^{0.9985}} \tag{4.17}$$

For polynomial equation:

$$WRFF_{pol} = -6.7899 + 5.1434D + 0.0313G + 0.0093S - 0.0062C + 0.2365V - 0.0084DS \tag{4.18}$$

For linear equation:

$$WRFF_{lin} = -3.3667 + 2.3678D + 0.0313G - 0.001S - 0.0062I + 0.2365V \tag{4.19}$$

The standard error of estimate, coefficient of multiple correlation and coefficient of determination are given table 4.5 for the equations (4.17) to (4.19). It is evident that the value of coefficient of multiple correlation of equation (4.18) is better than those of equations (4.17) and (4.19), but all equations are adequate.

Table 4.5 Analysis of variance tests for mathematical models for weld reinforcement shape factor

No. of equation	Standard error of estimate	Coefficient of multiple correlation	Coefficient of determination

Equation 4.17	0.485	0.9283	86.18
Equation 4.18	0.438	0.9429	88.90
Equation 4.19	0.465	0.9345	87.33

4.4.2.6 Weld Bead Total Area

The following curvilinear, polynomial and linear equations for predicting weld bead total area as well as correlating weld process parameters with weld bead total area were computed from the experimental results:

For curvilinear equation:

$$T_{Acur} = \frac{D^{0.4162} \; I^{1.027} \; V^{0.7669}}{S^{0.6938} \; 10^{0.2244}} \tag{4.20}$$

For polynomial equation:

$$A_{Tpol} = -57.4275 + 10.3466D + 3.5127G + 0.086S + 0.37I - 0.7728V$$
$$-0.0152GI - 0.0007SI + 0.0078IV \tag{4.21}$$

For linear equation:

$$A_{Tlin} = -10.6793 + 10.3466D - 0.095G - 0.0876S + 0.1725I + 1.0925V \tag{4.22}$$

Table 4.6 Analysis of variance tests for mathematical models for weld bead total area

No. of equation	Standard error of estimate	Coefficient of multiple correlation	Coefficient of determination
Equation 4.20	11.071	0.8703	75.74
Equation 4.21	11.067	0.8707	75.82
Equation 4.22	12.676	0.8183	66.97

The validity of the equations (4.20) to (4.22) can be judged from their high coefficient of multiple correlation in table 4.6, which shows the relationship between computed and measured weld bead total area. It is seen from table 4.6 that the values of coefficient of multiple correlation of equations (4.20) and (4.21) are higher than that of equation (4.22), while all equations could be equally used for prediction of weld bead total area.

4.4.2.7 Weld Bead Penetration Area

The following three equations to predict weld bead penetration area and to correlate weld process parameters with weld bead penetration area were obtained from the experimental results:

For curvilinear equation:

$$AP_{cur} = \frac{D^{1.6088} \quad I^{0.7856} \quad V^{2.2168}}{10^{4.1053}} \tag{4.23}$$

For polynomial equation:

$$AP_{pol} = -44.7832 + 14.6527D + 1.2393G + 0.1477S - 0.1393I + 0.9746V$$
$$-0.0053GI - 0.0067SV + 0.0091IV \tag{4.24}$$

For linear equation:

$$AP_{lin} = -31.215 + 14.6527D - 0.0056G - 0.0186S + 0.0352I + 0.9298V \tag{4.25}$$

Table 4.7 Analysis of variance tests for mathematical models for weld bead penetration area

No. of equation	Standard error of estimate	Coefficient of multiple correlation	Coefficient of determination
Equation 4.23	5.735	0.8135	66.18
Equation 4.24	5.282	0.8546	73.03
Equation 4.25	6.539	0.7547	56.96

Table 4.7 gives the details of variance analysis for equations (4.23) to (4.25). It is noted that the value of coefficient of multiple correlation of equation (4.24) is better than those of equations (4.23) and (4.25). However, those equations are sufficient.

4.4.2.8 Weld Bead Reinforcement Area

To predict weld bead reinforcement area and to correlate weld process parameters with weld bead reinforcement area, the three formulae below were obtained from the experimental results:

For curvilinear equation:

$$A_{Rcur} = \frac{I^{1.0848} \quad 10^{0.8442}}{D^{0.0381} \quad S^{0.7962}} \tag{4.26}$$

For polynomial equation:

$$A_{Rpol} = -64.578 + 10.1953D + 2.2218G + 0.0674S + 0.5029I + 0.1612V$$
$$-0.0637DI - 0.0098GI - 0.0006SI \tag{4.27}$$

For linear equation:

$$A_{Rlin} = 20.6281 - 4.3186D - 0.0896G - 0.0691S + 0.1372I + 0.1612V$$

(4.28)

The standard error of estimate, coefficient of multiple correlation and coefficient of determination for equations (4.26) to (4.28) are tabulated in table 4.8. The value of coefficient of multiple correlation of equation (4.27) is better than those of equations (4.26) and (4.28) as shown in table 4.8, while all equations are satisfactory.

Table 4.8 Analysis of variance tests for mathematical models for weld bead reinforcement area

No. of equation	Standard error of estimate	Coefficient of multiple correlation	Coefficient of determination
Equation 4.26	9.128	0.8042	64.67
Equation 4.27	8.319	0.8488	72.04
Equation 4.28	9.304	0.7973	63.57

4.4.2.9 Weld Bead Dilution

The following curvilinear, polynomial and linear equations for predicting weld bead dilution and correlating weld process parameters with weld bead dilution were obtained from the experimental results:

For curvilinear equation:

$$DI_{cur} = \frac{D^{1.1929} \; S^{0.2454} \; V^{1.4507}}{I^{0.2412} \; 10^{0.7572}} \tag{4.29}$$

For polynomial equation:

$$DI_{pol} = -106.6272 + 58.6711D + 0.1312G + 0.3241S - 0.3061I + 3.9757V$$
$$-0.0046DI - 1.2694DV - 0.012SV + 0.0115IV \tag{4.30}$$

For linear equation,

$$DI_{lin} = -34.9469 + 25.8823D + 0.1312G + 0.0231S - 0.0242I + 1.1581V \quad (4.31)$$

The statistical data for equations (4.29) to (4.31) are tabulated in table 4.9. It is evident from table 4.9 that the value of coefficient of multiple correlation of equation (4.30) is superior to those of equations (4.29) and (4.31), but those equations are sufficient for the purpose.

Table 4.9 Analysis of variance tests for mathematical models for weld bead dilution

No. of equation	Standard error of estimate	Coefficient of multiple correlation	Coefficient of determination
Equation 4.29	8.693	0.7466	55.74
Equation 4.30	8.214	0.7838	61.43
Equation 4.31	9.407	0.6823	46.56

4.4.2.10 Length of Weld Bead Penetration Boundary

For predicting length of weld bead penetration boundary and correlating weld process parameters with length of weld bead penetration boundary, the following equations were obtained from the experimental results:

For curvilinear equation:

$$BP_{cur} = \frac{D^{0.344} \; I^{0.4881} \; V^{0.783}}{S^{0.3637} \; 10^{0.2674}} \quad (4.32)$$

For polynomial equation:

$$BP_{pol} = 19.3066 - 1.6531D - 0.5342G - 0.05S - 0.0181I - 0.0416V$$

$$+0.0161DS + 0.0016GS + 0.0018IV \tag{4.33}$$

For linear equation:

$$B_{Plin} = -3.2684 + 3.6717D - 0.0139G - 0.0144S + 0.0275I + 0.3906V \tag{4.34}$$

Table 4.10 shows the standard error of estimate, coefficient of multiple correlation and coefficient of determination for the equations (4.32) to (4.34). It can be seen from table 4. 10 that the value of coefficient of multiple correlation of equation (4.32) is higher than those of equations (4.33) and (4.34), but all equations are similarly practical for use in estimating length of weld bead penetration boundary.

Table 4.10 Analysis of variance tests for mathematical models for length of weld bead penetration boundary

No. of equation	Standard error of estimate	Coefficient of multiple correlation	Coefficient of determination
Equation 4.32	1.897	0.8911	79.41
Equation 4.33	1.929	0.8880	78.86
Equation 4.34	2.055	0.8663	75.04

4.4.2.11 Length of Weld Bead Reinforcement Boundary

The following equations to predict length of weld bead reinforcement boundary and to correlate weld process parameters with length of weld bead reinforcement boundary were obtained from the experimental results below:

For curvilinear equation:

$$B_{Rcur} = \frac{D^{0.2731}\ C^{0.4975}\ V^{0.5442}\ 10^{0.0487}}{S^{0.3371}} \tag{4.35}$$

For polynomial equation:

$$B_{R_{pol}} = 8.1551 - 1.8479D - 0.0817G - 0.035S + 0.0295I + 0.3035V + 0.0161DS \quad (4.36)$$

For linear equation:

$$B_{R_{lin}} = 1.6075 + 3.4609D - 0.0817G - 0.0152S + 0.0295I + 0.3035V \quad (4.37)$$

The statistical data for equations (4.35) to (4.37) are given in table 4.11. The values of coefficient of multiple correlation of these equations are 0.8917, 0.8528, 0.8495, respectively. It is noted that the value of coefficient of multiple correlation for equation (4.35) is better than those of equation (4.35) and (4.37), but those equations are still adequate.

Table 4.11 Analysis of variance tests for mathematical models for length of weld bead reinforcement boundary

No. of equation	Standard error of estimate	Coefficient of multiple correlation	Coefficient of determination
Equation 4.35	2.004	0.8917	79.52
Equation 4.36	2.190	0.8528	72.73
Equation 4.37	2.198	0.8495	72.17

4.4.3 Interpretation of Mathematical Models

Based on the empirical mathematical models that determine a given weld bead geometry and provide useful guidelines for systems which control weld bead geometry, the effect of each welding process parameters and their significant interactions on weld bead geometric parameters were computed and plotted by using

mathematical equations with the highest coefficient of multiple correlation. Figures 4.15 to 4.19 indicate the effects of the five welding process parameters on the eleven weld bead dimensions within the ranges studied. The estimated effects of welding process parameters on weld bead geometry are presented only for parameter levels. The use of mathematical equations outside these boundaries is possible through extrapolation and should be only used with care. To stress the interaction of welding process parameters on weld bead geometry, figures 4.20 to 4.30 have been plotted taking account of the two major interactions for each of the mathematical model.

Figure 4.20 shows the effect of interaction between welding voltage and arc current on weld bead width at particular values of wire diameter, gas flow rate and welding speed. It is evident that the weld bead width increased with an increase in welding voltage and arc current. The influence of interaction between wire diameter and arc current on weld bead height at specific values of gas flow rate, welding speed and welding voltage is shown in figure 4.21.

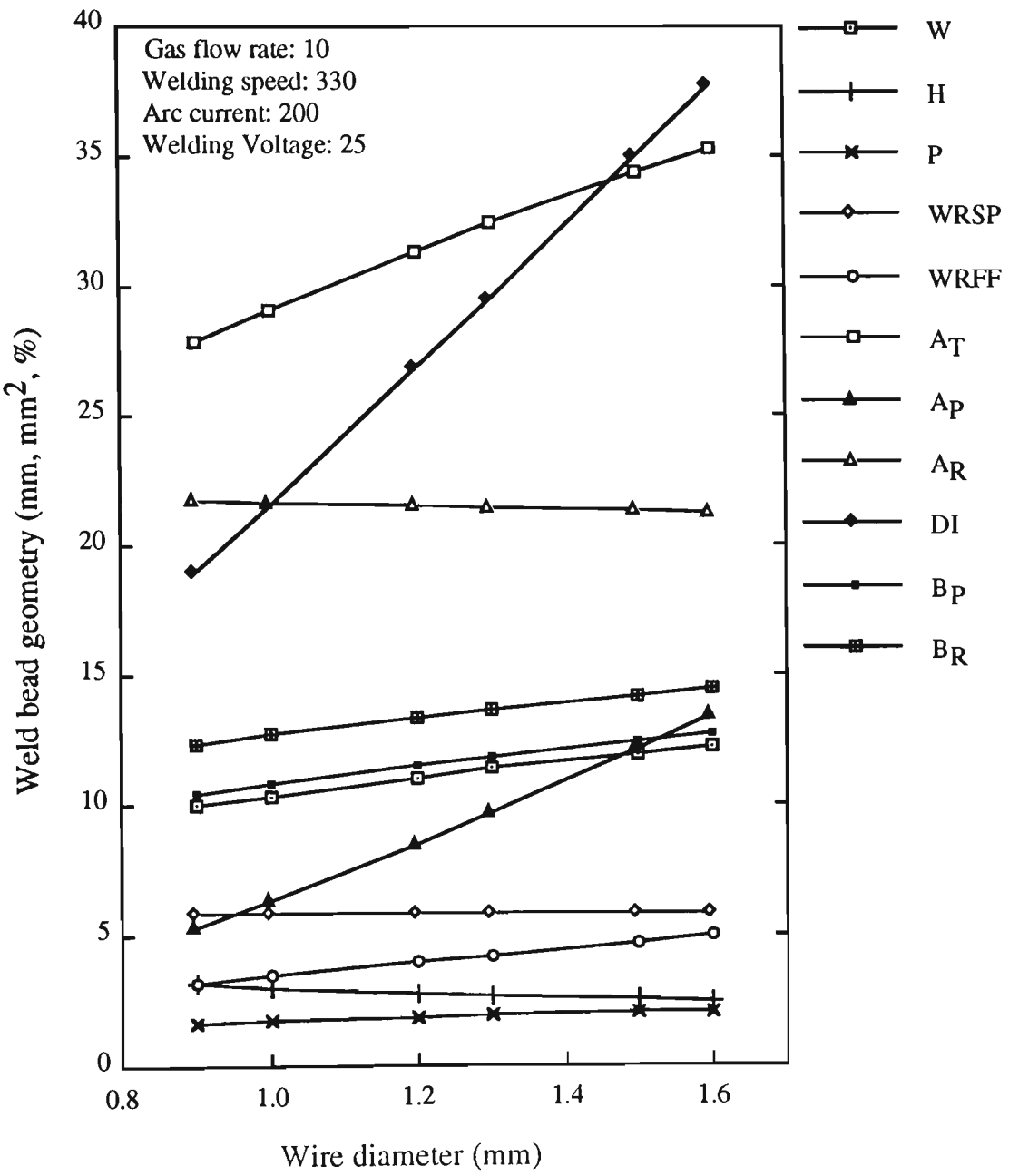

Figure 4.15 The effect of wire diameter on weld bead geometry.

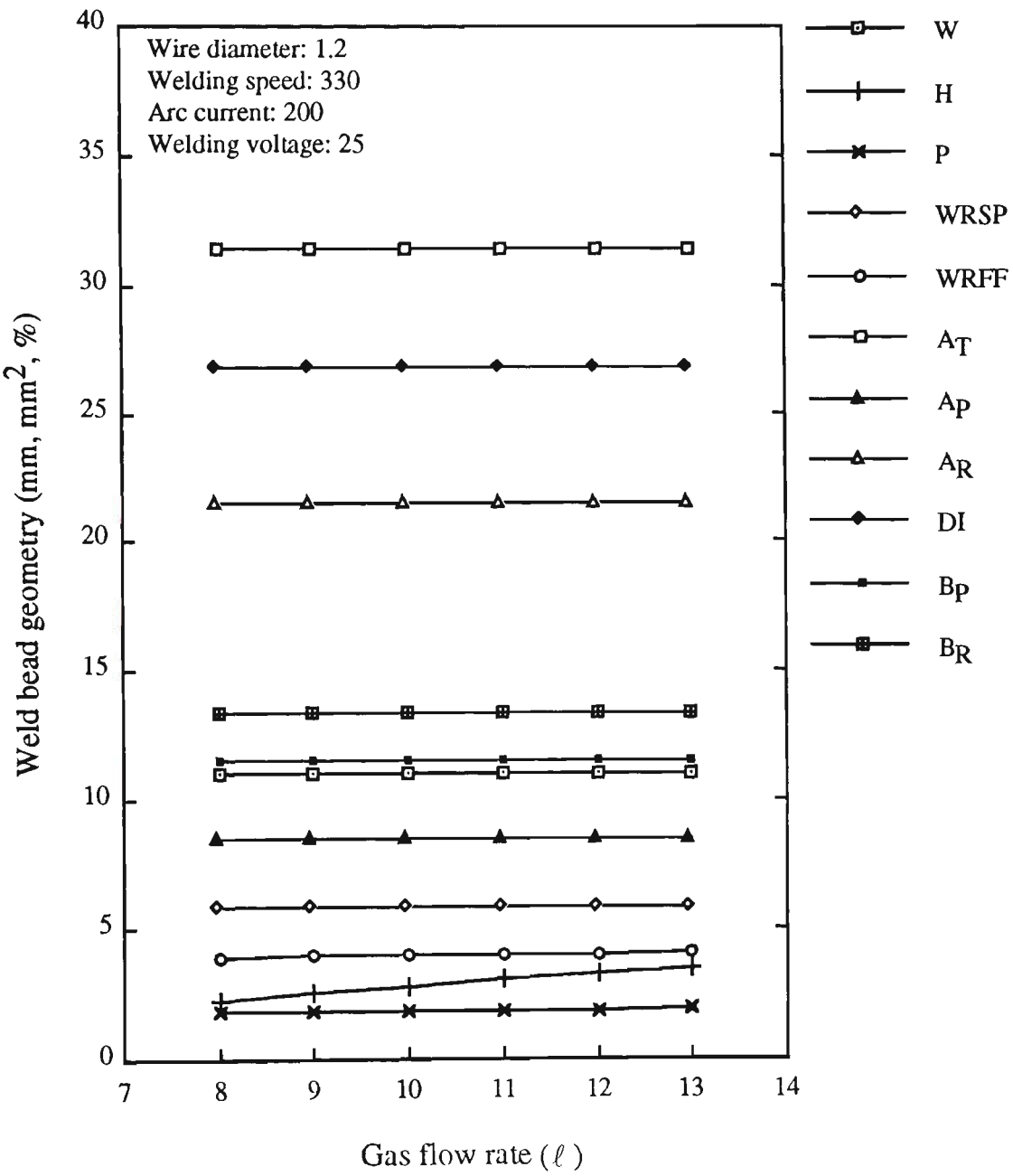

Figure 4.16 The effect of gas flow rate on weld bead geometry.

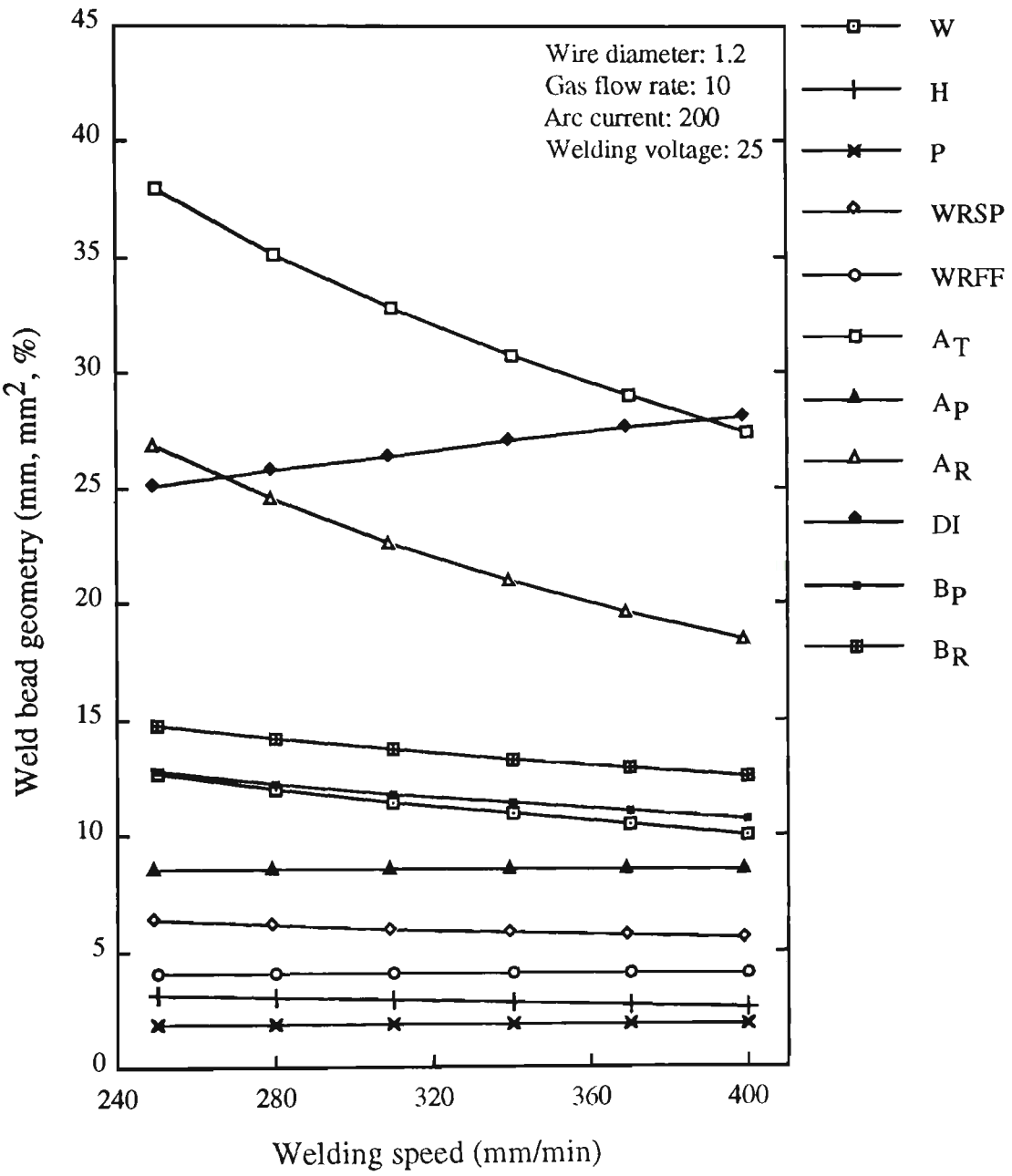

Figure 4.17 The effect of welding speed on weld bead geometry.

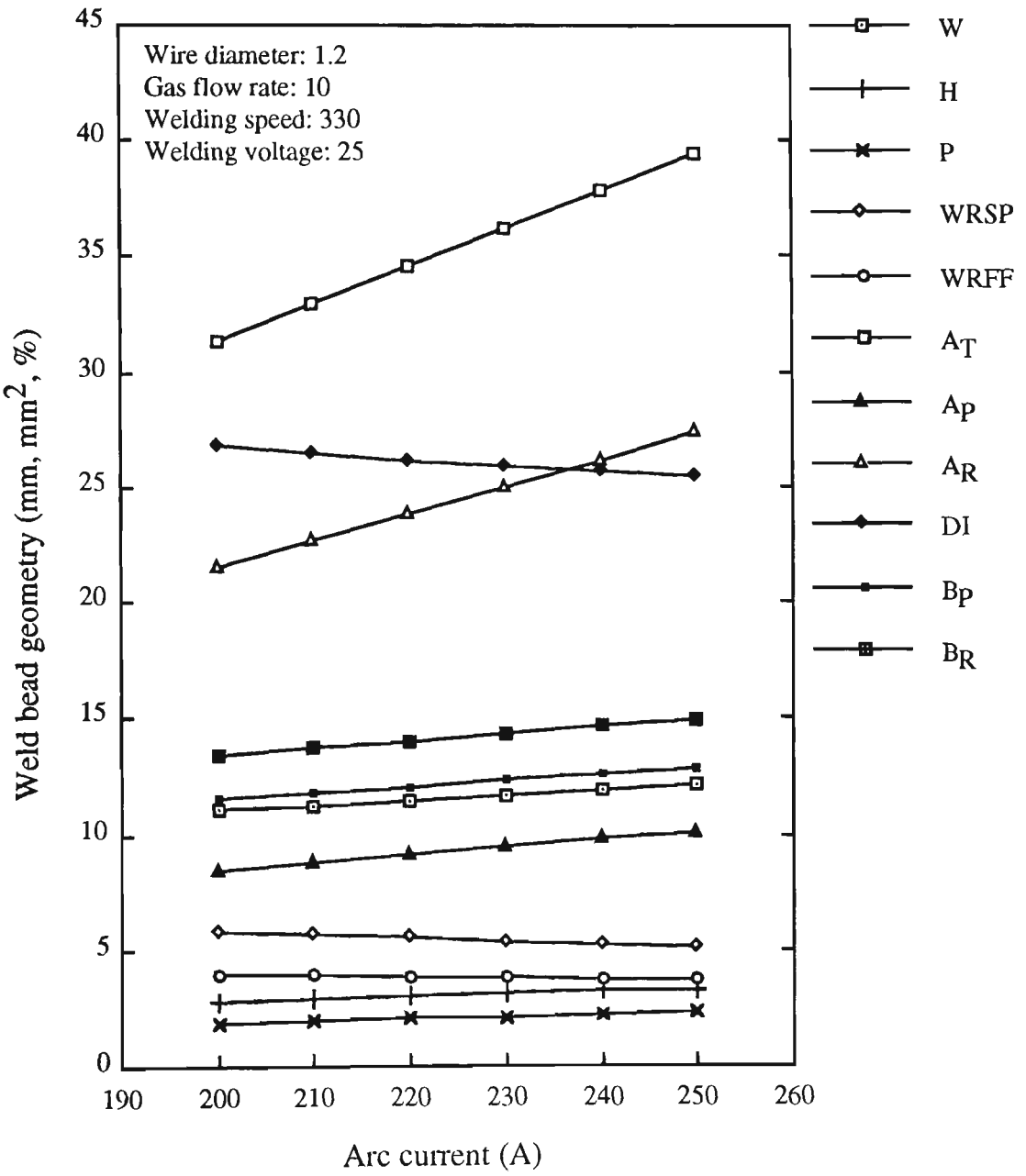

Figure 4.18 The effect of arc current on weld bead geometry.

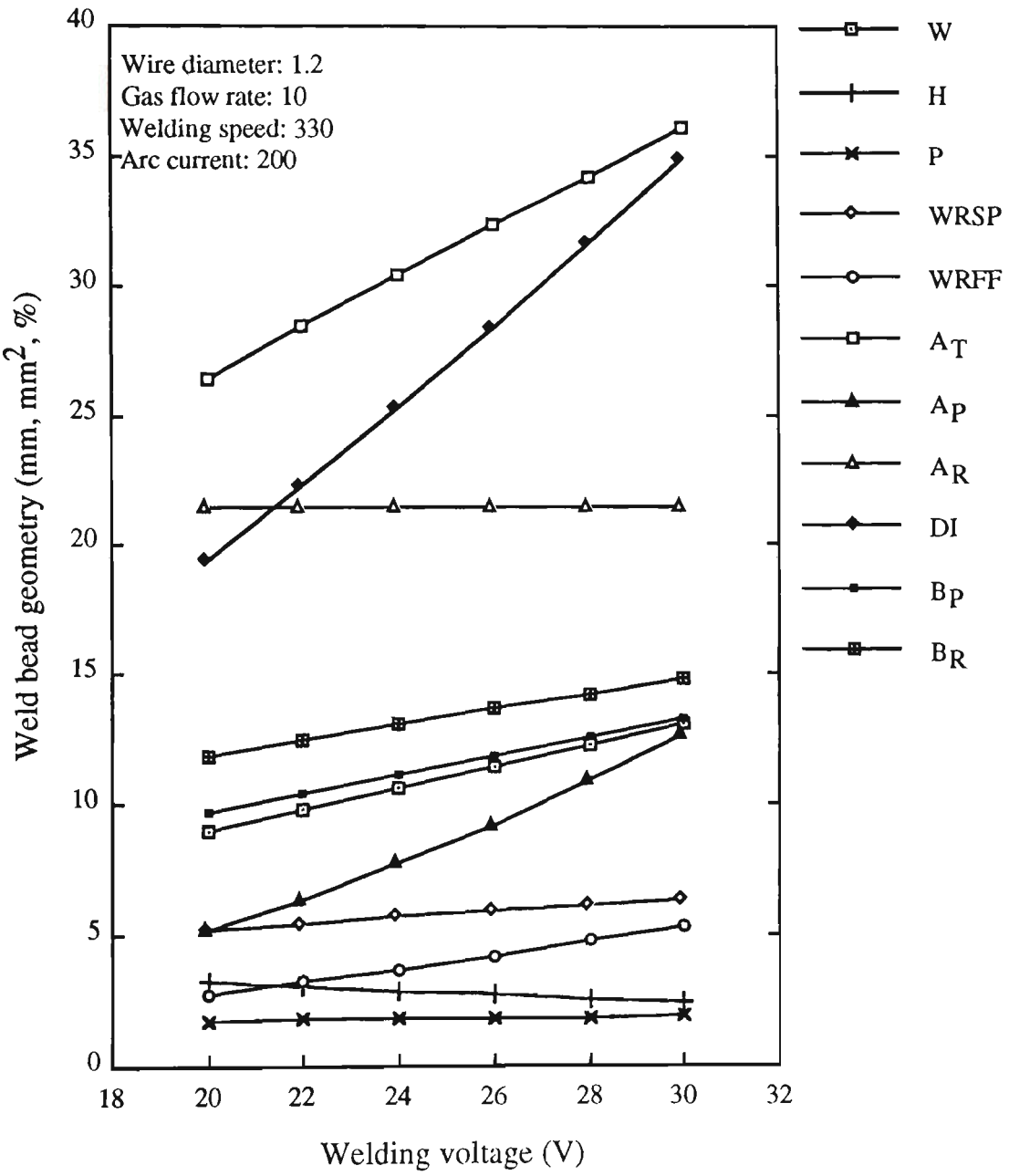

Figure 4.19 The effect of welding voltage on weld bead geometry.

Evidence from figure 4.21 shows that a larger weld bead height is obtained with a larger arc current and smaller wire diameter.

Figure 4.22 presents the influence of interaction between wire diameter and arc current on weld bead penetration at particular values of gas flow rate, welding speed and welding voltage. It is evidence from figure 4.22 that there is an increase of weld bead penetration with an increase in wire diameter and arc current.
The effect of interaction between welding voltage and arc current on weld penetration shape factor at particular values of wire diameter, gas flow rate and welding speed is displayed in figure 4.23. It is noted that the weld penetration shape factor increases when welding voltage increases and arc current decreases.

Figure 4.24 represents the effect of interaction between wire diameter and welding voltage on weld reinforcement shape factor at specific values of gas flow rate, welding speed and arc current. It can be seen figure 4.24 that weld reinforcement shape factor increases as both wire diameter and welding voltage increase. The influence of interaction between arc current and welding voltage on weld bead total area at particular values of wire diameter, gas flow rate and welding speed is shown in figure 4.25. When higher welding voltage and arc current are employed, a larger weld bead total area is achieved as can be seen figure 4.25.

Figure 4.26 shows the influence of interaction between welding voltage and wire diameter on weld bead penetration area at specific values of gas flow rate, welding speed and arc current. It is apparent from figure 4.26 that there is an increase in weld bead penetration area as both welding voltage and wire diameter increase. The effect of interaction between arc current and welding speed on weld bead reinforcement area at particular values of wire diameter, gas flow rate and welding voltage is displayed in figure 4.27. It is noted that weld bead reinforcement area increases as arc current increases and welding speed decreases.

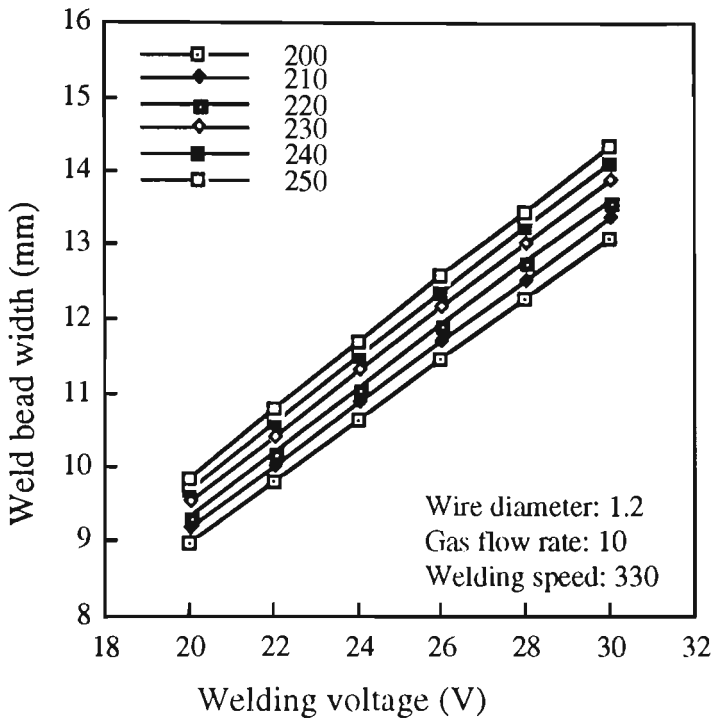

Figure 4.20 Interaction of welding voltage and arc current on weld bead width.

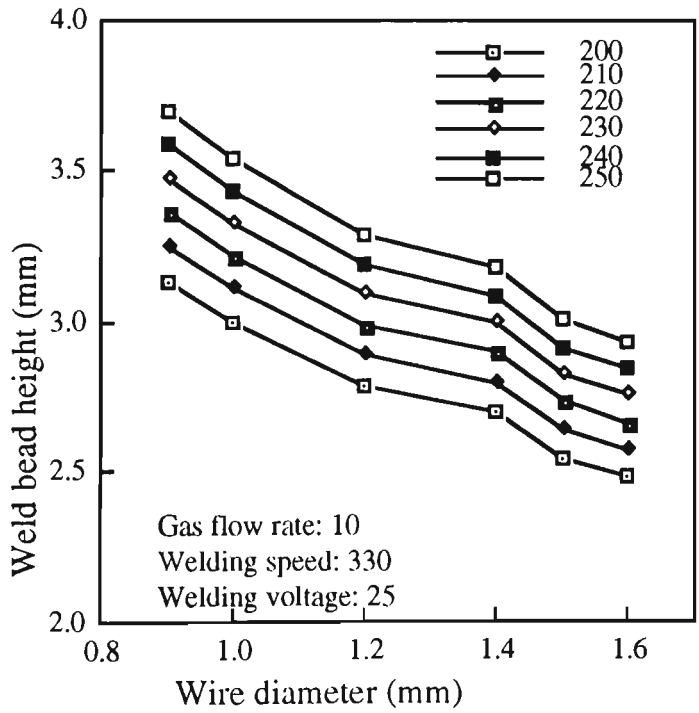

Figure 4.21 Interaction of wire diameter and arc current on weld bead height.

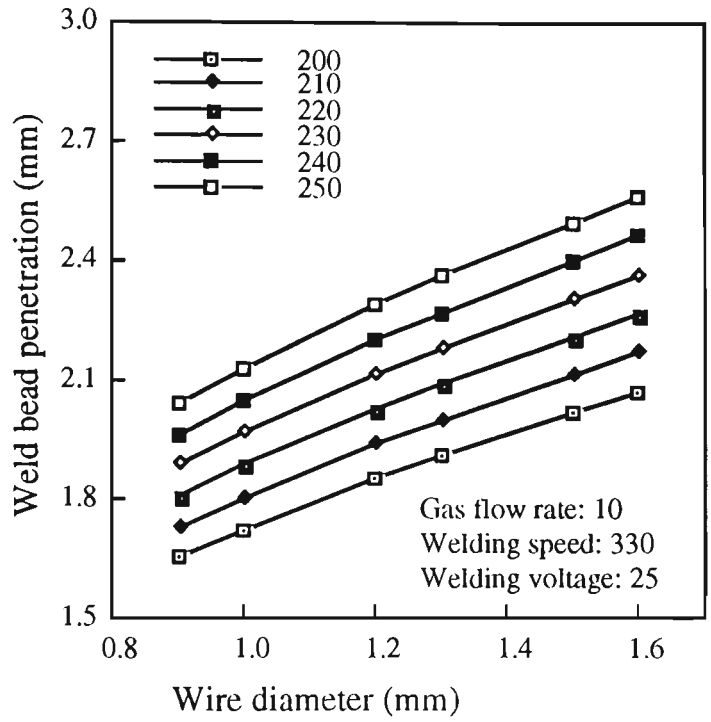

Figure 4.22 Interaction of wire diameter and arc current on weld bead penetration.

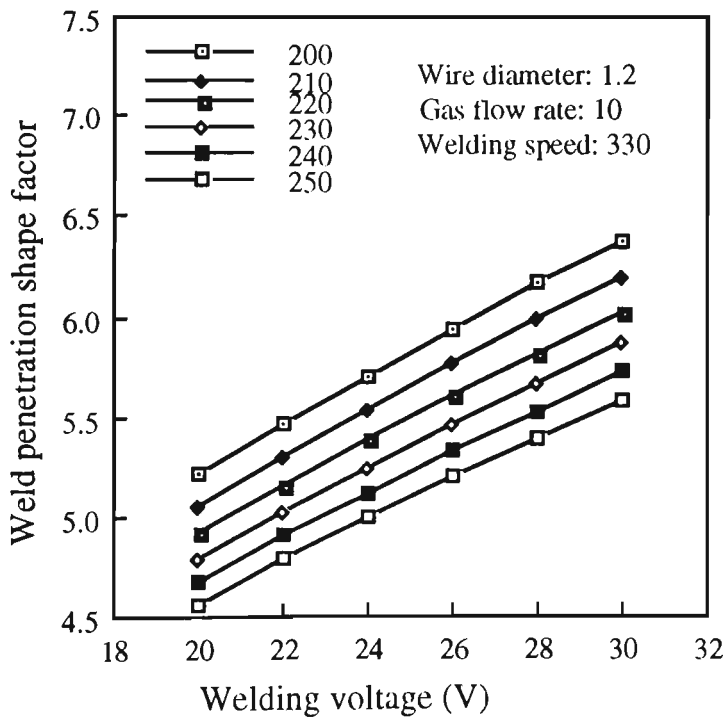

Figure 4.23 Interaction of welding voltage and arc current on weld penetration shape factor.

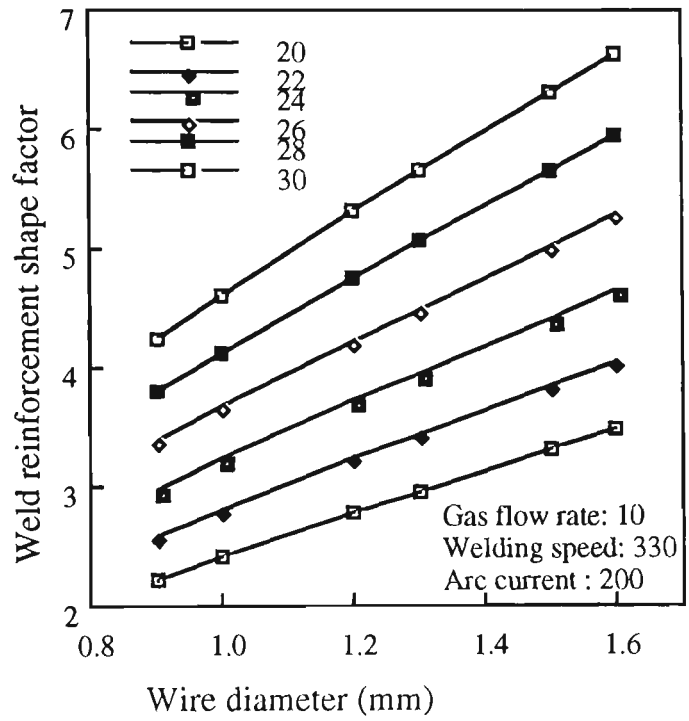

Figure 4.24 Interaction of wire diameter and welding voltage on weld reinforcement shape factor.

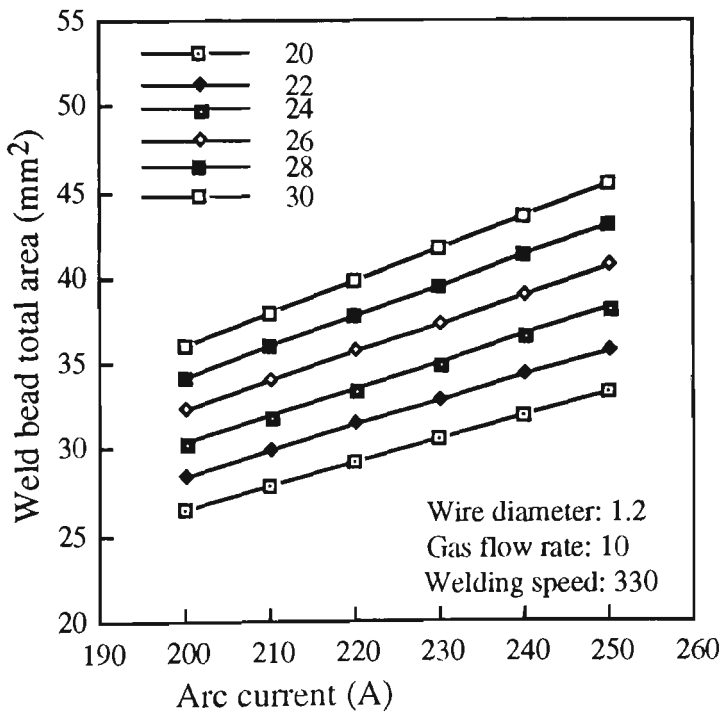

Figure 4.25 Interaction of arc current and welding voltage on weld bead total area.

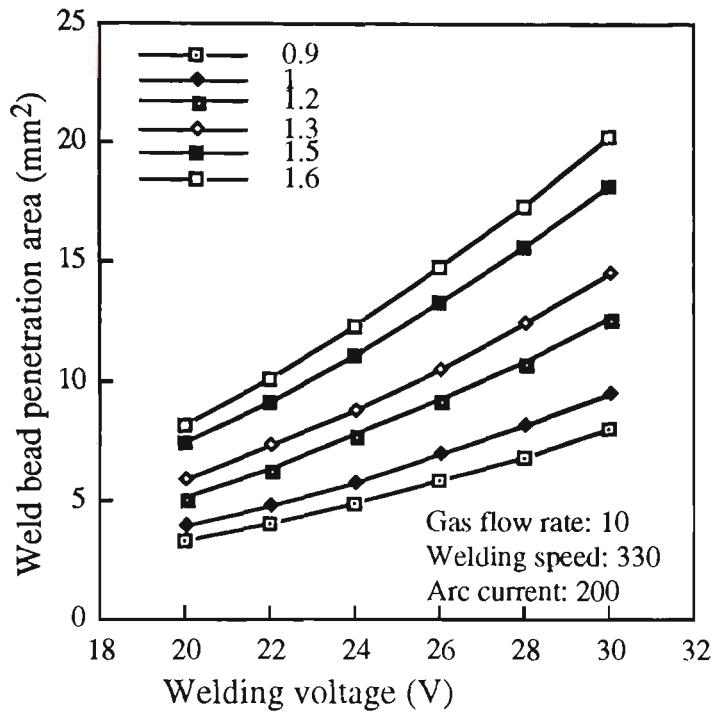

Figure 4.26 Interaction of welding voltage and wire diameter on weld bead penetration area.

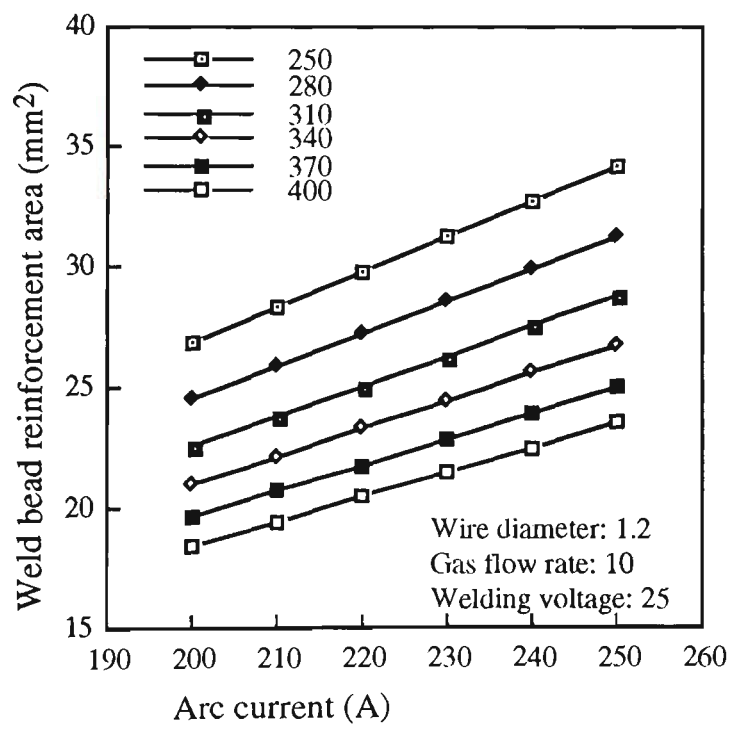

Figure 4.27 Interaction of arc current and welding speed on weld bead reinforcement area.

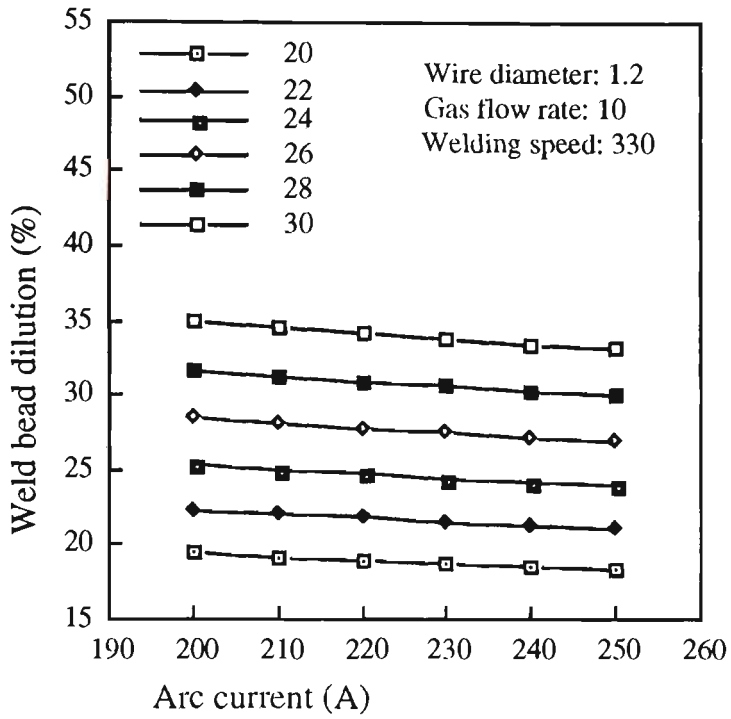

Figure 4.28 Interaction of arc current and welding voltage on weld bead dilution.

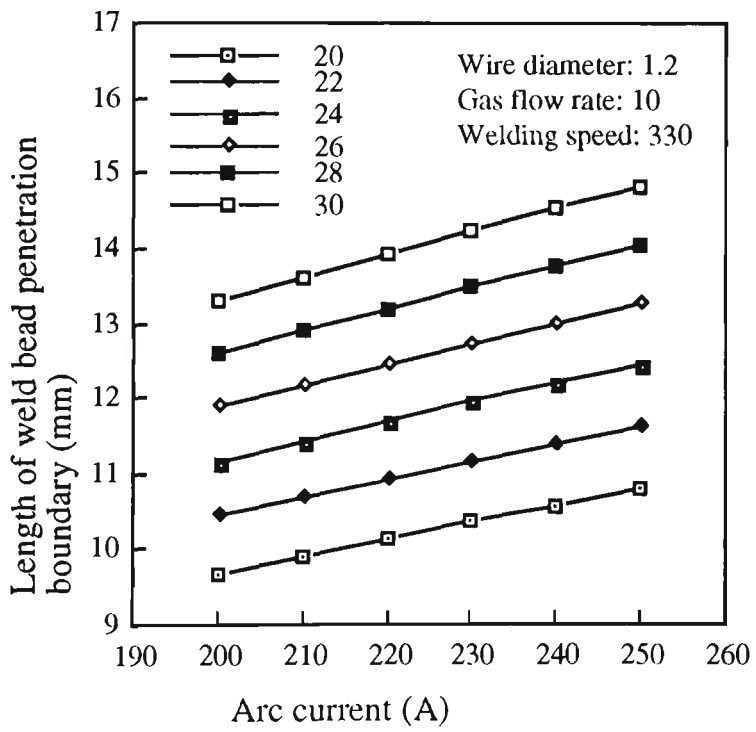

Figure 4.29 Interaction of arc current and welding voltage on length of weld bead penetration boundary.

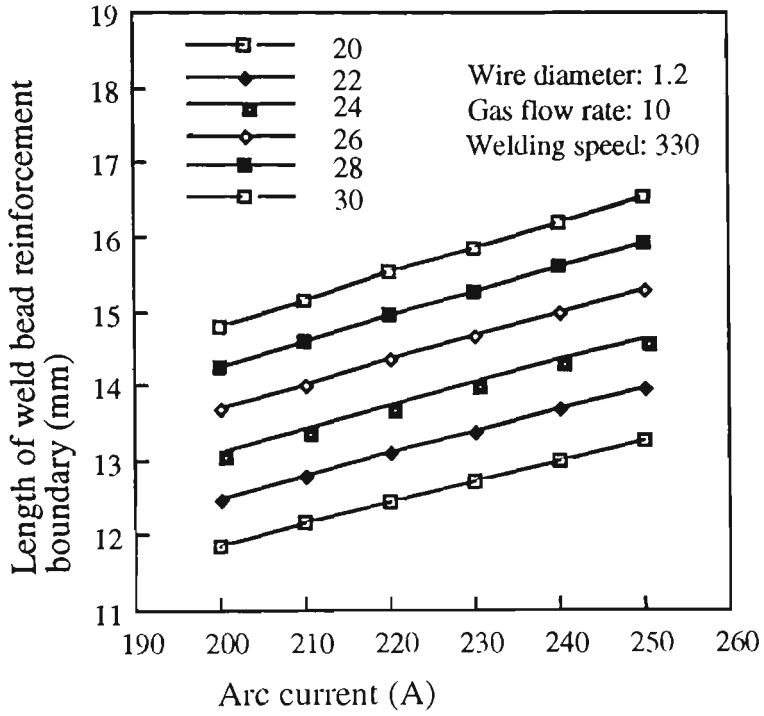

Figure 4.30 Interaction of arc current and welding voltage on length of weld bead reinforcement boundary.

Figure 4.28 presents the effect of interaction between arc current and welding voltage on weld bead dilution at specific values of wire diameter, gas flow rate and welding speed. As shown in figure 4.28, weld bead dilution decreases as arc current increases and welding voltage decreases. The influence of interaction between arc current and welding voltage on length of weld bead penetration boundary at particular values of wire diameter, gas flow rate and welding speed is shown in figure 4.29.

It is evident that there is an increase in length of weld bead penetration boundary as both arc current and welding voltage increase. Figure 4.30 represents the influence of interaction between arc current and welding voltage on length of weld bead reinforcement boundary at specific values of wire diameter, gas flow rate and welding speed. It can be seen in figure 4.30 that length of weld bead reinforcement boundary increases when both welding voltage and arc current increase.

For the automated and/or robotic arc welding system, the data must be available in the form of mathematical equations. It was in the light of these concluding remarks and suggestions for further developments outlined by previous researchers that the work in this chapter was undertaken.

4.5 SUMMARY OF RESULTS

The conclusions based on the experimental results and development of mathematical models can be summarised as follows:

1. Experimental results show that eleven weld bead dimensions in the GMAW process are affected by wire diameter, gas flow rate, welding speed, arc current and welding voltage.
2. The weld bead width, weld bead penetration, weld reinforcement shape factor, weld bead total area, weld bead penetration area, weld bead dilution, length of weld bead penetration boundary and length of weld bead reinforcement boundary increase with an increase in wire diameter, conversely an increase in wire diameter results in a decrease in weld bead height, weld penetration shape factor and weld bead reinforcement area.
3. The effect of gas flow rate on weld bead dimensions does not seem to have any significance except weld bead height.
4. There is a decrease in weld bead width, weld bead height, weld penetration shape factor, weld bead total area, weld bead reinforcement area, length of weld bead penetration boundary and length of weld bead reinforcement boundary with an increase in welding speed, but weld bead dilution increases as welding speed increases.
5. Weld bead width, weld bead height, weld bead penetration, weld bead total area, weld bead penetration area, weld bead reinforcement area, length of weld bead penetration boundary and length of weld bead reinforcement boundary

increase with an increase in arc current, but weld penetration shape factor, weld reinforcement shape factor and weld bead dilution decrease when arc current increases.

6. There is an increase in weld bead width, weld penetration shape factor, weld bead total area, weld bead dilution, length of weld bead penetration boundary and length of weld bead reinforcement boundary with an increase in welding voltage, while weld bead height decreases as welding voltage increases.
7. Mathematical models developed from experimental results can be used to investigate the relationship between welding process variables and weld bead geometry and to predict the weld bead dimensions with reasonable accuracy.
8. The comparison of coefficient of multiple correlation for curvilinear, polynomial and linear regression equations correlating welding process parameters to weld bead dimensions make no difference, which indicates that all equations are reasonably suitable.

CHAPTER 5

NUMERICAL ANALYSIS OF THE GMAW PROCESS

5.1 INTRODUCTION

Since it has been shown that the velocity and temperature distributions of molten metal affect weld pool geometry, the microstructure and mechanical properties of the weld produced, there has been a significant interest in the quantitative representation of heat transfer and fluid flow phenomena in weld pools. Experimental studies of the flow conditions in weld pools are limited to the measurement of the surface velocities only. Furthermore, accurate observation of the surface velocities is extremely difficult during the actual welding process because of the presence of the arc over the weld surface. Therefore mathematical modelling approaches for describing the phenomena happened during the arc welding and investigating how the welding process parameters affect the weld quality, have become an essential and systematic technique.

In recent years, considerable progress has been accomplished in modelling heat transfer and fluid flow conditions in weld pools during the GTAW, GMAW and laser welding process. However, a completely general mathematical model of the GMAW process incorporating the moving heat source and the details of the weld pool circulations is not currently available.

This chapter concentrates on the development of the unsteady 2D mathematical model which includes all important physical phenomena that control the heat transfer and convective flow condition in weld pools. The model developed was employed to investigate the heat transfer and the fluid flow in the GMAW process and to study the role of the various forces (buoyancy, electromagnetic, surface tension and plasma drag forces) and the molten metal droplets. Also, measurements of weld pool flow velocity and weld pool surface temperature are discussed.

5.2 THEORETICAL MODEL

A schematic diagram of weld pools in the GMAW process and the cylindrical coordinate system is presented (see figure 5.1) in order to assist in the development of the mathematical model. A spatially distributed heat and current fluxes fall on the free surface at $z = 0$, which is the surface on the workpiece. The weld bead penetration occurring in the GMAW process will be caused by the heat of the welding arc coming on the weld pool surface and the transfer of heat by the incoming droplets inside the workpiece. As a result, convection flow, free and forced, is induced in both radial and axial directions in molten weld pools. There are four distinct driving forces for weld pool convection. These were described earlier in chapter 2.4.1.

In modelling the system, the following assumptions were made for the present analysis:

(1) The flow is Newtonian and incompressible, in view of the relatively small size of weld pools expected.

(2) The flow is laminar and axisymmetric, with no circumferential variations in terms of the size of weld pools.

(3) All the physical properties of the liquid and solid metals are constant, independent of temperature except surface tension and thermal conductivity.

(4) A spatially distributed heat and current fluxes falling on the free surface are Gaussian characteristics.

(5) The Boussinesq approximation is employed.

(6) An undeformable pool surface is assumed for simplifying the problem.

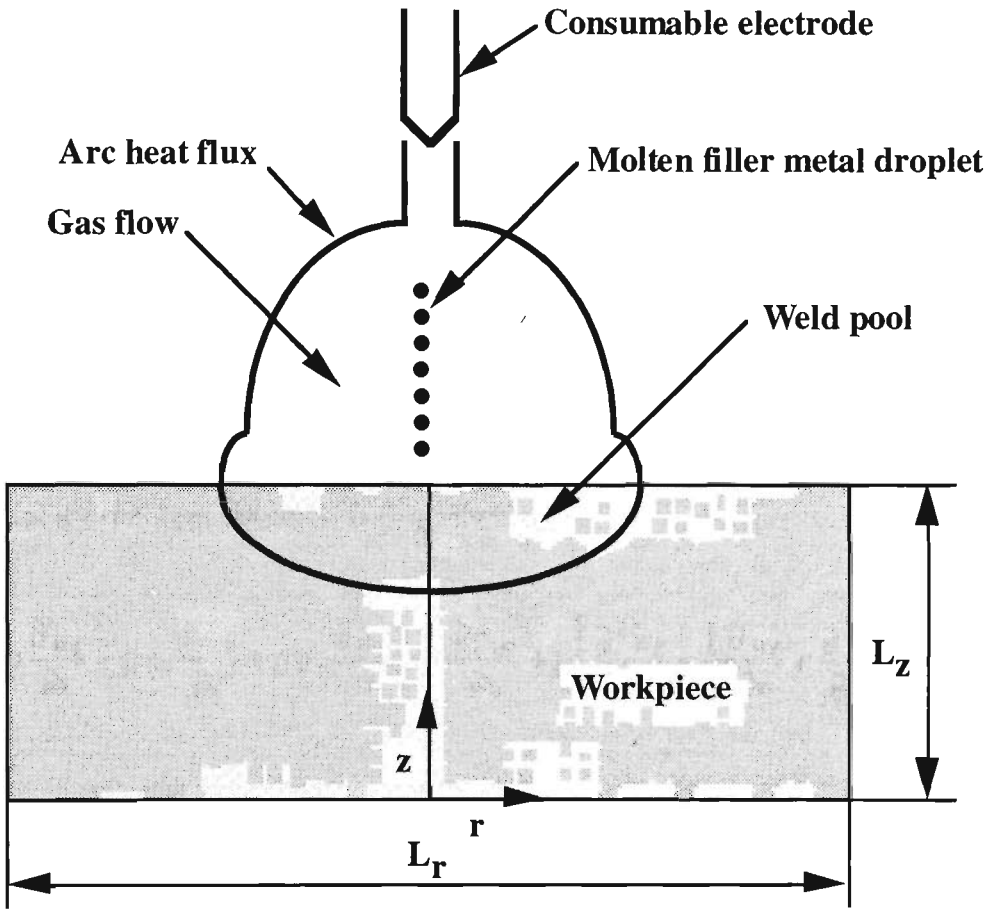

Figure 5.1 Schematic diagram of a GMAW and the weld pool.

5.2.1 Governing Equations

Using the assumptions stated above, the governing equations that describe the transient development of weld pools due to coupled conduction and convection heat transfer are the continuity, the momentum and the energy equations [Carslaw and Jaegar (1959)[18]].

The continuity equation is represented as

$$\frac{1}{r}\frac{\partial}{\partial_r}(\rho r u_r)+\frac{\partial}{\partial_z}(\rho u_z)=0 \tag{5.1}$$

The radial momentum equation is presented as

$$\rho\frac{\partial u_r}{\partial t}+\rho u_r\frac{\partial u_r}{\partial r}+\rho u_z\frac{\partial u_r}{\partial z}=-\frac{\partial p_m}{\partial r}+\mu\left[\frac{\partial^2 u_r}{\partial r^2}+\frac{1}{r}\frac{\partial u_r}{\partial r}-\frac{u_r}{r^2}+\frac{\partial^2 u_r}{\partial z^2}\right]$$

$$-J_z B_\theta \tag{5.2}$$

The axial momentum equation is described as

$$\rho\frac{\partial u_z}{\partial t}+\rho u_r\frac{\partial u_z}{\partial r}+\rho u_z\frac{\partial u_z}{\partial z}=-\frac{\partial p_m}{\partial z}+\mu\left[\frac{\partial^2 u_z}{\partial r^2}+\frac{1}{r}\frac{\partial u_z}{\partial r}+\frac{\partial^2 u_z}{\partial z^2}\right]$$

$$+J_r B_\theta+\beta\rho g(T-T_r) \tag{5.3}$$

The energy equation is expressed as

$$\rho C_p\frac{\partial T}{\partial t}+\rho C_p u_r\frac{\partial T}{\partial r}+\rho C_p u_z\frac{\partial T}{\partial z}=k\frac{\partial^2 T}{\partial r^2}+k\frac{\partial^2 T}{\partial z^2}+\frac{\Delta H\partial f_L}{\partial t} \tag{5.4}$$

5.2.2 Boundary Conditions

To complete the mathematical description of the problem, the boundary conditions are illustrated in figure 5.2 and specified as follows:

$$\Gamma 1\ (AB) \qquad u_r=0,\quad u_z=0,\quad -k\frac{\partial T}{\partial z}=h_c(T-T_o)+\sigma_o\varepsilon(T^4-T_o^4),\quad \frac{\partial\phi}{\partial z}=0$$

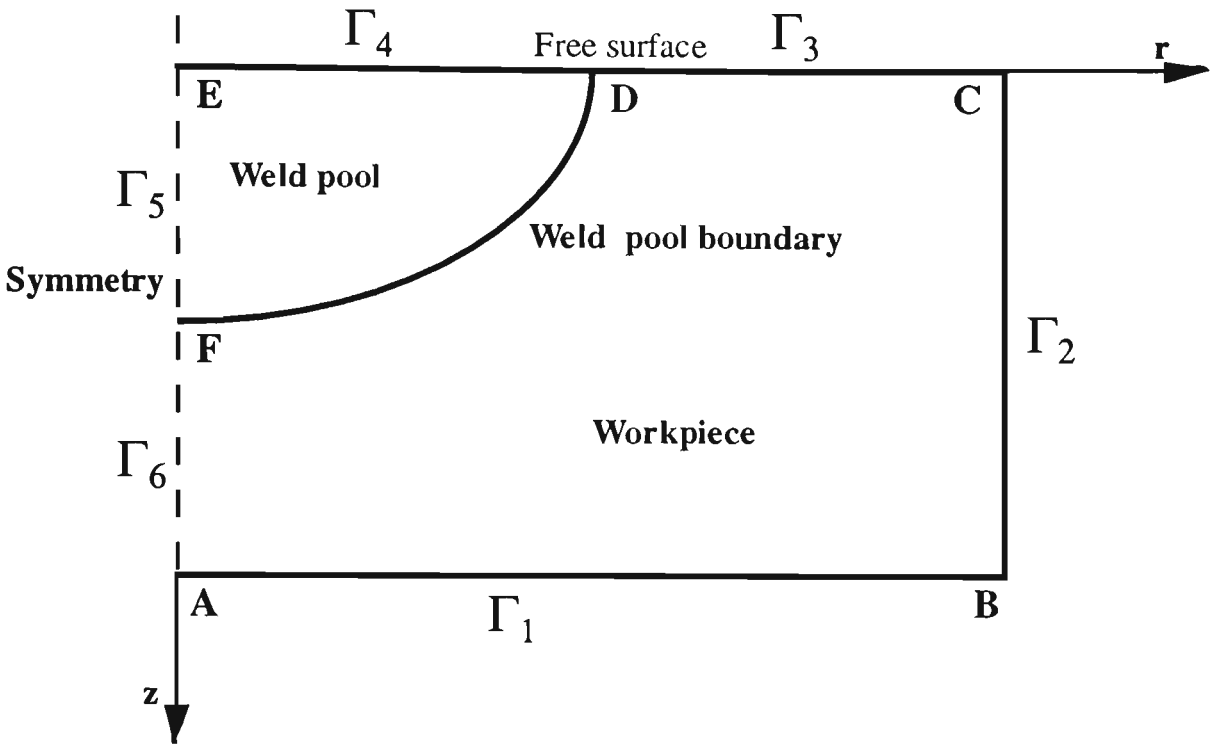

Figure 5.2 The boundary conditions employed in the mathematical model.

$$\Gamma 2\ (\text{BC}) \qquad u_r = 0, \quad u_z = 0, \quad -k\frac{\partial T}{\partial r} = h_c(T - T_o) + \sigma_o \varepsilon (T^4 - T_o^4) \quad \phi = 0$$

$$\Gamma 3\ (\text{CD}) \qquad u_r = 0, \quad u_z = 0, \quad -k\frac{\partial T}{\partial z} = q_a = \frac{3Q}{\pi r_q^2}\exp\left\{-3(r / r_q)^2\right\},$$

$$J_{suf} = -\sigma\frac{\partial \phi}{\partial z}$$

$$\Gamma 4\ (\text{DE}) \qquad \mu\frac{\partial u_r}{\partial z} = -\left\{\left(\frac{\partial \gamma}{\partial T}\right)\left(\frac{\partial T}{\partial r}\right)\right\} + \frac{3V_r}{\pi r_a^2} exp\left\{-3(r / r_a)^2\right\} + \tau_{drag}, \quad u_z = 0$$

$$-k\frac{\partial T}{\partial z} = \frac{3Q}{\pi r_q^2} exp\left\{-3(r / r_q)^2\right\} \qquad r < r_s$$

$$T = T_d \qquad r < r_d$$

$$J_{suf} = -\sigma \frac{\partial \phi}{\partial z}$$

$$\Gamma_5 \text{ (EF)} \quad u_r = 0, \quad \frac{\partial u_z}{\partial r} = 0, \quad \frac{\partial T}{\partial r} = 0, \quad \frac{\partial \phi}{\partial r} = 0$$

$$\Gamma_6 \text{ (FA)} \quad u_r = 0, \quad u_z = 0, \quad \frac{\partial T}{\partial r} = 0, \quad \frac{\partial \phi}{\partial r} = 0 \qquad (5.5)$$

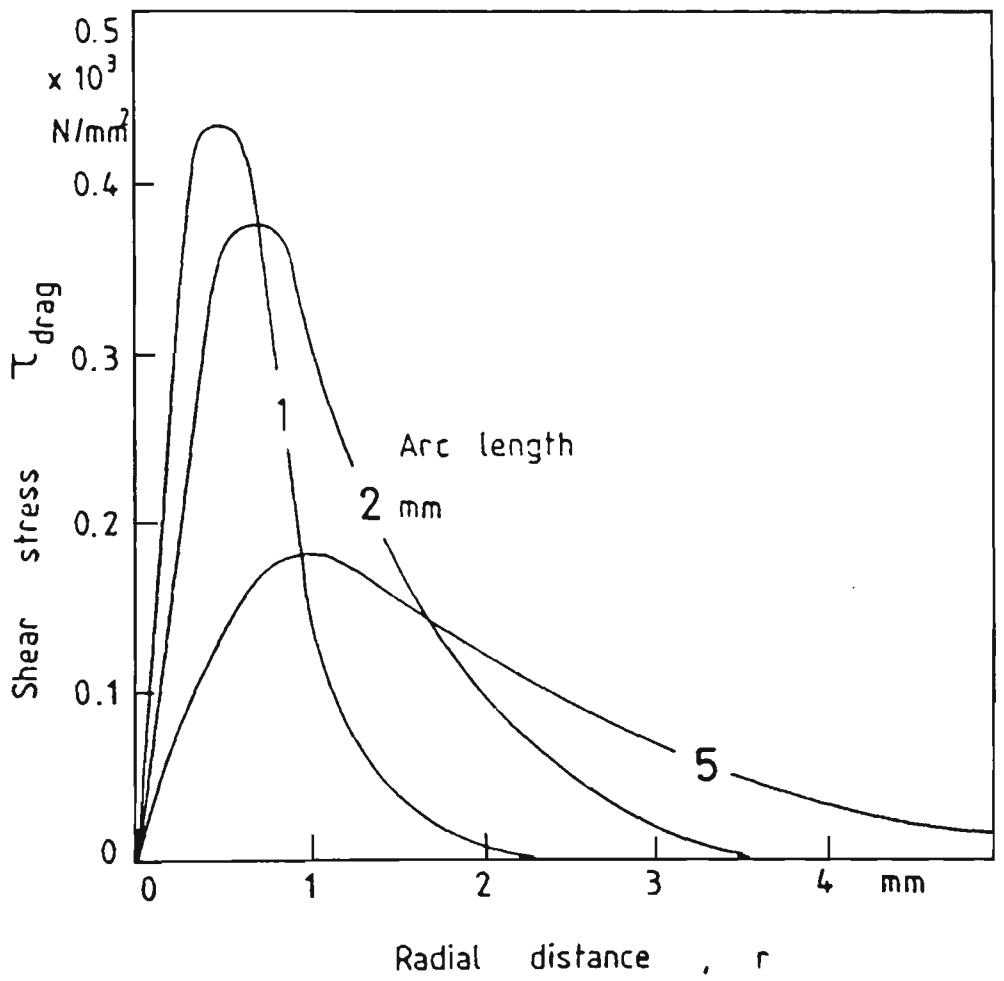

Figure 5.3 Distribution of shear stress at weld pool surface [Matsunawa et al. (1988)[114]].

The plasma drag and the surface tension forces are treated as boundary conditions. The radial distribution of shear stress τ_{drag} employed is shown in figure 5.3 [Matsunawa et al. (1988)[114]]. The liquid-solid phase change and the associated latent heat were modelled using the enthalpy method, which is the definition of the fraction

of liquid [Thomas et al. (1984)[176] and Brent et al. (1988)[11]]. The essential feature of this method is that the evolution of latent heat is taken account of the governing energy equation by defining a heat source terms.

The latent heat term is added to the energy equation via $-\frac{\Delta H \partial f_L}{\partial t}$ where

$$f_L = \begin{cases} 1 & T > T_{liq} \\ (T - T_{sol}) / (T_{liq} - T_{sol}) & T_{sol} \le T \le T_{liq} \\ 0 & T < T_{sol} \end{cases} \qquad (5.6)$$

This method easily adapts to the general algorithms of the PHOENICS code as it is designed to solve non-linear equations through iterative techniques. The latent heat content is directly coupled to the nodal temperature, which produces fairly accurate results, especially for non-isothermal solidification of metals.

5.2.3 Source Terms and Driving Forces for Fluid Flow

5.2.3.1 Molten Metal Droplets

In GMAW process, the shape of weld pools appears to be determined primarily by the momentum and special distribution of the stream of droplets from the melting electrode. To develop the numerical model in this study, it was assumed that not only the heat input distributions are described as uniform droplet temperature over a central circular area, equivalent to droplet radius and a Gaussian - distributed arc heat source, over a circular area equivalent to the arc, but also molten electrode is transferred from the melting electrode to the weld pool surface with the Gaussian - distributed velocities. The distributed velocities were added to the converged velocities of fluid components at the weld pool surface in the iterative calculation procedure. Tichellar et al. (1977)[179] determined the average temperature of droplets as 2400 ^{o}C for steel. The droplet radius has been taken from previously published experimental work

[Lancaster (1984)[97]] as 0.46 mm. Since there is a close relationship between gas flow rate and arc current in GMAW, arc current 360 A is calculated by wire feed rate of 0.207 m/s for 1.2 mm wire diameter from figure 5.4*. The volumetric feed rate of electrode was calculated from these date and effective radius of the velocity distribution was assumed 2 mm.

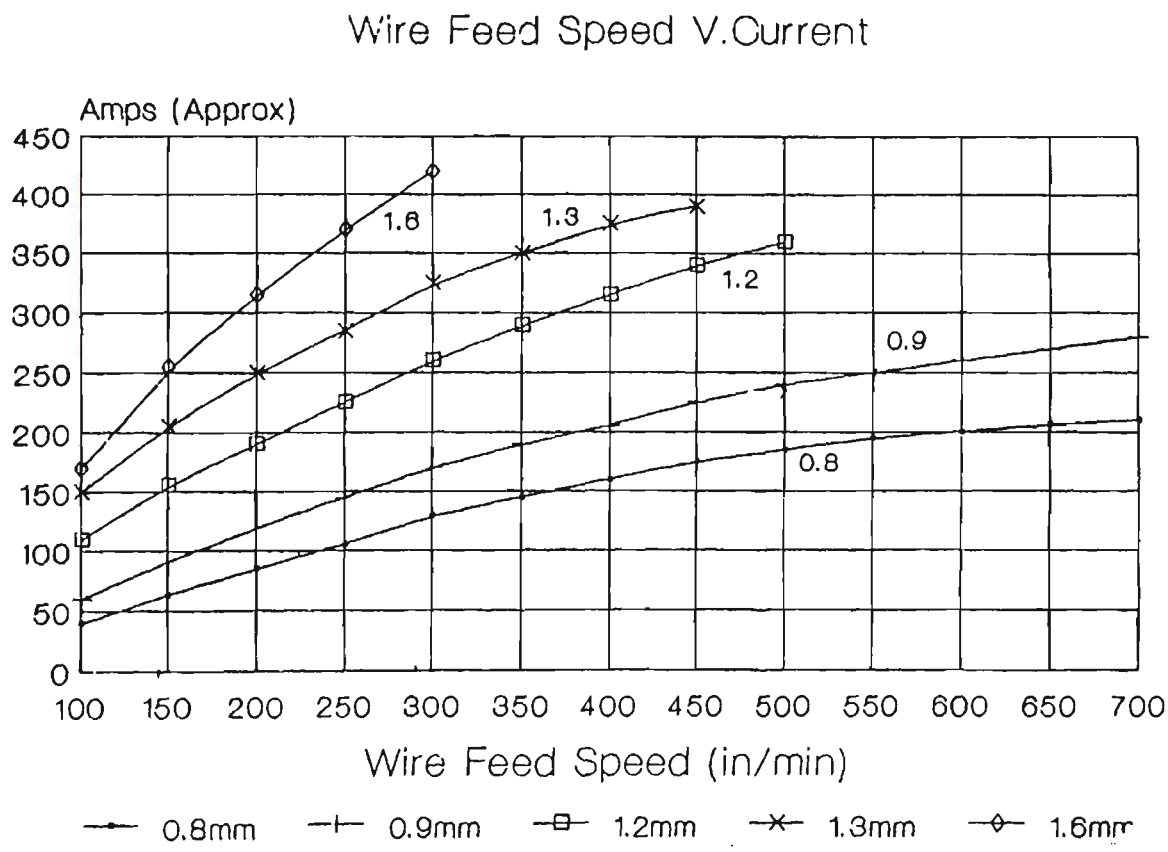

Figure 5.4 Relationship between wire feed speed and arc current.

Heat input efficiency which depends on welding process variables such as arc current, welding voltage, type of shielding gas, gas flow rate and electrode extension, has been found to range between 66 and 71 percent in the GMAW using plain carbon steels [Christensen et al. (1965)[36] and Allum and Quintino (1985)[3]], and 71 percent with 1.2 mm wire diameter argon + 7% CO_2 as the shielding gas [Essers and Walter (1981)[48]]. The heat input efficiency is taken as 70 percent in the present simulation.

* This data regarding relationship between arc current and wire feed rate was provided from the Lincon Electric Co.

5.2.3.2 Electromagnetic Force

In the GMAW, a current flow from wire electrode to the workpiece induces a magnetic field which interacts with arc current to create an electromagnetic or Lorentz force. The distribution of the arc current over weld pool surface can be written as:

$$J_{suf} = \frac{3I}{\pi r_j^2} \exp\left\{-3(r / r_j)^2\right\} \tag{5.7}$$

The charge continuity equation given by Gauss' law becomes:

$$\nabla J = 0 \tag{5.8}$$

assuming that the electric field is in a quasi-static state. For linear isotropic conducting media, the current density given by Ohm's law is represented:

$$J = \sigma E \tag{5.9}$$

Defining an electric potential by $E = -\nabla\phi$, the distribution of the electric potential in the workpiece from equations (5.8) and (5.9) is described:

$$\nabla^2 \phi = 0$$

or

$$\frac{1}{r}\frac{\partial}{\partial r}\left(r\frac{\partial \phi}{\partial r}\right) + \frac{\partial^2 \phi}{\partial z^2} = 0 \tag{5.10}$$

where steady flow and a constant electrical conductivity have been assumed.

From the calculated potential field, the distribution of current density in weld pools can be obtained from Ohm's law:

$$J_r = -\sigma \frac{\partial \phi}{\partial r} \tag{5.11}$$

$$J_z = -\sigma \frac{\partial \phi}{\partial z} \tag{5.12}$$

The magnetic field given by Ampere's law is presented:

$$\nabla B = \mu_m J \tag{5.13}$$

By symmetry, only the circumferential component of the self-induced magnetic flux vector B_θ is non-zero. With the help of the Maxwell equation, equation (5.13) is written as:

$$\frac{\partial B_\theta}{\partial z} = \mu_m J_r \tag{5.14}$$

$$\frac{1}{r}\frac{\partial}{\partial r}(r B_\theta) = \mu_m J_r \tag{5.15}$$

From equations (5.13) and (5.14) and the boundary condition that $B_\theta = 0$ is at $r = 0$, the self-induced magnetic field is obtained from Ampere's law:

$$B_\theta = \frac{\mu_m}{r}\int_0^r J_z r \partial r \tag{5.16}$$

Combining equations (5.10) through (5.16), the electromagnetic force $J \times B$ in weld pools is calculated:

$$(J \times B)_r = -J_r B_\theta \tag{5.17}$$

$$(J \times B)_z = -J_z B_\theta \tag{5.18}$$

A summary of the techniques for solving the electromagnetic force $J \times B$ with a distributed current source is useful at this time. Three methods for solving the electromagnetic force for the arc welding are known in the literature. Kou and Le (1983)[83], Kou and Sun (1985)[84] and Zacharia et al. (1989)[196] used an analytical solution derived by Atthey (1980)[7] for cylindrical coordinates, but experimental studies by Lu and Kou (1989)[108] showed that the current distribution did not certainly follow a Gaussian behaviour. The second technique by Oreper et al. (1986)[135] and Oreper and Szekely (1987)[136] was employed an electromagnetic stream function relation to derive the current density. This scheme is quite different from the first method of solving the electromagnetic force. The third technique by Correa and Sundell (1986)[40] and Choo et al. (1992)[34] was identical to the one used here. The technique proposed in this thesis has been individually originated from studies of Correa and Sundell (1986)[40] or Choo et al. (1992)[34].

5.2.3.3 Surface Tension Force

Surface tension force which is referred to as the Marangoni effect, describes the flow of liquid at a free surface from a region of low surface tension to a region of higher surface tension. At the surface of weld pools, the surface tension variation with temperature must be balanced by fluid shear stress since the surface must be continuous. Therefore, the shear stress at the surface is equated to the gradient of surface tension. At the free surface, the shear stress due to the Marangoni effect or the surface tension driven flow is included as a boundary condition for the momentum equation:

$$\mu \frac{\partial u_r}{\partial z} = -\frac{\partial \gamma}{\partial T}\frac{\partial T}{\partial r} \tag{5.19}$$

5.3 NUMERICAL PROCEDURE

5.3.1 The Discretization

In order to enhance the accuracy of calculation in the weld pool area and to reduce the cost of analysis, grids of variable spacing were employed. Finer grids were utilised near the heat source, while further away from it, a relatively coarse grid was employed. The mathematical model was employed a 40×41 non-uniform fixed rectangular grid system for calculation of temperature and velocity fields as shown in figure 5.5. Magnitude of weld pool zone was estimated as approximate 4 mm. The minimum radial grid was 0.15 mm, while the minimum axial grid was 0.14 mm.

For a numerical solution of equations (5.1) to (5.4), the problem domain is covered by a set of rectangular control volumes. Values of variables within a control volume are presented in terms of the values at the associated node point. A main grid was located at the centre of each control volume. The discretization was performed using a staggered grid [Patankar (1980)[141]] which consisted of two different grids; one for vector variables such as velocity and another for scalar variables such as temperature and pressure. Based on the staggered grid, a fully implicit control volume integration of the governing equations (5.1) to (5.4) results in the finite difference scheme below:

$$a_P\varphi_P = a_S\varphi_S + a_N\varphi_N + a_H\varphi_H + a_L\varphi_L + b \qquad (5.20)$$

where φ presents any of axial velocity, radial velocity, temperature and pressure. The subscripts indicate the appropriate nodal value of dependent variable. The value of **a** represents the coefficients which result from the equations, but **b** is the source term from the equations. To calculate the values of the relevant dependent variables at a set of chosen points called the grid points, the algebraic equations for these values, called

the discretization equations, were derived by integrating the governing differential equation over a each grid points.

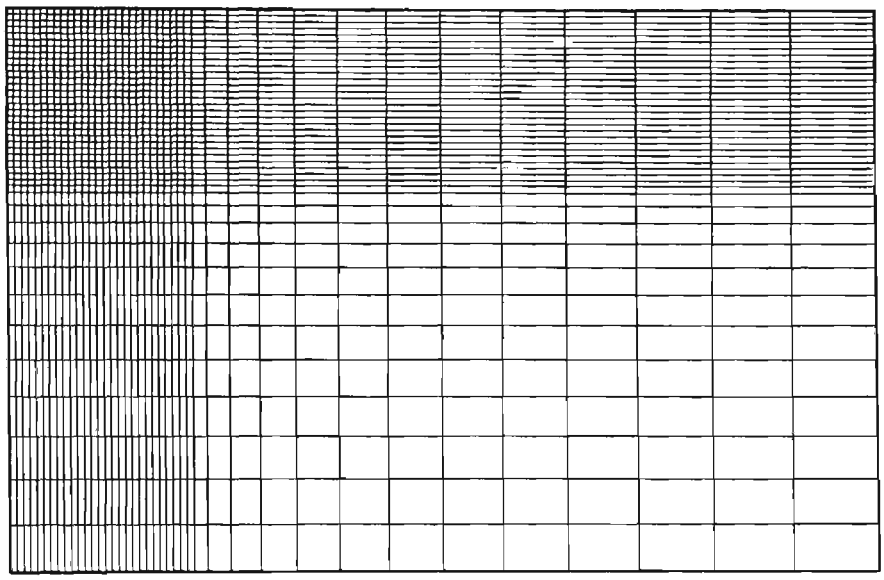

Figure 5.5 Grid employed for computations.

5.3.2 Method of Solution

To numerically solve the governing equations with the associated source terms, a general thermofluid-mechanics computer program, PHOENICS code [Spalding (1993)[170]] (which was based on the SIMPLE algorithm [Patankar (1980)[141]] and developed by CHAM Ltd. to solve coupled sets of partial differential equations governing heat, mass and momentum transfer) was used. The material properties and workpiece information employed in the calculation of temperature and velocity fields as well as weld bead geometry are summarised in table 5.1. They were taken from Oreper and Szekely (1987)[136] and Choo et al. (1992)[35]. In general, it is quite tedious to obtain accurate material properties since these properties are not only temperature dependant but also composition dependent [Zacharia et al. (1992)[199]]. As a result, the values reported here reflect order of magnitude approximation.

Table 5.1 Material properties data employed for modelling

Nomenclature	Symbol	Value
coefficient of thermal expansion	ß	$10^{-4}(K^{-1})$
density	ρ	7200 kg/m^3
electrical conductivity	σ_o	$7.14\times10^{5}\Omega^{-1}m^{-1}$
heat capacity	C_p	$753J/kg-K$
rate of addition of weld material	F	$1.37\times10^{-8}\ m^3/s$
latent heat of fusion	ΔH	$2.47\times10^{5}J/kg$
thermal conductivity (liquid steel)	k_l	$15.48W/m.K$
thermal conductivity (solid steel)	k_s	$31.39W/m.K$
plate radius	L_r	20 mm
plate thickness	L_z	12 mm
liquid temperature (steel)	T_{liq}	1723 K
Maximum surface temperature	T_{max}	2500 K
ambient temperature	T_o	300 K
solid temperature (steel)	T_{sol}	1523 K
surface tension coefficient	$\partial r/\partial T$	$10^{-5}N/m-K$
permeability of free space	μ_m	$1.26\times10^{-9}(H/mm)$
viscosity	μ	$6.0\times10^{-3}(kg/m.s)$

Initial convergence difficulties were overcome by using a simultaneous solver for the pressure-correction equation and false-time step relaxation on temperature and velocities. Convergence was accomplished when the spot values of the relevant dependent variables at the critical grid location remain fixed (<0.001), but the residuals of all governing equations keep decreasing. Generally, the residual must decrease by at least 3 orders of magnitude with respect to the first sweep before the run is terminated. The time step employed was 10^{-3}s. The number of sweeps needed to achieve a converged solution depends on a number of parameters such as initial guess, material properties, fine-turning of the relaxation parameters. The reference residual employed as a stopping criterion to determine when the calculations should advance to

the next time step, was assumed to be 10^{-9}* for radial velocities, axial velocities, temperature and pressure.

5.4 RESULTS AND DISCUSSION

The detailed information on the fluid flow and heat transfer that occur during the GMAW process was obtained by numerically solving the mathematical models that represent the essential physical features of the process. The computational model was employed to simulate the welding process in order to quantitatively understand the effects of different forces on the fluid flow and heat transfer, and the weld geometry. The arc current and welding voltage are 360 A and 25 V respectively. The effective radius of density distribution and effective radius of current distribution are 4 mm and 3 mm.

The gradual development of the interface between the liquid and solid regions with time has been shown in figure 5.6. The occurrence of the finger type of penetration can be easily observed. Contours of axial and radial velocity and of temperature as well as velocity field in weld pools at time of 0.75s due to the combined driving forces (electromagnetic, buoyancy, surface tension and plasma drag forces) are clearly shown in figures 5.7 to 5.10. During the GMAW process, all these forces are simultaneously applied in and on weld pools. The calculated temperature field in weld pools and shape of weld pools are shown in figure 5.7. The weld pool has a width of 4.26 mm and a depth of penetration of 4.09 mm. Figures 5.8 to 5.10 shows the contour of axial and radial velocity as well as velocity field which is composed of a double loop circulation pattern - a wider radial flow at surface and a central penetrating flow loop.

---

* The reference residual is 10^{-7} for the electric potential to aid in the stopping criterion as the charge continuity equation is time-independent.

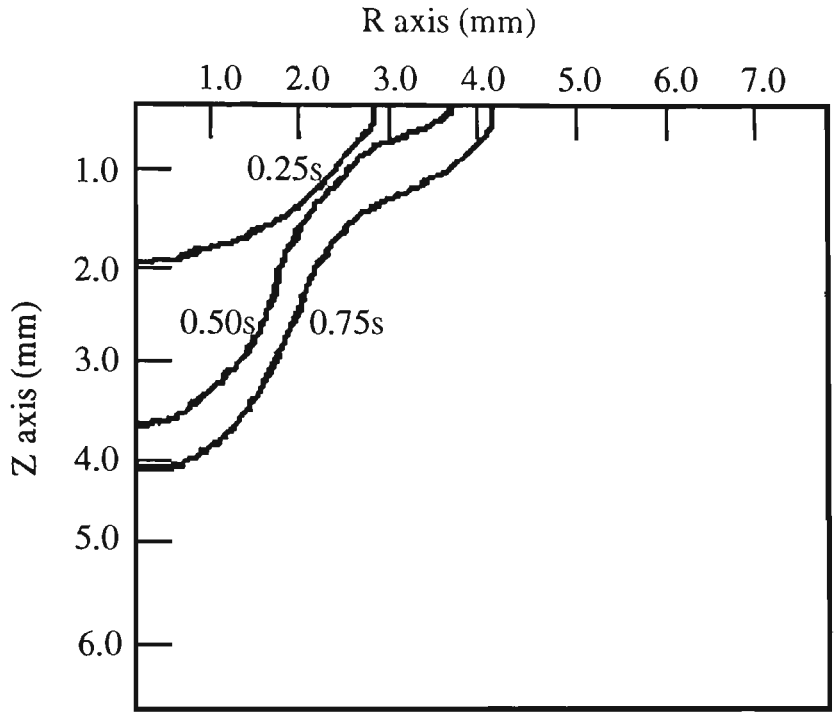

Figure 5.6 Liquid-solid interface of the GMAW process at different times.

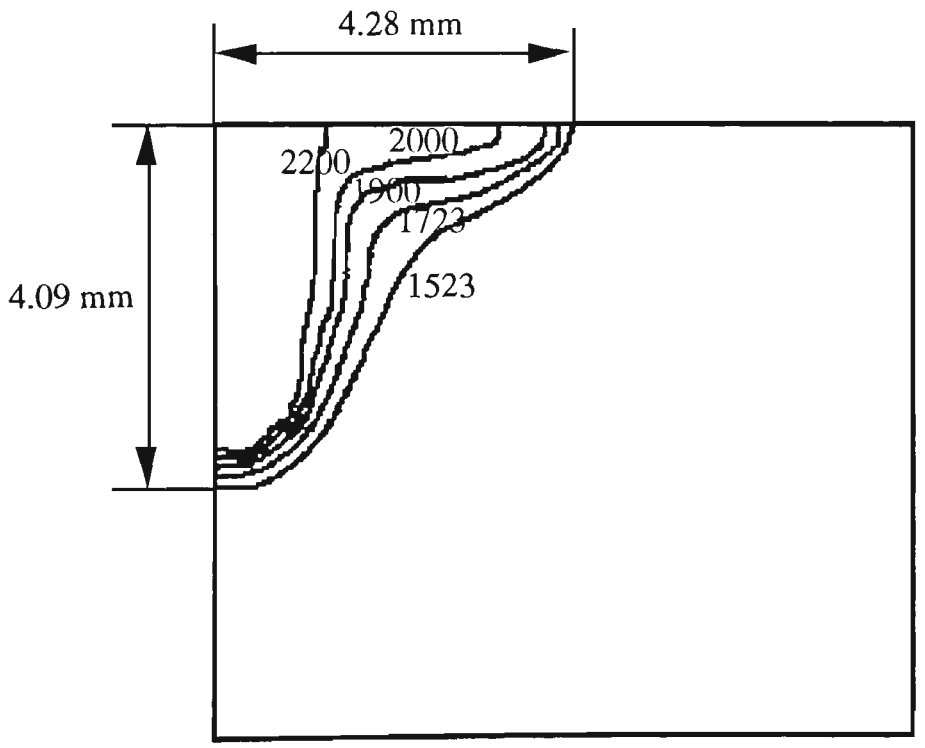

Figure 5.7 Temperature field in weld pools due to the combined driving forces.

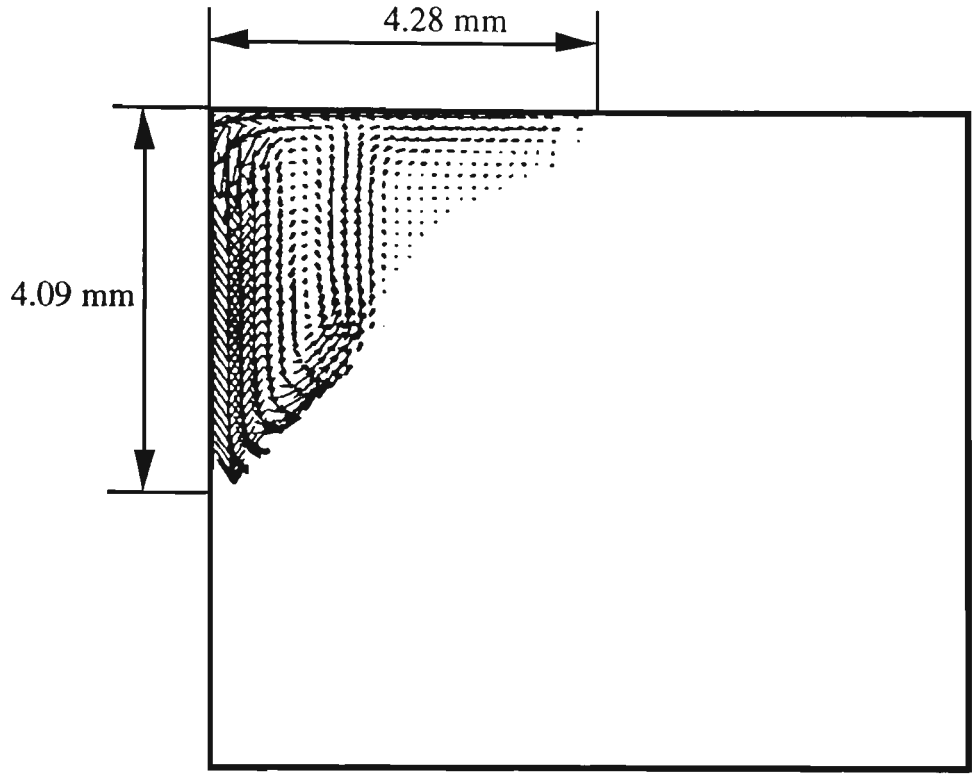

Figure 5.8 Velocity field in weld pools due to the combined driving forces.

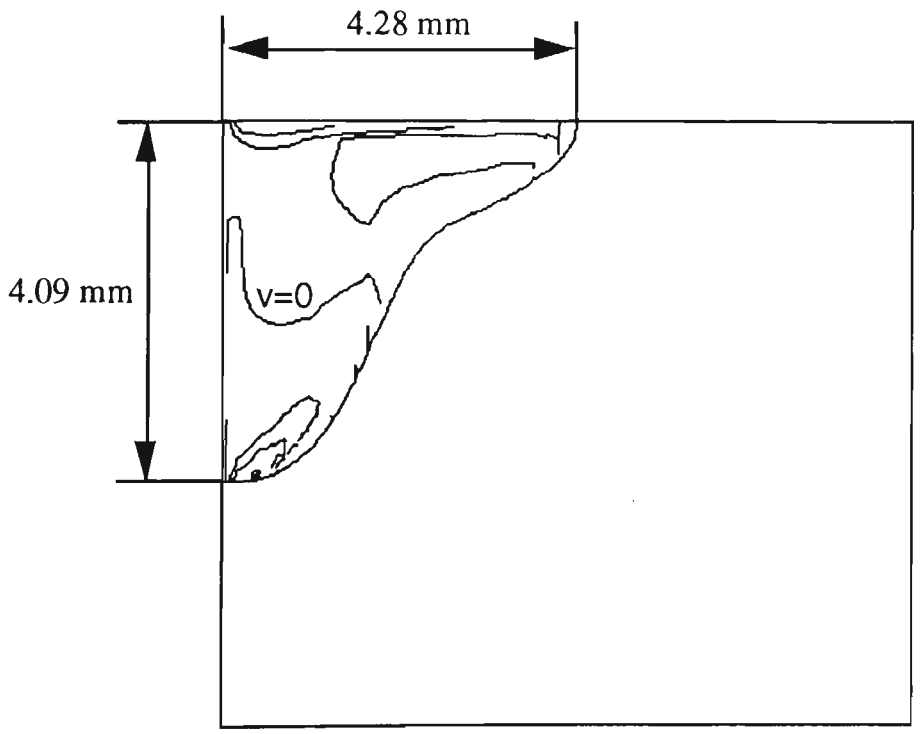

Figure 5.9 Radial velocity contour due to the combined driving forces.

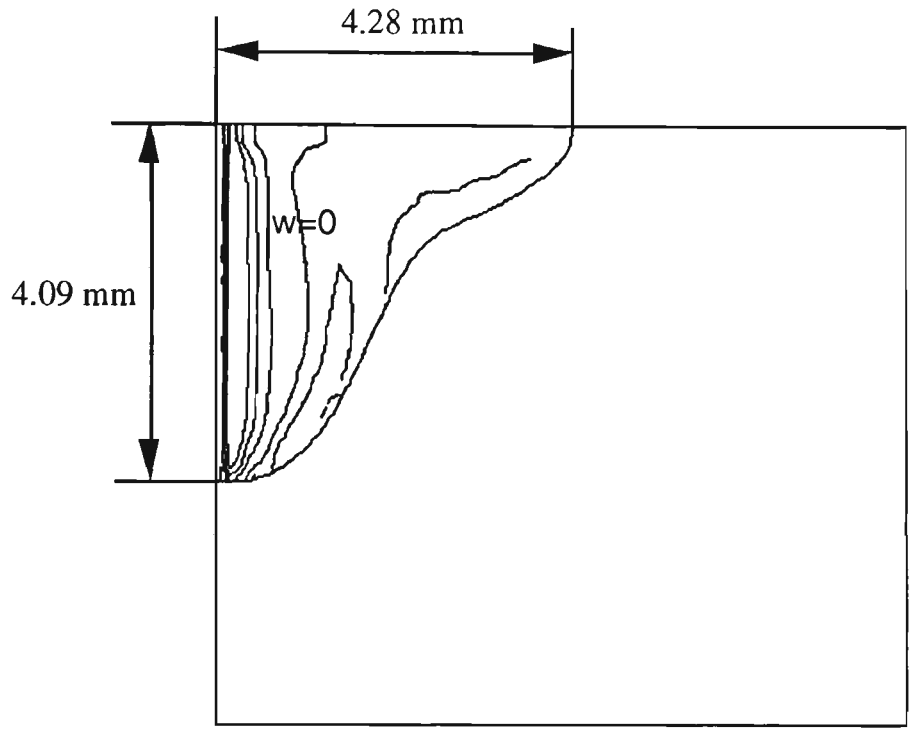

Figure 5.10 Axial velocity contour due to the combined driving forces.

The computed results indicate that there is the difference in the velocity scale between the first and second loop circulation patterns. The maximum surface velocity observed is of the order of 2.5 m/s.

A wider radial flow at surface is mainly induced by the surface tension force at the weld pool surface which is caused by temperature gradients at the weld pool surface and possibly by surface active agents in weld pools. Surface tension of the liquid metal at the weld pool surface is lower near the centre and higher near the boundary because surface tension of the liquid metal tends to decrease with increasing temperature. As a result, the calculated flow pattern by surface tension force was from centre to weld pool boundary.

A central penetrating flow loop is dominated by the electromagnetic force caused by the interaction between the divergent current path in weld pools and the magnetic field it generates. Since the divergence of the electric current fields in weld pools develops

a downward electromagnetic force near the central part of weld pools and pushes the liquid metal in the region downward to the weld root, the liquid metal by the electromagnetic force flows downward near the centre of weld pools and upward near the boundary. Since the flow pattern induced by the electromagnetic force promotes heat transfer from the heat source to the weld root, the transport of hot liquid metal down the axis of the weld pool will result in deep weld penetration. The results also indicate that the fluid flow has a significant effect on the weld pool temperature distribution and the development of the weld pool shape and size.

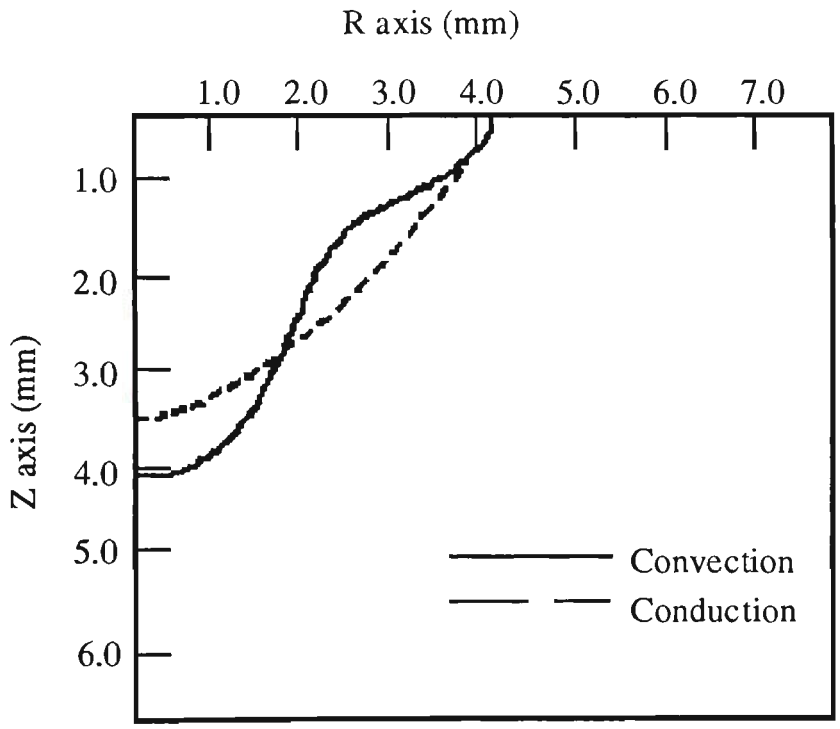

Figure 5.11 Comparison of weld pool boundaries with the same heat input.

Figure 5.11 depicts weld pool boundaries in comparison with those of calculation in only conduction mode while the input parameters and material properties were fixed. It is noted from figure 5.11 that convection mode makes deeper penetration in the workpiece than only conduction model, and weld pool convection which causes greater heat transfer from the heat source to the workpiece, plays a significant role in the formation of the finger penetration.

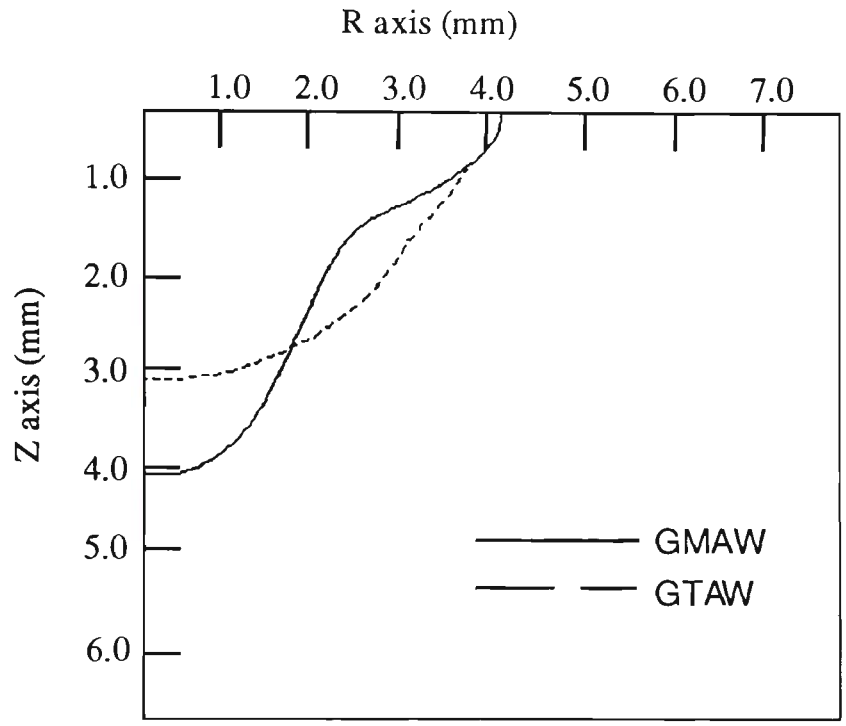

Figure 5.12 Comparison of the GMAW with GTAW weld pool dimensions.

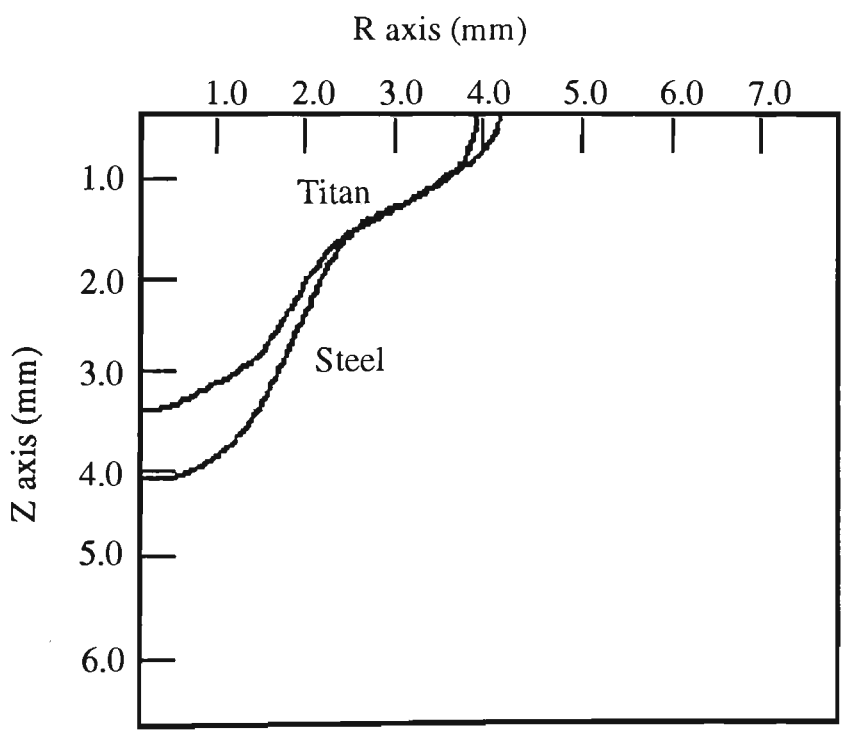

Figure 5.13 Comparison of mild steel with titanium weld pool boundaries at the same conditions.

Figure 5.12 illustrates the comparison of the GMAW with GTAW weld pool dimensions, while the input parameters and material properties were not changed. As shown in figure 5.12, the GMAW process makes a deeper weld bead penetration into the workpiece than the GTAW process, while a smaller weld pool because some of the input energy is employed to melt the filler metal and raise its temperature to that of the liquid metal. Figure 5.13 illustrates the comparison of mild steel with titanium weld pool profiles at the equal input parameters. These materials have different thermal and physical properties, which would cause different velocity and temperature fields.

5.5 SUMMARY OF RESULTS

1. Fluid flow and heat transfer in weld pools for the GMAW were theoretically investigated through a transient axisymmetrical solution of Navier-Stokes equation and the equation of conservation of energy.
2. The computer model incorporates the four distinct forces (electromagnetic, buoyancy, surface tension and plasma drag forces) and the molten metal droplets.
3. A double loop circulation pattern can coexist with weld pools: one in a central penetrating flow loop by the electromagnetic force and the other in a wider radial flow at surface by surface tension.
4. The computed results clearly indicate that the electromagnetic and surface tension forces as well as the molten metal droplets are the dominant factors that control the weld pool convection, while the buoyancy and plasma drag forces seem to have little significance.
5. With reference to figure 5.11, it is obvious that there is a significant difference between the results from models with and without convective heat transfer. Weld bead penetration is strongly affected by fluid flow in weld pools.

CHAPTER 6

INFRARED SENSING FOR AN ADAPTIVE ARC WELDING PROCESS

6.1 INTRODUCTION

The automated and/or robotic arc welding is widely employed in the fabrication industry for increasing productivity and enhancing product quality by its high processing speed, accuracy and repeatability. Reprogramming techniques have proved to be inadequate in taking into consideration of the component distortion, due to heat imperfections and seam misalignment which can take place during the welding process. To fully automate the welding process and adaptively control, it is needed sensors that monitor the process output in real-time and feedback to the controller the generated information so that welding process parameters are adjusted accordingly and in-process variations are compensated [Cook et al. (1989)[39]]. These variations can be either in the weld pool shape and size, weld seam, or both.

Tactile sensors have been employed for seam tracking and weld bead penetration control. Even if these are simple to use, their major limitation lies with their inherent inflexibility and wear characteristics that can give rise to measurement inaccuracies [Malin (1986)[111] and Hanright (1986)[61]]. On the other hand, non-contact type sensing is preferable, but the cost associated with the sophisticated system constrain their extensive applications. Machine vision systems have been developed and used in

conjunction with low power laser beams. The latter is utilised to intercept the area of sight, while the former is employed to extract information from the welding scene regarding seam positioning and the unfused zone area [Boillet et al. (1985)[9]]. Control is performed in real-time and an adaptive manner via an integrated microprocessor capable of taking appropriate corrective action and ensuring that the welding head follows the seam path and deposits the optimum amount of filler material to fuse the joint. A number of variations of systems based on this principle exist, most of which have been miniaturised and made robust over the years [Richardson (1986)[153]]. For sensors incorporated within the welding torch or attached to the robotic manipulator, an ability to withstand the harsh welding environment is a major prerequisite.

In general, remote sensing techniques are currently under considerable flux and constitute the preferred means for dynamically detecting welding process variations. Accumulated information at each point is employed to compensate for deficiencies including incomplete penetration and lack of side wall fusion. A system of this type that employs infrared thermography principles and computer imaging techniques is described in the following section. The sensing system has been implemented in real-time monitoring of the robotic GMAW process.

Infrared thermography is finding increasing application in the area of non-destructive testing and evaluation as well as in condition monitoring of plant equipment and facilities. Temperature differences down to 0.1 ^{o}C can be monitored with today's thermoelectrically cooled infrared scanners. Thermal signatures can be stored on video tapes or on other forms of permanent records including computer disk and photographs. However, this sophisticated technique is expensive and this is the only drawback to its wide utilisation in industry. It is believed that the more the laboratory applications are researched and developed, the more possibilities for industry implementations may be found.

In welding, infrared thermography has been used to monitor weld quality and the bond strength of resistance welded electrical components in real-time. The system employed was integrated with a microprocessor which compared the measured data against stored models of acceptable weld thermal signatures. Another example is that of monitoring the on-line weld quality of electrical switches used in automobile air bag components. Information related to tensile strength of the weld was extracted from the temperature profiles and heat distribution areas. Infrared thermography has also been used to assess the integrity of critical fusion welds in industries such as air craft and petrochemical [Ramsey et al. (1963[149]), Lukens and Morris (1982)[109] and Chin et al. (1983)[28]].

Preliminary investigations [Chen and Chin (1990)[26] and Nagarajan et al. (1989)[128]] using infrared thermography for welding process status information showed that variations in weld process parameters produce changes in surface temperature distributions on the plates being welded. During these works, front side scanning infrared camera was used to monitor molten pool and surface temperature distributions during the welding. Welding process parameters were varied to alter the weld bead penetration and corresponding changes in the temperature distribution were recorded. It was established that a linear relationship between weld bead width and infrared image profile width exists. Additionally, the weld bead penetration was exponentially correlated to the area under the measured surface temperature profile taken at the centre-line of the molten metal pool [Nagarajan et al. (1989)[129]]. Such findings clearly indicate that the above mentioned information from the surface temperature of plates being welded can be utilised to control the weld bead penetration and weld bead width in real-time. A recent study [Chen and Chin (1990)[26]] revealed that by measuring the amount of visible and near infrared emitted from the rear of the weld joint, weld bead penetration over a range of welding process parameters can be controlled. The system employed proved to be sensitive enough to employ fibre-optics for transmitting the light from the weld to the sensor. The fibre-optics

technology helped the facilitation of welding assemblies with limited access to the underside of the weld is most suited to relatively small diameter tubes. This may be an expensive application but it can be seen as a tool for ensuring specification compliance and minimising the amount of rework needed, especially on critical and valuable components [Smartt et al. (1993)[168]].

The above mentioned techniques have substantially advanced the concept of remote monitoring of weld bead penetration during the automated and/or robotic arc welding using infrared sensing, but make no reference to the technique's additional potential capability for seam tracking. In other words, the studies document only the capacity of the emerged technology to accommodate deficiencies related to acceptable penetration variations in real-time. While the correct weld volume deposition is necessary to fuse the joint, it's correct placement on the joint that is equally desirable in order to allow quality to be built into the product rather than inspected into it [Marburger (1990)[113]]. Although there exists a plethora of seam tracking systems that can be used in conjunction with infrared thermography to complement the seam following capabilities of these systems by controlling weld bead penetration, it would be more advantageous to fully explore the potential of a single system to control both tasks. It was against this background that the research and development discussed below was carried out.

The primary purpose of this chapter is (1) to find relationships between welding process parameters and thermal image from infrared thermography, (2) to obtain the thermal profile characteristics, (3) to calculate the weld bead geometry using image analysis techniques and (4) to finally relate the surface temperature distribution of the welded part to the weld bead width and height.

6.2 EXPERIMENTAL PROCEDURE

6.2.1 Experimental Equipment

The AGA thermovision 680 employed in this study consists of infrared camera and thermal picture display. The camera unit converts the invisible infrared radiation given off by an object into equivalent electronic video signals which are then amplified and transferred via an interconnecting cable to the display unit [AGA (1983)[1]].

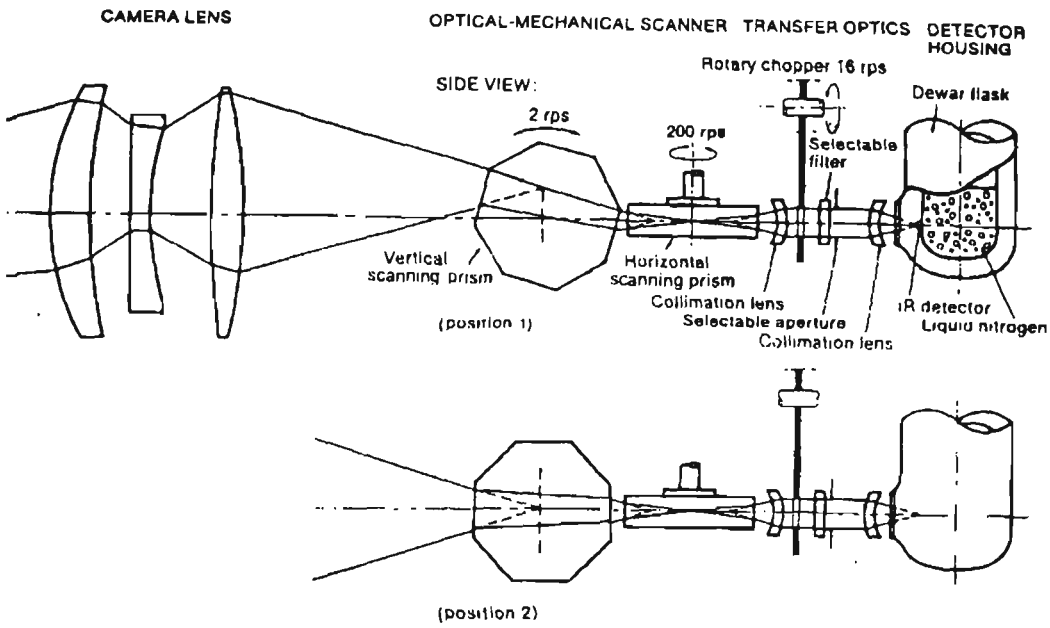

Figure 6.1 Various optical paths with the system 680 camera unit.

The infrared scanner in the 680 camera is made up of two rotating (vertical and horizontal) scanning prisms, that are driven by a pair of hysteresis synchronous drive motors. Power to the motors is supplied from a built-in 200 Hz solid state inverter located in the display unit. The functions of the scanner are as follows: A virtual image is formed by the front lens of camera on a plane within the first prism. The image is scanned vertically by the rotation of the prism about its horizontal axis. This

results in a horizontal, virtual line-image being formed within the second scanning prism. The line-image is then scanned horizontally in turn by the rotation of the second prism about its vertical axis (shown in figure 6.1).

Both prisms are eight sided. The horizontal scanning prism is flat in form, and rotates at high speed about its short axis at a speed of 12000 revolutions per minute. The prism is mounted together with a position pick-off ring on a single flange coupled directly to the shaft of the horizontal-drive motor. Due to the high horizontal rotational speed, the entire assembly must be carefully balanced dynamically before installed inside the camera unit. The vertical scanning prism is drum-shaped. It rotates at right angles to the horizontal prism, scanning the image approximately once vertically for every 70 horizontal scans. Due to its greater mass, the vertical prism is supported separately on both sides by precision ball bearings and carefully centred. It is coupled through a set of precision reduction gears to the second drive motor, which operates at 4000 rpm. Figure 6.2 shows the internal arrangement of the infrared camera.

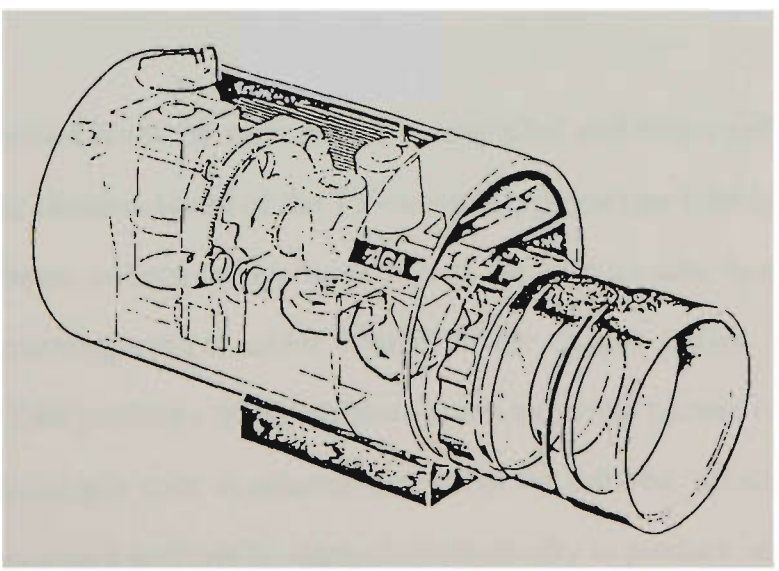

Figure 6.2 Internal arrangement of infrared camera.

The infrared sensitive detector in the standard 680 camera consists of an indium antimonite (InSb) photovoltaic cell, sensitive to the middle infrared wavelength band. The detector cell must be cooled to the temperature of liquid nitrogen (-196°C) to obtain its maximum sensitivity. The liquid nitrogen coolant is stored in a 100 cm^3 dewar within the camera. When the dewar is full, it provides coolant for at least four hours of camera operation before refilling is necessary.

The dimensions of the infrared detector are kept as small as possible consistent with required temperature resolution in order to obtain the best possible spatial resolution. The small size of the detector enables mounting it within the double walls of the dewar vessel, providing both temperature-shielding and protection from contamination of the sensitive detector surface by exposure to the atmosphere. The infrared beam enters the detector housing through a sapphire window set in the outer wall of the dewar. In front of the detector, window is a flange for mounting the detector assembly on the chopper housing. This flange that contains the second lens of the collimating system, used to focus the parallel rays emerging from the chopper assembly onto the surface of the detector.

The signal derived from the camera unit is amplified and employed to modulate the intensity of the electron beam of the TV-monitor type picture tube in the display unit. The electron beam sweeps across the screen of the monitor tube in synchronism with the camera scanning-optics, under control of the trigger pulses derived from the camera unit. This produces on the display screen a thermal picture of the object being scanned by the camera unit. A selected amount of the infrared radiation focused on the detector in the camera unit can be marked electronically to produce isothermal contours on the display screen. Whenever the detector video signal level corresponds to the preset isothermal level selected, the electron beam of the picture tube is automatically switched to maximum intensity. This causes all areas in the thermal picture with the selected temperature level to be outlined in saturated white. The isothermal contours

thus produced can be used to measure the exact amount of temperature variation existing between details of the thermal image of the weld in progress if required.

6.2.2 Welding Procedure

Experiments were designed to study the effects of welding process parameters on weld bead geometry and the surface temperature distributions, and to develop the adaptive control system. In the first series of test, a 2^3 factorial experiment was employed to investigate the relationship between welding process parameters and thermal images as well as welding bead geometry as a function of arc current, welding speed and welding voltage. Appendix C shows the welding process parameters for experiment.

The second series of experiments were performed using various arc currents of 150 to 240 Amps and a constant welding speed of 180 mm/min, welding voltage of 20 V, wire diameter of 1.2 mm and gas flow rate of 14 ℓ. These experimental results were employed to investigate the relationship between the thermal images produced by infrared thermography and welding bead geometry (weld bead width and height) in order to achieve an adaptive welding process.

All experiments were carried out using AS 1204 mild steel plates having dimensions 200 mm in length, 100 mm in width and 5 and 10 mm in thickness. The chemical composition of weld material and 1.2 mm wire diameter were the same employed in chapter 3. The experimental setup was composed of the welding power source by Lincoln arc welding, Hitachi process robot and AGA thermovision 680 system. An automatic wire feeding unit was employed to provide variable wire feed rates, according to arc current level employed. A six axis robotic manipulator was utilised to provide the welding process speed and welding direction. The robotic and welding controller was interfaced with the welding power source with an adjustable range of

output current between 50-350 Amps and an adjustable range of output voltage between 16-36 Volts. A microcomputer was employed to address the robotic arc welding controller and to access its menu containing combinations of welding process parameters to achieve the desired quality output. The schematic diagram of the experimental setup employed is illustrated in figure 6.3.

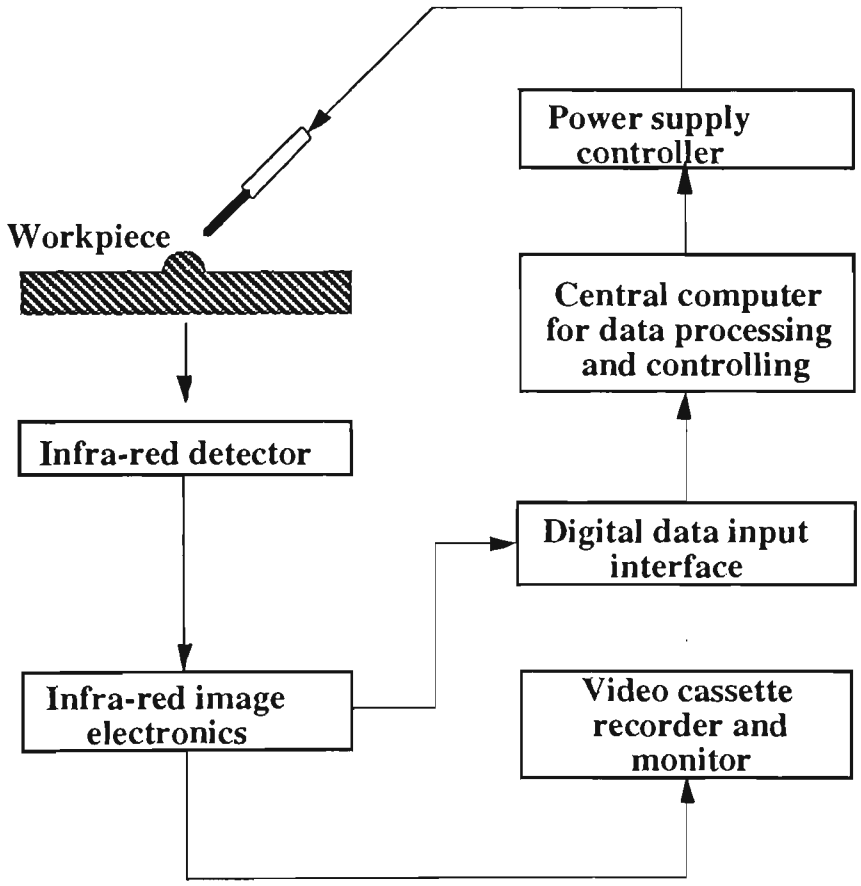

Figure 6.3 The schematic diagram of the experiment.

A solid electronics cooled infrared vision camera was employed to convert the invisible infrared given off during welding into equivalent electronic video signals which were then amplified and transferred to the display unit during the welding. The unit was positioned away from, but directly in view of, the rear of the weld steel plates to be welded and was interfaced with the same microprocessor as the robotic welding controller through the video output connection. The output was fed to an image frame grabber and after being digitised it was processed using an image analysis software

package. The scanning rate of the camera was 30 frames per second and computer image sampling and storage rate was 5 frames per second. Digitised frames were stored in a C. D. erasable / rewritable laser facility for analysis and processing. During the welding, the planner position coordinates of the welding torch in relation to the plate surface were also recovered.

After each welding run, test pieces were sectioned and metallographically examined. Polishing and etching of the welding zone revealed weld bead dimensions, which were recorded using machine vision facilities. Figure 6.4 illustrates measurements of weld bead width and height taken from the metallographic weld samples. Measurements of weld bead width and height were performed after welding, using a standard metallographic technique.

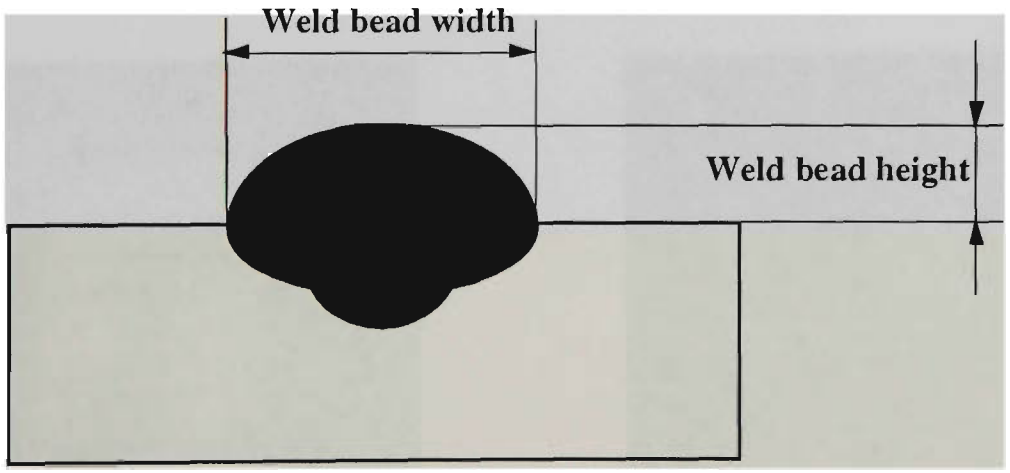

Figure 6.4 Metallographic weld sample showing measurements of weld bead width and weld bead height.

6.3 RESULTS AND DISCUSSION

Figure 6.5 depicts the temperature distribution obtained during the GMAW process for four welds of varying welding process parameter. As shown in figure 6.5, there are identifiable changes in the surface temperature distribution.

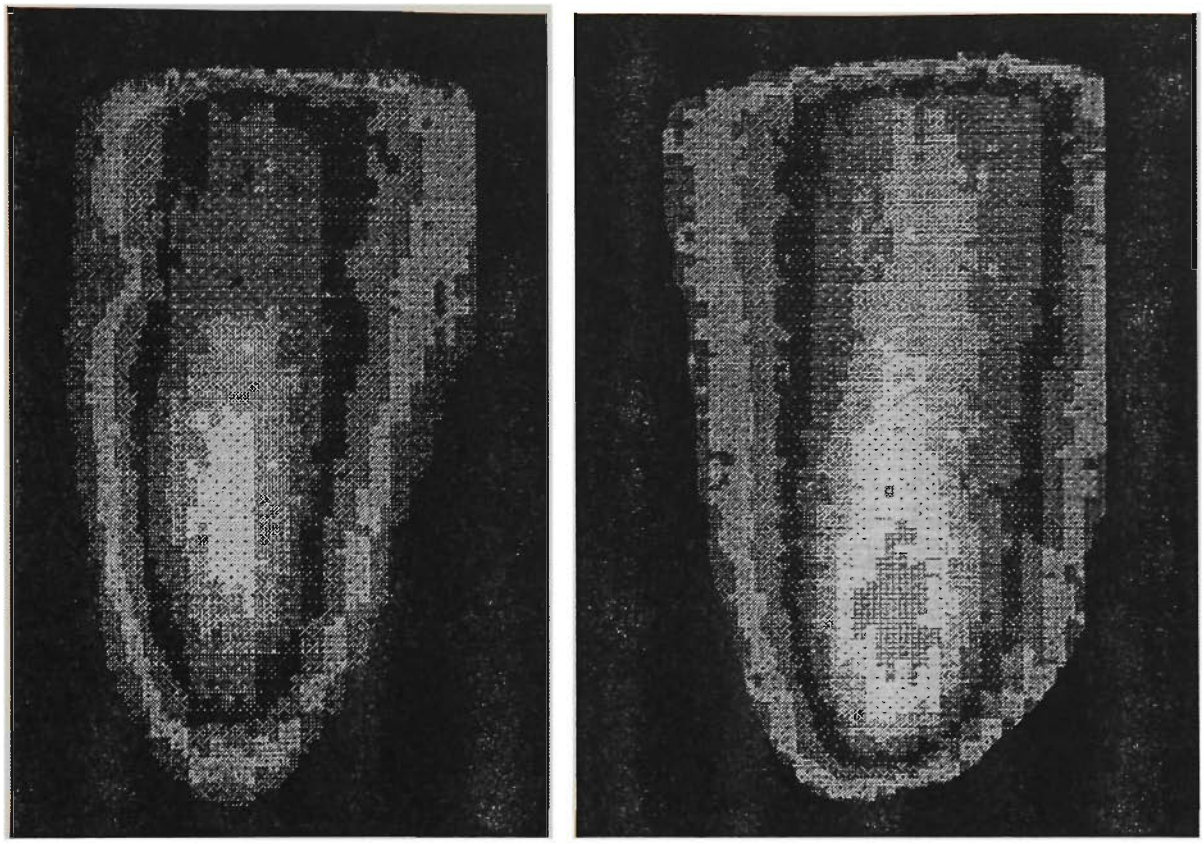

(a) Arc current=150A and thickness=5mm (b) Arc current=150A and thickness=10mm

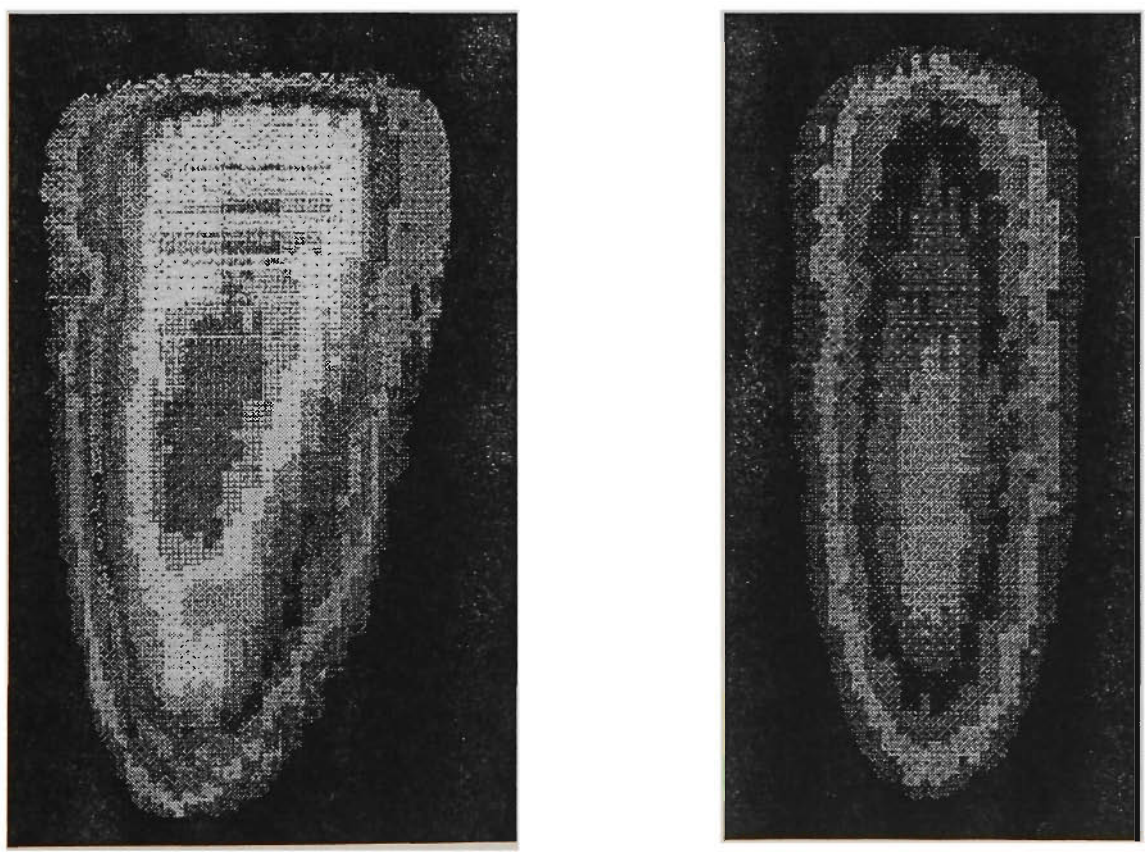

(c) Arc current=240A and thickness=5mm (d) Arc current=240A and thickness=10mm

Figure 6.5 Isothermal colour plots showing surface temperature distribution.

Figure 6.6 shows temperature versus distance from the thermal images to calculate the width of the temperature peak by measuring the profile width at the temperature midway between the peak and background temperature, its unit is called an "isotherm unit" [AGA (1983)[1]].

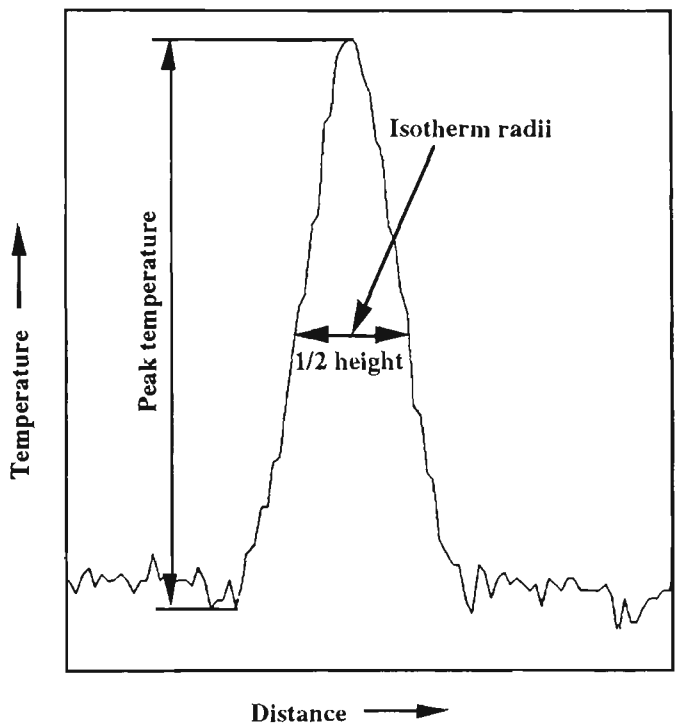

Figure 6.6 Diagram showing thermal scan characteristics used.

In the first experiments, the three welding process parameters (arc current, welding speed and welding voltage) were varied independently. Other welding process parameters were held constant during the each experiment. The results of experiment were given in Appendix C and figures 6.7 to 6.18. Figure 6.7 shows the relationship between arc current and isotherm radii. The average isotherm radii were calculated by taking the average of all measured values with the same arc current for a 5 mm and 10 mm thickness of mild steel test pieces respectively, but without considering the effects of welding speed and welding voltage. It can be seen here that as arc current increases, the isotherm radii also increases. The relationship between arc current and weld bead width shown in figure 6.8 indicates that there is an increase in weld bead width with an increase in arc current. Weld bead widths were produced by taking the

average of all values for welds deposited with the same arc current for 5 mm and 10 mm thickness of mild steel test pieces respectively, but ignoring the effects of welding speed and welding voltage. When a higher arc current is employed, a higher weld bead height is achieved as can be shown in figure 6.9. The average weld bead heights were found by taking the average of all measured values with the same arc current for 5 mm and 10 mm thickness of mild steel test pieces respectively, without taking account of the effects of welding speed and welding voltage. The relationship between isotherm radii and weld bead geometry is shown in figure 6.10, which indicates that there is an increase in weld bead geometry as isotherm radii increases.

The relationship between welding speed and the isotherm radii is represented in figure 6.11. The average isotherm radii were computed by taking the average of all measured values for welds deposited with the same welding speed for 5 mm and 10 mm thickness of mild steel test pieces respectively, but without considering the effects of arc current and welding voltage. It is evident that as welding speed increases the isotherm radii decreases. The relationship between welding speed and weld bead width shown in figure 6.12 represents that there is a decrease in weld bead width with an increase in welding speed. Weld bead widths were produced by taking the average of all values for welds with the same welding speed, ignoring the effects of arc current and welding voltage. When a higher welding speed is employed, a lower weld bead height is achieved as seen in figure 6.13. The average weld bead heights were found by taking the average of all measured values with the same welding speed for 5 mm and 10 mm thickness of mild steel test pieces respectively, but without taking account of the effects of arc current and welding voltage.

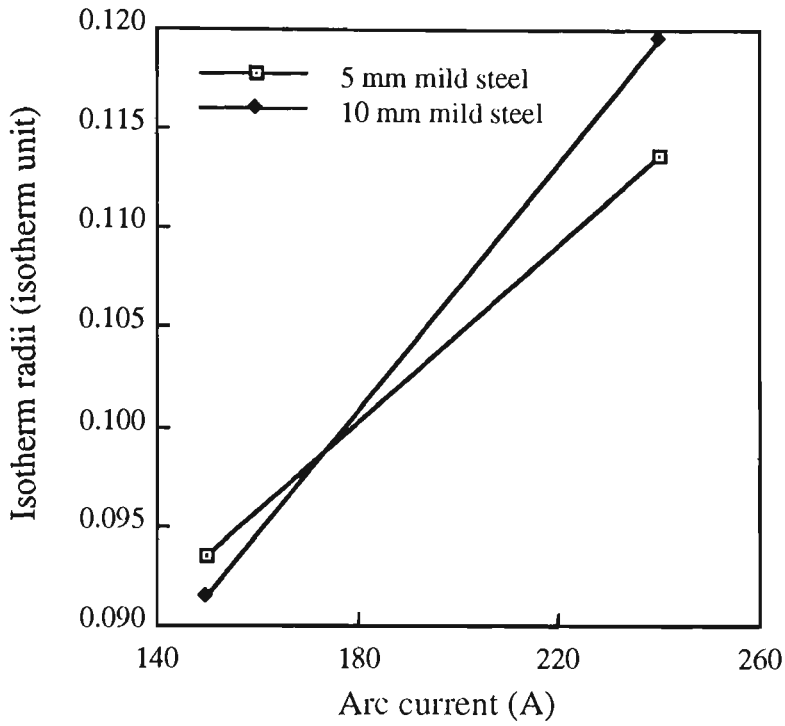

Figure 6.7 Arc current versus isotherm radii.

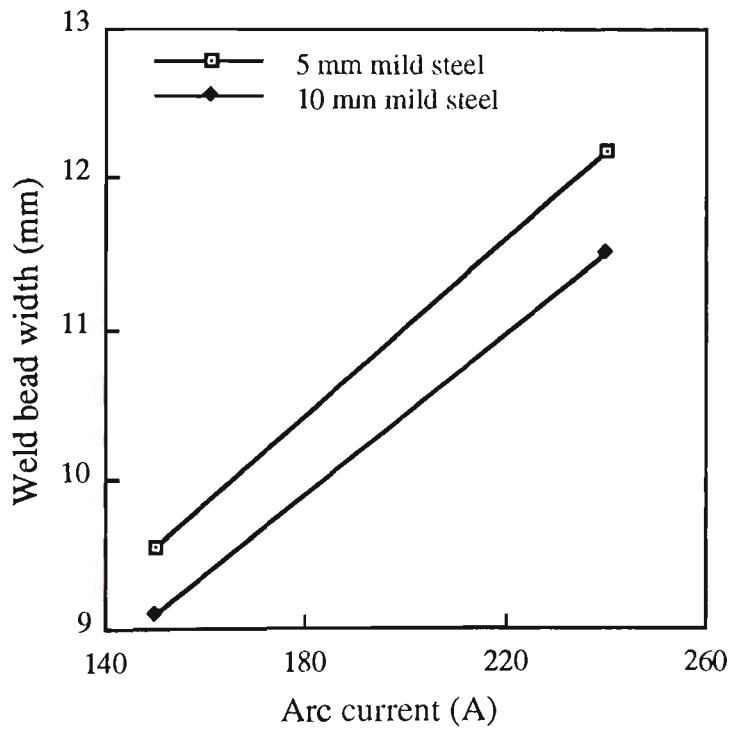

Figure 6.8 Arc current versus weld bead width.

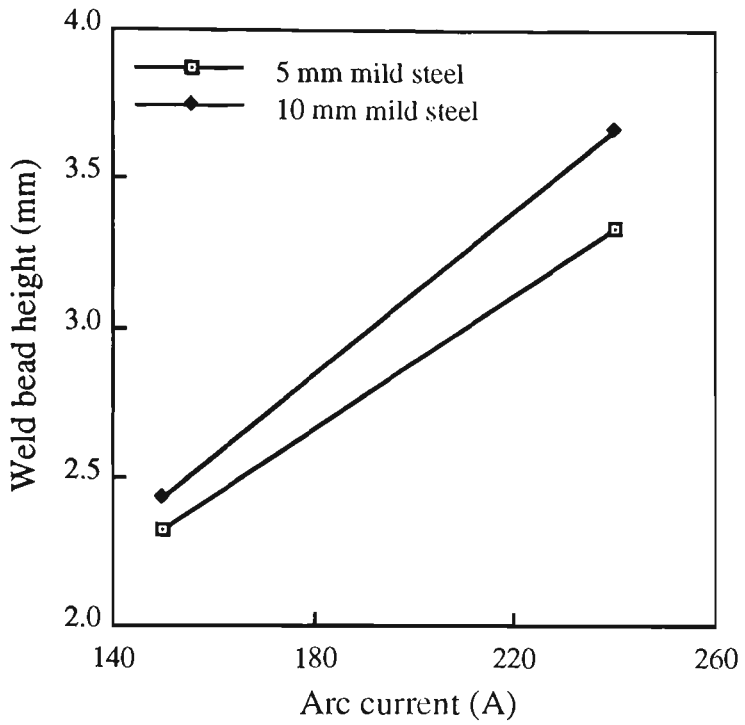

Figure 6.9 Arc current versus weld bead height.

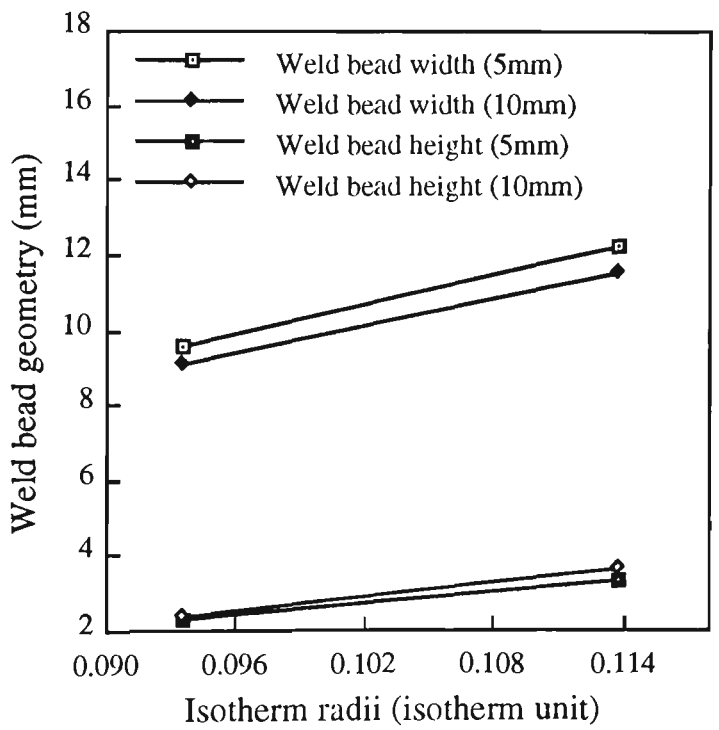

Figure 6.10 Isotherm radii versus weld bead geometry.

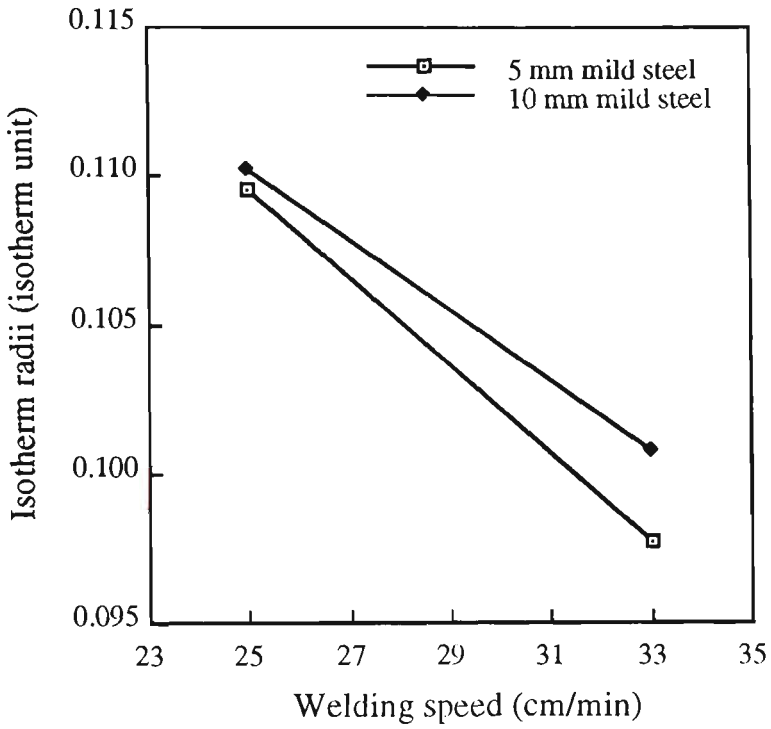

Figure 6.11 Welding speed versus isotherm radii.

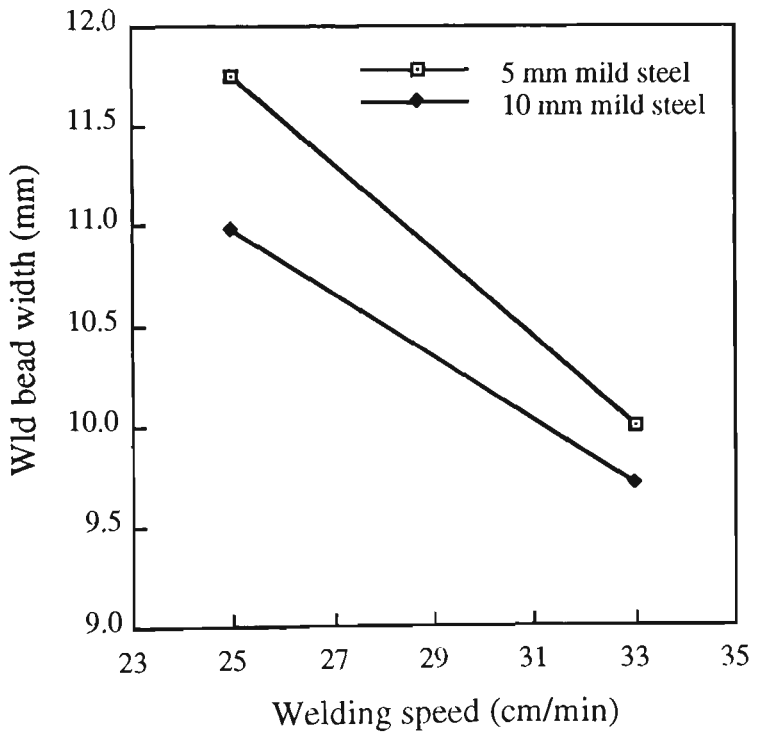

Figure 6.12 Welding speed versus weld bead width.

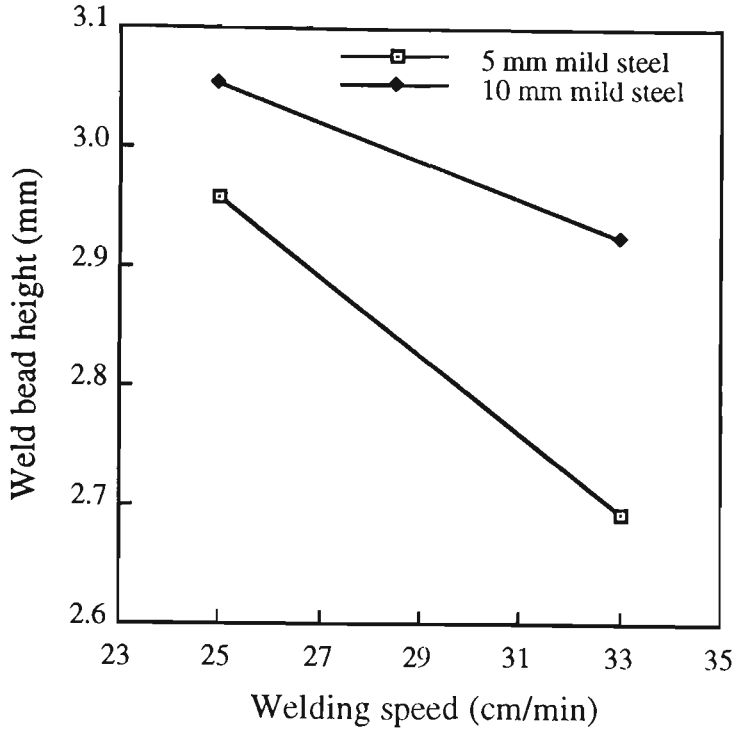

Figure 6.13 Welding speed versus weld bead height.

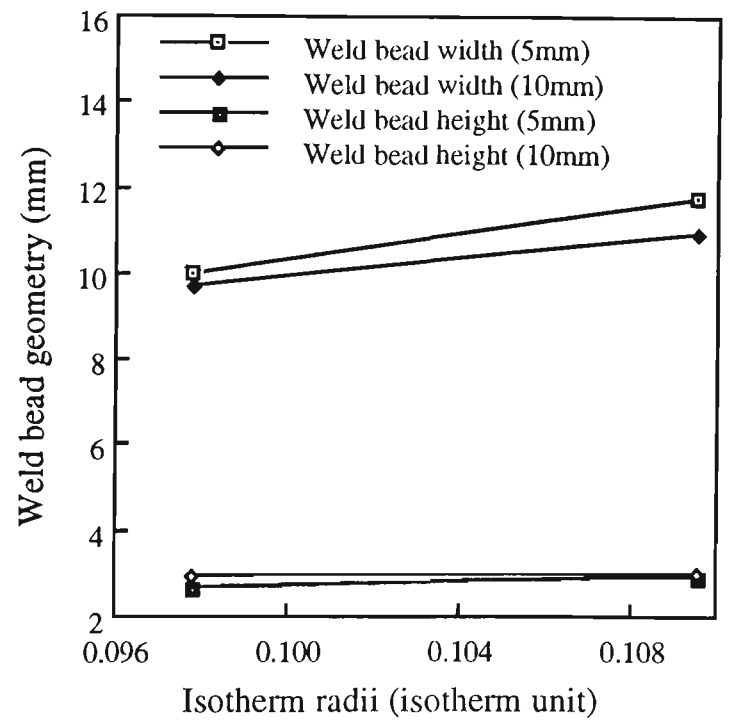

Figure 6.14 Isotherm radii versus weld bead geometry.

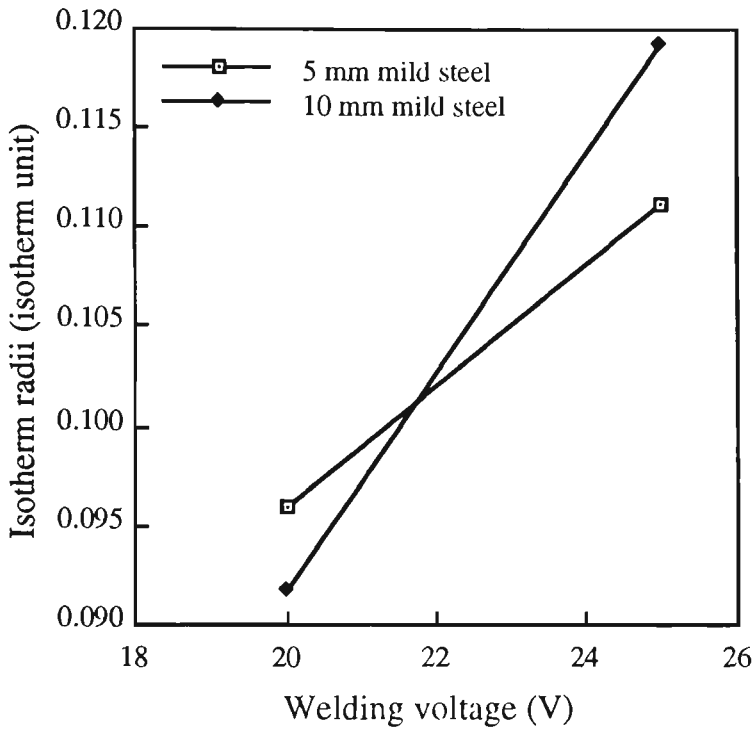

Figure 6.15 Welding voltage versus isotherm radii.

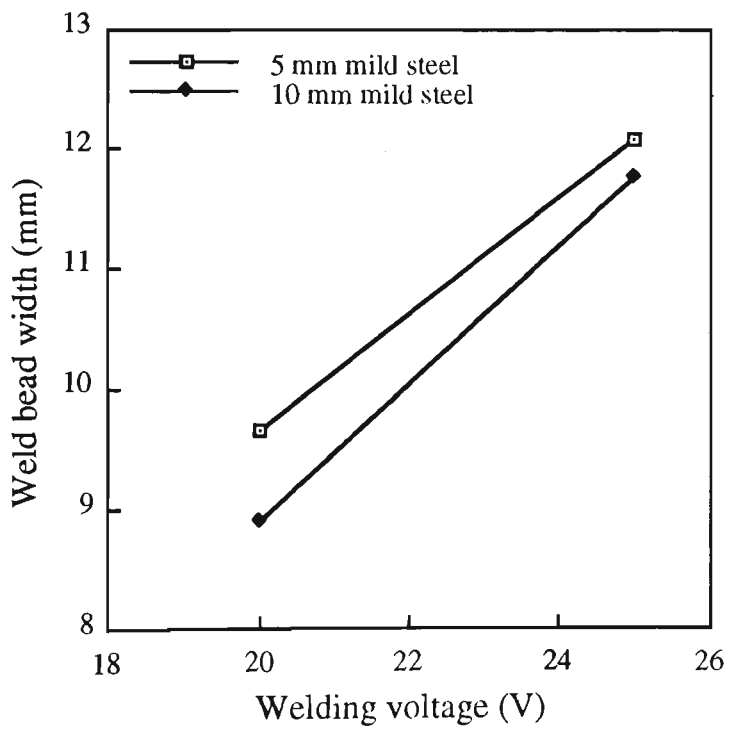

Figure 6.16 Welding voltage versus weld bead width.

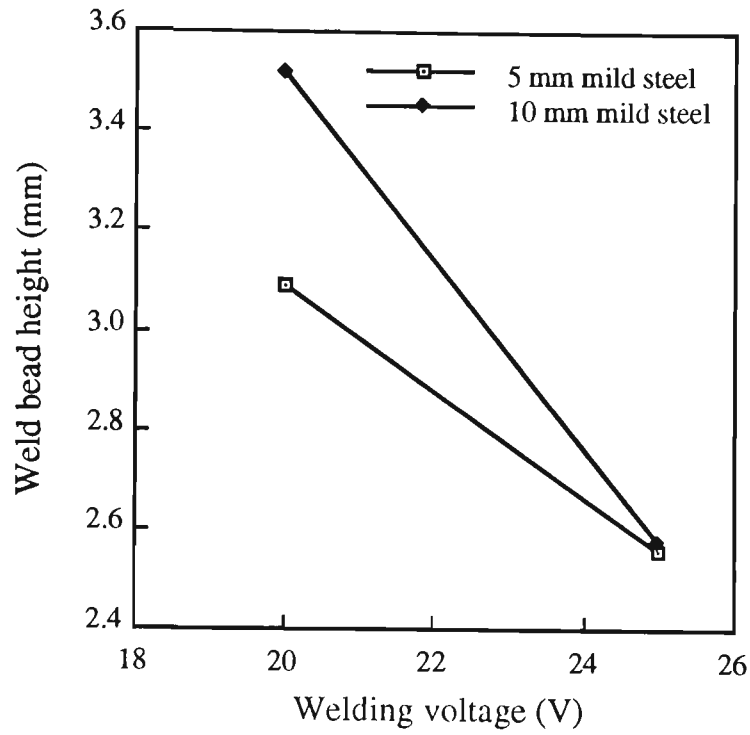

Figure 6.17 Welding voltage versus weld bead height.

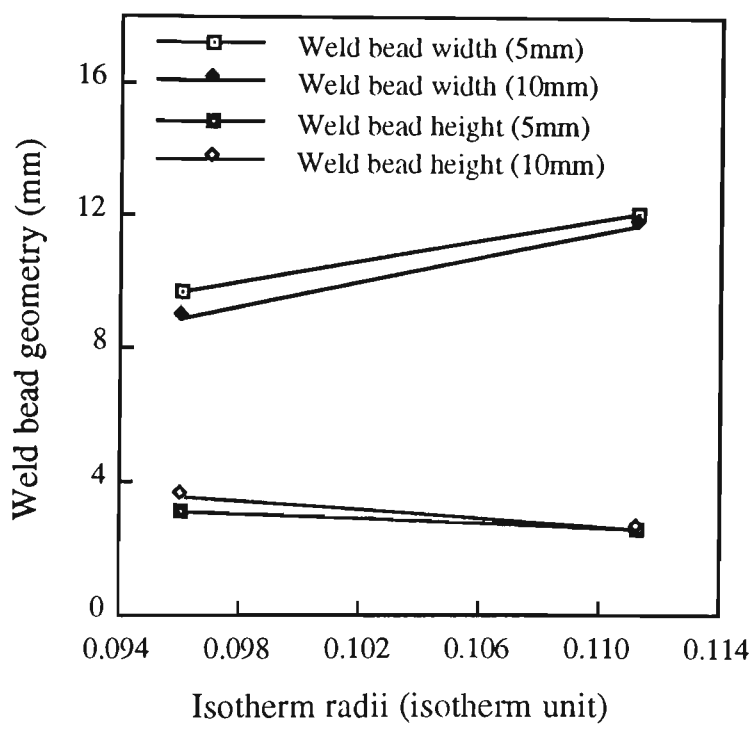

Figure 6.18 Isotherm radii versus weld bead geometry.

The relationship between isotherm radii and weld bead geometry is presented in figure 6.14, which shows that there is an increase in weld bead geometry as isotherm radii increases.

Figure 6.15 displays the relationship between welding voltage and the isotherm radii. The average isotherm radii were adjusted by taking the average of all measured values with the same welding voltage for 5 mm and 10 mm thickness of mild steel test pieces respectively, but without considering the effects of arc current and welding speed. It is apparent from figure 6.15 that the isotherm radii also increases as welding voltage increases. The relationship between welding voltage and weld bead width shown in figure 6.16 depicts an increase in weld bead width with an increase in welding voltage. The average weld bead widths were produced by taking the average of all values for welds deposited with the same welding voltage for 5 mm and 10 mm thickness of mild steel test pieces respectively, but ignoring the effects of arc current and welding speed. When a higher welding voltage is employed, a lower weld bead height is achieved as seen in figure 6.17. Weld bead heights were produced by taking the average of all measured values for welds deposited with the same welding voltage for 5 mm and 10 mm thickness of mild steel test pieces respectively, but ignoring the effects of arc current and welding speed. The relationship between isotherm radii and weld bead geometry is shown in figure 6.18, which indicates that there is an increase in weld bead width as isotherm radii increases, while weld bead height decreases when isotherm radii increases.

In the second experiments, Appendix C show the variations in arc current and the isotherm radii for both 5 mm and 10 mm plate thickness respectively. Different arc current were employed to produce the variation in weld bead dimensions. Figure 6.19 depicts arc current versus isotherm radii for 5 mm and 10 mm thickness measured using computer imaging analysis.

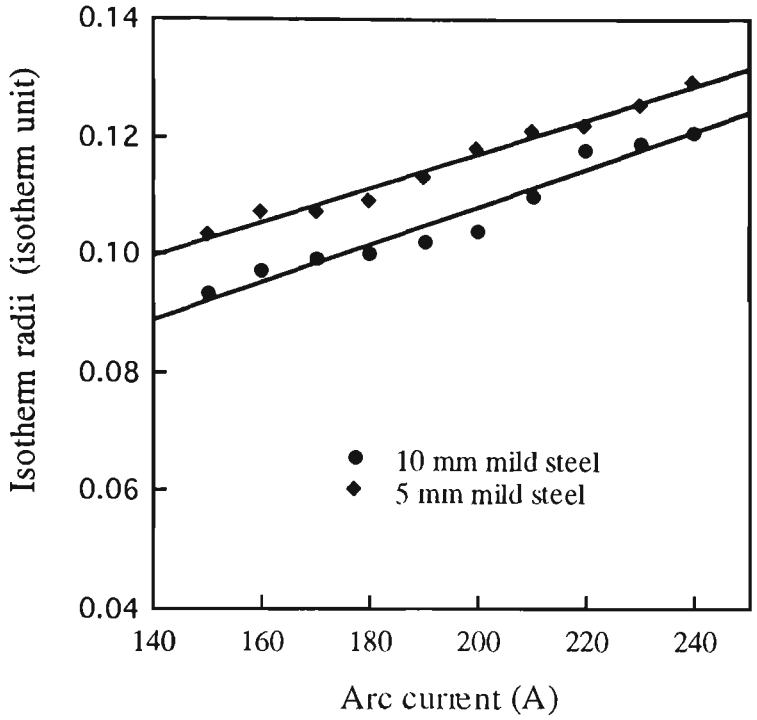

Figure 6.19 Arc current versus isotherm radii.

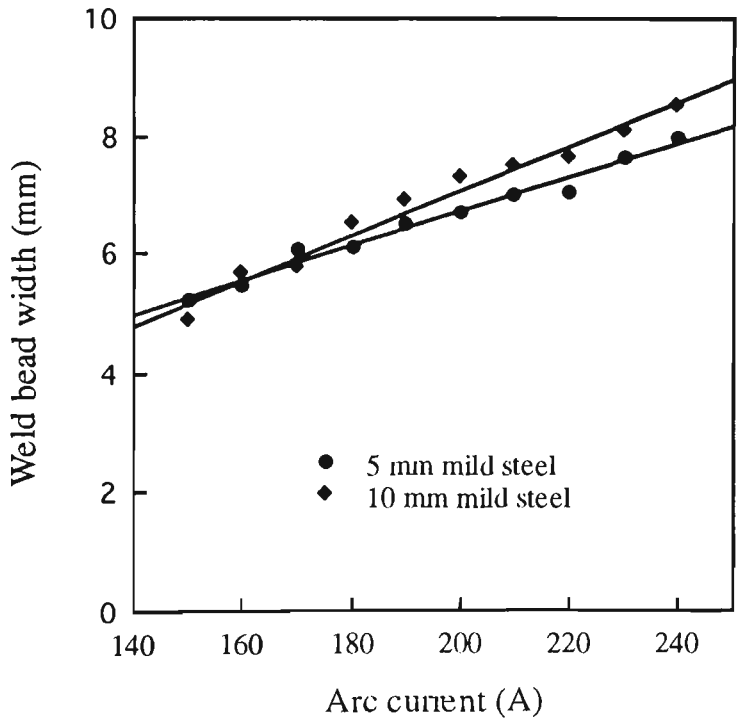

Figure 6.20 Arc current versus weld bead width.

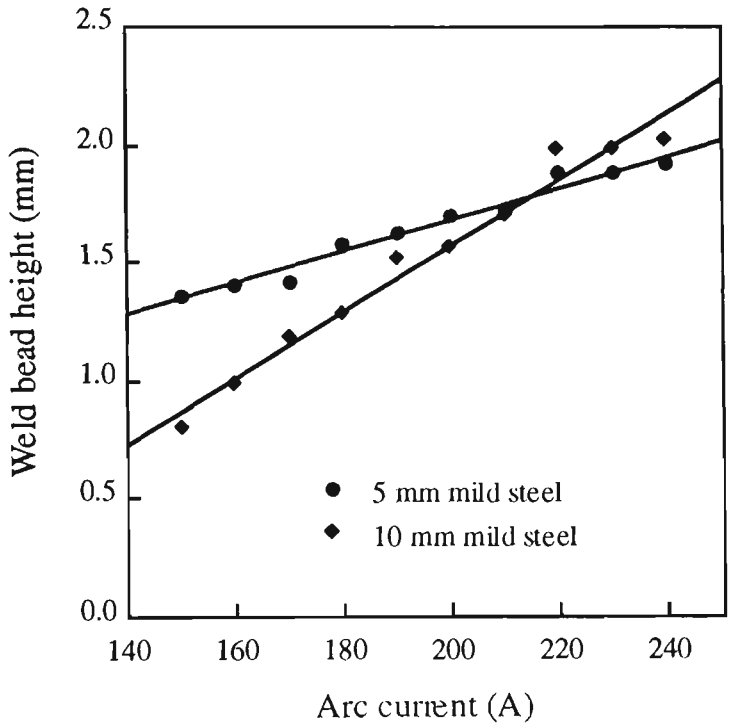

Figure 6.21 Arc current versus weld bead height.

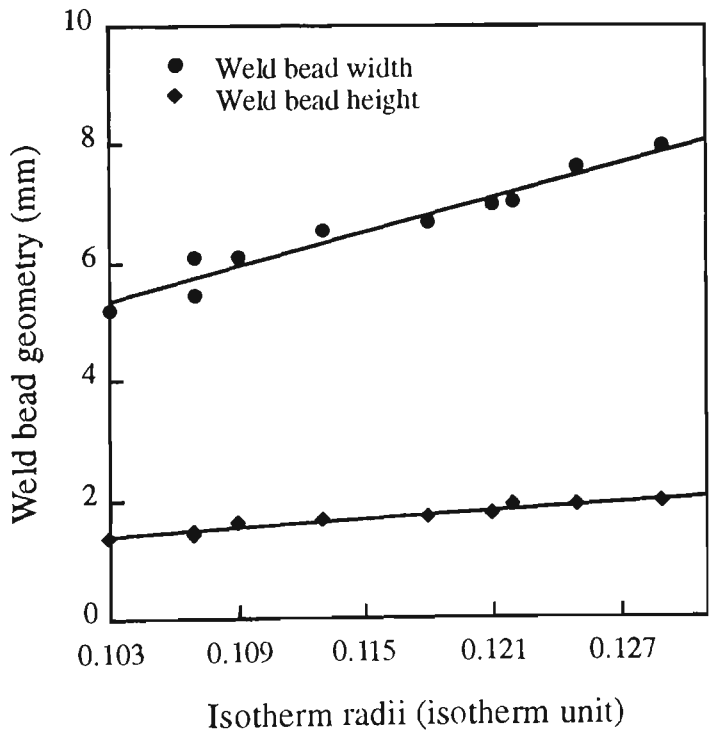

Figure 6.22 Isotherm radii versus weld bead geometry for 5 mm mild steel.

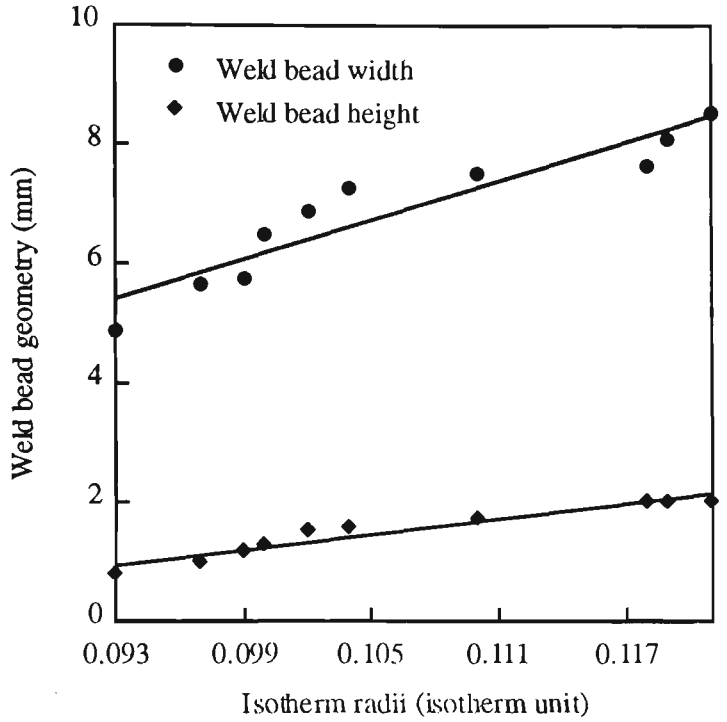

Figure 6.23 Isotherm radii versus weld bead geometry for 10 mm mild steel.

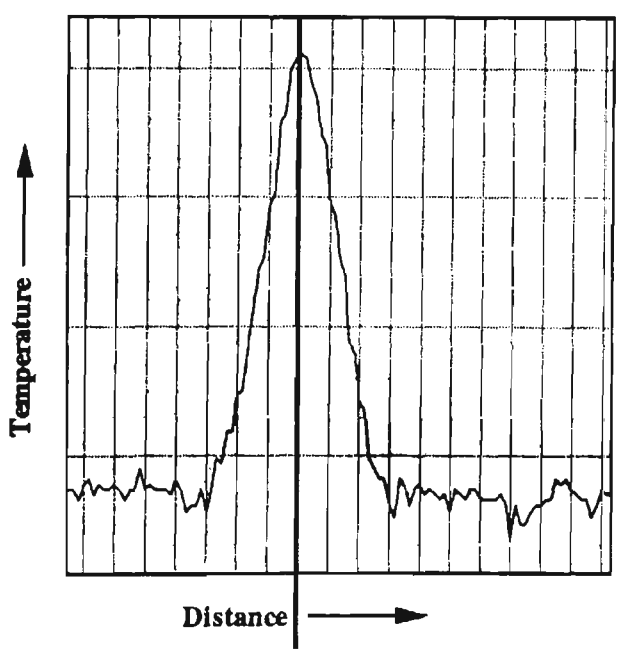

(a) Arc position - on seam

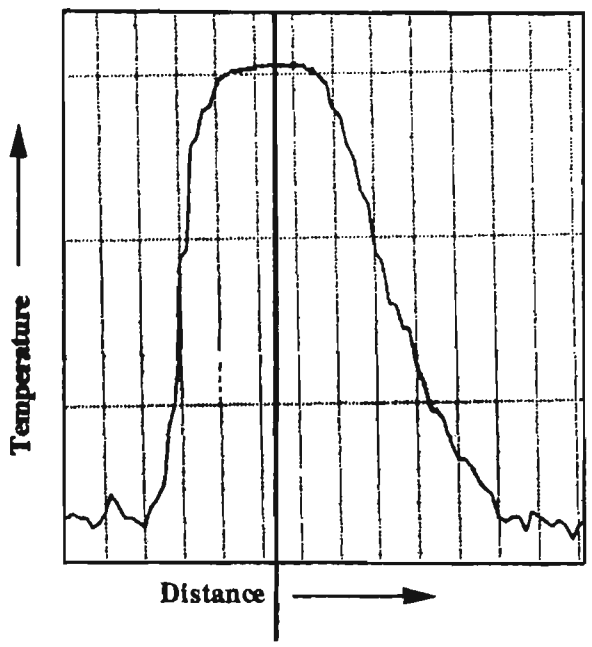

(b) Arc position - off seam

Figure 6.24 Temperature versus distance profiles.

As shown in figure 6.19, there is a linear relationship between arc current and isotherm radii. Results relating arc current to weld bead width and height are illustrated in figures 6.20 and 6.21 for 5 mm and 10 mm thickness respectively. It is evident that a linear relationship existed between process output parameters and the welding current input variation when primary process input parameters such as welding voltage and welding speed were kept constant.

The thermographic profile measurements of the same welds are shown in figures 6.22 and 6.23. Here, welding output parameters are plotted against the isotherm radii measured for 5 mm and 10 mm thickness of mild steel specimens respectively. A linear relationships obtained suggested that adaptive control of weld bead shape and size can be achieved during the robotic arc welding process.

Further experiments on close fit butt welds using the same process parameters revealed that seam tracking can be also achieved (figure 6.24). Isothermal contours obtained during welding of these specimens indicated that a leading spike on the thermographic profile is presented during the welding which indicates the seam path direction. Aligning the pointing direction of this isothermal spike with the reference point from where the isothermal radii were obtained can lead to the correct placement of the weld on the seam. Although the potential of the technique for adaptive control during robotic arc welding has been proved, future research and development work is needed to assess its viability.

6.4 SUMMARY OF RESULTS

1. Experimental results show that both weld bead geometry and thermal images from infrared thermography are affected by welding process parameters (arc current, welding speed and welding voltage).
2. Thermal image, weld bead width and height increase with an increase in arc current.
3. An increase in the welding speed results in a decrease in thermal image, weld bead width and height.
4. Thermal image and weld bead width increase with an increase in welding voltage, while weld bead height decreases as welding voltage increases.
5. Infrared thermography may be appropriate for adaptive control of weld bead width and height during the GMAW process.
6. A linear relationship exists between the isotherm radii produced during the GMAW process and the weld bead width as well as the weld bead height.
7. Adaptive control using infrared thermography may be achieved with the development of appropriate computer interface with both the welder control and the technique used for infrared thermography.

CHAPTER 7

CONCLUSIONS

7.1 CONCLUSIONS

The complete mathematical models to predict welding process parameters on the required weld bead dimensions and to investigate the effects of weld process variables on the weld bead geometry for the GMAW process have been achieved in this research by the separation of theoretical studies and empirical findings, and the following conclusions reached:

1. Mathematical models are able to predict the welding process parameters required to achieve desired weld bead geometry and weld criteria, help the development of automatic control system and expert system and establish guidelines and criteria for the most effective joint design.
2. Results have demonstrated that empirical equations can find the interrelationship between welding process parameters (wire diameter, gas flow rate, welding speed, arc current and welding voltage) and weld bead geometry (weld bead width, weld bead height, weld bead penetration, weld penetration shape factor, weld reinforcement shape factor, weld bead total area, weld bead penetration area, weld bead reinforcement area, weld bead dilution, length of weld bead penetration boundary and length of weld bead reinforcement boundary) for the

GMAW process. Gas flow rate shows no significant effect on the weld bead dimensions except weld bead height.

3. Weld bead geometry can be expressed in terms of welding process parameters using empirical equations obtained by statistical analysis, with the help of a standard statistical package program SAS. The comparison with values of coefficient of multiple correlation for curvilinear, polynomial and linear equations presents no differences, which indicates that all equations are reasonably suitable.

4. A transient 2D mathematical model for prediction of the temperature and velocity fields in weld pools for the GMAW process was developed. The computed results show the significant influence of convective heat transfer on the development of weld pools. The model was also able to predict the effects of various welding process parameters on the mean weld pool dimensions with reasonable accuracy.

5. According to figures 6.19 to 6.23, it can be concluded that the infrared thermography and the machine vision sensing have shown to control the weld bead width and weld bead height during the GMAW of AS 1204 mild steel plates. It was also found that the width of the thermal line scan was directly proportional to the weld bead width and weld bead height. Adaptive control using infrared thermography may eventually be achieved with the development of appropriate computer interface with both the weld control and the technique employed in infrared thermography.

7.2 SUGGESTIONS FOR FUTURE WORK

The work carried out in this thesis was mainly aimed at the development of mathematical models for the automated and/or robotic welding system. The following are summaries of major work identified for future research.

1. The empirical formulae based on experimental results are valid for current welding process parameters and welding bead geometry. It is proposed that the these equations are extended to multipeds welds, shielding gas composition, weld joint position, polarity and many other parameters which are not included in this research.
2. 3. In this work the weld pool was modelled independently of the weld arc and the Gaussian heat and current distributions were applied as boundary conditions for flat surface. It is well known that the measured heat and current fluxes is not a trivial matter, and can be complicated if the free surface deforms. To overcome these problems, a fundamental approach would be to model the arc directly using fundamental transport equations. Such methods involve the simultaneous solution of the continuity, momentum, energy, and Maxwell's electromagnetic equations. Temperature distribution, velocity profile, anode heat and current fluxes in the welding arc should be determined through the governing equations. The results from the welding arc will be served as boundary conditions for weld pools so that the weld pool characteristics such as surface temperature and weld bead geometry can be predicted from a identical set of governing equations. Virtually, a mathematical model to simulate the heat and fluid flow phenomena for the GMAW process must be coupled with the welding arc and weld pools. In this method, a comprehensive mathematical model of the GMAW process is described from the welding process variables through the coupling of the welding arc with weld pools.
3. It is desirable to interface the existing infrared display unit directly to the image analysis software in order to establish a closed loop feedback control system and to minimise possible errors from uncontrolled variations. Figure 7.1 presents the appropriate layout.

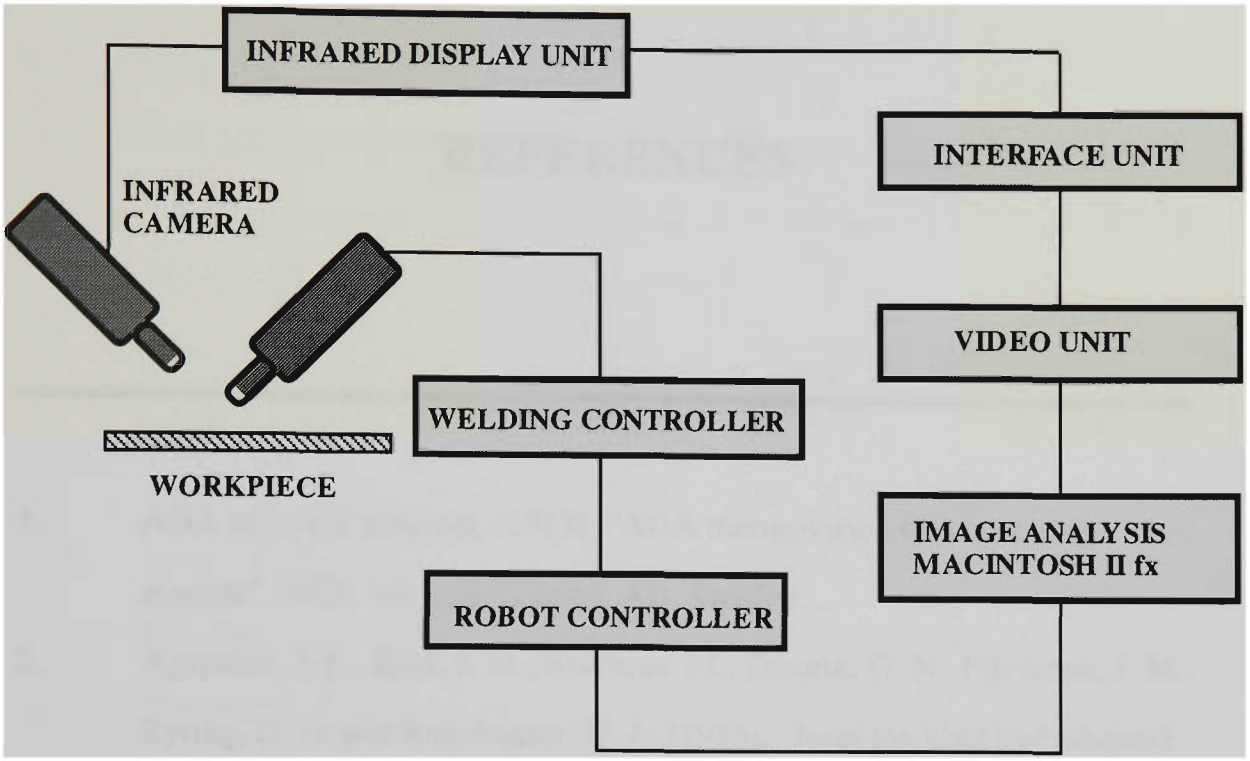

Figure 7.1 The feedback control system.

Research towards accomplishing this would be a worthwhile effort.

REFERENCES

1. AGA infra-red Systems, (1983), "AGA thermovision 680 operating manual", AGA Infrared Systems, AB, Sweden.
2. Agapakis, J. E., Katz, J. M., Koifman, M., Epstein, G. N., Friedman, J. M., Eyring, D. O. and Rutishauser, H. J., (1986), "Joint tracking and adaptive robotic welding using vision sensing of the weld joint geometry", *Welding Journal*, Vol. 65, No. 11, P. 33 - 41.
3. Allum, C. J. and Quintino, L., (1985), "Control of fusion characteristics in pulsed current MIG welding - Part 1", *Metal Construction*, Vol. 17, No. 4, P. 242R - 245R.
4. Allum, C. J. and Quintino, L., (1985), "Control of fusion characteristics in pulsed current MIG welding - Part 2", *Metal Construction*, Vol. 17, No. 5, P. 314R - 317R.
5. Andrews, J. G. and Crane, R. E., (1978), "Fluid flow in a hemisphere induced by a distributed source of current", *Journal of Fluid Mechanics*, Vol. 84, No. 2, P. 281 - 290.
6. Apps, R. L., Gourd, L. M. and Nelson, K. A., (1963), "Effect of welding variables upon bead shape and size in submerged-arc welding", *Welding and Metal Fabrication*, No. 11, P. 453 - 457.
7. Atthey, D. R., (1980), "A mathematical model for fluid flows in a weld pool at high currents", *Journal of Fluid Mechanics*, Vol. 98, No. 4, P. 787 - 801.
8. Automatix Inc., (1990), "Image analyst user's manual", AI Document, No. MN-SP-08, USA.

9. Boillet, J. P., Cielo, P., Begin, G., Michel, C., Lessard, M., Fafard, P. and Villemure, D., (1985), "Adaptive welding by fiber optic thermographic sensing : An analysis of thermal and instrumental considerations", *Welding Journal,* Vol. 64, No. 7, P. 209-s - 217-s.

10. Box, G. E. P., Hunter, W. H. and Hunter, J. S., (1978), "Statistics for experimenters: An introduction to design data analysis and model building", John Wiley and Sons, 10th Edition, New York, P. 165 - 240.

11. Brent, A. D., Voller, V. R. and Reid, K. J., (1988), "Enthalpy porosity technique for modelling convection-diffusion phase change: Application to the melting of a pure metal", *Numerical Heat Transfer*, Vol. 13, P. 297 - 318.

12. Brien R. L., (1990), "Welding handbook", American Welding Society, Vol. 2, P. 110 - 155.

13. Brown, B. and Bangs, E., (1985), "The measurement and monitoring of resistance spot welds using infrared thermography", *Proceedings of SPIE - The International Society for Optical Engineering*, Cambridge, Massachusetts, 17 - 20, September, P. 57 - 69.

14. Brown, S. B. and Song, H., (1992), "Implications of three-dimensional numerical simulations of welding of large structures", *Welding Journal*, Vol. 71, No. 2, P. 55-s - 62-s.

15. Burleigh, T. D. and Eagar, T. W., (1983), "Measurement of the force exerted by a welding arc", *Metallurgical Transactions,* Vol. 14A, P. 1223 - 1224.

16. Carlson, N. M. and Johnson, J. A., (1988), "Ultrasonic sensing of weld pool penetration", *Welding Journal*, Vol. 67, No. 11, P. 239-s - 246-s.

17. Carlson, N. M., Johnson, J. A. and Kunerth, D. C., (1990), "Control of GMAW: Detection of discontinuities in the weld pool", *Welding Journal,* Vol. 69, No. 7, P. 256-s - 263-s .

18. Carslaw, H. S. and Jaegar. J. C., (1959), "Conduction of heat in solids", Clarendon Press, Oxford.

19. Cary, H. B., (1979), "Modern welding technology", Englewood Cliffs, Prentic-Hall, New Jersey, USA, P. 25 - 85.

20. Chan, C., Mazumder, J. and Chen, M. M., (1984), "A two-dimensional transient model for convection in laser melted pools", *Metallurgical Transactions,* Vol. 15A, P. 2175 - 2184.

21. Chan, C. L., Zehr, R., Mazumder, J. and Chen, M. M., (1986), "Three-dimensional model for convection in laser weld pool", Modeling and Control of Casting and Welding Processes : *Proceedings of the Third Conference on Modeling of Casting and Welding Processes*, Santa Barbara, CA, USA, 12 - 17, January, P. 229 - 246.

22. Chandel, R. S. and Bala, S. R., (1986), "Effect of welding parameters and groove angle on the soundness of root beads deposited by the SAW process", *Advances in Welding Science and Technology : Proceedings of an International Conference on Trends in Welding Research*, Gatlinburg, Tennessee, USA, 18 - 22, May, P. 379 - 385.

23. Chandel, R. S., Bala, S. R. and Malik, L., (1987), "Effect of submerged arc process variables", *Welding and Metal Fabrication*, No. 6, P. 302 - 304.

24. Chandel, R. S., (1988), "Mathematical modelling of gas metal arc weld features", *Modeling and Control of Casting and Welding Processes IV : Proceedings of the Fourth International Conference on Modeling of Casting and Welding Processes*, Palm Coast, Florida, 17 - 22, April, P. 109 - 120.

25. Chen, L. and Yang, B. T., (1985), "Design principle for simultaneous emissivity and temperature measurements", *Proceedings of SPIE - The International Society for Optical Engineering*, 20 - 21, August, P. 83 - 88.

26. Chen, W. and Chin, B. A., (1990), "Monitoring joint penetration using infrared sensing techniques", *Welding Journal*, Vol. 69, No. 4, P. 181-s - 185-s.

27. Chen, W. H., Banjerjee, P. and Chin, B. A., (1989), "Study of penetration variations in automated gas tungsten arc welding", *Recent Trends in Welding Science and Technology: TWR '89 : Proceedings of the 2nd International Conference on Trends in Welding Research*, Gatlinburg, Tennessee, USA, 14 - 18, May, P. 517 - 522.

28. Chin, B. A., Madsen, N. H. and Goodling, J. S., (1983), "Infrared thermography for sensing the arc welding process", *Welding Journal*, Vol. 62, No. 9, P. 227-s - 234-s.

29. Choi, M., Greif, R. and Salcudean, M., (1987), "A study of the heat transfer during arc welding with applications to pure metals or alloys and low or high boiling temperature materials", *Numerical Heat Transfer,* Vol. 11, P. 477 - 489.

30. Choo, R. T. C., Mukai, K. and Toguri, J. M., (1992), "Marangoni interaction of a liquid droplet falling onto a liquid pool", *Welding Journal,* Vol. 71, No. 4, P. 139-s - 146-s.

31. Choo, R. T. C., Szekely, J. and David, S. A., (1990), "Modeling of high-current arcs with emphasis on free surface phenomena in the weld pool", *Welding Journal*, Vol. 69, No. 9, P. 346-s - 361-s.

32. Choo, R. T. C. and Szekely, J., (1991), "The effects of gas shear stress on Marangoni flows in arc welding", *Welding Journal*, Vol. 70, No. 9, P. 223-s - 233-s.

33. Choo, R. T. C. and Szekely, J., (1992), "Vaporization kinetics and surface temperature in a mutually coupled spot gas tungsten arc weld and weld pool", *Welding Journal*, Vol. 71, No. 3, P. 77-s - 93-s.

34. Choo, R. T. C. and Szekely, J. and Westhoff, R. C., (1992), "On the calculation of the free surface temperature of gas-tungsten-arc weld pools

from first principles: Part I. Modeling the welding arc", *Metallurgical Transactions*, Vol. 23B, P. 357 - 369.

35. Choo, R. T. C. and Szekely, J. and David, S. A., (1992), "On the calculation of the free surface temperature of gas-tungsten-arc weld pools from First principles: Part II. Modeling the weld pool and comparison with experiments", *Metallurgical Transactions*, Vol. 23B, P. 371 - 384.

36. Christensen, N., Davies, V. de L. and Gjermundsen, K., (1965), "Distribution of temperatures in arc welding", *British Welding Journal*, No. 2, P. 54 - 75.

37. Cook, G. E., (1981),"Feedback and adaptive control in automated arc welding system", *Metal Construction*, Vol. 13, No. 9, P. 551 - 556.

38. Cook, G. E., (1983), "Through-the-arc sensing for arc welding", *Proceedings of the Tenth Conference on Production Research and Technology*, National Science Foundation, ISBN 0-89883-087-7, March, P. 141 - 151.

39. Cook, G. E., Andersen, K. and Barrett, R. J., (1989), "Keynote address: Feedback and adaptive control in welding", *Recent Trends in Welding Science and Technology: TWR '89 : Proceedings of the 2nd International Conference on Trends in Welding Research,* Gatlinburg, Tennessee, USA, 14 - 18, May, P. 891 - 903.

40. Correa, S. M. and Sundell, R. E., (1986), "A computational and experimental study of the fluid flow in weld pools", *Modeling and Control of Casting and Welding Processes : Proceedings of the Third Conference on Modeling of Casting and Welding Processes*, Santa Barbara, CA, USA, 12 - 17, January, P. 211 - 227.

41. Davis, M., Kapadia, P. and Dowden, J., (1986), "Modeling the fluid flow in laser beam welding", *Welding Journal*, Vol. 65, No. 7, P. 167-s - 174-s.

42. Davis, O. L., (1978), "The design and analysis of industrial experiments", Longman Group Ltd, New York.

43. Deam, R. T., (1989), "Weld pool frequency : A new way to define a weld procedure", *Recent Trends in Welding Science and Technology: TWR '89 : Proceedings of the 2nd International Conference on Trends in Welding Research*, Gatlinburg, Tennessee, USA, 14 - 18, May, P. 967 - 971.

44. Doherty, J. and McGlone, J. C., (1977), "Relationships between process variables and weld geometry", *The Welding Institute Report* 52/1977/PE.

45. Doherty, J., Shinoda, T. and Weston, J., (1978), "The relationships between arc welding parameters and fillet weld geometry for MIG welding with flux cored wires", *The Welding Institute Report* 82/1978/PE.

46. Doumanidis, G., Hale, M. and Hardt, D. E., (1986), "Multivariable control of arc welding processes", *Advances in Welding Science and Technology : Proceedings of an International Conference on Trends in Welding Research*, Gatlinburg, Tennessee, USA, 18 - 22, May, P. 449 - 457.

47. Drayton, P. A., (1972), "An examination of the influence of process parameters on submerged arc welding", *The Welding Institute Report* PE/4/72.

48. Essers, W. G. and Walter, R., (1981), "Heat transfer and penetration mechanisms with GMA and plasma-GMA welding", *Welding Journal,* Vol. 60, No. 2, P. 37-s - 42-s.

49. Fenn, R., (1985), "Ultrasonic monitoring and control during arc welding", *Welding Journal*, Vol. 64, No. 9, P. 18 - 22.

50. Fortunko. C. M. and Schramm, R. E., (1982), "Ultrasonic nondestructive evaluations of butt welds using electromagnetic-acoustic transducers", *Welding Journal*, Vol. 61, No. 2, P. 39 - 46.

51. Friedman, E., (1975), "Thermomechanical analysis of the welding process using the finite element method", *Journal of Pressure Vessel Technology*, No. 8, P. 206 - 213.

52. Friedman, E. and Glickstein, S. S., (1976), "An investigation of the thermal response of stationary gas tungsten arc welds", *Welding Journal,* Vol. 55, No. 12, P. 408-s - 420-s.

53. Friedman, E., (1978), "Analysis of weld puddle distortion and its effect on penetration", *Welding Journal*, Vol. 57, No. 6, P. 161-s - 166-s.

54. Galopin, M. and Boridy, E., (1986), "Statistical experiment in arc welding", *Advances in Welding Science and Technology : Proceedings of an International Conference on Trends in Welding Research,* Gatlinburg, Tennessee, USA, 18 - 22, May, P. 719 - 722.

55. Geidt, W. H. and Wei, X.-C. and Wei, S.-R. (1984), "Effect of surface convection on stationary GTA weld zone temperatures", *Welding Journal,* Vol. 63, No. 12, P. 376-s - 383-s.

56. Goldak, J., Chakravarti, A. and Bibby, M., (1984), "A new finite element model for welding heat sources", *Metallurgical Transaction,* Vol. 15B, P. 299 - 305.

57. Goldak, J., Bibby, M., Moore, J., House, R. and Patel, B., (1986), "Computer modeling of heat flow in welds", *Metallurgical Transactions,* Vol. 17B, P. 587 - 600.

58. Goldak, J., McDill, M., Oddy, A., House, R., Chi, X. and Bibby, M., (1986), "Computational heat transfer for weld mechanics ", *Advances in Welding Science and Technology : Proceedings of an International Conference on Trends in Welding Research*, Gatlinburg, Tennessee, USA, 18 - 22, May, P. 15 - 20.

59. Gonseth, P. M. and Blanc, P., (1983), "Optiguide - A new optical joint tracking device", *Welding Journal*, Vol. 62, No. 9, P. 27 - 29.

60. Grosh, R. J. and Trabant, E. A., (1956), "Arc welding temperatures", *Welding Journal*, Vol. 35, No. 8, P. 396-s - 400-s.

61. Hanright, J., (1986), "Robotic arc welding under adaptive control - A survey of current technology", *Welding Journal*, Vol. 65, No. 11, P. 19 - 24.

62. Hardt, D. E. and Katz, J. M., (1984), "Ultrasonic measurement of weld penetration", *Welding Journal*, Vol. 63, No. 9, P. 273-s - 281-s.

63. Hardt, D. E., (1986), "Measuring weld pool geometry from pool dynamics", *Modeling and Control of Casting and Welding Processes : Proceedings of the Third Conference on Modeling of Casting and Welding Processes*, Santa Barbara, California, USA, 12 - 17, January, P. 3 - 17.

64. Harris, P. and Smith, B. L., (1983), "Factorial techniques for weld quality prediction", *Metal Construction,* Vol. 15, No. 11, P. 661 - 666.

65. Heiple, C. R. and Roper, J. R., (1981), "Effect of selenium on GTAW fusion zone geometry", *Welding Journal,* Vol. 60, No. 8, P. 143-s - 145-s.

66. Heiple, C. R. and Roper, J. R., (1982), "Mechanism for minor element effect on GTA fusion zone geometry", *Welding Journal*, Vol. 61, No. 4, P. 97-s - 102-s.

67. Heiple, C. R. and Roper, J. R., (1990), "The geometry of gas tungsten arc, gas metal arc and submerged arc weld beads", *Welding: Theory and Practice*, Elsevier Science Publishers, B. V., P. 1 - 33.

68. Hibbit, H. D. and Marcal, P. V., (1973), "A numerical, thermo-mechanical model for the welding and subsequent loading of a fabricated structure", *Computer & Structures*, Vol. 3, P. 1145 - 1174.

69. Hobart Brothers Company, (1964), "Microwire manual", Hobart Industrial Tech. Centre, Ohio, P. 12/14 - 14/15.

70. Hohn, R. E. and Holmes, J. G., (1986), "Robotic arc welding adding science to the art", *Robotic Welding a Guide to Selection and Application,* SME Publications, P. 14 - 25.

71. Holmsten, D., (1985), "Precision infrared on-line scanning for process control", *Proceedings of SPIE - The International Society for Optical Engineering,* Cambridge, Massachusetts, 17 - 20, September, P. 35 - 46.

72. Hunter, J. J., Bryce, G. W. and Doherty, J., (1988), "On-line control of the arc welding process", *Proceedings of the 2nd International Conference on*

Computer Technology in Welding, Cambridge, UK, June, P. 37-1 - 37-12.

73. Jackon, C. E., (1960), "The science of arc welding", *Welding Journal*, Vol. 39, No. 6, P. 225-s - 230-s.

74. Johnson, J. A., Carlson, N. M. and Smartt, H. B., (1989), "Detection of. metal transfer mode in GMAW", *Recent Trends in Welding Science and Technology: TWR '89 : Proceedings of the 2nd International Conference on Trends in Welding Research,* Gatlinburg, Tennessee, USA, 14 - 18, May, P. 337 - 181.

75. Jon, M. C., (1985), "Noncontacting acoustic emission monitoring of laser beam welding", *Welding Journal,* Vol. 64, No. 9, P. 43 - 47.

76. Jones, S. B., (1976), "Process tolerance in submerged arc welding : Initial report", *The Welding Institute Report* 1/1976/PE.

77. Kamala, V. and Goldak, J. A., (1993), "Error due to two dimensional approximation in heat transfer analysis of welds", *Welding Journal*, Vol. 72, No. 9, P. 440-s - 446-s.

78. Kaskinen, P. and Mueller, G. J., (1986), "Acoustic arc length control", *Advances in Welding Science and Technology : Proceedings of an International Conference on Trends in Welding Research*, Gatlinburg, Tennessee, USA, 18 - 22, May, P. 763 - 765.

79. Kim, I. S., Basu, A. and Siores, E., (1993), "Relationships between process parameters and weld bead geometry for GMAW process", *WTIA/AINDT Conference - Towards Competitive Edge*, 27 September - 1 October, Wollongong, Australia, P. 170 - 176.

80. Kim, I. S. and Basu, A., (1994), "Mathematical models for open loop control in GMAW process", *Proceedings of the 1st International Symposium on Advances in Intelligent Computer Integrated Manufacturing System,* 21 - 23, November, Seoul, Korea, P. 165 - 172.

81. Kim, J. W. and Na, S. J., (1994), "A study on the three-dimensional analysis of heat and fluid flow in gas metal arc welding using boundary-fitted coordinates", *Journal of Engineering for Industry,* Vol. 116, No. 2, P. 78 - 85.

82. Kim, S. D. and Na, S. J., (1992), "Effect of weld pool deformation on weld penetration in stationary gas tungsten arc welding", *Welding Journal*, Vol. 71, No. 5, P. 179-s - 193-s.

83. Kou, S. and Le, Y., (1983), "Three-dimensional heat flow and solidification during the autogenous GTA welding of aluminium plates", *Metallurgical Transactions,* Vol. 14A, P. 2245 - 2253.

84. Kou, S. and Sun, D. K., (1985), "Fluid flow and weld penetration in stationary arc welds", *Metallurgical Transactions,* Vol. 16A, P. 203 - 213.

85. Kou, S. and Wang, Y. H., (1986), "Three-dimensional convection in laser melted pools", *Metallurgical Transactions*, Vol. 17A, P. 2265 - 2270.

86. Kou, S. and Wang, Y. H., (1986), "Weld pool convection and its effect",. *Welding Journal*, Vol. 65, No. 3, P. 63-s - 70-s.

87. Kovitay, P. and Lowke, J., (1985), "Two-dimensional analysis of free burning arcs in argon", *Journal of physics. D, Applied physics*, Vol. 18, P. 53 - 70.

88. Kovitya, P. and Cram, L. E., (1986), "A two-dimensional model of gas-tungsten welding arcs", *Welding Journal*, Vol. 65, No. 12, P. 34 - 39.

89. Kovitya, P., Cram, L. E. and Little, L., (1986), "Theoretical prediction of weld pool and weld bead shapes", *Australia Welding Research*, December, P. 94 - 98.

90. Kraus, H. G., (1986), "Thermal finite element formulation and solution versus experimental results for thin-plate GTA welding", *Journal of Heat Transfer*, Vol. 108, No. 8, P. 591 - 596.

91. Kraus, H. G., (1987), "Experimental measurement of thin plate 304 stainless steel GTA weld pool surface temperatures", *Welding Journal*, Vol. 66, No. 12, P. 353-s - 359-s.

92. Kraus, H. G., (1988), "Experimental measurement of weld pool temperatures - A review", *Modeling and Control of Casting and Welding Processes IV : Proceedings of the Fourth International Conference on Modeling of Casting and Welding Processes*, Palm Coast, Florida, 17 - 22, April, P. 205 - 212.

93. Kraus, H. G., (1989), "Experimental measurement of stationary SS304, 316L and 8630 GTA weld pool surface temperatures", *Welding Journal*, Vol. 68, No. 7, P. 269-s - 279-s.

94. Krutz, G. W. and Segerlind, L. J., (1978), "Finite element analysis of welding structures", *Welding Journal*, Vol. 57, No. 7, P. 211-s - 216-s.

95. Kuhne, A. H., Cary, H. B. and Prinz, F. B., (1988), "Expert system improves the robotic welding procedure", *Welding Quality - The Role of Computers*, International Institute of Welding, Pergamon Press, P. 175 - 180.

96. Kumar, R. S. and Parmar, R. S., (1986), "Weld bead geometry prediction for pulse MIG welding", *Advances in Welding Science and Technology : Proceedings of an International Conference on Trends in Welding Research*, Gatlinburg, Tennessee, USA, 18 - 22, May, P. 647 - 652.

97. Lancaster, J. F., (1984), "The physics of welding", Pergamon Press, P. 1 - 293.

98. Lawson, C. L. and Hanson, R. J., (1974), "Solving least squares problems", Englewood Cliffs, N. J., USA.

99. Lee, H-J. and Na, S-j., (1991), "A study on heat flow in circumferential pipe welding using a semi-analytical finite element method", *Journal of Engineering Manufacture*, Vol. 205, P. 180 - 185.

100. Lewis, G. K. and Dixon, R. D., (1985), "Plasma monitoring of laser beams welds", *Welding Journal,* Vol. 64, No. 2, P. 49-s - 54-s.

101. Lin, M. L. and Eagar, T. W., (1985), "Influence of arc pressure on weld pool geometry", *Welding Journal,* Vol. 64, No. 6, P. 163-s - 169-s.

102. Lin, M. L. and Eagar, T. W., (1986), "Pressure produced by gas tungsten arcs", *Metallurgical Transactions*, Vol. 17B, P. 601 - 607.

103. Lin, M. L. and Eagar, T. W., (1986), "Effects of surface depression and convection in GTA welding", *Advances in Welding Science and Technology : Proceedings of an International Conference on Trends in Welding Research*, Gatlinburg, Tennessee, USA, 18 - 22, May, P. 47 - 56.

104. Liu, J. T., Weckman, D. C. and Kerr, H. W., (1993), "The effects of process variables on pulsed Nd: YAG laser spot welding: Part 1. AISI 409 stainless steel", *Metallurgical Transactions*, Vol. 24B, No. 12, P. 1065 - 1076.

105. Liu, S., Siewert, T. A. and Lan, H., (1989), "Metal transfer mode in gas metal arc welding", *Recent Trends in Welding Science and Technology: TWR '89 : Proceedings of the 2nd International Conference on Trends in Welding Research,* Gatlinburg, Tennessee, USA, 14 - 18, May, P. 475 - 479.

106. Lott, L. A., (1984), "Ultrasonic detection of molten/solid interfaces in weld pools", *Materials Evaluation,* Vol. 42, No. 3, P. 337 - 341.

107. Lu, M. J. and Kou, S., (1989), "Power input in gas metal arc welding of aluminium - Part 1", *Welding Journal*, Vol. 68, No. 9, P. 382-s - 388-s.

108. Lu, M. J. and Kou, S., (1989), "Power input in gas metal arc welding of aluminium - Part 2", *Welding Journal*, Vol. 68, No. 11, P. 452-s - 456-s.

109. Lukens , W. E. and Morris, R. A., (1982),"Infrared temperature sensing of cooling rates for arc welding control", *Welding Journal*, Vol. 61, No. 1, P. 27 - 33.

110. Mahin, K. W., Shapiro, A. B. and Hallquist, J., (1986), "Assessment of boundary condition limitations on the development of a general computer

model for fusion welding", *Advances in Welding Science and Technology : Proceedings of an International Conference on Trends in Welding Research,* Gatlinburg, Tennessee, USA, 18 - 22, May, P. 215 - 223.

111. Malin, V., (1986), "Problems in design of integrated welding automation - Part 1: Analysis of welding related operations as objects for welding automation", *Welding Journal*, Vol. 65, No. 11, P. 53 - 60.

112. Manz, A. F., (1981), "Welding arc sounds", *Welding Journal*, Vol. 60, No. 5, P. 23 - 27.

113. Marburger, S. J., (1990), "Welding automation and computer control", *Welding: Theory and Practices*, Elsevier Science Publishers, B. V., P. 209 - 233.

114. Matsunawa, A., Yokoya, S. and Asako, Y., (1988), "Convection in weld pool and its effects on penetration shape in stationary arc welds", *Journal of Japan Welding Society*, Vol. 6, No. 4, P. 455 - 462.

115. Matsunawa, A. and Yokoya, Y., (1989), "Fluid flow and its effect on penetration shape in stationary arc welds", *Recent Trends in Welding Science and Technology: TWR '89 : Proceedings of the 2nd International Conference on Trends in Welding Research,* Gatlinburg, Tennessee, USA, 14 - 18, May, P. 31 - 35.

116. Maxfield, B. W., Kuramoto, A. and Hulbert, J. K., (1987), "Evaluating EMAT designs for selected applications", *Materials Evaluation,* Vol. 45, No. 10, P. 1166 - 1183.

117. McGlone, J. C., (1978), "The submerged arc butt welding of mild steel Part 1: The influence of procedure parameters on weld bead geometry", *The Welding Institute Report* 79/1978/PE.

118. McGlone, J. C. and Chadwick, D. B., (1978), "The submerged arc butt welding of mild steel Part 2: The prediction of weld bead geometry from the procedure parameters", *The Welding Institute Report* 80/1978/PE.

119. McGlone, J. C., (1980), "The submerged arc butt welding of mild steel - A decade of procedure optimization", *The Welding Institute Report* 13/1980/PE.

120. McGlone, J. C., (1982), "Weld bead geometry prediction - A review", *Metal Construction*, Vol. 14, No. 7, P. 378 - 384.

121. Mckee, K. E., (1982), "Welding, robots and productivity", *Welding Journal,* Vol. 61, No. 9, P. 30 - 35.

122. Mclay, R. and Carey, G. F., (1989), "Coupled heat transfer and viscous flow, and magnetic effects in weld pool analysis", *International Journal for Numerical Methods in Fluids*, Vol. 9, P. 713 - 730.

123. Miller, R. K., (1987), "Industrial robot handbook", SEIA Technical Publications, P. 153 - 158.

124. Montgomery, D. C., (1984), "Design and analysis of experiments", John Wiley and Sons, 2nd Edition, New York, P. 387 - 433.

125. Mundra, K., Debroy, T., Zacharia, T. and David, S. A., (1992), "Role of thermophysical properties in weld pool modeling", *Welding, Journal*, Vol. 71, No. 9, P. 313-s - 320-s.

126. Murti, K. G. K. and Sundaresan, S., (1983), "Parameter optimisation in friction welding dissimilar materials", *Metal Construction*, Vol. 15, No. 6, P. 331 - 335.

127. Myers, P. S., Uyehara, O. A. and Borman, G. L., (1967), ."Fundamentals of heat flow in welding", *Welding Research Council Bulletin* 123, July.

128. Nagarajan, S., Chen, W. H. and Chin, B. A., (1989), "Infrared sensing for adaptive arc welding", *Welding Journal*, Vol. 68, No. 11, P. 462-s - 466-s.

129. Nagarajan, S., Groom, K. N. and Chin, B. A., (1989), "Infrared sensors for seam tracking in gas tungsten arc welding processes", R*ecent Trends in Welding Science and Technology: TWR '89 : Proceedings of the 2nd International Conference on Trends in Welding Research*, Gatlinburg, Tennessee, USA, 14 - 18, May, P. 951 - 955.

130. Nagarajan, S. and Chin, B. A., (1990), "Infrared image analysis for on-line monitoring of arc misalignment in gas tungsten arc welding processes", *Materials Evaluation,* Vol. 48, No. 12, P. 1469 - 1990.

131. Oddy, A. S., Goldak, J. A. and Mcdill J. M. J., (1989), "Transformation effect in the 3D finite element analysis of welds", R*ecent Trends in Welding Science and Technology: TWR '89 : Proceedings of the 2nd International Conference on Trends in Welding Research*, Gatlinburg, Tennessee, USA, 14 - 18, May, P. 97 - 101.

132. Oreb, B. F., (1990), "Holographic interferometry for nondestructive testing in manufacture", *Proceedings from the Fifth International Conference on Manufacturing Engineering*, IEAust, Vol. 2, P. 365 - 369.

133. Oreper, G. M., Eagar, T. W. and Szekely, J., (1983), "Convection in arc weld pools", *Welding Journal*, Vol. 62, No. 11, P. 307-s - 312-s.

134. Oreper, G. M. and Szekely, J., (1984), "Heat - and fluid flow phenomena in weld pools", *Journal of Fluid Mechanics*, Vol. 147, No. 1, P. 53 - 79.

135. Oreper, G. M., Szekely, J. and Eagar, T. W., (1986), "The role of transient convection in melting and solidification in arc weld pools", *Metallurgical Transactions,* Vol. 17B, P. 735 - 744.

136. Oreper, G. M. and Szekely, J., (1987), "A comprehensive representation of transient weld pool development in spot welding operations", *Metallurgical Transactions,* Vol. 18A, P. 1325 - 1332.

137. Paley, Z. and Hibbert, P. D., (1975), "Computation of temperatures in actual weld designs", *Welding Journal,* Vol. 54, No. 11, P. 385-s - 392-s.

138. Pandey, S. and Parmar R. S., (1989), "Mathematical models for predicting bead geometry and shape relationships for MIG welding of aluminium alloy 5083", *Recent Trends in Welding Science and Technology: TWR '89 : Proceedings of the 2nd International Conference on Trends in Welding Research,* Gatlinburg, Tennessee, USA, 14 - 18, May, P. 37 - 41.

139. Pardo, E. and Weckman, D., (1988), "A numerical model of the gas metal arc welding process", *Modeling and Control of Casting and Welding Processes IV : Proceedings of the Fourth International Conference on Modeling of Casting and Welding Processes*, Palm Coast, Florida, April, 17 - 22, P. 187 - 195.

140. Pardo, E. and Weckman, D., (1989), "Prediction of weld pool and reinforcement dimensions of GMA welds using a finite-element model", *Metallurgical Transactions,* Vol. 20B, P. 937 - 947.

141. Patankar, S. V., (1980), "Numerical heat transfer and fluid flow", McGraw-Hill, New York, USA.

142. Patankar, S. V., (1981), "A calculation procedure for two-dimensional elliptic situations", *Numerical Heat Transfer*, Vol. 4, P. 409 - 425.

143. Paul, A and Debroy, T., (1986), "Heat transfer and fluid flow in laser melted weld pools", *Advances in Welding Science and Technology : Proceedings of an International Conference on Trends in Welding Research*, Gatlinburg, Tennessee, USA, 18 - 22, May, P. 29 - 33.

144. Paul, A. and Debroy, T., (1988), "Free surface flow and heat transfer in conduction mode laser welding", *Metallurgical Transactions*, Vol. 19B, P. 851 - 858.

145. Pavelic, V., Tanbakuchi, R., Uyehara, O. A. and Myers, P. S., (1969), "Experimental and computed temperature histories in gas tungsten-arc welding of thin plates", *Welding Journal*, Vol. 48, No. 7, P. 295-s -305-s.

146. Quintino, L. and Allum, C. J., (1984), "Pulsed GMAW: Interactions between process parameters - Part 1", *Welding and Metal Fabrication*, No. 3, P. 85 - 89.

147. Quintino, L. and Allum, C. J., (1984), "Pulsed GMAW: Interactions between process parameters - Part 2", *Welding and Metal Fabrication,* No. 4, P. 126 - 129.

148. Ramanan, N. and Korpela, S. A., (1990), "Fluid dynamics of a stationary weld pool", *Metallurgical Transactions,* Vol. 21A, P. 45 - 57.

149. Ramsey, P. W., Chyle, J. J., Kuhr, J. N., Myers, P. S., Weiss, M. and Groth, W., (1963), "Infrared temperature sensing system for automatic fusion welding", *Welding Journal,* Vol. 42, No. 8, P. 337-s - 346-s.

150. Raveendra, J. and Parmar, R. S., (1987), "Mathematical models to predict weld bead geometry for flux cored arc welding", *Metal Construction,* Vol. 19, No. 2, P. 31R - 35R.

151. Remwick, R. J. and Richardson, R. W., (1983), "Experimental investigation of GTA weld pool oscillation", *Welding Journal,* Vol. 62, No. 2, P. 29-s - 35-s.

152. Richardson, R. W., Gutow, A., Anderson, R. A. and Farson, D. F., (1984), "Coaxial weld pool viewing for process monitoring and control", *Welding Journal,* Vol. 63, No. 3, P. 43 - 50.

153. Richardson, R. W., (1986), "Robotic weld joint tracking systems - Theory and implementation methods", *Welding Journal,* Vol. 65, No. 11, P. 43 - 51.

154. Roberts, D. K. and Wells, A. A., (1954), "Fusion welding of aluminium alloys", *British Welding Journal,* No. 12, P. 553 - 559.

155. Roget, J., Debiez, J. and Meyer, J. L., (1984), "Application of acoustic emission to in-process monitoring of submerged arc welding", *The Winter Annual Meeting of the American Society of Mechanical Engineers*, New Orleans, Louisiana, USA, 9 - 14, December, P. 77 - 94.

156. Rosenthal, D., (1941), "Mathematical theory of heat distribution during welding and cutting", *Welding Journal*, Vol. 20, No. 5, P. 220-s - 231-s.

157. Rykalin, N., Uglov, A. and Kokora, A., (1960), "Laser machining and welding", MIR, Moscow.

158. Salter, G. R. and Doherty, J., (1981), "Procedure selection for arc welding", *Metal Construction*, Vol. 13, No. 9, P. 544 - 550.

159. Salter, R. J. and Deam, R. T., (1987), "A practical front face penetration control system for TIG welding", *Developments in Automated and Robotic Welding,* Cambridge, UK, The Welding Institute, P. 38-1 - 38-12.

160. SAS Institute, Inc., (1988), "SAS/STAT User's Guide", 1988 Edition, SAS Institute Inc., Cary, NC.

161. Schauer, D. A., Giedt, W. H. and Shintaku, S. M., (1978), "Electron beam welding cavity temperature distributions in pure metals and alloys", *Welding Journal*, Vol. 57, No. 5, P. 127-s - 133-s.

162. Shercliff, J. A., (1970), "Fluid motions due to an electric current source", *Journal Fluid Mechanics,* Vol. 40, P. 241 - 250.

163. Shinoda, T. and Doherty, J., (1978), "The relationship between arc welding parameters and weld bead geometry : A literature survey", *The Welding Institute Report* 74/1978/PE.

164. Silk, M. G., (1984), "Ultrasonic transducers for nondestructive testing", Adam Hilger Ltd, Bristol, P. 120 - 134.

165. Siores, E., (1988), "Development of a real-time ultrasonic sensing system for automated and robotic welding", Ph. D Thesis, Brunel University.

166. Smartt, H. B., Einerson, P., Watkins, A. D. and Morris, R. A., (1986), "Gas metal arc welding process sensing and control", *Advances in Welding Science and Technology : Proceedings of an International Conference on Trends in Welding Research*, Gatlinburg, Tennessee, USA, 18 - 22, May, P. 461 - 465.

167. Smartt, H. B., (1990), "Arc-welding process", *Welding: Theory and Practice*, Elsevier Science Publishers, P. 175 - 208.

168. Smartt, H. B., Johnson, J. A. and Einerson, C. J., (1993), "The role of intelligent systems in weld process control", *Materials Evaluation*, Vol. 51, No. 10, P. 1166 - 1173.

169. Sozou, C. and Pickering, W. M., (1976), "Magnetohydrodynamic flow due to the discharge of an electric current in a hemispherical container", *Journal of Fluid Mechanics*, Vol. 73, P. 641 - 650.

170. Spalding, D. B., (1993), "A guide to the PHOENICS input language - CHAM TR/100", CHAM, London, UK.

171. Szekely, J., (1989), "Keynote address transport phenomena in welds with emphasis on free surface phenomena", *Recent Trends in Welding Science and Technology: TWR '89 : Proceedings of the 2nd International Conference on Trends in Welding Research,* Gatlinburg, Tennessee, USA, 14 - 18, May, P. 3 - 11.

172. Tekriwal, P., Stitt, M. and Mazumder, J., (1987), "Finite element modelling of heat transfer for gas tungsten arc welding", *Metal Construction*, Vol. 19, No. 7, P. 599R - 606R.

173. Tekriwal, P. and Mazumder, J., (1988), "Effect of torch angle and shielding gas flow on TIG welding - A mathematical model", *Metal Construction*, Vol. 20, No. 6, P. 275R - 279R.

174. Tekriwal, P. and Mazumder, J., (1988), "Finite element analysis of three-dimensional transient heat transfer in GMA welding", *Welding Journal,* Vol. 67, No. 7, P. 150-s - 156-s.

175. Tekriwal, P. and Mazumder, J., (1988), "Three-dimensional finite element analysis of multi-pass GMA welding", *Modeling and Control of Casting and Welding Processes IV : Proceedings of the Fourth International Conference on Modeling of Casting and Welding Processes,* Palm Coast, Florida, 17 - 22, April, P. 167 - 176.

176. Thomas, B. G., Samarasekara, I. V. and Brimacombe, J. K., (1984), "Comparison of numerical modeling techniques for complex two-dimensional, transient heat conduction problems", *Metallurgical Transactions*, Vol. 15B, P. 307 - 318.

177. Thompson, M. E. and Szekely, J., (1989), "The transient behaviour of weld pools with a deformed free surface", *International Journal Heat and Mass Transfer*, Vol. 32, No. 6, P. 1007 - 1019.

178. Thorn, K., Feenstra, M., Young, J. C., Lawson, W. H. S. and Kerr, H. W., (1982), "The interaction of process variables - Their influence on weld dimensions in GMA welds on steel plate", *Metal Construction*, Vol. 14, No. 3, P. 128 - 133.

179. Tichellar, G. W., Jelmorini, G. and van der Heuvel, G. J. P. M., (1977), "Droplet temperature measurements in arc welding", *IIW Document 212-411-77.*

180. Tsai, C. L., Dai, W. L., Dickinson, D. W. and Papritan, J. C., (1991), "Analysis and development of real-time control methodology in resistance spot welding", *Welding Journal*, Vol. 70, No. 12, P. 339-s - 351-s.

181. Tsai, M. C., and Kou, S., (1988), "The advantages of orthogonal curvilinear coordinates in simulating Marangoni convection in deformed weld pools", *Modeling and Control of Casting and Welding Processes IV : Proceedings of the Fourth International Conference on Modeling of Casting and Welding Processes,* Palm Coast, Florida, 17 - 22, April, P. 409 - 420.

182. Tsai, M. C. and Kou, S., (1990), "Electromagnetic-force-induced convection in weld pools with a free surface", *Welding Journal*, Vol. 69, No. 6, P. 241-s - 246-s.

183. Tsai, M. C. and Kou, S., (1990), "Heat transfer and fluid flow in welding arcs produced by sharpened and flat electrode", *International Journal Heat Mass Transfer*, Vol. 33, No. 10, P. 2089 - 2098.

184. Tsao, K. C., and Wu, C. S., (1988), "Fluid flow and heat transfer in GMA weld pools", *Weld Journal*, Vol. 67, No. 3, P.70-s - 75-s.

185. Ule, R. L., Joshi, Y. and Sedy, E. B., (1990), "A new technique for three-dimensional transient heat transfer computations of autogenous arc welding", *Metallurgical Transactions*, Vol. 21B, P. 1033 - 1047.

186. Walsh, D. W. and Savage, W. F., (1982), "Autogenous GTA weldment - Bead geometry variation due to minor elements", *Welding Journal,* Vol. 61, No. 4, P. 97-s - 102-s.

187. Wei, P. S. and Giedt, W. H., (1985), "Surface tension gradient driven flow around an electrode beam welding cavity", *Welding Journal,* Vol. 64, No. 9, P. 251-s - 259-s.

188. Wells, A. A., (1952), "Heat flow in welding", *Welding Journal*, Vol. 31, No. 5, P. 263-s - 267-s.

189. Woods, R. A. and Milner, D. R., (1971), "Motion in the weld pool in arc welding", *Welding Journal,* Vol. 50, No. 4, P. 163-s - 173-s.

190. Yang, L. J., Chandel, R. S. and Bibby, M. J., (1992), "The effects of process variables on the bead height of submerged-arc weld deposits", *Canadian Metallurgical Quarterly,* Vol. 31, No. 4, P. 289 - 297.

191 Yang, L. J., Chandel, R. S. and Bibby, M. J., (1993), "The effects of process variables on the weld deposit area of submerged arc welds", *Welding Journal,* Vol. 72, No. 1, P. 11-s - 18-s.

192. Yokoya, S. and Matsunawa, A., (1983), "Surface tension driven flow in a semi-spherical basin", *International Institute of Welding Document 212-563-83.*

193. Zacharia, T., Eraslan, A. H. and Aidun, D. K., (1988), "Modeling of autogenous welding", *Welding Journal*, Vol. 67, No. 3, P. 53-s - 62-s.

194. Zacharia, T., Eraslan, A. H. and Aidun, D. K., (1988), "Modeling of non-autogenous welding", *Welding Journal*, Vol. 67, No. 1, P. 18-s - 27-s.

195. Zacharia, T., Eraslan, A. H. and Aidun, D. K., (1988), "Welder: A computer code for simulating welding processes", *Modeling and Control of Casting and Welding Processes IV : Proceedings of the Fourth International Conference on Modeling of Casting and Welding Processes*, Palm Coast, Florida, 17 - 22, April, P. 177 - 185.

196. Zacharia, T., Eraslan, A. H., Aidun, D. K. and David, S. A., (1989), "Three-dimensional transient model for arc welding process", *Metallurgical Transactions*, Vol. 20B, P. 645 - 659.

197. Zacharia, T., David, S. A., Vitek, J. M. and Debroy, T., (1989), "Weld pool development during GTA and laser beam welding of type 304 stainless steel, Part II - Experimental correlation", *Welding Journal*, 68, No. 12, P. 510-s - 519-s.

198. Zacharia, T., David, S. A., Vitek, J. M. and Debroy, T., (1989), ",Weld pool development during GTA and laser beam welding of type 304 stainless steel, Part I - Theoretical analysis", *Welding Journal*, Vol. 68, No. 12, P. 499-s - 509-s.

199 Zacharia, T., David, S. A. and Vitek, J. M., (1991), "Effect of evaporation and temperature - Dependent material properties on weld pool development", *Metallurgical Transactions*, Vol. 22B, P. 233 - 241.

200. Zacharia, T., David, S. A., Vitek, J. M. and Kraus, H. G., (1991), "Computational modeling of stationary gas-tungsten-arc weld pools and comparison to stainless steel 304 experimental results", *Metallurgical Transactions*, Vol. 22B, P. 243 - 257.

APPENDICES

Appendix A: Experimental Data for Weld Bead Geometry

Table A.1 Welding Process Variables and Limits (As used in Chapter 3)

Variable	Unit	Level			Coding		
		Low	Middle	High	Low	Middle	High
Wire diameter	mm	1.2		1.6	0		1
Welding voltage	Volts	20	25	30	0	1	2
Welding speed	cm / min	25	33	41	0	1	2
Arc current	Amps	180	260	360	0	1	2

Table A.2 Design Matrix and Treatment Combinations (As used in Chapter 3)

Number of trial	Wire diameter	Welding voltage	Welding speed	Arc current
1	0	0	0	0
2	0	0	0	1
3	0	0	0	2
4	0	0	1	0
5	0	0	1	1
6	0	0	1	2
7	0	0	2	0
8	0	0	2	1
9	0	0	2	2
10	0	1	0	0
11	0	1	0	1
12	0	1	0	2
13	0	1	1	0
14	0	1	1	1
15	0	1	1	2
16	0	1	2	0
17	0	1	2	1
18	0	1	2	2
19	0	2	0	0
20	0	2	0	1
21	0	2	0	2
22	0	2	1	0

23	0	2	1	1
24	0	2	1	2
25	0	2	2	0
26	0	2	2	1
27	0	2	2	2
28	1	0	0	0
29	1	0	0	1
30	1	0	0	2
31	1	0	1	0
32	1	0	1	1
33	1	0	1	2
34	1	0	2	0
35	1	0	2	1
36	1	0	2	2
37	1	1	0	0
38	1	1	0	1
39	1	1	0	2
40	1	1	1	0
41	1	1	1	1
42	1	1	1	2
43	1	1	2	0
44	1	1	2	1
45	1	1	2	2
46	1	2	0	0
47	1	2	0	1
48	1	2	0	2
49	1	2	1	0
50	1	2	1	1
51	1	2	1	2
52	1	2	2	0
53	1	2	2	1
54	1	2	2	2

Table A.3 The Results of Experiment (As used in Chapter 3)

No. of trial	Weld bead width	Weld bead height	Weld bead penetration
1	9.65	3.43	2.04
2	12.12	4.18	3.53
3	13.71	5.39	6.68
4	8.96	2.91	1.82
5	11.38	4.04	2.89
6	13.00	5.09	5.42
7	8.08	2.75	1.84
8	9.27	3.25	2.97
9	10.30	4.64	4.13
10	12.56	2.80	2.12
11	13.04	3.49	3.43
12	14.56	4.92	5.93
13	10.09	2.79	1.78

14	12.46	2.95	3.36
15	14.20	4.52	5.34
16	10.12	2.45	1.66
17	10.22	3.02	2.34
18	13.10	4.26	4.12
19	14.20	2.09	2.12
20	16.50	3.06	3.08
21	15.36	2.64	6.25
22	13.45	2.52	1.26
23	15.75	2.58	3.05
24	14.70	1.95	5.10
25	10.91	2.20	1.81
26	11.40	2.24	2.54
27	14.10	2.95	5.81
28	12.49	3.37	1.79
29	13.07	3.51	2.67
30	14.26	4.87	3.85
31	10.37	2.38	1.75
32	11.49	3.08	2.45
33	13.83	4.65	3.40
34	8.94	2.24	1.75
35	10.92	2.92	2.67
36	12.35	4.18	3.82
37	13.73	2.57	1.94
38	16.05	2.68	2.28
39	18.00	4.02	4.00
40	11.76	2.4	1.89
41	12.82	2.98	2.53
42	15.35	3.93	3.90
43	11.03	2.18	1.80
44	11.94	2.40	2.41
45	13.45	3.39	3.32
46	16.20	2.51	2.00
47	17.63	2.78	2.83
48	20.06	3.51	5.37
49	14.08	2.30	1.66
50	15.48	2.53	2.53
51	18.47	3.74	4.50
52	12.55	2.32	1.14
53	14.25	2.81	2.33
54	16.83	4.93	5.14

Appendix B: Experimental Data for Mathematical Models

Table B.1 Welding Process Parameters and Limits (As used in Chapter 4)

Parameter	Symbol	Unit	Limits
Wire diameter	D	mm	0.9, 1.2, 1.6
Gas flow rate	G	ℓ	6, 10, 14
Welding speed	S	mm/min	250, 330, 410
Arc current	I	Amp	90, 190, 250 180, 260, 360
Welding voltage	V	Volt	20, 25, 30

Table B.2 Design Matrix (As used in Chapter 4)

No. of trial	D	G	S	I	V
1	0	0	0	0	0
2	0	0	0	1	2
3	0	0	0	2	1
4	0	0	1	0	2
5	0	0	1	1	1
6	0	0	1	2	0
7	0	0	2	0	1
8	0	0	2	1	0
9	0	0	2	2	2
10	0	1	0	0	2
11	0	1	0	1	1
12	0	1	0	2	0
13	0	1	1	0	1
14	0	1	1	1	0
15	0	1	1	2	2
16	0	1	2	0	0
17	0	1	2	1	2
18	0	1	2	2	1
19	0	2	0	0	1
20	0	2	0	1	0
21	0	2	0	2	2
22	0	2	1	0	0
23	0	2	1	1	2
24	0	2	1	2	1
25	0	2	2	0	2
26	0	2	2	1	1
27	0	2	2	2	0
28	1	0	0	0	2
29	1	0	0	1	1
30	1	0	0	2	0
31	1	0	1	0	1

32	1	0	1	1	0
33	1	0	1	2	2
34	1	0	2	0	0
35	1	0	2	1	2
36	1	0	2	2	1
37	1	1	0	0	1
38	1	1	0	1	0
39	1	1	0	2	2
40	1	1	1	0	0
41	1	1	1	1	2
42	1	1	1	2	1
43	1	1	2	0	2
44	1	1	2	1	1
45	1	1	2	2	0
46	1	2	0	0	0
47	1	2	0	1	2
48	1	2	0	2	1
49	1	2	1	0	2
50	1	2	1	1	1
51	1	2	1	2	0
52	1	2	2	0	1
53	1	2	2	1	0
54	1	2	2	2	2
55	2	0	0	0	1
56	2	0	0	1	0
57	2	0	0	2	2
58	2	0	1	0	0
59	2	0	1	1	2
60	2	0	1	2	1
61	2	0	2	0	2
62	2	0	2	1	1
63	2	0	2	2	0
64	2	1	0	0	0
65	2	1	0	1	2
66	2	1	0	2	1
67	2	1	1	0	2
68	2	1	1	1	1
69	2	1	1	2	0
70	2	1	2	0	1
71	2	1	2	1	0
72	2	1	2	2	2
73	2	2	0	0	2
74	2	2	0	1	1
75	2	2	0	2	0
76	2	2	1	0	1
77	2	2	1	1	0
78	2	2	1	2	2
79	2	2	2	0	0
80	2	2	2	1	2
81	2	2	2	2	1

Table B.3 Measured Weld Bead Dimension from Experiment (As used in Chapter 4)

Trial No.	W	H	P	WRSP	WRFF	A_T	A_R	A_P	DI	B_R	B_P
1	7.51	4.30	1.65	4.5515	1.7465	10.697	9.933	0.764	7.143	7.894	5.823
2	12.91	2.87	1.74	7.4195	4.4983	33.708	25.097	8.611	25.545	14.827	12.838
3	13.36	4.15	1.96	6.8163	3.2193	49.371	37.263	12.108	24.524	16.245	15.807
4	8.49	1.70	0.64	13.2656	4.9941	14.018	11.931	2.087	14.885	10.226	8.148
5	9.96	2.83	1.26	7.0948	3.5194	26.126	20.865	5.260	20.135	11.769	10.248
6	8.49	4.54	1.45	5.8552	1.8700	34.589	29.417	5.172	14.953	12.999	9.638
7	6.86	1.53	0.93	7.3763	4.4837	9.815	6.113	3.703	37.725	7.185	7.953
8	6.42	3.22	1.33	4.8271	1.9938	18.544	16.281	2.263	12.203	9.307	6.830
9	12.50	2.69	1.94	6.4433	4.6468	37.440	25.273	12.166	32.496	15.615	12.972
10	8.81	1.75	0.66	13.3485	5.0343	16.046	12.490	3.556	22.161	10.359	9.809
11	11.14	3.01	1.79	6.2235	3.7100	33.619	27.624	5.995	17.832	13.359	12.237
12	9.75	4.88	1.55	6.2903	1.9980	43.729	37.616	6.113	13.978	14.450	10.743
13	7.31	1.66	0.72	10.1528	4.4036	9.815	7.729	2.087	21.257	8.004	6.770
14	7.22	3.50	1.18	6.1186	2.0629	22.717	21.012	1.704	7.503	10.375	7.689
15	13.63	3.13	2.21	6.1674	4.3546	48.048	33.502	14.547	30.275	15.485	14.702
16	4.68	1.67	1.05	4.571	2.8024	7.523	5.172	2.351	31.250	6.101	4.918
17	9.83	2.25	0.97	10.1340	4.3689	20.219	15.252	4.966	24.564	11.849	8.769
18	10.03	3.18	2.16	4.6435	3.1541	19.014	12.343	6.671	35.085	12.002	8.247
19	8.05	1.88	1.01	7.9703	4.2819	15.987	12.137	3.850	24.081	8.486	9.003
20	8.29	3.90	1.31	6.3282	2.1256	28.888	23.804	5.084	17.599	11.784	9.233
21	16.53	3.46	2.61	6.3333	4.7775	60.803	42.045	18.749	30.836	18.941	17.203
22	5.45	1.76	1.17	4.6581	3.0966	7.641	5.525	2.166	27.692	6.648	5.397
23	10.99	2.60	0.96	11.4479	4.2269	26.860	19.778	7.082	26.368	13.365	10.517
24	11.46	3.39	2.07	5.5362	3.3805	38.968	30.210	8.757	22.474	13.315	13.135
25	7.44	1.15	0.80	9.3000	6.4696	27.830	25.303	2.527	9.081	8.018	8.283
26	9.53	2.40	1.51	6.2697	3.9708	32.121	23.304	8.816	27.447	10.203	9.874

27	7.51	4.25	1.52	4.9408	1.7671	9.022	5.466	3.556	39.414	12.192	11.661
28	13.62	2.71	1.24	10.9839	5.0258	35.559	22.217	13.342	37.521	16.262	13.383
29	14.82	3.55	2.53	5.8577	4.1746	50.282	39.262	11.020	21.917	17.436	15.249
30	14.90	5.64	1.59	9.3711	2.6418	78.435	74.115	4.320	5.508	20.187	13.798
31	11.46	2.52	1.33	8.6165	4.5476	28.065	19.602	8.464	30.157	13.678	10.495
32	10.05	4.22	2.05	4.9024	2.3815	34.295	27.536	6.759	19.709	12.559	10.905
33	16.36	4.68	5.39	3.0353	3.4957	82.285	56.218	26.067	31.679	19.725	19.085
34	8.18	2.55	1.84	4.4457	3.2078	20.924	14.341	6.583	31.461	9.787	9.387
35	13.54	3.39	2.03	6.6700	3.9941	45.609	32.062	13.548	29.704	18.723	13.615
36	10.98	4.64	4.37	2.5126	2.3664	51.781	33.112	18.669	16.742	16.032	13.771
37	12.73	2.84	1.78	7.1517	4.4824	34.619	23.451	11.167	32.258	16.781	12.070
38	12.18	5.43	1.87	6.5134	2.2431	51.987	48.196	3.791	7.292	16.846	13.779
39	17.25	5.15	5.65	3.0531	3.3495	105.44	68.561	36.881	34.978	21.483	21.694
40	8.57	3.34	1.59	5.3899	2.5659	23.863	19.102	4.761	19.951	10.629	8.271
41	14.41	3.42	1.72	8.3779	4.2135	50.429	33.884	16.545	32.809	16.774	14.657
42	13.27	5.07	2.97	4.4680	2.6174	63.830	54.249	9.580	15.009	17.727	14.959
43	11.17	2.16	1.41	7.9220	5.1713	25.567	13.842	11.726	45.862	12.101	10.473
44	11.44	3.14	2.04	5.6078	3.6433	34.472	22.070	12.402	35.976	13.755	11.438
45	11.46	5.44	1.32	8.6667	2.1029	45.815	44.816	0.999	2.181	17.645	10.572
46	9.65	3.43	2.04	4.7304	2.8134	31.792	27.360	4.438	13.956	11.787	9.996
47	16.50	3.06	3.08	5.3571	5.3922	62.801	35.089	27.712	44.127	20.097	15.886
48	14.56	4.92	5.93	2.4553	2.9593	73.645	54.543	19.102	25.938	18.408	17.225
49	13.45	2.52	1.26	10.6746	5.3373	30.592	20.938	9.610	31.412	15.555	13.413
50	12.46	2.95	3.36	3.7083	4.2237	40.085	27.536	12.548	31.305	14.547	12.531
51	13.00	5.09	5.42	2.3985	2.5540	50.018	47.402	2.615	5.229	17.121	13.190
52	10.12	2.45	1.66	6.0964	4.1306	22.246	13.195	9.051	40.687	11.760	9.338
53	9.27	3.25	2.97	3.1212	2.8523	27.448	22.452	4.996	18.201	11.095	8.904
54	14.10	2.95	5.81	2.4269	4.7797	42.083	26.508	15.575	37.011	15.794	14.955
55	12.95	2.41	1.72	7.5291	5.3734	33.825	19.778	14.047	41.529	15.999	12.969
56	12.78	3.80	2.56	4.9922	3.3632	44.610	28.006	16.604	37.220	15.360	12.898

57	20.22	3.81	4.71	4.2930	5.3071	101.51	57.747	43.758	43.109	24.144	22.692
58	9.67	2.45	2.18	4.4358	3.9469	24.068	15.046	9.022	37.485	10.486	10.767
59	16.50	2.57	2.47	6.6802	6.4202	56.454	25.009	31.445	55.700	17.943	18.710
60	15.45	3.68	3.65	4.2329	4.1984	62.067	40.555	21.512	34.659	25.771	19.929
61	12.16	2.21	1.35	9.0074	5.5023	26.860	20.219	6.642	24.726	13.898	13.442
62	12.15	2.67	2.46	4.9390	4.5506	36.029	18.367	17.662	49.021	15.033	12.204
63	10.70	4.02	3.04	3.5197	2.6617	46.961	27.477	19.484	41.489	14.676	12.202
64	10.58	2.86	1.69	6.2604	3.6993	29.858	20.806	9.051	30.315	13.668	10.658
65	19.08	2.59	2.64	7.2273	7.3668	63.418	30.916	32.503	51.251	20.871	19.863
66	18.16	3.95	4.69	3.8721	4.5975	82.785	60.509	22.276	26.908	20.316	20.626
67	13.94	2.13	1.38	10.1014	6.5446	31.121	20.277	10.844	34.844	18.542	12.055
68	13.86	2.90	2.63	5.2700	4.7793	43.611	21.424	22.188	50.876	15.429	14.438
69	11.95	4.34	3.50	3.4143	2.7535	59.392	42.054	17.339	29.193	15.345	15.214
70	11.17	2.21	1.71	6.5322	5.0543	25.450	19.308	6.142	24.134	14.266	10.313
71	9.53	3.12	2.03	4.6946	3.0545	30.005	17.250	12.754	42.507	12.372	9.411
72	17.07	3.36	5.70	2.9947	5.0804	78.759	36.911	41.484	53.134	18.242	22.191
73	16.20	2.51	2.00	8.1000	6.4542	25.773	12.402	13.371	51.881	10.718	9.125
74	16.05	2.68	2.28	7.0395	5.9888	28.741	17.926	10.815	37.628	13.390	12.653
75	14.26	4.87	3.85	3.7039	2.9281	36.852	28.623	8.229	22.329	13.987	11.916
76	11.76	2.40	1.89	6.2222	4.9000	83.137	45.081	38.057	45.776	21.487	20.062
77	11.49	3.08	2.45	4.6898	3.7305	77.965	57.600	20.366	26.121	20.205	16.663
78	18.47	3.74	4.50	4.1044	4.9385	47.461	26.665	20.806	43.839	16.334	17.187
79	8.94	2.24	1.75	5.1086	3.9911	51.252	26.478	24.774	48.337	15.963	14.388
80	14.25	2.81	2.33	6.1159	5.0712	47.167	36.247	10.903	23.115	17.513	14.642
81	13.45	3.39	3.32	4.0512	3.9676	46.227	29.858	16.396	35.410	17.412	16.373

Appendix C: Experimental Data for Infrared Sensing

Table C.1 Welding process parameters for experiment (As used in Chapter 6)

No. of Trial	Thickness (mm)	Arc current (A)	Welding speed (cm/min)	Welding voltage (V)
1	5	150	25	20
2	5	150	25	25
3	5	150	33	20
4	5	150	33	25
5	5	240	25	20
6	5	240	25	25
7	5	240	33	20
8	5	240	33	25
9	10	150	25	20
10	10	150	25	25
11	10	150	33	20
12	10	150	33	25
13	10	240	25	20
14	10	240	25	25
15	10	240	33	20
16	10	240	33	25

Table C.2 Measured isotherm radii and weld bead geometry (As used in Chapter 6)

No. of Trial	Isotherm Radii (isotherm unit)	Bead width (mm)	Bead height (mm)
1	0.087	8.96	2.55
2	0.113	11.59	2.39
3	0.083	8.08	2.46
4	0.091	9.57	1.87
5	0.113	11.63	3.72
6	0.125	14.80	3.17
7	0.101	9.98	3.64
8	0.116	12.35	2.8

9	0.085	8.36	2.57
10	0.108	11.09	2.05
11	0.079	7.41	3.22
12	0.094	9.51	1.86
13	0.100	10.54	4.33
14	0.148	13.89	3.26
15	0.103	9.34	3.95
16	0.127	12.56	3.14

Table C.3 Measurement of weld process parameters for 5 mm mild steel plates (As used in Chapter 6)

No. of Trial	Arc current (A)	Isotherm radii (isotherm unit)	Bead width (mm)	Bead height (mm)
1	150	0.103	5.20	1.36
2	160	0.107	5.46	1.40
3	170	0.107	6.08	1.42
4	180	0.109	6.10	1.58
5	190	0.113	6.52	1.62
6	200	0.118	6.68	1.70
7	210	0.121	7.00	1.72
8	220	0.122	7.02	1.88
9	230	0.125	7.64	1.88
10	240	0.129	7.96	1.92

Table C.4 Measurement of weld process parameters for 10 mm mild steel plates (As used in Chapter 6)

No. of Trial	Arc current (A)	Isotherm radii (isotherm unit)	Bead width (mm)	Bead height (mm)
1	150	0.093	4.86	0.80
2	160	0.097	5.66	0.98
3	170	0.099	5.74	1.18
4	180	0.100	6.50	1.28

5	190	0.102	6.88	1.52
6	200	0.104	7.28	1.56
7	210	0.110	7.50	1.70
8	220	0.118	7.65	1.98
9	230	0.119	8.08	1.98
10	240	0.121	8.54	2.02